

*Università degli Studi del Piemonte Orientale*

Department of Pharmacological Science.

Ph.D. in Chemistry and Biology

XXXIV cycle a.y. 2021/2022

*Characterization of a mouse model for  
Tubular Aggregate Myopathy and  
development of small molecules*



**PhD Candidate:** Celia Cordero Sánchez

**Supervisor:** Prof. Armando Genazzani

**PhD program Coordinator:** Prof. Gian Cesare Tron





UNIVERSITÀ DEL PIEMONTE ORIENTALE  
DOTTORATO DI RICERCA  
IN CHEMISTRY & BIOLOGY

Via Duomo, 6  
13100 - Vercelli (ITALY)

### DECLARATION AND AUTHORISATION TO ANTIPLAGIARISM DETECTION

The undersigned CELIA CONDINO SANCI student of the Chemistry & Biology  
Ph.D course (~~XXX~~ Cycle)

#### declares:

- to be aware that the University has adopted a web-based service to detect plagiarism through a software system called "Turnit.in",
- his/her Ph.D. thesis was submitted to Turnit.in scan and reasonably it resulted an original document, which correctly cites the literature;

#### acknowledges:

- his/her Ph.D. thesis can be verified by his/her Ph.D. tutor and/or Ph.D Coordinator in order to confirm its originality.

Date: 03.11.2021 Signature: Celia Condino





En primer lugar quiero dedicar mi tesis, sin lugar a dudas, a mis padres. Me faltan páginas para agradecerlos todo lo que me gustaría. Fuisteis el apoyo incondicional que necesité y del cual aprendí para mi vida personal y profesional. Un cóctel equilibrado que me sirvió de referente para mi personalidad. Mamá, has sido el mejor ejemplo de mujer trabajadora y apasionada que podríamos haber tenido. Nuestra super heroína. Has sido el ejemplo del sudor del trabajo, pero más aún de la gratificación de las recompensas y del constante estudio requerido para avanzar profesionalmente, hecho que caracteriza el mundo en el que me sumerjo, la investigación. Papá, has sido un ejemplo intelectual, cultural, y pasional, queriendo lo mejor, no solo para mí, sino para nuestra familia bajo toda circunstancia. Me has enseñado la pasión por la informática, el análisis y la resolución de problemas, esencial en el mundo de la investigación. Siempre he pensado que mi vocación por la ciencia, viene directamente de vosotros. Gracias por haberme dado las bases para ser como soy. Ha sido duro desde el primer momento, pero lo tengo claro: no estaría aquí sin vosotros. Ejemplo de constancia, trabajo y lucha por una vida equilibrada es mi hermana. Andrea, eres el ejemplo de lo que me gustaría ser, y no te pierdo como referente. Tu fortaleza me fascina. Te admiro muchísimo, hermana. Aunque no lo creas, me has dado bocanadas de aire cuando más lo necesitaba. Soy muy afortunada de teneros y tengo que agradecerlos a cada uno de vosotros el estímulo y el calor que habéis siempre proyectado en mí. Prima, parecía que no, pero finalmente ha salido. Gracias.

En segundo lugar, agradecer a Armando Genazzani, por haberme dado la grandísima oportunidad de participar en uno de sus emocionantes proyectos, del cual me enamoré perdidamente en solo 3 meses. Has sido un gran mentor, y los encuentros contigo, aunque fugaces, estaban siempre cargados de la inspiración y estímulo científico más que necesaria para continuar.

Gracias a todos los integrantes de su laboratorio: Ambra Grolla, Giorgia Colombo, Cristina Travelli, Dmitry Lim, Giulia Dematteis, Mariana Moro, Sara Boumya y Arash Foroutan, que siempre han estado más que disponibles para darme una mano ante cualquier ayuda que he podido necesitar. Laura Tapella, hay una mención especial para ti. Has llenado sobre todo los últimos días con tu alegría juvenil, y las conversaciones contigo, científicas y personales. Han sido un absoluto placer. Siento haberte abandonado este último año. Gracias a todos nuestros colaboradores que han hecho posible esta investigación y a la fundación Telethon, por la financiación. No puedo agradecer más de lo que ya lo he hecho a Nausicaa Clemente, por ser un referente en la experimentación *in vivo*, y por tu eterna disponibilidad, que tan fundamental ha sido. Gracias especialmente a Alessandra Bertoni. Alessandra, sin tu siempre gentil apoyo no habría podido realizar la mayor parte de los experimentos en las plaquetas. Tu experiencia y profesionalidad me han abierto las puertas a un mundo totalmente desconocido, y que a día de hoy, sigo intrigada a conocer aún más. Muchísimas gracias.

Así mismo, agradecer a Asia Fernández Carvajal. Asia, fuiste y siempre serás mi madre científica. Mi referente científico y la que me transmitió la pasión por la ciencia. Gracias a ti soy una microbióloga frustrada, pero seré una orgullosísima y apasionadísima doctora en Química y Biología, dedicada a intentar mejorar la vida de unos pocos olvidados, pero igualmente super importantes. El mundo del calcio me interesó (más de lo que esperaba) desde nuestro primer encuentro. Has marcado cada uno de los pasos y elecciones que he hecho en mi vida profesional. No puedo agradecerte más la oportunidad que me diste, acogéndome en tu laboratorio, y permitiéndome conocer a tus colaboradores, que me han permitido continuar en mi camino hacia mi sueño final: ser doctora.

Mi elección de dedicarme a la investigación, no fue más que la buena influencia de un gran profesor en el instituto, Juan Jesús Campos. Siempre insistiré en esa clase de plásmidos e ingeniería genética que dio en

una inocente clase, que marcó en 1 hora el resto de mi vida. Sali de esa clase con un nudo en la garganta y la sensación de explosión en el pecho. Supe en aquel entonces que quería dedicarme a la investigación. Gracias a ti, me metí en la cabeza que quería hacer biotecnología, y aunque no fue una elección fácil, fui hasta todos los rincones inexplorados que se presentaron como oportunidad para realizar mi sueño. Siempre sin olvidar dónde todo empezó.

No puedo continuar mis agradecimientos sin mencionar a Javi. Estuviste en los momentos más difíciles, apoyándome. Fuiste fundamental en Bachiller y la carrera, donde no dejaste, y a día de hoy no dejas de creer en mí y en mi potencial. No podías no estar presente en mis agradecimientos.

Por último, pero para nada menos importante, eres tú, Bea. Has sido la hermana mayor que no tengo, personal y profesionalmente. Todo un estímulo, una bomba de pasión y energía. No puedo decirte nada que ya no te haya dicho. Me enamoré del proyecto y de tu pasión. Tus rizos alocados corriendo por los pasillos, en busca de financiación y nuevos artículos me asustaron, pero al mismo tiempo me involucró en la montaña rusa de sentimientos y locura que fueron nuestros años juntas, pero sobretodo, trabajo en equipo. Mi infierno, pero a la vez, mi mayor paraíso. Contigo aprendí la incondicionalidad y la lealtad en la pasión científica. Aprendí que todo merece la pena si la satisfacción personal es una prioridad. He aprendido también a la importancia de ponerse límite. Hemos crecido juntas, personal y profesionalmente, y eso hará que sienta una unión muy especial contigo. No dejaré de llevarte kínder-bueno cada vez que pueda. Eres el ejemplo de lo que quería ser profesionalmente, como siempre te he dicho. Eso sí, espero no trabajar el resto de mi vida tanto como lo que he trabajado contigo. Espero también encontrar compañeros que me den la fuerza, el estímulo y la dinamita que me das tú, aunque sé que esto no será así.

Obviamente este doctorado no podría haber sido realizado sin los animales de experimentación, uno de los mayores orígenes de estrés de mi doctorado. A pesar de la fundamental necesidad de realizar experimentos en animales para desarrollar fármacos para tratamientos de enfermedades en humanos o en otros animales, no podemos olvidar que ellos, como los mismos científicos (diría que más), dedican su vida para el desarrollo de la ciencia.

Quiero también agradecerme a mí misma. Por no haber dejado de luchar por mi pasión, y no haber perdido la esperanza aunque no viera la luz al final del túnel. Ha merecido la pena. He madurado y crecido, personal y profesionalmente. Mi crecimiento ha sido apoyado y acentuado gracias a ti, Federico. Aunque no lo creía, me has dado la estabilidad y la templanza que necesitaba en el periodo donde más me estaba perdiendo a mí misma. Me has ayudado y animado a buscar mi Zen y mi tranquilidad psicológica, a poner los pies sobre la tierra, que especialmente en estos últimos años que el mundo ha tenido, lo necesitaba. Me has ayudado a separarme emocionalmente del trabajo, de los problemas, a intentar mantener la calma, haciéndome más eficaz y productiva. Aún con el coronavirus y con la experiencia al extranjero, conseguí hacer todo lo que me propuse. Has luchado contra mí, para que yo misma dejara de hacerlo. Gracias.

Gracias a todos.





# Index

1. <b>Introduction</b> .....	1
a. Store-Operated Calcium Entry .....	1
i. <i>ORAI1</i> .....	4
ii. <i>STIM1</i> .....	6
iii. <i>Store-Operated Calcium Entry in skeletal muscle</i> .....	8
iv. <i>Store-Operated Calcium Entry in platelets</i> .....	10
b. CRAC channelopathies .....	12
i. <i>Tubular Aggregate Myopathy, Stormorken syndrome, and York Platelet syndrome</i> .....	16
c. Contemporary mouse models .....	18
d. Current Store-Operated Calcium Entry inhibitors .....	19
2. <b>Outline of the thesis</b> .....	23
3. <b>PART I: Characterization of KI-STIM1<sup>1115F</sup> mouse model</b> .....	25
a. Validation of KI-STIM1 <sup>1115F</sup> mouse model for Tubular Aggregate Myopathy.....	25
i. <i>Synopsis</i> .....	27
ii. <i>A luminal EF-hand mutation in STIM1 in mice causes the clinical hallmarks of tubular aggregate myopathy</i> .....	29
iii. <i>Supplementary information</i> .....	41
iv. <i>Author contributions</i> .....	49
b. Validation of KI-STIM1 <sup>1115F</sup> mouse model for York Platelet Syndrome.....	51
i. <i>Synopsis</i> .....	53
ii. <i>CIC-39Na reverses the thrombocytopenia that characterizes Tubular Aggregate Myopathy</i> .....	55
iii. <i>Supplementary data</i> .....	77

iv. <i>Author contributions</i> .....	79
<b>4. PART II: Development of small molecules</b> .....	<b>81</b>
a. Screening of putative Store-Operated Calcium Entry inhibitors .....	83
i. <i>Synopsis</i> .....	87
ii. <i>Store-Operated Calcium Entry as a Therapeutic Target in Acute Pancreatitis: Discovery and Development of Drug-Like SOCE Inhibitors</i> .....	85
iii. <i>Supporting information</i> .....	105
iv. <i>Author contributions</i> .....	127
<b>5. Discussion and conclusions</b> .....	<b>129</b>
<b>6. References</b> .....	<b>145</b>
<b>Abbreviations</b> .....	<b>179</b>
<b>Publications and patent</b> .....	<b>181</b>
<b>Curriculum vitae</b> .....	

## 1.- Introduction

### *a. Store Operated Calcium Entry*

Calcium ( $\text{Ca}^{2+}$ ) is a well-known second messenger able to regulate boundless cellular processes. Its versatility is due to the ability to modulate  $\text{Ca}^{2+}$ -rises in terms of concentration, as well as in terms of spatial and temporal localization. A huge repertoire of cellular components, known collectively as the calcium toolkit, drives the coding and the decoding of  $\text{Ca}^{2+}$ -signals (Berridge et al. 2000; Bootman et al. 2019; Carafoli et al. 2001; Schulte et al. 2022).

In cells, basal cytosolic  $\text{Ca}^{2+}$  is maintained at low nanomolar levels (10-50 nM) by the combination of  $\text{Ca}^{2+}$ -buffering proteins and the action of ion-exchange mechanisms (e.g.  $\text{Na}^+/\text{Ca}^{2+}$  exchanger and  $\text{Ca}^{2+}$ -pumps) into the extracellular space or in intracellular organelles (e.g. endosarcoplasmic reticulum ER/SR). A  $\text{Ca}^{2+}$ -signal is given by a rise in cytosolic  $\text{Ca}^{2+}$  which can derive from the extracellular space, for example via the opening of  $\text{Ca}^{2+}$ -channels located on the plasma membrane (PM), or from the opening of receptors (e.g.  $\text{IP}_3\text{R}$ , RYR, TRP) located on the intracellular organelles (Amini et al. 2021; Berridge et al. 2003; Bootman et al. 2002; Lewis, 2019; Putney et al. 1981; Schulte et al. 2022). Store-Operated Calcium Entry (SOC Entry) is a ubiquitous cellular mechanism that allows the influx of extracellular calcium after the depletion of the ER/SR. The two principal protagonists of SOC Entry are (i) STIM (STromal Interaction Molecule),  $\text{Ca}^{2+}$ -sensor on the ER membrane; and (ii) ORAI, as principal Calcium Release-Activated Calcium (CRAC) channel located in the PM (Lacruz and Feske, 2015; Lewis, 2019; Noble et al. 2020; Putney, 1986; Schulte et al. 2022).

As represented in Figure 1, SOC Entry begins with the depletion of ER/SR calcium through channels sensitive to  $\text{Ca}^{2+}$  located on the ER/SR membrane, as Inositol-1,4,5-triPhosphate Receptor ( $\text{IP}_3\text{R}$ ) or RYanodine Receptor (RYR) (Carafoli et al. 2001; Noble et al. 2020; Pallipadan et al. 2017; Putney, 2014). The drop in stored  $\text{Ca}^{2+}$  concentrations then leads to a reduced ion binding to the intraluminal binding domains of STIM1 and the subsequent conformational change leading to the formation of dimers that accumulate at the ER-PM junctions. Then, these dimers of STIM1 interact and

activate ORAI1, allowing the influx of calcium to the cytosol and the consecutive replenishment of the depleted organelles through the Endo(Sarco)plasmic Reticulum  $\text{Ca}^{2+}$  ATPase (SERCA; Fahrner et al. 2020; Lewis, 2019; Noble et al. 2020; Putney, 2014; Prakriya and Lewis, 2015; Schulte et al. 2022; Yang et al. 2021). Cytosolic calcium level after SOC Entry is not only restored at resting levels by SERCA, but also by plasma membrane ATPases (PMCA),  $\text{Na}^+/\text{Ca}^{2+}$  exchangers, and (Conte et al. 2021; Gehlert et al. 2021).

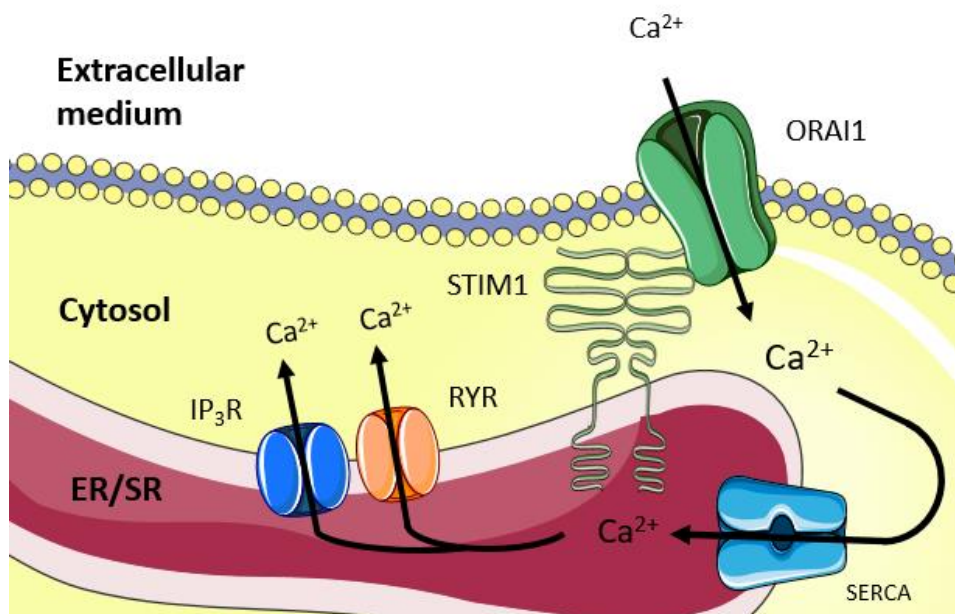


Figure 1.- *Store-Operated Calcium Entry (SOC Entry) mechanism.* SOC Entry begins with the depletion of the stores through IP<sub>3</sub>R and RYR (Left) and follows with the dimerization of STIM1 and interaction with ORAI1 (Right) for the refilling of the stores. ER/SR: Endo(Sarco)plasmic Reticulum; IP<sub>3</sub>R: Inositol-1,4,5-triPhosphate Receptor; RYR: Ryanodine Receptor; STIM: STromal Interaction Molecule; SERCA: Sarco(Endo)plasmic Reticulum  $\text{Ca}^{2+}$  ATPase. (Figure created through Smart Servier Medical Art.)

Calcium fluxes through SOC Entry have a key role in a number of specific cellular functions, recapitulated in Table 1. The implication of SOC Entry in skeletal muscle and platelets will be detailed in chapters (1.a.iii) and (1.a.iv) respectively.

**Table 1. Cellular functions modulated by SOC Entry.**

<b>Function</b>	<b>Reference</b>
Apoptosis	Sukumaran et al. 2021
Bone-forming osteoblasts	Hwang and Putney, 2012;
Bone-resorbing osteoblasts	Hwang et al. 2012
Contraction in skeletal muscle	Wei-Lapierre et al. 2013
Keratinocyte differentiation	Numaga-Tomita and Putney, 2012
Milk expulsion from mammary glands	Davis et al. 2015
Neutrophil chemotaxis	Steinckwich et al. 2015
Secretion	Balghi et al. 2011; Sabourin et al. 2015; Xing et al. 2014
Sperm development	Davis et al. 2016
Platelet functionality	Galan et al. 2009; Gilio et al. 2010
Vascular smooth muscle proliferation	Dominguez-Rodriguez et al. 2012

### *i. ORAI1*

Three homolog proteins (ORAI1, ORAI2, and ORAI3) of ~33 KDa with 4 highly conserved transmembrane domains (TM) constitute the ORAI family, with ORAI1 as the principal subunit composing the CRAC channel (Figure 2; Cai et al. 2007; Feske et al. 2006; McNally and Prakriya, 2012; Vig et al. 2006).

TM domains are responsible for the permeability and selectivity of the ORAI channels. Specifically, the TM1 domain, rich in cross-linking cysteine residues forming  $\alpha$ -helices, constitutes the central pore of the ORAI1, highly selective for calcium (Mignen et al. 2008). Concretely, amino acids R91C, L95C, G98C, and V102C are crucial in conductance in ORAI1, although other substitutions in TM2, TM3, or TM4 also affected ORAI1 conductance (Bohm et al. 2017; Bulla et al. 2019; Endo et al. 2015; McNally et al. 2009; Nesin et al. 2014). Moreover, TM3 has been associated with calcium permeation, since the E178N mutant directly abolishes calcium permeation, and the V174A mutant is constitutively activated (Yang et al. 2021). Indeed, E190Q mutation has been demonstrated to increase pore diameter (from 3.8 to 7.0 Å), compromising calcium selectivity (Pakriya and Lewis, 2015; Zhou et al. 2010).

Besides, negatively charged residues held by extracellular loop 1 (E106, D110, D112, and D114) are crucial for calcium selectivity, and mutations in this location lead to a loss of calcium selectivity (Bulla et al. 2019; Prakriya et al. 2006; Vig et al. 2006). Instead, intraluminal loop 2 is responsible for calcium-dependent inactivation, where mutations such as R155S, K159S, and K163S lead to a permanent close ORAI1 channel (Yang et al. 2021).

Last, as shown in Figure 2, both N and C-termini are extended to the cytosol, making ORAI a teardrop-shaped molecule that allows the exposure of crucial domain for STIM direct interaction (Amcheslavsky et al. 2015; Derler et al. 2013; McNally et al. 2013; Maruyama et al 2009; Palty et al. 2015; Palty and Isacoff. 2016; Zhang et al. 2006). Indeed, the interaction of N-termini and intraluminal loop 2 has been demonstrated to be crucial for the pH-dependent property of ORAI1 (Rychkov et al. 2022).

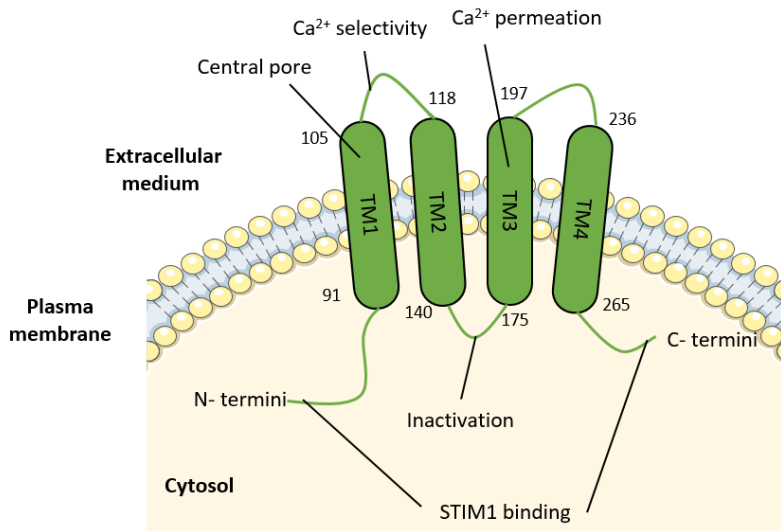


Figure 2-. **Scheme of overall human ORAI1 subunit structure.** ORAI1 subunit scheme comprehends a summary of the principal function of each structural component. TM: Transmembrane domain. Numbers correspond to number of amino acid. (Figure created through Smart Servier Medical Art.)

Some authors have suggested that ORAI channels are constituted by tetramers (Maruyama et al 2009; Mignen et al. 2008; Penna et al. 2009; Zhou et al. 2010) while others hinted at hexamers (Cai et al. 2016; Thompson and Shuttleworth, 2013; Yen et al. 2016). Stoichiometry studies of STIM1 and ORAI1 studies indicate that 8 molecules of STIM1 interact with a single channel of ORAI1 (Hoover and Lewis, 2011), reinforcing the hypothesis of ORAI tetramers since STIM1 forms dimers. Unfortunately, higher-resolution structural studies are needed to characterize and understand better the behaviour and functionality of ORAI channels and their subunits.

## ii. *STIM1*

Two family members of STIM have been reported: (i) STIM1 with 685 amino acids; and (ii) STIM2, with 833 amino acids. STIM1 is the principal stored-calcium sensor that activates CRAC channels and therefore SOC Entry. This was demonstrated by (i) the increase of SOC Entry when co-overexpression of STIM1 and ORAI1 (Mercer et al. 2006; Soboloff et al. 2006), and (ii) the strong reduction of CRAC entry after STIM1 knockdown (Liou et al. 2005; Roos et al. 2005). The function of STIM2 has been associated with the control of basal calcium homeostasis due to (i) its lower affinity for calcium than STIM1; and (ii) the interaction with ORAI1 at resting ER  $\text{Ca}^{2+}$  levels (Grabmayr et al. 2021; Stathopoulos et al. 2006; Zheng et al. 2011). This evidence has been supported by the formation of STIM2 but not STIM1 puncta upon subtle decreases of ER-stored calcium (Bird et al. 2013; Brandman et al. 2007).

Both STIM proteins bear a single-pass transmembrane (TM) domain (Figure 3; Fahrner et al. 2020; Grabmayr et al. 2021; Prakriya and Lewis, 2015), and share highly conserved domains within cytosolic and luminal regions (Roos et al. 2005; Liou et al. 2005).

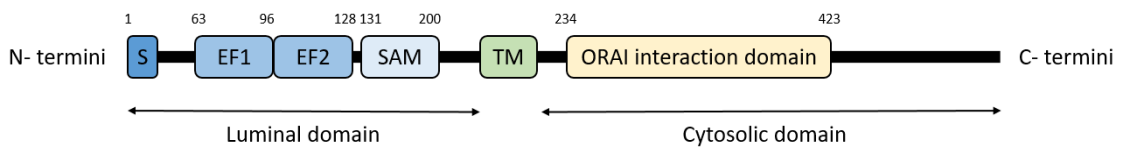


Figure 3.- **Scheme of human STIM1 structure.** S: signal peptide; EF1: Canonical EF-hand; EF2: non canonical EF-hand; TM: transmembrane region. Numbers correspond to number of amino acid. (*Figure created through Powerpoint*)

The cytosolic domain contains the ORAI1 interaction region (Figure 3), which is responsible for (i) the oligomerization of STIM1 upon depletion of  $\text{Ca}^{2+}$  (Convington et al. 2010); (ii) of the targeting of STIM1 to the ER-PM junctions; and (iii) of the interaction with ORAI1 (Baba et al. 2006; Huang et al. 2006; Liou et al. 2007; Li et al. 2007).



The intraluminal domain is composed of a highly conserved EF-SAM domain, which is formed by two EF-hands and a SAM domain (Figure 3; Collins and Meyer, 2011; Fahrner et al. 2020; Grabmayr et al. 2021). The canonical EF-hand (EF1) is capable of calcium-binding, while the non-canonical (EF2) domain is responsible for the stabilization of that binding. Both EF-hands consist of helix-loop-helix motifs and create the hydrophobic core for cation binding in the presence of stored calcium. In STIM1, side chains of 12 amino acids head the calcium-binding side: Val68, Ile71, Hist72, Leu74, Met75, Val83, Leu92, Leu96, Lys104, Phe108, Ile115 and Leu120 (Figure 4). Therefore, mutations in these amino acids directly lead to a defect in calcium-sensing and consequently lead to constitutive activation of STIM1 and SOC Entry (Jinhui et al. 2017).

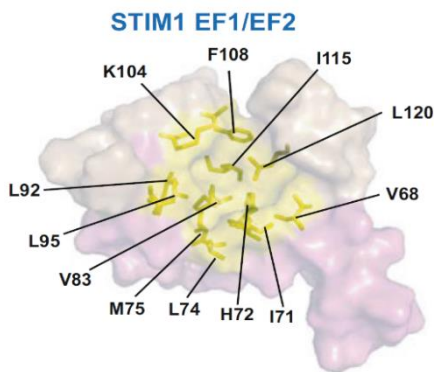


Figure 4.- *Scheme of EF hands of STIM1.*  
(Jinhui et al. 2017)

The SAM domain folds in five-helix compact bundles and increases the hydrophobic pocket and the stability of the EF-SAM domain (Stathopoulos et al. 2006). Furthermore, other STIM stability studies have revealed that EF-SAM domains lose the  $\alpha$ -helicity in the absence of calcium, and consequently become less stable. The calcium-lacking instability leads to a quaternary conformational change, resulting in dimerization of STIM (Stathopoulos et al. 2006; Zheng et al. 2008).

### iii. Store-Operated Calcium entry in skeletal muscle

Skeletal muscle contraction initiates with the membrane depolarization of the muscle fiber that leads to a conformational change of voltage-gated  $\text{Ca}^{2+}$  channels. At this point, the excitation-contraction coupling process starts, where calcium influx activates RYR channels that release to sarcoplasm calcium stored in SR (Figure 5, point A; Launikonis et al. 2003; Launikonis & Rios, 2007).

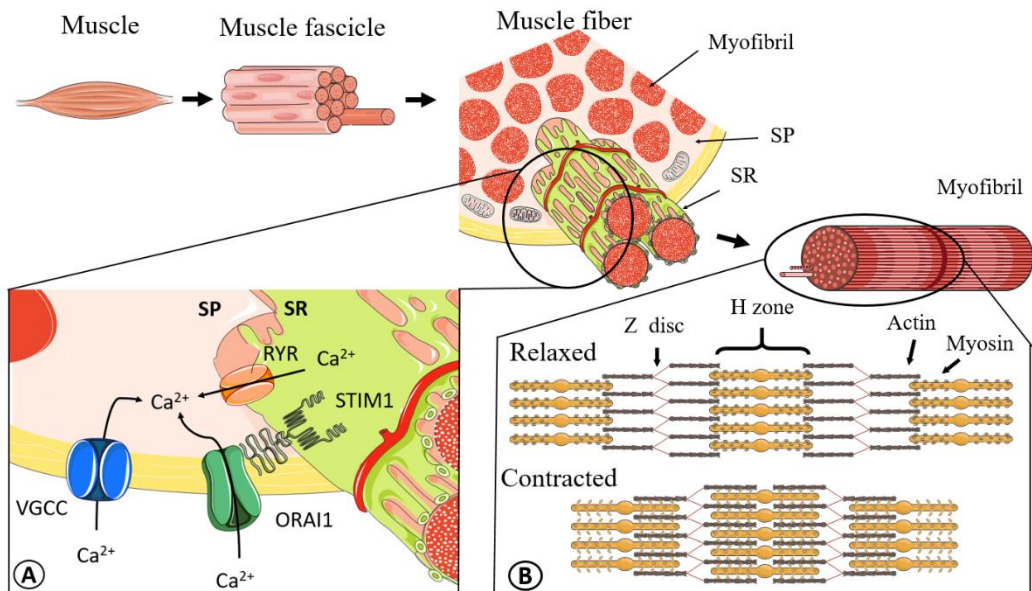


Figure 5.- **Scheme of skeletal muscle.** Muscle is formed by muscle fascicle composed at the same time by muscle fibers. Muscle fiber cells contain myofibrils, constituted by contractile units of actin and myosin. **(A) Calcium signalling in muscle fibers.** VGCC allow calcium influx that activates RYR channels. Emptiness of stored calcium lead to activation of SOC Entry mechanism, heading to further calcium influx. **(B) Myofibril sarcomere composition.** Sarcomere unit comprehends from one Z disc to the next. Contraction of sarcomeres consist in  $\text{Ca}^{2+}$ -dependent progression on actin and myosin filaments, carrying to the reduction of H zone. SP: Sarcoplasm; SR: Sarcoplasmic Reticulum; Receptor; RYR: Ryanodine Receptor; STIM: STromal Interaction Molecule; SERCA: Sarco(Endo)plasmic Reticulum  $\text{Ca}^{2+}$  ATPase VGCC: Voltage-gated calcium channels. (Figure created through Smart Servier Medical Art.)

The increase of sarcoplasmic calcium has been demonstrated to be critical for the interaction of myosin and actin of the myofibrils, direct conductors of muscle contraction by the regulatory troponin-tropomyosin complex. In the absence of calcium, troponin I and tropomyosin blocks myosin-binding sites in actin. After calcium binding,

troponin C interacts with troponin I, liberating actin and allowing the rotation of tropomyosin on the actin filament. This movement allows the myosin-actin binding and the progression of actin filaments through myosin filament which leads to the reduction of the H zone, and therefore, to myofibril contraction (Figure 5, point B; Schiaffino and Reggiani, 2011).

Since SOC Entry kinetics is slower than the influx of calcium from SR through RYR1, SOC Entry has a key role in the maintenance of sarcoplasmic calcium concentrations and consequently the maintenance of the contractile function (Bulla et al. 2019; Gehlert et al. 2021; Koenig et al. 2018). Indeed, reduction of contractility of skeletal muscle with age has been proposed to be due to a reduction in SOC Entry contribution (Thornton et al. 2011).

Apart from this, repetitive muscle contraction requires a fast and huge calcium mobilization and a high calcium sensitivity of myofilaments (Gehlert et al. 2021). Surprisingly, recent studies demonstrated that mice pre-exercised, that display higher resistance to fatigue compared to non-pre-exercised mice, show a co-localization of STIM1 and ORAI1 in skeletal muscle, suggesting that training molecularly prepares fibers to overcome faster responses (Boncompagni et al 2017; Protasi et al. 2021).

During muscle relaxation, calcium levels have to be restored to resting conditions. SERCA is the main responsible for calcium removal, refilling the SR store at the expense of ATP. Different isoforms of SERCA have been found according to the fiber type: SERCA1 is present in type II myofibers while SERCA2 is in type I myofibers. Uptake comparison between the different isoforms of SERCA differs, conferring dissimilar fatigue resistance, leading to more fatigable type II fibers (Lilliu et al. 2021; Schiaffino and Reggiani, 2011). As in other cell types, also PMCA contributes to the restoration of cytosolic calcium levels (Conte et al. 2021; Gehlert et al. 2021).

iv. *Store-Operated Calcium entry in platelets*

Stored calcium is the principal conductor of cytosolic calcium increase that triggers the cellular cascade pathway for platelets functionality, emphasized by the contribution of SOC Entry and other calcium channels in the plasma membrane. Dense tubular system (DTS) and lysosomal-like acidic organelles are the principal responsible for calcium storage in platelets (Figure 6; Lopez et al. 2005; Mammadova-Bach et al. 2019; Münzer and Borst, 2022).

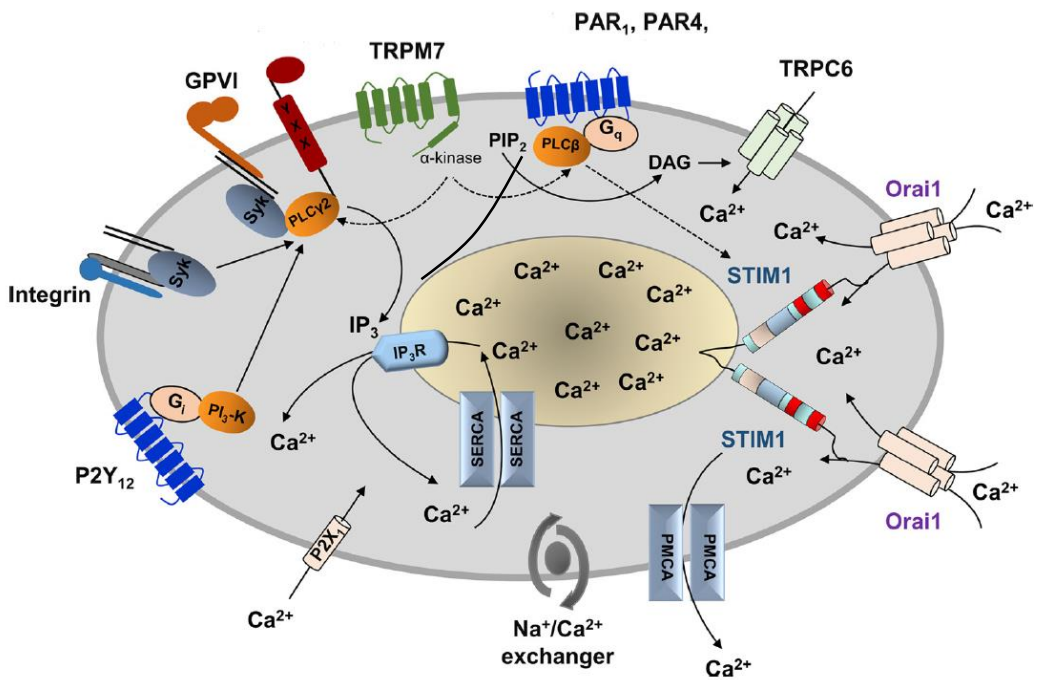


Figure 6.- *Calcium implication in cellular pathway in platelet functionality.* PLC isoforms activation by a wide number of plasma membrane receptors lead to DAG and IP<sub>3</sub> formation from PIP<sub>2</sub>. IP<sub>3</sub> open IP<sub>3</sub>R allowing the release of stored calcium and activation of Stored-Operated Calcium entry (SOC Entry). In the meanwhile, DAG proceed with the opening of TRPC6 channels evoking an additional influx of calcium. P2X<sub>1</sub> channels contribute in cytosolic calcium increase while PMCA, Na<sup>+</sup>/Ca<sup>2+</sup> exchanger and SERCA contribute in cytosolic calcium level restore. Ca<sup>2+</sup>: calcium ion ;P2X<sub>1</sub>: receptor-operated calcium channel; P2Y<sub>12</sub>: purinergic G protein-coupled receptor 12; PI<sub>3</sub>-K: phosphatidylinositol 3-kinase; GPVI: glycoprotein VI; Syk: spleen tyrosine kinase; PLCγ2 and PLCβ: phospholipase C isoforms; TRPM7: Transient receptor potential melastanin 7; PAR1 and 4: protease-activated receptor 1 and 4; TRPC6: Transient receptor potential canonical 6; PIP<sub>2</sub>: hydrolysephosphatidilinositol-4,5-bisphosphate; DAG: diacylglycerol;IP<sub>3</sub>: Inositol-1,4,5-triPhosphate; IP<sub>3</sub>R: IP<sub>3</sub> Receptor; SERCA: endoplasmic reticulum Ca<sup>2+</sup> ATPases; STIM: STromal Interaction Molecule I; PMCA: plasma membrane Ca<sup>2+</sup> ATPases. (Simplified Mammadova-Bach et al. 2019)

Concretely, stored calcium and SOC Entry orchestrate (i) activation by agonists, such as thrombin, adenosine diphosphate (ADP), or thromboxane A<sub>2</sub> (Rink and Sage, 1990; Varga-Szabo et al. 2009) and (ii) adhesion and spreading on collagen, the trigger for aggregation and thrombus formation (Gavin et al. 2020; Gresele et al. 2002; Inoue et al. 2003 Mazzucato et al. 2002;). Thrombus formation is induced by thrombin-stimulation which activates protease-activated receptors (PARs), PAR-1, and PAR-4 (Jardin et al. 2007; Gilio et al. 2010; Münzer and Borst, 2022). Other agonists are also able to evoke thrombus formation such as collagen or ADP, which activate GPVI or P2Y<sub>12</sub> receptors, respectively (Gilio et al. 2010; Mammadova-Bach et al. 2019). Activation of these receptors directly or indirectly activates PLC, leading to calcium store depletion by IP<sub>3</sub>R activation with IP<sub>3</sub> (Figure 6) and to the influx of calcium through P2Y<sub>12</sub> or TRPC channels. This increase of cytosolic calcium orchestrates granule exocytosis by Ca<sup>2+</sup>-dependent regulatory proteins of actin filaments, which are simultaneously critical for the spreading of platelets in the aggregation process as well (Marcu et al. 1996; Münzer and Borst, 2022; Ren et al. 2010). Granule exocytosis liberates collagen and fibrinogen, among other autocrine and paracrine agonists indispensable in platelet recruitment for aggregation (Amor et al. 2009; Gresele et al. 2002; Yoshioka et al. 2001).

The role of stored calcium and SOC Entry have been shown in the STIM1<sup>Sax/+</sup> mouse model, partly elucidating the direct role of STIM1 in platelet function. The gain-of-function mutation of STIM1 in this mouse model leads to the overloading of calcium through the SOC Entry mechanism, even in the absence of previous store depletion. Impairment in STIM1 function perturbs physiological responsiveness of platelets to GPVI and integrin stimulation, pointing to stored calcium and SOC Entry mechanisms as central regulators of platelet function (Grosse et al. 2007; Liou et al. 2005; Zhang et al. 2005).

Concomitantly, mutations in ORAI1 lead to GPVI and integrin deficient signalling, as well (Bergmeier et al. 2009; Braun et al 2009; Gilio et al. 2010). Indeed, further studies have demonstrated that ORAI1 is the principal CRAC channel in platelet SOC Entry (Braun et al 2009; Varga-Szabo 2008)

The importance of SOC Entry in platelet activation and aggregation processes is the main reason why mutations in STIM1 and ORAI1 lead to bleeding diathesis (Münzer and Borst, 2022).

### ***b. CRAC channelopathies***

Due to the importance of SOC entry in all processes described above, mutations in Stim1 and ORAI1 genes consequently head to pathophysiological phenotypes, leading to several human disorders. Table 2 recapitulates diseases associated with SOC Entry impairment. Both loss-of-function and gain-of-function mutations in SOC Entry members give rise to a wide range of rare-genetic disorders (Bohm and Laporte, 2018; Feske, 2010; Lacruz and Feske, 2015; Silvio-Rojas et al. 2020).

The best-known disorder caused by loss-of-function mutations is Severe Combined Immunodeficiency (SCID) despite the lack of ORAI1 is not the most common aetiology (la Marca et al. 2013; Sauer et al. 2017; Vaeth et al. 2021). The families identified with this inherited immunodeficiency bear a missense mutation in ORAI1 in the highly conserved arginine (R91W) in the TM1 of the ORAI1 subunit and this leads to the lack of the CRAC current ( $I_{CRAC}$ ; Feske et al. 2006). Other loss-of-function mutations have been related to SCID. In particular, (i) missense mutations in the TM1 (A103E) and TM3 (L149P) of ORAI1 (McCarl et al. 2009); (ii) an insertion in ORAI1 (A88SfsX25) resulting in a premature stop codon at TM1; and (iii) insertion mutation in STIM1 (E128RfsX9) resulting in a premature stop codon (Lacruz and Feske, 2015). Several loss of function mutations of STIM1 or ORAI1 has also been directly associated with other diseases as:

- (i) autoimmune hemolytic anemia (AIHA), where the selection of mature auto-reactive T cells and B cells is altered; (Feske, 2020; Lacruz and Feske, 2015; Lian et al. 2018).
- (ii) anhidrotic ectodermal dysplasia (EDA), in which case T-cell cytokine production is affected; (Eckstein and Lacruz, 2018; Feske, 2020; Lacruz and Feske, 2015; Lian et al. 2018).

- (iii) hypocalcified *amelogenesis imperfecta*, where ameloblasts maturation is seriously compromised (Eckstein and Lacruz, 2018; Feske, 2020; Lacruz and Feske, 2015; Lian et al. 2018).

Gain-of-function mutations of STIM1 or ORAI1 lead to an increased or constitutively active influx of calcium that primarily affects skeletal muscle and platelets. Both STIM1 and ORAI1 gain-of-function mutations are directly linked to the three separate, but overlapping, disorders: Tubular Aggregate Myopathy (TAM), Stormorken syndrome, and York Platelet Syndrome (YPS; Feske, 2010; Lacruz and Feske, 2015). Given their rarity compared to other myopathies, the disorders have not been tackled systematically in the clinic, and disease registries are not currently available nor is the exact prevalence known. Unfortunately, the lack of a fast and solid platform or method of diagnosis of rare diseases incentivizes this drastic situation. The diseases will be deeply explained in the next chapter (1.b.i.).

Concurrently, some disorders are not directly associated with genetic mutations of SOC Entry players but are characterized by an overload of intracellular calcium orchestrated by this mechanism (Gukovskaya et al. 2016; Lee et al. 2019; Lur et al. 2011; Prakriya and Lewis, 2015; Parekh and Putney, 2005; Zhen-Dong et al. 2018). In acute pancreatitis case, exacerbated SOC Entry activity evokes an uncontrolled release of digestive enzymes in pancreatic acinar cells (Gerasimenko et al. 2014; Gerasimenko et al. 2018) leading to necrosis that can even injure extra-pancreatic organs (Lee et al. 2019). Interestingly, it has been demonstrated that one of the principal originators of acute pancreatitis, metabolic alcohol products, triggers the opening of IP<sub>3</sub>R, provoking the emptying of stored calcium and consequently SOC Entry (Lur et al. 2011).

Apart from this, a role for SOC Entry has been also postulated in psoriasis, since some studies have reported the implication of calcium signalling in neutrophil chemotaxis and the release of pro-inflammatory cytokines (Steinckwich et al. 2015). Besides, hyperactivity of SOC Entry has been associated with cell migration, proliferation, metastasis, and angiogenesis in cancer (Hammad et al. 2021; Jardin and Rosado, 2016; Shapovalov et al. 2021; Smani et al. 2015). Concretely, SOC Entry has been proposed

as the mechanism of apoptosis resistance, except in prostate cancer cells, lymphoma and myeloma, and fibrosarcoma (Hammad et al. 2021; Dubois et al. 2014; Jardin and Rosado, 2016). Last, hyperactivity of STIM1 in platelets in diabetes mellitus type 2, increasing prone to thrombosis (Xia et al. 2015), has been shown. Evidence of SOC Entry dysfunction in myotubes of both Duchenne Muscular Dystrophy (DMD) patients and the mdx mice have also been found (Harrisseh et al. 2013; Goonaseka et al. 2014; Millay et al. 2009).



**Table 2. Diseases associated with SOC Entry impairment.**

<b>Disease</b>	<b>Aetiology</b>	<b>Reference</b>
<b>Severe Combined Immunodeficiency (SCID)</b>	ORAI1 LoF mutations	A88SfsX25
		R91W
		A103E
		L149P
		E128RfsX9
<b>Autoimmune hemolytic anemia (AIHA) and/or Hypocalcified <i>amelogenesis imperfecta</i></b>	STIM1 LoF mutation	P165Q
		R426C
		R429C
		E128RfsX9
<b>Anhidrotic ectodermal dysplasia (EDA) with/without hypocalcified <i>amelogenesis imperfecta</i></b>	ORAI1 LoF mutation	A88SfsX25
		R91W
		G98R
		A103E
		H165PfsX1
		V181SfsX8
		L194P
<b>Tubular Aggregate Myopathy (TAM)</b>	GoF mutation ORAI1 and STIM1 (Chapter 1.b.i.).	Lacruz and Feske, 2015
<b>Stormorken Syndrome</b>	GoF mutation ORAI1 and STIM1 (Chapter 1.b.i.).	Lacruz and Feske, 2015
<b>York Platelet Syndrome (YPS)</b>	GoF mutation ORAI1 and STIM1 (Chapter 1.b.i.).	Lacruz and Feske, 2015
<b>Acute pancreatitis</b>	Hyperactivity of SOC Entry	Lee et al. 2019
<b>Psoriasis</b>	Hyperactivity of SOC Entry	Steinckwich et al. 2015
<b>Cancer disease</b>	Hyperactivity of SOC Entry	Hammad et al. 2021
<b>Diabetes mellitus type 2</b>	Hyperactivity of SOC Entry	Xia et al. 2015
<b>Duchenne Muscular Dystrophy (DMD)</b>	Hyperactivity of SOC Entry	Goonaseka et al. 2014

LoF: Loss of function. GoF: gain of function

*i. Tubular Aggregate Myopathy, Stormorken syndrome, and York Platelet Syndrome*

Tubular Aggregate Myopathy (TAM) is characterized by variable combinations of myalgias, cramps, and muscle stiffness, with or without muscle weakness (Bohm et al, 2014; Nesin et al, 2014) and the characteristic presence of tubular aggregates (Schiaffino, 2012). Tubular aggregates appear in skeletal muscle, specifically in type II fibers and especially in rat male muscles kept in hypoxic medium (Schiaffino, 2012). These aggregates are inclusions of regular arrays of tubules originally from the sarcoplasmic reticulum (SR) that were firstly described in 1970 (Engel, 1970). Several SR proteins have been found in tubular aggregates, such as calsequestrin, SERCA, or RYR. Tubular aggregates are usually identified by electron microscopy, but histochemistry staining as Gomori trichrome or NADH tetrazolium reductase dye them (Jain et al. 2008).

Only Stormorken Syndrome and York Platelet Syndrome are characterized by bleeding diathesis and thrombocytopenia besides myopathy (Feske, 2010; Lacruz and Feske, 2015).

Stormorken syndrome (Stormorken et al, 1995) is variably characterized by myopathic signs, including tubular aggregate myopathy and proximal muscle weakness, mild bleeding tendency due to platelet premature activation, thrombocytopenia, anemia, asplenia, congenital miosis, ichthyosis, headache, and recurrent stroke-like episodes (Nesin et al, 2014; Misceo et al, 2014, Morin et al. 2014). Human platelets of Stormorken patients are less responsive to stimulation and present a higher PS exposure than healthy donors, lighting that the platelets are in a constitutively activated state. This condition evokes a decrease in the lifespan of platelets and causes thrombocytopenia and bleeding diathesis (Misceo et al. 2014).

Last, York Platelet Syndrome (YPS) shows blood dyscrasias as the main phenotype, thrombocytopenia, altered morphology, delta granule deficiency in platelets, and myopathy (Markello et al. 2015).

Patients with autosomal dominant mutations of STIM1, as R304W, have been diagnosed as both Stormorken and YPS. Concretely, this is a missense mutation in the exon 7 of STIM1 gene replace the arginine at 304 with a tryptophan (R304W) located in the coiled-coil region, responsible for the interaction with ORAI1. Other mutations in STIM1 have been related to TAM, as H72Q, D84G, or H109N/R (Bohm et al. 2014). Figure 7 comprises all mutations reported in literature associated with this cluster of rare genetic diseases (Bohm et al. 2014; Bohm et al. 2017; Claeys et al. 2020; Conte et al. 2021; Garibaldi et al. 2017; Endo et al. 2015; Harris et al. 2017; Morin et al. 2020; Noury et al. 2017; Okuma et al. 2016; Walter et al. 2015). At the same time, mutation p.I115F has been associated with both TAM and YPS (Lacruz and Feske, 2015). Indeed, some authors defend that all these three disorders are the spectra of the same disease since all of them have the presence of myopathy and tubular aggregates (Bohm and Laporte, 2018a; Markello et al. 2015; Morin et al. 2020; Silvio-Rojas et al. 2019; Hedberg et al. 2014; Misceo et al. 2014). Concretely, Peche et al. have recently demonstrated that TAM and Stormorken syndrome share the pathomechanism, where a constitutive clustering of STIM1 and consequent recruitment of ORAI1 occurs. Instead, differences in patients' symptomatology are explained by a divergent inactivation capacity according to the location of the mutation (Peche et al. 2020).

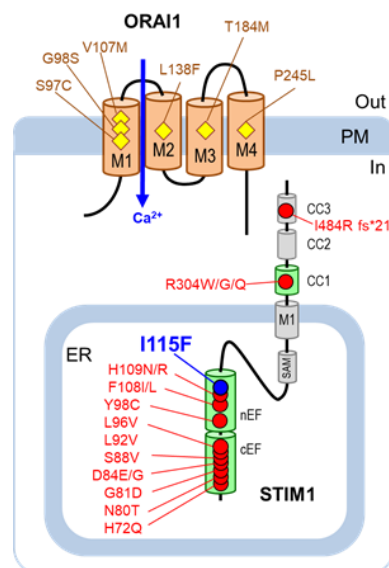


Figure 7.- *Graphical representation of gain-of-function mutation of ORAI1 and STIM1 associated to TAM, Stormorken, and YPS.* (updated Cordero-Sanchez et al. 2019)

### *c. Contemporary mouse models*

Up to now, three mouse models bearing gain-of-function mutations of STIM1 have been reported. The first model bears a spontaneous mutation of STIM1 (STIM1<sup>Sax</sup>; D84G) located in the intraluminal EF-hand domain. STIM1<sup>Sax</sup> model displayed a reduced lifespan and is characterized by severe thrombocytopenia, but no muscular phenotype was reported (Grosse et al. 2007). Recently, two groups described mice bearing the R304W mutation, which leads to Stormorken syndrome (Gamage et al. 2018; Silva-Rojas et al. 2018). Both groups found strong thrombocytopenia and myopathic-like phenotype but the absence of tubular aggregates, the principal hallmark of TAM, Stormorken syndrome, and YPS.

Since each disease is an ultra-rare disease, the frequency of each mutation is extremely low. No mouse model has been designed bearing a luminal STIM1 mutation associated with the clinical diagnosis of any of the diseases. Therefore, we believe that a mouse model bearing I115F mutation is extremely needed, to guarantee the effectiveness of putative treatment in patients bearing luminal STIM1 mutations. We esteem that models mimicking both luminal and cytosolic mutations are complementary, and that decidedly increase the likelihood of success of the development of effective treatments for these patients uncared of therapeutic options.

#### ***d. Current Store-Operated Calcium Entry Inhibitors***

Hitherto, many allosteric modulators of SOC Entry, recapitulated in Table 3, have been identified and clinically developed for a wide variety of diseases.

The first of the compounds that demonstrated an effect *in vitro* in acute pancreatitis is GSK-7975A. This compound has been identified as a concentration-dependent CRAC channel inhibitor (Gerasimenko et al. 2013), ceasing the necrotic cell death pathway in human and mouse pancreatic acinar cells.

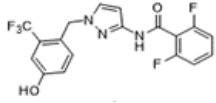
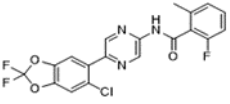
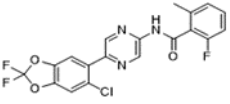
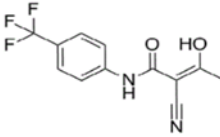
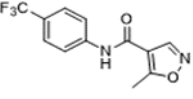
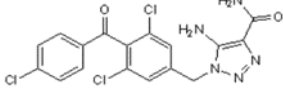
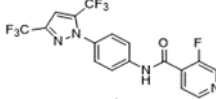
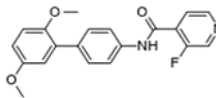
Afterward, a second SOC Entry inhibitor, CM4620, was demonstrated to prevent acute pancreatitis in three different murine models (Wen et al. 2015; Waldron et al. 2019). At present, CM4620 has already completed the preclinical phase and Phase II trial for acute pancreatitis (NCT03401190). Indeed, CM4620 has initiated an ongoing Phase I/II trial for asparaginase-associated acute pancreatitis, a rare condition of the disease triggered by asparaginase treatment (NCT04195347). Noteworthy, CM4620 recently initiated Phase II for severe COVID-19 pneumonia (NCT04345614). The recent worldwide pandemic virus, SARS-CoV2, causes severe pulmonary injury by increasing pro-inflammatory cytokine signals in the lungs. Due to its already demonstrated effects in acute inflammation, CM4620 appears to be also able to reduce pulmonary inflammation (Miller et al. 2020).

Furthermore, two approved drugs have shown SOC Entry inhibition activity at therapeutic doses (Rahman et al. 2017): Teriflunomide, a dihydroorotate dehydrogenase (DHODH) inhibitor (Davis et al. 1996), and leflunomide its pro-drug (Breedveld and Dayer, 2000; Schattenkirchner et al. 2000). Both drugs have been approved for rheumatoid arthritis and multiple sclerosis, respectively.

L-651582 has been the first SOC Entry inhibitor to enter clinical trials for cancer. While its development was initially discontinued due to lack of promising efficacy in tumors, it is now gaining novel impulse in glioblastoma (NCT01107522; Omuro A. et al, 2018).

Besides, other two SOC Entry modulators whose structure has not been disclosed, PRCL-02 and RP3128, have been clinically studied. PRCL-02 has initiated a Phase II

trial for psoriasis (NCT03614078) while RP3128 has been demonstrated to be well tolerated with no limiting toxicities for autoimmune disorders (NCT02958982; Barde et al. 2021).

<i>Chemical structure</i>	<b>Compound</b>	<b>Targeted disease</b>	<b>Development</b>	<b>Reference</b>
	<b>GSK-7975A</b>	Acute pancreatitis	<i>In vivo</i> murine model	Gerasimenko et al. 2013
	<b>CM4620</b>	Acute pancreatitis	Phase II trial	NCT03401190
		Asparaginase-associated acute pancreatitis	Phase I/II trial	NCT04195347
	<b>CM4620</b>	Severe COVID-19 pneumonia	Phase II	NCT04345614
	<b>Teriflunomide</b>	-	<i>In vitro</i>	Rahman et al. 2017
	<b>Leflunomide</b>	-	<i>In vitro</i>	Rahman et al. 2017
	<b>L-651582</b>	Glioblastoma	Phase I	NCT01107522
-	<b>PRCL-02</b>	Psoriasis	Phase II	NCT03614078
-	<b>RP3128</b>	Mild Asthmatics	<i>Phase I/IIa</i>	NCT02958982
	<b>Pyr6</b>	-	<i>In vitro</i>	Riva et al. 2018
	<b>Synta66</b>	-	<i>In vitro</i>	Di Sabatino et al. 2009

Recently, our group has characterized a chemical library of modulators of SOC Entry derivate of Pyr6, a well-known SOC Entry probe (Riva et al. 2018). Compound CIC-37 (39) has been proposed as a promising drug candidate, able to ameliorate acute cerulein-induced pancreatitis. CIC-37 showed a short half-life (1.3 h) and high volume of distribution (32 L/kg), without any sign of toxicity.

This pharmacokinetic profile is not generally suitable for drugs, pushing us to synthesize and develop further inhibitors. Consequently, another class of compounds has been created based on another chemical probe, Synta66, a known inhibitor of CRAC channel with an  $IC_{50}$  of 1.4-3.0  $\mu$ M (Di Sabatino et al. 2009; Ng et al. 2008; WO2005009954; WO2005009539). the precise mechanism of action of Synta66 is unclear, but (i) it has been demonstrated that it does not interfere with STIM1 clustering (Li et al. 2011); and (ii) ORAI1 has been proposed as a putative target (Ng et al. 2008), strengthened by *in silico* data (Waldherr et al. 2020). Furthermore, Synta66 has been demonstrated selective over other ion channels or receptors, including  $Ca^{2+}$  ATPase pump, voltage-gated  $Ca^{2+}$ ,  $Na^{+}$  channels, and TRPC1/5 channels (Di Sabatino et al. 2009; Ng et al. 2008; Li et al. 2011). All this data made us, in collaboration with Prof. Pirali's group, bet on Synta66 as a reliable starting point to synthesize new SOC Entry modulators.





## 2.- Outline of the Thesis

My thesis project is focused on the characterization of a novel mouse model for Tubular Aggregate Myopathy (TAM). Up to now, there is no mouse model bearing a mutation in the intraluminal domains of STIM1 clinically associated with TAM. This project intends to fulfil this gap: the lack of a valid platform for testing future putative treatments that guarantee efficacy in patients with intraluminal mutations in STIM1. Consequently, Prof. Genazzani and Dr. Riva designed the mouse model (KI-STIM1<sup>I115F</sup>) bearing the p.I115F mutation in STIM1, diagnosed both TAM and York Platelet Syndrome (YPS).

The principal aims of my thesis are:

- To validate the KI-STIM1<sup>I115F</sup> mouse model for TAM by demonstrating the myopathy picture.
- To study whether the KI-STIM1<sup>I115F</sup> mouse model present also YPS-like disease or not and to identify aetiology of thrombocytopenia, if exists.
- To find a hit compound from a chemical library of putative modulators of SOC Entry for treating KI-STIM1<sup>I115F</sup> mice.

Taking the aims of my thesis into account, to characterize the mouse model for TAM/YPS and the screening of compounds, my thesis will be divided into two parts. The first part of my thesis is focused on demonstrating the presence of myopathy and bleeding dyscrasia in KI-STIM1<sup>I115F</sup> mice. The second part of my thesis is dedicated to the characterization of a chemical library of putative modulators of SOC Entry.

Since most of the results obtained have been published, each part of the thesis will have a chapter for each published or submitted article/s. I am the first or co-first author of the three articles composing this thesis.

This project has been possible thanks to our collaborators, the groups of Prof. Pirali, Prof. Bertoni, Prof. Filigheddu (University of Piemonte Orientale), and Dr. Sanghalini (Istituto di Tumori di Milano). The project has been supported by Telethon foundation funding to Armando Genazzani (GGP19110).



### ***3. PART I:***

## **Characterization of the KI- STIM1<sup>I115F</sup> mouse model**

- a. Validation of KI-STIM1<sup>I115F</sup> mouse model for Tubular Aggregate Myopathy***



## *i. Synopsis*

### *Aim*

The aim of this article is (i) to characterize the KI-STIM1<sup>I115F</sup> mouse model which was generated in the lab and (ii) to bridge its phenotype to that of patients bearing the same mutation (STIM1 p.I115F).

*The main findings of the manuscript are that:*

- (i) Heterozygous are fertile and viable, while no live homozygous mouse was found;
- (ii) KI-STIM1<sup>I115F</sup> mice are smaller in size;
- (iii) SOC Entry was enhanced in KI-STIM1<sup>I115F</sup> myotubes;
- (iv) KI-STIM1<sup>I115F</sup> muscle were underweight and presented fiber frequency alteration, necrosis, and regeneration evidence;
- (v) Morphological aggregation similar to tubular aggregates was observed in KI-STIM1<sup>I115F</sup> muscles;
- (vi) KI-STIM1<sup>I115F</sup> mice presented muscle functional deficits and bleeding diathesis. This is in accord with the clinic diagnosis since p.I115F has been associated with both Tubular Aggregate Myopathy and York Platelet Syndrome (Lacruz and Feske 2015; Morin et al. 2020).

### *Key take-home message*

KI-STIM1<sup>I115F</sup> mouse model displays both myopathy and bleeding diathesis.

### *Personal Contribution*

In the present contribution, I managed the colony and designed and performed all experiments except those contained in figure 4, under the supervision of Prof. Filigheddu and Prof. Genazzani. KI-STIM1<sup>I115F</sup> founders in a C57Bl/6N background were commissioned to PolyGene transgenics (CH, <https://www.polygene.ch/>) and the conceptualization of the mouse occurred before my arrival in the lab by Dr. Riva and Prof. Genazzani.



## RESEARCH ARTICLE

# A luminal EF-hand mutation in STIM1 in mice causes the clinical hallmarks of tubular aggregate myopathy

Celia Cordero-Sanchez<sup>1,‡</sup>, Beatrice Riva<sup>1,‡</sup>, Simone Reano<sup>2,‡</sup>, Nausicaa Clemente<sup>2</sup>, Ivan Zaggia<sup>2</sup>, Federico A. Ruffinatti<sup>1</sup>, Alberto Potenzieri<sup>1,\*</sup>, Tracey Pirali<sup>1</sup>, Salvatore Raffa<sup>3</sup>, Sabina Sangaletti<sup>4</sup>, Mario P. Colombo<sup>4</sup>, Alessandra Bertoni<sup>2</sup>, Matteo Garibaldi<sup>5</sup>, Nicoletta Filigheddu<sup>2,‡,§,¶</sup> and Armando A. Genazzani<sup>1,‡,§,¶</sup>

## ABSTRACT

STIM and ORAI proteins play a fundamental role in calcium signaling, allowing for calcium influx through the plasma membrane upon depletion of intracellular stores, in a process known as store-operated Ca<sup>2+</sup> entry. Point mutations that lead to gain-of-function activity of either STIM1 or ORAI1 are responsible for a cluster of ultra-rare syndromes characterized by motor disturbances and platelet dysfunction. The prevalence of these disorders is at present unknown. In this study, we describe the generation and characterization of a knock-in mouse model (KI-STIM1<sup>I115F</sup>) that bears a clinically relevant mutation located in one of the two calcium-sensing EF-hand motifs of STIM1. The mouse colony is viable and fertile. Myotubes from these mice show an increased store-operated Ca<sup>2+</sup> entry, as predicted. This most likely causes the dystrophic muscle phenotype observed, which worsens with age. Such histological features are not accompanied by a significant increase in creatine kinase. However, animals have significantly worse performance in rotarod and treadmill tests, showing increased susceptibility to fatigue, in analogy to the human disease. The mice also show increased bleeding time and thrombocytopenia, as well as an unexpected defect in the myeloid lineage and in natural killer cells. The present model, together with recently described models bearing the R304W mutation (located on the coiled-coil domain in the cytosolic side of STIM1), represents an ideal platform to characterize the disorder and test therapeutic strategies for patients with STIM1 mutations, currently without therapeutic solutions.

This article has an associated First Person interview with Celia Cordero-Sanchez, co-first author of the paper.

<sup>1</sup>Department of Pharmaceutical Sciences, University of Piemonte Orientale, Via Bovio 6, Novara 28100, Italy. <sup>2</sup>Department of Translational Medicine, Università del Piemonte Orientale, Via Solaroli 17, Novara 28100, Italy. <sup>3</sup>Laboratory of Ultrastructural Pathology, Department of Clinical and Molecular Medicine, SAPIENZA University of Rome, Sant'Andrea Hospital, Rome 00189, Italy.

<sup>4</sup>Department of Experimental Oncology and Molecular Medicine, Fondazione IRCCS Istituto Nazionale Tumori, Milan 20133, Italy. <sup>5</sup>Unit of Neuromuscular Disorders, Department of Neuroscience, Mental Health and Sensory Organs (NESMOS), Sapienza University of Rome, Sant'Andrea Hospital, Rome 00189, Italy. \*Present address: NBT - Department of Neuroscience and Brain Technologies, Istituto Italiano di Tecnologia, Via Morego 30, Genova, Italy.

<sup>‡</sup>These authors contributed equally to this work

<sup>§</sup>These authors contributed equally to this work

<sup>¶</sup>Authors for correspondence (armando.genazzani@uniupo.it; nicoletta.filigheddu@med.uniupo.it)

© N.F., 0000-0002-3848-611X; A.A.G., 0000-0003-1923-7430

This is an Open Access article distributed under the terms of the Creative Commons Attribution License (<https://creativecommons.org/licenses/by/4.0>), which permits unrestricted use, distribution and reproduction in any medium provided that the original work is properly attributed.

Received 21 June 2019; Accepted 24 October 2019

**KEY WORDS:** STIM1, Calcium signaling, Mouse model, Rare disease, Store-operated calcium entry

## INTRODUCTION

High concentrations of calcium ions are present in intracellular organelles [in particular in the endoplasmic reticulum (ER)/ sarcoplasmic reticulum (SR)], and the opening of Ca<sup>2+</sup> channels located on these membranes (e.g. ryanodine receptors, inositol 1,4,5-trisphosphate receptors) allows this ion to flux out of the deposit and elicit cellular signals. A crosstalk mechanism between the ER and the plasma membrane exists that allows for the refilling of the depleted organelles (Putney, 2011). This crosstalk is known as store-operated Ca<sup>2+</sup> entry (SOCE). The principal components of SOCE are a Ca<sup>2+</sup> sensor on the ER membrane (STIM protein) and a plasma membrane Ca<sup>2+</sup> channel (ORAI protein) (Lacruz and Feske, 2015; Berna-Ero et al., 2012). STIM proteins are single-span membrane proteins, highly conserved across species. Two members of the family have been described, STIM1 and STIM2, of which the former appears more expressed. ORAI channels reside on the plasma membrane, and three members of the family (ORAI1, ORAI2 and ORAI3) have been described, with ORAI1 being the most abundant. Importantly, other crucial proteins participate in the SOCE process, including transient receptor potential canonical (TRPC) channels (Ong and Ambudkar, 2015).

Genetic defects of STIM and ORAI proteins have been described that give rise to loss-of-function and gain-of-function genetic disorders (Lacruz and Feske, 2015; Böhm and Laporte, 2018; Feske, 2010). Gain-of-function disorders primarily affect skeletal muscles and platelets, although other organs also seem to be affected. Given the rarity of the disorders, compared to other myopathies, their prevalence is currently unknown; they have not been tackled systematically in the clinic, and disease registries are not available at present. Both STIM1 and ORAI1 mutations are linked to three separate, but overlapping, disorders: tubular aggregate myopathy (TAM), Stormorken syndrome and York platelet syndrome. TAM is characterized by variable combinations of myalgias, cramps and muscle stiffness, with or without weakness with a predominantly proximal distribution (Böhm et al., 2014), and by the presence of tubular aggregates, which are regular arrays of tubules derived from the SR (Schiaffino, 2012). Stormorken syndrome (Stormorken et al., 1995) is variably characterized by myopathic signs, mild bleeding tendency due to platelet dysfunction, thrombocytopenia, anemia, asplenia, congenital miosis, ichthyosis, headache and recurrent stroke-like episodes (Nesin et al., 2014; Misceo et al., 2014; Noury et al., 2017). In York platelet syndrome, blood dyscrasias is the main phenotype (Markello et al., 2015). Fig. 1A illustrates the mutations reported

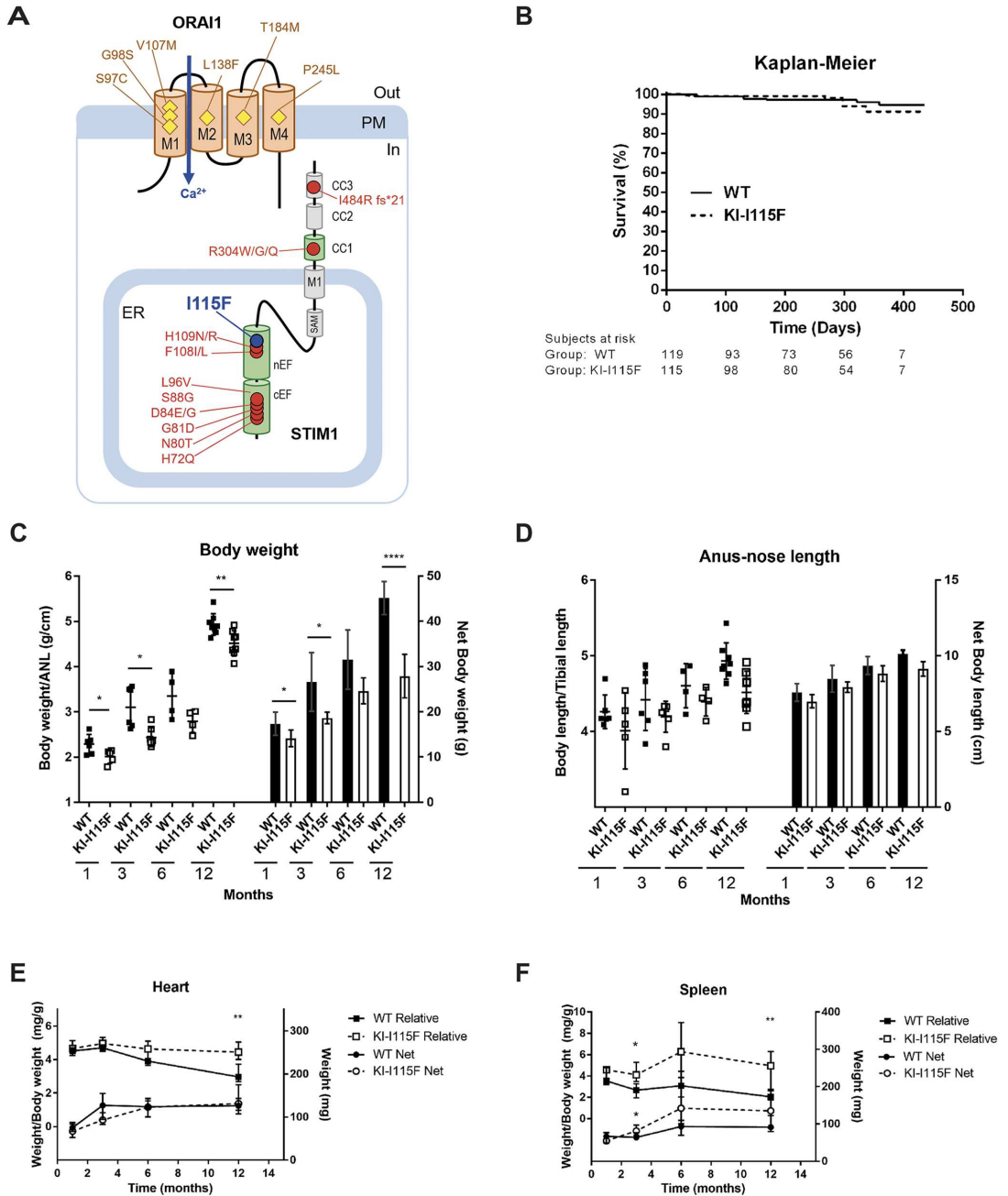


Fig. 1. See next page for legend.

so far. Briefly, mutations of STIM1 mostly reside in the EF-hand  $Ca^{2+}$ -binding motifs, most likely modifying the affinity for  $Ca^{2+}$  ions of the protein, with few exceptions located on the cytosolic coiled-coil domains. The R304W mutation has recently been

shown to affect the dimerization and resting state of STIM1 (Fahrner et al., 2018). A second substitution at the same position (R304Q; Harris et al., 2015) and a deletion on the third coiled-coil domain have also been reported (I484R fs\*21; Okuma et al., 2016).



### Fig. 1. Characterization of KI-STIM1<sup>I115F</sup> mice multi-systemic phenotype.

(A) Known point mutations leading to gain-of-function phenotypes in humans. ER, endoplasmic reticulum; PM, plasma membrane. (B) Kaplan–Meier for survival of WT and KI-I115F. Numbers below the graph indicate numbers at risk, i.e. the number of true observations made to estimate survival. (C) Body weight at 1 (WT  $n=6$ , KI-I115F  $n=5$ ), 3 (WT  $n=6$ , KI-I115F  $n=6$ ), 6 (WT  $n=4$ , KI-I115F  $n=4$ ) and 12 (WT  $n=8$ , KI-I115F  $n=8$ ) months, shown as ratio to anal-nose length (ANL) on the left axis and net body weight on the right axis. Scatter plots and histograms show the means $\pm$ s.e.m. of the indicated number of mice. Unpaired Student's *t*-test with Welch's correction. \* $P\leq 0.0386$ , \*\* $P=0.0068$ , \*\*\*\* $P<10^{-4}$  versus WT. (D) Body length at 1 (WT  $n=6$ , KI-I115F  $n=5$ ), 3 (WT  $n=6$ , KI-I115F  $n=6$ ), 6 (WT  $n=4$ , KI-I115F  $n=4$ ) and 12 (WT  $n=8$ , KI-I115F  $n=8$ ) months, shown as ratio to tibial length on the left axis and net body length on the right axis. Scatter plots and histograms show the means $\pm$ s.e.m. of the indicated number of mice. Unpaired Student's *t*-test with Welch's correction. (E) Heart weight at 1 (WT  $n=6$ , KI-I115F  $n=5$ ), 3 (WT  $n=6$ , KI-I115F  $n=6$ ), 6 (WT  $n=4$ , KI-I115F  $n=4$ ) and 12 (WT  $n=8$ , KI-I115F  $n=8$ ) months, shown as ratio to body weight on the left axis and net weight on the right axis. Graph shows median and IQR of heart weight/body weight, or heart net weight. Mann–Whitney *U*-test. \*\* $P=0.003$  versus WT. (F) Spleen weight at 1 (WT  $n=6$ , KI-I115F  $n=5$ ), 3 (WT  $n=6$ , KI-I115F  $n=6$ ), 6 (WT  $n=4$ , KI-I115F  $n=4$ ) and 12 (WT  $n=8$ , KI-I115F  $n=8$ ) months, shown as ratio to body weight on the left axis and net weight on the right axis. Graph shows median and IQR of spleen weight/body weight, or spleen net weight. Mann–Whitney *U*-test. \* $P\leq 0.026$ , \*\* $P=0.0037$  versus WT.

The mutations of ORAI1 are located in the transmembrane domains in positions that might lead to the assumption that the resultant amino acids participate in the channel lining.

There are three reported mouse models bearing gain-of-function mutations of STIM1. The first model originated from a mutation of STIM1 (STIM1<sup>Sax</sup>; D84G), generated via random chemical mutagenesis, located in the intraluminal EF-hand domain. STIM1<sup>Sax</sup> is characterized by severe thrombocytopenia, but no muscular phenotype was reported (Grosse et al., 2007). Recently, two groups have described mice bearing the R304W mutation, which leads to Stormorken syndrome (Silva-Rojas et al., 2018; Gamage et al., 2018). Both groups found bleeding disorders and a muscular phenotype. Surprisingly, no models exist that investigate and reproduce clinically relevant mutations located on the luminal side of STIM1.

In this study, we have generated and characterized a knock-in animal bearing a mutation in one of the two EF-hand motifs. Heterozygous mice bearing the I115F mutation display important histological and functional muscle dysfunctions associated with thrombocytopenia, and unexpected hematological defects related to the myeloid lineage and natural killer (NK) cells.

## RESULTS

### Development of the KI-STIM1<sup>I115F</sup> mouse colony

The knock-in (KI) STIM1<sup>I115F</sup> mouse model was generated by homologous recombination by PolyGene Transgenetics. Details are provided in the Materials and Methods section.

Both male and female mice are fertile. Given that the disorder is a dominant gain-of-function, it was decided to routinely breed wild-type (WT) and heterozygous (KI-STIM1<sup>I115F</sup>) mice. The genotype ratio of born pups was 120:118 and did not significantly deviate from the expected Mendelian ratio of 1:1. Average litter size was 7.2 $\pm$ 0.5 ( $n=36$  litters). Anecdotally, two matings were attempted between heterozygous animals. One of the matings did not result in a litter, while the other resulted in two pups (one WT and one heterozygous). Given that characterization of homozygosity was not an aim, we did not analyze whether this was a result of embryonic lethality, and we did not breed between heterozygous animals further.

The Kaplan–Meier of survival shows that there are no signs of early mortality, and KI-STIM1<sup>I115F</sup> mice survive over 1 year, like WT animals (Fig. 1B). Animals were not bred for longer, and therefore data are not sufficient to define the median survival of animals and whether the mutation leads to a decreased lifespan. With age, KI-STIM1<sup>I115F</sup> mice may display an arched back that worsens with age, may limp and show tremors, and manifest an instantaneous post-mortem rigidity.

On visual inspection, KI-STIM1<sup>I115F</sup> mice are smaller than WT mice, and this rendered blinding difficult for behavioral tests. The size difference (Fig. 1C) could be better appreciated when mice were weighed, and a significant difference between KI-STIM1<sup>I115F</sup> and WT could be observed at all time points evaluated (1, 3, 6, 12 months), when net weight or body weight adjusted for length (anus-nose) were considered (Fig. 1D). Animal length was not significantly different between KI-STIM1<sup>I115F</sup> and WT mice, also when normalized for tibial length.

At necropsy, the weights of the heart and spleen from KI-STIM1<sup>I115F</sup> animals were determined and were not statistically different from those of WT (Fig. 1E,F). However, when body weight was taken into account, a statistically significant increase in heart size was evident at 12 months, while an increased spleen/body weight ratio was already observable at 3 months.

We also proceeded to analyze whether males (50 WT and 58 KI-STIM1<sup>I115F</sup>) and females (71 WT and 59 KI-STIM1<sup>I115F</sup>) differed. We did not find any significant differences between the sexes regarding survival at 1 year, body weight, animal length, heart size and spleen size (Figs S1 and S2), thereby suggesting that there is not a sex difference in penetrance of the disease.

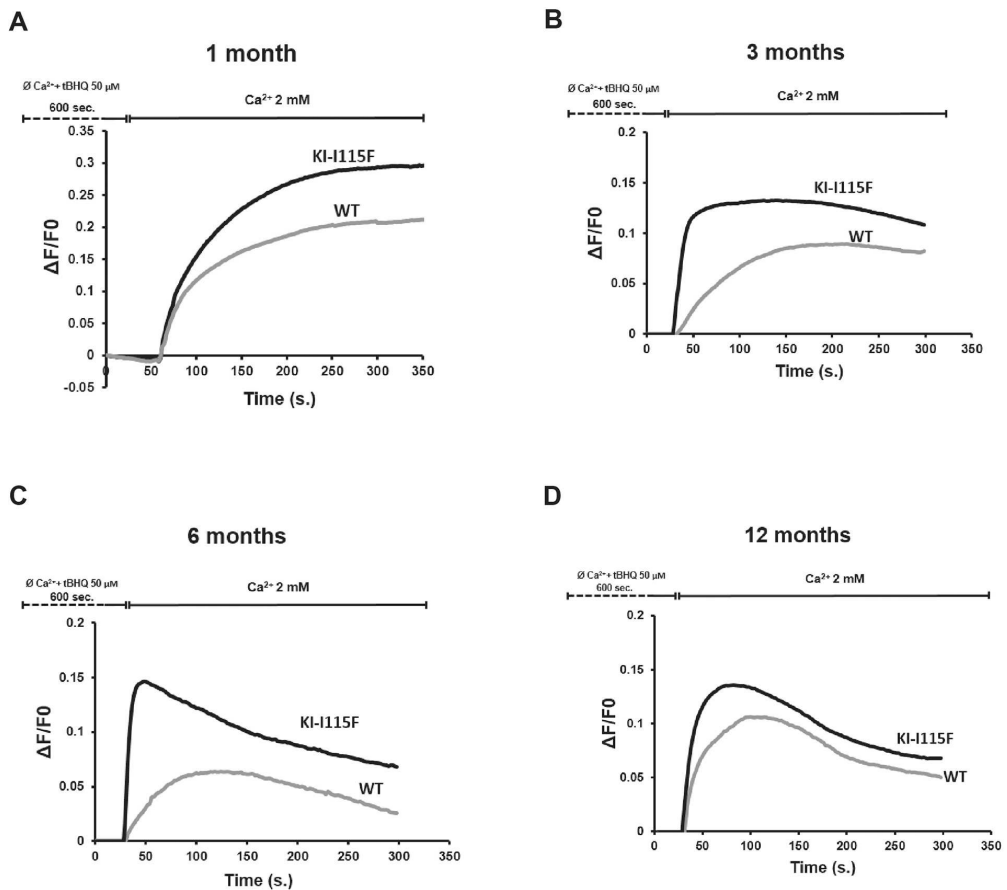
### Myotubes from the KI-STIM1<sup>I115F</sup> mouse colony retain increased SOCE

We next examined whether myotubes from KI-STIM1<sup>I115F</sup> mice retained the fundamental cellular characteristic of increased Ca<sup>2+</sup> entry upon store depletion (SOCE). Myotubes were generated from four animals in each condition. We also analyzed whether SOCE in WT myotubes was modified during the lifespan of these animals. To do this, we employed a classical protocol for Ca<sup>2+</sup> entry, in which stores are depleted with 2,5-t-butylhydroquinone (tBHQ) in a Ca<sup>2+</sup>-free buffer, and, after 10 min, cells are perfused in a Ca<sup>2+</sup>-containing solution (2 mM).

As can be observed in Fig. 2, myotubes from KI-STIM1<sup>I115F</sup> display a significantly augmented SOCE compared to WT at 1 month. The increased SOCE was retained throughout all time points examined (1, 3, 6, and 12 months). Interestingly, SOCE from WT myotubes appeared to be higher in younger animals (1 month) and decreased at the subsequent time points. It is also interesting to note that, in myotubes from mice at 6 and 12 months, there was a reduced sustained entry compared to the earlier time points.

We next analyzed the Ca<sup>2+</sup> entry pattern and found that slope, peak Ca<sup>2+</sup> entry and area under the curve differed between KI-STIM1<sup>I115F</sup> and WT mice, except at 1 month, when the slope appeared similar (Fig. 2; Fig. S3). We also investigated whether we could observe any spontaneous oscillations in intracellular Ca<sup>2+</sup>, or whether there were changes in basal Ca<sup>2+</sup> between WT and KI-STIM1<sup>I115F</sup> mice. No difference in basal Ca<sup>2+</sup> between the two groups was observed when considering the same age group. Furthermore, analysis for 20 min of ~50 cells per time point did not yield any oscillations, in any of the two strains.

We evaluated whether Ca<sup>2+</sup> entry genes (*Trpc1*, *Trpc2*, *Trpc3*, *Trpc4*, *Trpc5*, *Orai1*, *Orai2*, *Orai3*, *Stim1* and *Stim2*) were modified



**Fig. 2. SOCE alterations in myotubes.** Evaluation of SOCE by calcium imaging in myotubes from WT and KI-115F at (A) 1, (B) 3, (C) 6 and (D) 12 months of age. Traces are the average of at least 180 myotubes from 6-well plates on two different experimental days. At all time points, myotubes from four animals (two males, two females) for each condition were used.

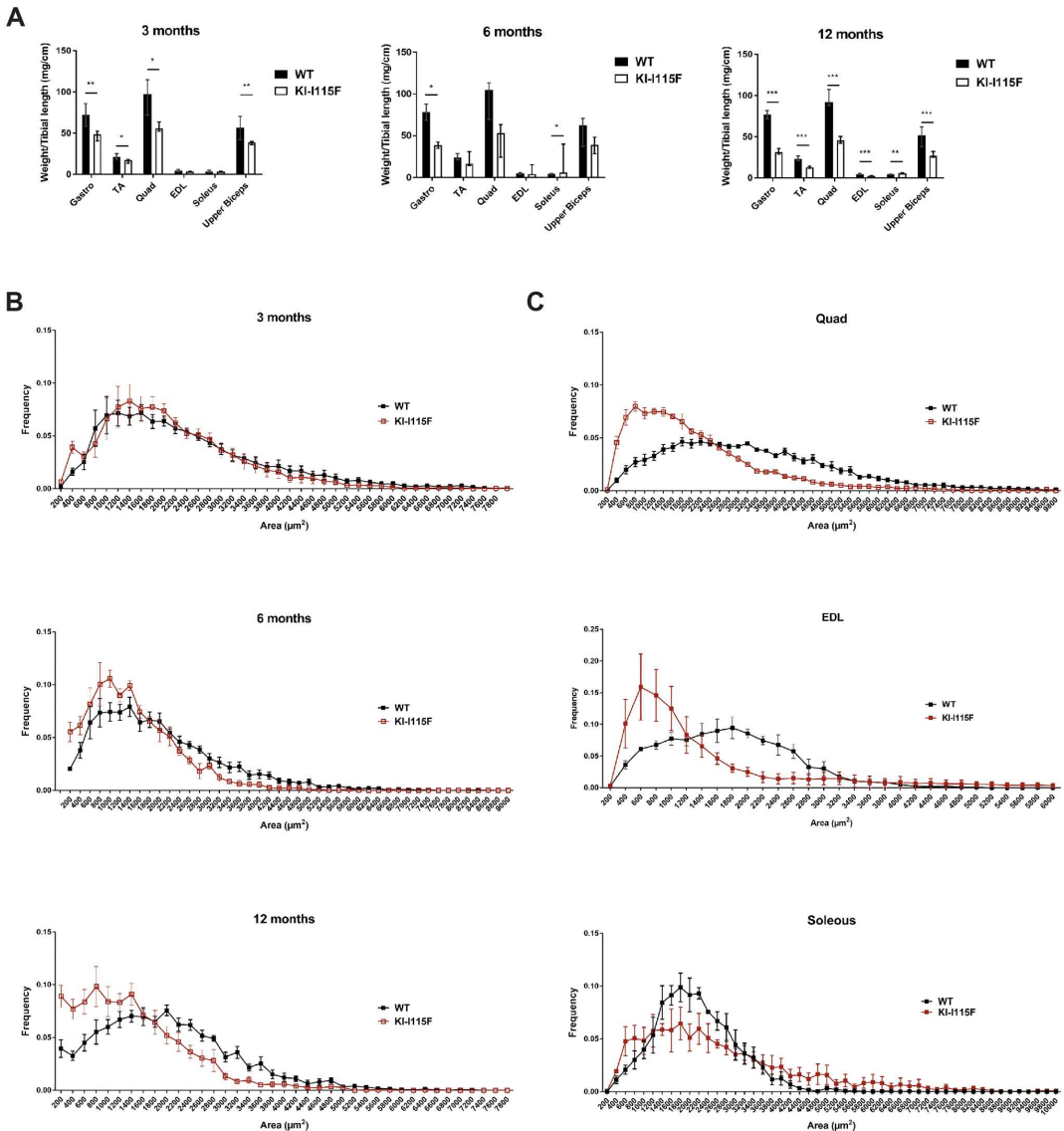
in their expression between the two groups at 1, 3, 6, and 12 months (Fig. S4). No major differences were observed by quantitative real-time PCR (qRT-PCR). Indeed, we did not observe a compensatory decrease in *Stim1* mRNA expression. Although we did observe some minor, albeit statistically significant, differences at different time points, these were not consistent and are most likely a result of bias for multiple testings.

#### Muscles in KI-STIM1<sup>I115F</sup> mice present significant histological and functional alterations

We then analyzed muscle weight in animals of different ages. As shown in Fig. 3A, the gastrocnemius and quadriceps muscles in KI-STIM1<sup>I115F</sup> animals weigh significantly less compared to in WT animals at 3 months (no change was observed at 1 month; data not shown), and all muscles evaluated, except for the soleus, weigh less in KI-STIM1<sup>I115F</sup> than in WT animals at 12 months. Similar trends were observed when a subanalysis was performed between male and female animals (Fig. S5). The paradoxical finding of the increased weight of the soleus at 6 and 12 months parallels the report on R304W mice by Silva-Rojas et al. (2018). Cross-sectional area

(CSA) analysis of the tibialis anterior (TA) fibers shows a higher frequency of smaller areas in KI-STIM1<sup>I115F</sup> animals compared to WT, and this worsens with age (Fig. 3B). A similar trend was observed in the quadriceps and extensor digitorum longus, but not in the soleus (Fig. 3C), in accord with the data obtained from muscle weight analyses (Fig. 3A).

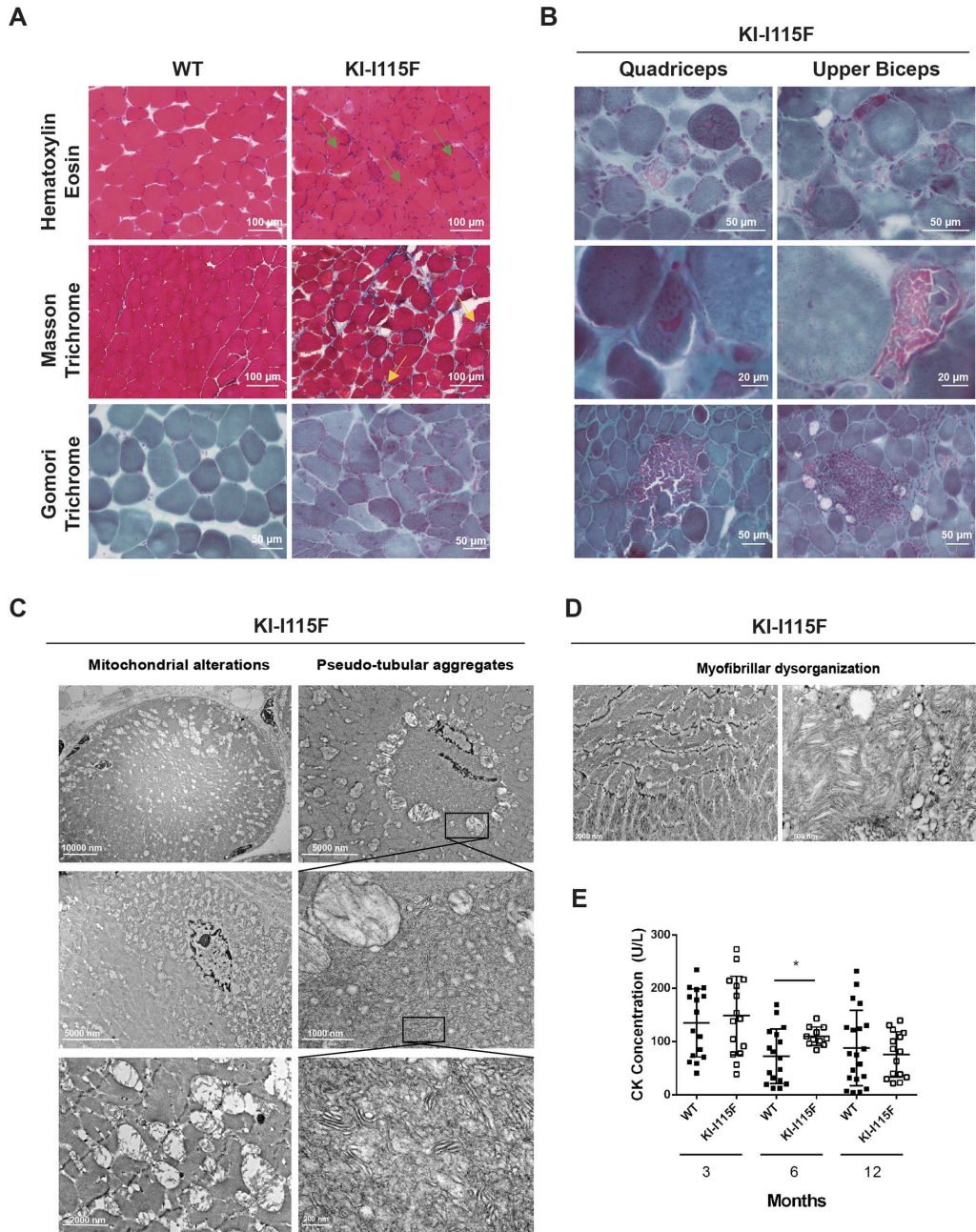
Histological sections of the quadriceps and upper biceps were obtained to evaluate muscle morphology. Hematoxylin-Eosin, Masson Trichrome and Gomori Trichrome stainings were performed (Fig. 4A,B). A myopathic process was evident from 1 month and worsened with age. It was characterized by marked fiber size variability, necrosis and regeneration with newly formed myofibers with central nuclei, and increased connective tissue. Interestingly, in the quadriceps and upper biceps of 6-month-old animals, endomysial inflammatory infiltrates as well as cytoplasmic fusciphilic areas in Gomori Trichrome staining were observed (Fig. 4B). In electron microscopy of 6-month-old animals (quadriceps and upper biceps), enlarged mitochondria with abnormal morphology were observed (for example, hypertrophic with loss of the mitochondrial crest; Fig. 4C, left column), which at



**Fig. 3. Reduced muscle growth and damage in KI-STIM1<sup>1115F</sup> mice.** (A) Muscle weight in WT and KI-1115F mice at 3 (WT  $n=6$ , KI-1115F  $n=6$ ), 6 (WT  $n=4$ , KI-1115F  $n=4$ ) and 12 (WT  $n=8$ , KI-1115F  $n=8$ ) months. (Gastro, gastrocnemius; TA, tibialis anterior; Quad, quadriceps; EDL, extensor digitorum longus). Histograms show median and IQR of muscle weight. Mann–Whitney  $U$ -test.  $^*P \leq 0.0303$ ,  $^{**}P \leq 0.0022$ ,  $^{***}P \leq 0.0003$  versus WT. (B) Cross-sectional area (CSA) frequency distribution of fibers in TA at 3 (WT  $n=6$ , KI-1115F  $n=6$ ), 6 (WT  $n=4$ , KI-1115F  $n=4$ ) and 12 (WT  $n=6$ , KI-1115F  $n=6$ ) months. (C) CSA frequency distribution of fibers in quadriceps (Quad, top; WT  $n=4$ , KI-1115F  $n=3$ ), extensor digitorum longus (EDL, middle; WT  $n=3$ , KI-1115F  $n=4$ ) and soleus (bottom; WT  $n=3$ , KI-1115F  $n=3$ ) at 6 months.

times formed circular structures (Fig. 4C, top left). Some mitochondria were located in a subplasmalleal position (Fig. 4C, middle and bottom left), which might explain some features observed in Gomori staining (e.g. Fig. 4B, bottom row). Inside the circular structures formed by mitochondria, no sarcomeric structures were observed, although pseudo-aggregate structures were at times visible (Fig. 4C, middle and bottom right),

and they resembled, in part, the characteristics of the human disorders, but were disorganized and chaotic. However, no true tubular aggregates were observed at either 6 or 12 months, and these pseudo-aggregates were not observable in 12-month-old animals. These features were accompanied by a partial disorganization of myofibrils (Fig. 4D). Subsequently, we proceeded to analyze myosin in fibers. The frequency distribution of type IIa fibers



**Fig. 4. Muscle histology of KI-STIM1<sup>H115F</sup> mice.** (A) Representative images of Hematoxylin-Eosin (top row), Masson Trichrome (middle row) and Gomori Trichrome (bottom row) staining of the quadriceps at 6 months of age. Green arrows indicate fibrotic tissue and inflammatory cell infiltration; yellow arrows indicate necrotic fibers. (B) Representative images of Gomori Trichrome staining in the quadriceps (left column) and upper biceps (right column) from 6-month-old KI-I115F mice that show cytoplasmic fuscophilic areas (top and middle rows) and inflammatory infiltrates (bottom row). (C) Representative electron microscopic images of the quadriceps of 6-month-old KI-I115F mice, showing pseudo-tubular aggregates (right column) and mitochondrial alterations (left column). (D) Representative electron microscopic images of the quadriceps of 6-month-old KI-I115F mice, showing myofibrillar dysorganization. (E) Creatine kinase (CK) plasma concentrations. Mean±s.e.m. at 3 (WT *n*=16, KI-I115F *n*=15), 6 (WT *n*=17, KI-I115F *n*=11) and 12 (WT *n*=20, KI-I115F *n*=15) months. \**P*=0.011 versus WT.

was increased in the quadriceps, whereas no differences were observed in the extensor digitorum longus. In the soleus, both type IIa and type I fibers were decreased in KI-STIM1<sup>1115F</sup> compared to WT animals, but this was paralleled by a marked increase in fibers that were negative for both type IIa and type I myosin (Fig. S6).

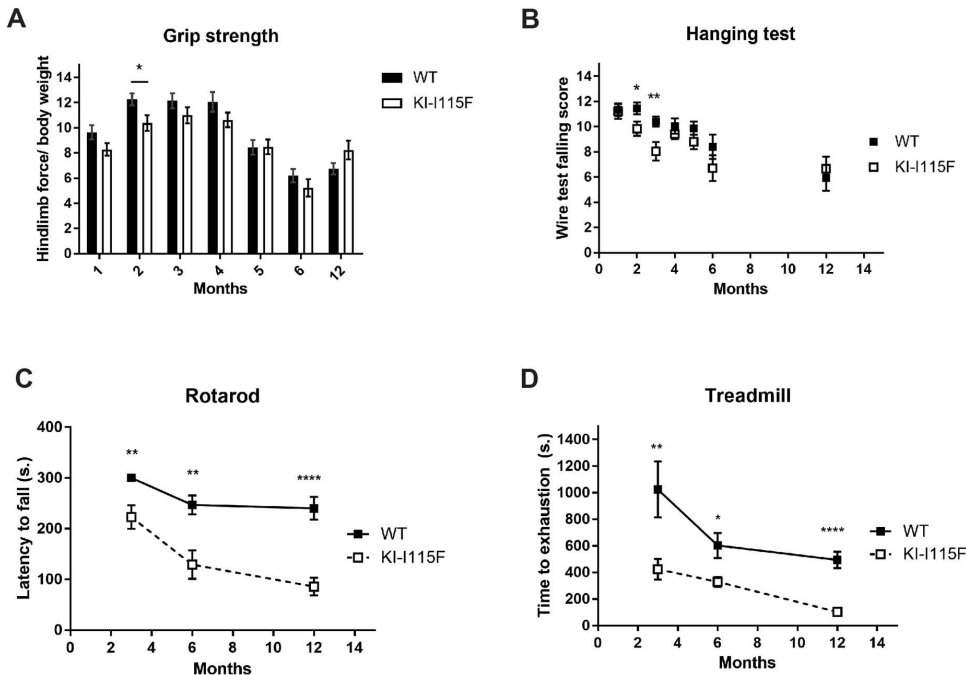
Despite the marked histopathological alterations in muscle tissue, only small differences in serological creatine kinase (CK) levels were observed between KI-STIM1<sup>1115F</sup> and WT during the entire lifespan (Fig. 4E). A significant variability in CK levels was observed, presumably due to the low levels detected. Similar trends were observable in a subanalysis of male and female animals (Fig. S7).

Finally, we analyzed the motor and strength performances of the animals. KI-STIM1<sup>1115F</sup> mice performed similarly to WT mice, both in the grip strength and hanging test, although a reduced performance was evident at around 2-3 months, which then recovered to levels comparable to WT (Fig. 5A,B). In contrast, when animals were tested on the rotarod or the treadmill, an underperformance of KI-STIM1<sup>1115F</sup> with respect to WT was already evident at 3 months (the earliest age at which these tests can be performed reproducibly) and was maintained up to 1 year (Fig. 5C,D).

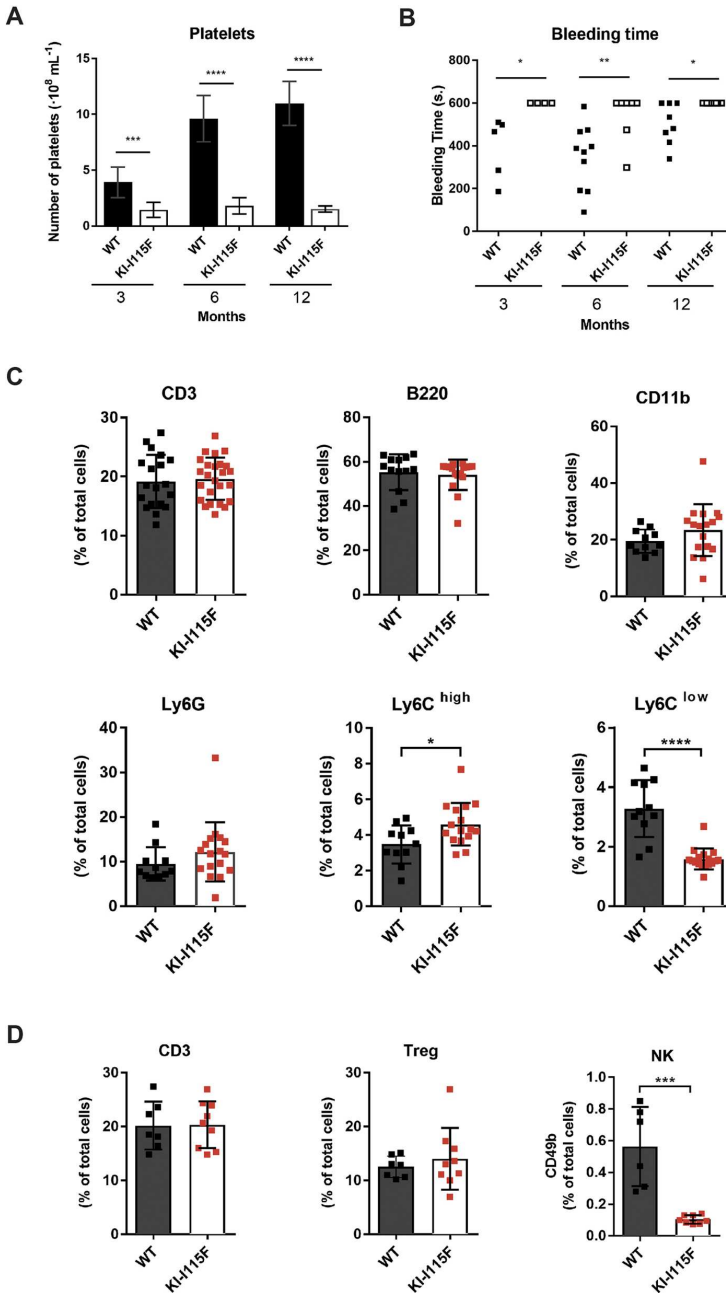
### KI-STIM1<sup>1115F</sup> mice display hematological defects

We next proceeded to determine platelet count in animals at 3, 6 and 12 months. As shown in Fig. 6A, significant thrombocytopenia was evident in KI-STIM1<sup>1115F</sup> mice of all ages. This reduced number of platelets was reconciled with an increased bleeding time, which was evaluated via the tail test (Fig. 6B). Of the 19 KI-STIM1<sup>1115F</sup> mice tested, only two stopped bleeding within 10 min of the incision, compared to 20 out of 23 in the WT animals.

To gain an insight into other hematological dyscrasias, we next evaluated the frequency of circulating B and T lymphocytes in WT or KI-STIM1<sup>1115F</sup> mice at 6 months of age. As shown in Fig. 6C (top row), we could not detect any difference in the frequency of T cells (CD45<sup>+</sup>CD3<sup>+</sup> cells), B cells (CD45<sup>+</sup>B220<sup>+</sup> cells) and CD11b<sup>+</sup> cells (CD45<sup>+</sup>Cd11b<sup>+</sup>) between KI-STIM1<sup>1115F</sup> and WT. We also evaluated the myeloid populations, and found that KI-STIM1<sup>1115F</sup> mice displayed similar levels of total granulocytes (CD45<sup>+</sup>Cd11b<sup>+</sup>Ly6G<sup>+</sup>) compared to WT (Fig. 6C, bottom row). In contrast, KI-STIM1<sup>1115F</sup> showed impairment of the monocyte subsets. As shown in Fig. 6C (bottom row), the number of Ly6C<sup>high</sup> monocytes (CD45<sup>+</sup>Cd11b<sup>+</sup>Ly6G<sup>-</sup>Ly6C<sup>high</sup> cells) was increased in KI-STIM1<sup>1115F</sup> mice, with a marked reduction in the levels of Ly6C<sup>low</sup> monocytes (CD45<sup>+</sup>Cd11b<sup>+</sup>Ly6G<sup>-</sup>Ly6C<sup>low</sup> cells),



**Fig. 5. Characterization of muscular functionality of KI-STIM1<sup>1115F</sup> mice.** (A) Grip strength performance at 1 (WT  $n=45$ , KI-115F  $n=40$ ), 2 (WT  $n=35$ , KI-115F  $n=27$ ), 3 (WT  $n=39$ , KI-115F  $n=34$ ), 4 (WT  $n=34$ , KI-115F  $n=30$ ), 5 (WT  $n=34$ , KI-115F  $n=25$ ), 6 (WT  $n=19$ , KI-115F  $n=14$ ) and 12 (WT  $n=13$ , KI-115F  $n=12$ ) months. Graph shows the means  $\pm$  s.e.m. of the falling score. Unpaired Student's *t*-test with Welch's correction. \* $P=0.02$  versus WT. (B) Hanging test performance at 1 (WT  $n=45$ , KI-115F  $n=37$ ), 2 (WT  $n=37$ , KI-115F  $n=32$ ), 3 (WT  $n=42$ , KI-115F  $n=33$ ), 4 (WT  $n=35$ , KI-115F  $n=29$ ), 5 (WT  $n=32$ , KI-115F  $n=26$ ), 6 (WT  $n=17$ , KI-115F  $n=14$ ) and 12 (WT  $n=18$ , KI-115F  $n=18$ ) months. Graph shows the means  $\pm$  s.e.m. of the latency to fall in WT and KI-115F. Unpaired Student's *t*-test with Welch's correction. \*\* $P=0.0034$  KI-115F versus 300 s. \*\* $P=0.0096$ , \*\*\*\* $P<10^{-4}$  versus WT. (C) Rotarod test performance at 3 (WT  $n=11$ , KI-115F  $n=17$ ), 6 (WT  $n=13$ , KI-115F  $n=10$ ) and 12 (WT  $n=13$ , KI-115F  $n=13$ ) months. The 3-month data were analyzed by one-sample Student's *t*-test KI-115F versus 300 s. All WT mice achieved the endpoint of the experiment (300 s). Graph shows the means  $\pm$  s.e.m. of the latency to fall in WT and KI-115F. Unpaired Student's *t*-test with Welch's correction. \*\* $P=0.0034$  KI-115F versus 300 s. \*\* $P=0.0096$ , \*\*\*\* $P<10^{-4}$  versus WT. (D) Treadmill test performance at 3 (WT  $n=7$ , KI-115F  $n=9$ ), 6 (WT  $n=15$ , KI-115F  $n=15$ ) and 12 (WT  $n=16$ , KI-115F  $n=8$ ) months. Graph shows the means  $\pm$  s.e.m. of the time to exhaustion. Unpaired Student's *t*-test with Welch's correction. \* $P=0.0116$ , \*\* $P=0.0041$ , \*\*\*\* $P<10^{-4}$  versus WT.



**Fig. 6. Evaluation of hematological defects in KI-STIM1<sup>1115F</sup> mice.** (A) Platelet count at 3 (WT  $n=8$ , KI-1115F  $n=7$ ), 6 (WT  $n=9$ , KI-1115F  $n=11$ ) and 12 (WT  $n=8$ , KI-1115F  $n=10$ ) months. Histogram shows the means  $\pm$  s.e.m. of the number of platelets in WT and KI-1115F. Unpaired Student's *t*-test with Welch's correction. \*\*\* $P=0.0015$ , \*\*\*\* $P<10^{-4}$  versus WT. (B) Bleeding time at 3 (WT  $n=5$ , KI-1115F  $n=4$ ), 6 (WT  $n=10$ , KI-1115F  $n=7$ ) and 12 (WT  $n=8$ , KI-1115F  $n=8$ ) months. Scatter plots show bleeding time. Unpaired Student's *t*-test with Welch's correction. \* $P\leq 0.0256$ , \*\* $P=0.0064$  versus WT. (C) CD3 (CD45<sup>+</sup>CD3<sup>+</sup>), B220 (CD45<sup>+</sup>B220<sup>+</sup>), CD11b (CD45<sup>+</sup>CD11b<sup>+</sup>), Ly6G (CD45<sup>+</sup>CD11b<sup>+</sup>Ly6G<sup>+</sup>), Ly6C<sup>high</sup> (CD45<sup>+</sup>CD11b<sup>+</sup>Ly6G<sup>-</sup>Ly6C<sup>high</sup>) and Ly6C<sup>low</sup> (CD45<sup>+</sup>CD11b<sup>+</sup>Ly6G<sup>-</sup>Ly6C<sup>low</sup>) cell populations in blood from mice at 6 months (WT  $n=11$ , KI-1115F  $n=17$ ). Unpaired two-tailed Student's *t*-test was used for statistical analysis. \* $P=0.0193$ , \*\*\*\* $P<0.0001$  versus WT. (D) CD3 (CD45<sup>+</sup>CD3<sup>+</sup>), Treg (CD4<sup>+</sup>Foxp3<sup>+</sup>CD25<sup>+</sup>) and NK (CD3<sup>-</sup>CD11b<sup>-</sup>CD49b<sup>+</sup>) cells in spleen from mice at 6 months (WT  $n=6$ , KI-1115F  $n=8$ ). Unpaired two-tailed Student's *t*-test was used for statistical analysis. \*\*\*\* $P=0.0002$  versus WT.

compared to WT. These data demonstrate that KI-STIM1<sup>1115F</sup> mice have a normal T and B subset, but suggest an alteration in monocyte differentiation. Furthermore, to investigate the impact of the mutation on the immune system, we quantified regulatory T (Treg) (CD4<sup>+</sup>FOXP3<sup>+</sup>CD25<sup>+</sup>) and NK (CD3<sup>-</sup>CD11b<sup>-</sup>CD49b<sup>+</sup>) cells in the spleen of WT and KI-STIM1<sup>1115F</sup> mice. As shown in

Fig. 6D, only the number of NK cells was significantly reduced in KI-STIM1<sup>1115F</sup> compared to WT animals, suggesting a putative role of the STIM1 p.1115F mutation in the differentiation/maturation of NK cells (Abel et al., 2018). The gating strategies of fluorescence-activated cell sorting (FACS) analyses are reported in Fig. S8.

## DISCUSSION

TAM, Stormorken syndrome and York platelet syndrome represent a cluster of ultra-rare genetic diseases that can be attributed to overactivation of SOCE, a fundamental mechanism that allows calcium replenishment after ER store emptying. These disorders are driven by mutations in one of two key proteins involved in SOCE (STIM and ORAI). These mutations lead to gain-of-function proteins, and the clinical hallmarks are muscle weakness and platelet dysfunction. The two hallmarks may have variable penetrance in each individual, also according to the mutation.

In the present study, we generated a mouse colony bearing the I115F (c.343A>T) constitutive knock-in point mutation (KI-STIM1<sup>I115F</sup>), on a C57Bl/6 background. This mutation is located in one of the two luminal EF-hand Ca<sup>2+</sup>-binding motifs, and has been associated in the clinic with TAM and York platelet syndrome (Lacruz and Feske, 2015). Although a mouse bearing a mutation in the EF-hand motifs (STIM1<sup>Sax</sup>; D84G) has been described, the muscle phenotype was either not present or was not investigated (Grosse et al., 2007), as only a severe thrombocytopenia was reported. Two independent groups have reported the generation and characterization of mouse colonies that bear the R304W mutation, which is characteristic of TAM and Stormorken syndrome (Silva-Rojas et al., 2018; Gamage et al., 2018). The R304W mutation is located on the cytosolic domains of STIM1, and therefore our model is perfectly complementary to that described earlier.

KI-STIM1<sup>I115F</sup> mice are fertile, breed well in heterozygosity and ~50% of newborns display the mutation. The Mendelian ratio obtained when heterozygous animals were mated with WT was 1:1, which was as expected. This is partly in contrast to results reported by Silva-Rojas et al. (2018) for STIM1<sup>R304W</sup>, as fewer than expected heterozygous pups were observed.

KI-STIM1<sup>I115F</sup> mice are lighter than WT mice, which might reconcile with the decreased muscle weight that is observed. Importantly, this manifestation can be observed at 1 month of age, making it a good surrogate early endpoint to investigate drugs in the future. Similarly, platelet dysfunction can also be observed early, providing a further early read-out.

KI-STIM1<sup>I115F</sup> mice showed a normal performance in the grip strength and hanging tests. This somehow differs from the model described by Silva-Rojas et al. (2018), in which STIM1<sup>R304W</sup> mice showed impaired performance at 9 weeks (the only time assessed). We found, instead, a strong impairment in both the rotarod and treadmill tests, which also contrasts with observations by Silva-Rojas et al. (2018) (at 9 weeks) and Gamage et al. (2018) (at 5-6 months). Our model, therefore, appears to show functional deficits in tests that evaluate motor coordination (rotarod test) and speed activity (treadmill test), suggesting a prevalent impairment in actions that require running or sprinting, a deficit also reported in TAM patients (Walter et al., 2015). The negative performance of KI-STIM1<sup>I115F</sup> mice in the rotarod test is unlikely to be attributable to balance impairment, as this is not supported by the hanging test (a functional test that also requires coordination), demonstrating muscle involvement but not a cerebellar deficit.

In line with the Ca<sup>2+</sup> overload detected in myotubes from TAM patients, in KI-STIM1<sup>I115F</sup> myotubes, we observed a SOCE overactivation that was maintained during the entire lifespan, unlike what was observed in WT mice. However, in contrast to previous data reported in TAM patient myotubes (Garibaldi et al., 2016), we did not observe any increase in basal calcium levels or spontaneous oscillations in KI-STIM1<sup>I115F</sup> myotubes. This observation at present has no explanation, although preliminary

evidence reveals that platelets from KI-STIM1<sup>I115F</sup> animals instead show an increased basal Ca<sup>2+</sup> level (C.C.-S., unpublished).

Histopathological findings in KI-STIM1<sup>I115F</sup> mice revealed a progressive muscle degeneration. Muscle tissue showed histological features consistent with a myopathic process, similar to those observed in the other mice models (Silva-Rojas et al., 2018; Gamage et al., 2018). Given the different times at which muscles were evaluated in the different models, comparison of the severity of the myopathy is not possible. In our model, at 12 months, muscles showed a severe myopathic process. When evaluating different muscles at 6 months, we found mitochondrial alterations and the presence of aggregates that, in part, may represent the counterpart of the human hallmark, although they were not superimposable. It is worth noting, therefore, that all three models lack true tubular aggregates (Silva-Rojas et al., 2018; Gamage et al., 2018), although the pseudo-aggregates observed in KI-STIM1<sup>I115F</sup> mice will require more investigation in the future. Interestingly, we detected in some mice abundant endomysial inflammatory infiltrates, a pathological feature that has been reported in a mouse model overexpressing STIM1 (Goonasekera et al., 2014). In KI-STIM1<sup>I115F</sup>, the myopathic process was not paralleled by significant increases in CK levels. Although an increasing trend was observed, the variability, which might have been due to the technology used or to true inter-individual variability, did not lead to consistent statistical significance.

As reported in patients carrying the STIM1 p.I115F mutation, our mouse model also displays a severe platelet dysfunction. At all time points evaluated, we observed a marked reduction in platelet number, which is likely to be linked to the increased bleeding time. It has previously been reported in the STIM1<sup>Sax</sup> mouse that thrombocytopenia is associated with increased basal calcium in platelets, resulting in a pre-activation state (Grosse et al., 2007). Such a mechanism would be compatible with our findings; indeed, in preliminary experiments, we confirmed this increase in basal Ca<sup>2+</sup>. Importantly, the two R304W models have contradictory findings on platelets: whereas Silva-Rojas et al. (2018) found a significantly decreased platelet number, Gamage et al. (2018) found no differences in heterozygous animals and attributed this negative finding to a compensatory reduction in STIM1 protein. The KI-STIM1<sup>I115F</sup> model did not display compensatory mechanisms, at least at the mRNA level.

Considering the crucial role of SOCE in the immune system (Feske et al., 2010) and the involvement of STIM and ORAI loss-of-function mutations in severe immunodeficiencies (Lacruz and Feske, 2015), we investigated the impact of the STIM1<sup>I115F</sup> mutation on circulating T lymphocytes, B lymphocytes, neutrophils and monocytes. In contrast to observations by Silva-Rojas et al. (2018), in STIM1<sup>R304W</sup>, we did not find impairment of T cells or a significant increase in the levels of neutrophils, but found alterations in monocyte subsets and in NK cells, which are worth exploring in patients in the future.

To date, 12 point mutations have been reported on the intraluminal EF-hand motifs and four mutations/deletions described in the cytosolic coiled-coil domains of STIM1. Given the extremely low frequency of these mutations, it is plausible that only drugs that will be able to counteract most of these mutations will find sufficient patients to treat in clinical trials and be approved. In this respect, we believe the presence of complementary models mimicking luminal and cytosolic mutations will increase the likelihood of success for the development of effective drugs for patients that are – at present – lacking therapeutic options.

## MATERIALS AND METHODS

### KI-STIM1<sup>I115F</sup> mouse model generation and animal care

The care and husbandry of animals were in conformity with the institutional guidelines, in compliance with national and international laws and policies. Mice were housed in ventilated cages in 22±1°C monitored rooms with 12 h light/dark cycles, had access to food and water *ad libitum*, and were weaned at 23 days by sex. The procedures were approved by the local animal-health and ethical committee (Università del Piemonte Orientale) and authorized by the national authority (Istituto Superiore di Sanità; authorization number N. 194/2019-PR).

KI-STIM1<sup>I115F</sup> founders in a C57Bl/6N background were obtained from PolyGene Transgenics (<https://www.polygene.ch/>). Briefly, this knock-in mouse model was generated by homologous recombination in electroporation-transfected embryonic stem (ES) cells on exon 3 of the *Stim1* gene, located on chromosome 7, inserting the c.343A>T mutation (corresponding to isoleucine to phenylalanine substitution; I115F). The linearized targeting vector F118.3 TV, with a flippase recognition target (FRT)-flanked neomycin resistance cassette, inserted in an unsuspicious region in intron 3 of *Stim1*, was used for the electroporation. The integrity of the targeting vector was confirmed by sequencing exonic regions and by restriction analysis. G418 selection was used to maintain stable transfection, and the clones obtained were analyzed and validated by PCR and Southern blotting using BstEII-digested DNA (internal probe) and a 3' external probe (LA probe).

The selected ES clones were injected into 49 blastocysts from gray C57Bl/6N mice. Forty-one surviving blastocysts were transferred to two CD-1 foster mice. Resulting chimeras were mated to gray Flp-deleter mice. The offspring from the chimeras were screened for the Flp-mediated deletion of the neomycin cassette and the corresponding presence of the remaining FRT site.

Mice were identified with the ear punch method at weaning and the piece of tissue obtained was used to perform genotyping using a PCR BIO Rapid Extract PCR Kit (PCR Biosystems, UK). DNA extraction was performed according to the manufacturer's instructions (5× PCR BIO Rapid Extract Buffer A, 10× PCR BIO Rapid Extract Buffer B). For tissue lysis, the samples were incubated at 75°C for 5 min. Another incubation at 95°C for 10 min was performed to deactivate proteases. Subsequently, the reaction was stopped by adding mQ H<sub>2</sub>O, and centrifugation at 13,000 g for 1 min was performed to eliminate the debris. The PCR reaction was conducted using the following primers: FW, 5'-CCGCAACTGAGGCATTC-3'; REV, 5'-AAGAGTGGAGTAGGCAGAG-3'. A single band was obtained as a final PCR product in WT mice (617 bp), whereas a double band was obtained in heterozygotes KI-STIM1<sup>I115F</sup> (617 bp and 746 bp), related to the presence of the remaining FRT site.

### Bleeding time

From an isoflurane-anesthetized animal, a segment of 2 mm was cut from the tail tip and immersed in a solution of 0.9% NaCl (Sigma-Aldrich, Italy) at 37°C. Bleeding time was measured for a maximum of 10 min to avoid unnecessary suffering.

### Behavioral tests

All behavioral tests were performed according to the Standard Operating Protocols (SOPs) of the TREAT-NMD neuromuscular network (<http://www.treat-nmd.eu/research/preclinical/dmd-sops/>).

### Grip strength test

To measure the forelimb force *in vivo*, mice were suspended by the tail and allowed to grasp on a rod. A force transducer, attached to the rod by the mice grasp, was used to measure the force and the time of peak resistance. Five trials per mouse were performed and data were normalized to mouse weight (DMD\_M.2.2.001). Experiments were performed in WT and KI-STIM1<sup>I115F</sup> mice at 1, 2, 3, 4, 5, 6 and 12 months.

### Hanging wire test

To determine 'subacute' muscle function and coordination, mice were allowed to grasp onto the middle of a wire. Mice attempted to reach one of the wire ends and the number of 'falls' or 'reaches' was recorded. From an initial score of 10, each fall decreased the score by one and each reach

increased the score by 1. The experiment was terminated after 180 s or when the animal reached zero as a score, whichever was earlier. A Kaplan-Meier-like curve was created with all data obtained (DMD\_M.2.1.004). Experiments were performed in WT and KI-STIM1<sup>I115F</sup> mice at 1, 2, 3, 4, 5, 6 and 12 months.

### Rotarod test

To assess motor coordination and balance, animals were placed on a rotarod with fixed speed (2.8 m/min or 10 rpm). Experiments were terminated after five falls or after 5 min, whichever was earlier. Before the test, mice were left to acclimatize to the experimental room, and mice habituation to the rotarod for 1 min at low speed was performed (ESLIM\_010\_001; Shiotsuki et al., 2010).

### Treadmill test

To assess the resistance and fatigue of mice, enforced running on a treadmill with no inclination at a fixed speed (12 m/min) was performed. The experiment was terminated after 30 min or after the fifth grid-stop, whichever came earlier. An acclimation period of 15 min in the experimental room was needed, and training for a maximum of 30 min was performed the previous day. Following the SOPs, no electric shock was used on the grid and it was substituted by a gentle touch of the tail, requiring two experimenters for continuous supervision of this test (DMD\_M.2.1.003, DMD\_M.2.1.001).

### CK assay

Blood was collected from isoflurane-anesthetized mice by submandibular vein puncture. Approximately 250 µl of blood was collected into heparin tubes to obtain plasma by centrifuging samples at 1200 g for 10 min at room temperature (RT). CK determination was performed according to the manufacturer's instructions using a standard spectrophotometric method with enzyme-coupled assay reagent from Point Scientific (C7522-150). Absorbance at 340 nm was measured every minute for 2 min at 37°C to calculate enzyme activity. Duplicate measurements were performed on each serum sample.

### Histological analysis

Muscles were trimmed of tendons and adhering non-muscle tissue, mounted in Killik embedding medium (Bio-optica, Italy), frozen in liquid nitrogen-cooled isopentane and stored at -80°C.

For conventional histological techniques, 8- to 10-µm-thick cryostat sections were stained with Hematoxylin-Eosin, Masson Trichrome and modified Gomori Trichrome (GT), to reveal general muscle architecture and myopathological features.

For ultrastructural studies, small muscle specimens were fixed with glutaraldehyde (2%, pH 7.4), then fixed with osmium tetroxide (2%), dehydrated and embedded in resin. Longitudinally oriented ultra-thin sections were obtained at different depths from one to three small blocks, and stained with uranyl acetate and lead citrate. Ultra-thin sections of transversally oriented blocks were obtained for only the most significant findings. The grids were observed using a Morgagni Fei electron microscope (The Netherlands) and were photo-documented using a Mega View II Camera (SYS Technologies).

For CSA distribution, muscle slices were fixed in 4% paraformaldehyde (PFA), permeabilized with 0.2% Triton X-100 in 1% bovine serum albumin (BSA) for 15 min and blocked with 4% BSA for 30 min. They were then incubated for 1 h with anti-laminin antibody (1:200; Dako, Agilent Technologies) and for a further 45 min with secondary antibody (1:400; anti-rabbit Alexa Fluor 488, Thermo Fisher Scientific) at RT. Images were acquired using a Leica CTR5500 B fluorescent microscope (Leica Biosystems, Germany) with the Leica Application SuiteX 1.5 software. CSA of the total muscle fibers was quantified with ImageJ software (v1.49o). For myosin heavy chain studies, muscle slices were not fixed with PFA and were stained with anti-laminin antibody (1:200; Dako, Agilent Technologies), BA-D5, Myosin Heavy Chain Type I (IgG2b; 1:50), SC-71, Myosin Heavy Chain Type IIA (IgG1; 1:500), BF-F3 and Myosin Heavy Chain Type IIB (IgM; 1:5), all obtained from the Developmental Studies Hybridoma Bank (Iowa City, IA, USA).



## Characterization of blood cell population

### T cell, B cell, Treg cell, NK cell, monocyte and granulocyte determination

Blood cells were collected from the eye vein of anesthetized mice, and splenocytes from the spleen after filtration through cell strainers (70  $\mu$ m). Ammonium-chloride-potassium lysing buffer was used for the lysis of red blood cells. Blood cells were labeled for 15 min at 4°C with fluorochrome-conjugated monoclonal antibodies: CD45-FITC BD Biosciences Clone 30-F11 (1:100), Ly6G BV421 BioLegend Clone 1A8 (1:500), Ly6C BV605 BD Biosciences Clone AL-21 (1:500), CD3e BV786 BD Biosciences Clone 500A2 (1:500), CD45R (B220) PE BD Biosciences Clone RA3-6B2 (1:500) and CD11b PE-Cy7 eBioscience Clone MI-70 (1:500). Splenocytes were labeled for 15 min at 4°C with fluorochrome-conjugated monoclonal antibodies: CD3 BV786 BD Biosciences (1:500), CD11b BV510 BD Biosciences (1:500), CD49b PE eBioscience (1:500), CD4 BV650 BD Biosciences (1:500), CD25 FITC BioLegend (1:500) and Foxp3 PerCP-Cy5.5 eBioscience (1:100). Samples were acquired with a BD LSRII Fortessa (BD Biosciences) and analyzed with FlowJo software.

### Number of platelets

To determine platelet number, 18  $\mu$ l of blood extracted from the submandibular vein was mixed with 2  $\mu$ l acid citrate dextrose (Sigma-Aldrich). Ten microliters of the mixture was then blended with 190  $\mu$ l NaNH<sub>2</sub> (Sigma-Aldrich) for 5 min at RT to induce the lysis of red blood cells. Then, 10  $\mu$ l of this solution was diluted in 90  $\mu$ l of phosphate-buffered saline (PBS). Counts were performed in a Burkert chamber on a microscope with a 40 $\times$  objective (Dhanjal et al., 2007).

### Cell cultures

WT and KI-STIM1<sup>1115F</sup> primary myoblasts were obtained from the following muscles: gastrocnemius, TA, quadriceps femoris, extensor digitorum longus, soleus, biceps brachii and diaphragm. Each muscle was placed in a 60-mm dish in PBS, removed from the tendon, separated longitudinally and subsequently chopped into smaller pieces. The small fragments were incubated with Pronase<sup>®</sup> (Protease, *Streptomyces griseus*, Calbiochem<sup>®</sup>, 25 KU) for 1 h at 37°C with shaking and neutralized with Dulbecco's modified Eagle medium (DMEM, Sigma-Aldrich), supplemented with 10% heat-inactivated fetal calf serum (Gibco, Italy), 50 mg/ml L-glutamine (Sigma-Aldrich), 10 U/ml penicillin and 100 mg/ml streptomycin (Sigma-Aldrich), and 1% chicken embryo extract (Sigma-Aldrich). Tissues were then chopped into smaller pieces and passed through pipettes of 10 ml and 5 ml, and the supernatant obtained was filtered in a 40- $\mu$ m strainer and centrifuged at RT for 10 min at 1200 rpm (235 g). The pellets were re-suspended and myoblasts were plated in a 100-mm dish in DMEM, supplemented with 10% heat-inactivated fetal bovine serum (FBS) (Gibco), 50 mg/ml L-glutamine (Sigma-Aldrich), 10 U/ml penicillin and 100 mg/ml streptomycin (Sigma-Aldrich), and 1% chicken embryo extract (Sigma-Aldrich) for 90 min at 37°C, in a 5% CO<sub>2</sub> humidified atmosphere, to separate cells from debris. Supernatants were then centrifuged and plated in a 2% gelatine-treated 35-mm dish in DMEM (Sigma-Aldrich), supplemented with 20% heat-inactivated FBS (Gibco), 10% horse serum (Gibco), 50 mg/ml L-glutamine (Sigma-Aldrich), 10 U/ml penicillin and 100 mg/ml streptomycin (Sigma-Aldrich), 1% chicken embryo extract (Sigma-Aldrich) and 10 ng/ml fibroblast growth factor (Peprotech, UK) at 37°C, in a 5% CO<sub>2</sub> humidified atmosphere for 6-7 days, with a medium change every 24-36 h.

For differentiation into myotubes, myoblasts were transferred for 48 h into differentiation medium consisting of DMEM with 5% horse serum and 1% penicillin-streptomycin.

For calcium-imaging experiments, myotubes were further maintained in the same medium for 24 h upon plating onto glass coverslips at a concentration of 20 $\times$ 10<sup>4</sup> per well (24-mm diameter coverslips in 6-well plates) and maintained in DMEM supplemented with 10% heat-inactivated FBS (Gibco), 50 mg/ml L-glutamine (Sigma-Aldrich), and 10 U/ml penicillin and 100 mg/ml streptomycin (Sigma-Aldrich), at 37°C in a 5% CO<sub>2</sub> humidified atmosphere. Experiments were performed 6-7 days after the extraction at cell passage number (P)2 and P3.

## Fura-2 Ca<sup>2+</sup> experiments

Myotubes from WT and KI-STIM1<sup>1115F</sup> mice were loaded with 5  $\mu$ M Fura-2 AM in the presence of 0.02% Pluronic-127 (both from Life Technologies, Italy) and 10  $\mu$ M sulfapyrazone (Sigma-Aldrich) in Krebs-Ringer buffer (KRB; 135 mM NaCl, 5 mM KCl, 0.4 mM KH<sub>2</sub>PO<sub>4</sub>, 1 mM MgSO<sub>4</sub>, 5.5 mM glucose, 20 mM HEPES, pH 7.4) containing 2 mM CaCl<sub>2</sub> (30 min, RT). Then, cells were washed and incubated with KRB for 30 min to allow the de-esterification of Fura-2.

To measure SOCE, changes in cytosolic Ca<sup>2+</sup> were monitored upon depletion of the intracellular Ca<sup>2+</sup> stores. Experiments were carried out prior to and during exposure of the cells to the Ca<sup>2+</sup>-free solution. In the absence of Ca<sup>2+</sup>, the intracellular Ca<sup>2+</sup> stores were depleted by inhibition of the vesicular Ca<sup>2+</sup> pump by tBHQ (50  $\mu$ M; Sigma-Aldrich). Re-addition of 2 mM Ca<sup>2+</sup> allowed assessment of the SOCE.

During the experiments, the coverslips were mounted into an acquisition chamber and placed on the stage of a Leica DMI6000 epifluorescent microscope equipped with S Fluor  $\times$ 40/1.3 objective. Fura-2 was excited by alternating 340 nm and 380 nm using a Polychrome IV monochromator (Till Photonics, Germany), and the probe emission light was filtered through a 520/20 bandpass filter and collected by a cooled CCD camera (Hamamatsu, Japan). The fluorescence signals were acquired and processed using MetaFluor software (Molecular Devices, USA). To quantify the differences in the amplitudes of Ca<sup>2+</sup> transients, the ratio values were normalized using the formula  $\Delta F/F_0$ .

## qRT-PCR

Total RNA from WT and KI-STIM1<sup>1115F</sup> myotubes was isolated using TRI-Reagent<sup>®</sup> and reverse transcribed according to the manufacturer's instructions (Life Technologies). cDNA was then stored at -20°C until further use. qRT-PCRs were performed on 96-well plates (CFX96™ Real-Time PCR Detection Systems, Bio-Rad, Italy), in triplicate, and fluorescence intensity was assessed.

Primers used are listed in Table S1. Transcripts were normalized to the expression of ribosomal protein S18 mRNAs; for each gene, the threshold cycle ( $\Delta$ Ct) was calculated.

## Statistical analysis

The normality of data distributions was assessed using Shapiro-Wilk test and data are presented as mean $\pm$ s.e.m. or median and interquartile range (IQR), according to distribution. Parametric [unpaired Student's *t*-test and one-way analysis of variance (ANOVA) followed by Tukey's post-hoc] or non-parametric (Mann-Whitney *U*-test and one-way Kruskal-Wallis H test followed by Dunn's post-hoc) statistical analyses were used. All statistical assessments were two-sided and *P*<0.05 was considered statistically significant. Statistical analyses were performed using Prism software (GraphPad Software, USA). Statistical significance was tested between the two mouse strains at the same age and was not tested for changes in time.

In calcium-imaging *in vitro* experiments, *n* represents the number of cells, and the number of independent experiments (defined as experiments performed on different days) is provided in the respective figure legends. For *in vivo* experiments, *n* represents the number of animals studied. In experiments involving histology, the figures shown are representative of at least three experiments (histologic coloration), performed on different experimental days on the tissue sections collected from all animals in each group.

This article is part of a special collection 'A Guide to Using Neuromuscular Disease Models for Basic and Preclinical Studies', which was launched in a dedicated issue guest edited by Annemieke Aartsma-Rus, Maaïke van Putten and James Dowling. See related articles in this collection at <http://dmm.biologists.org/collection/neuromuscular>.

## Acknowledgements

We thank Dr Gioia Merlonghi and Dr Andrea Micaloni for help with histological analyses.

## Competing interests

The authors declare no competing or financial interests.

**Author contributions**

Conceptualization: B.R.; Methodology: C.C.-S., B.R., S. Reano, N.C., I.Z., A.P., S. Raffa, S.S., M.P.C., M.G.; Validation: N.C.; Formal analysis: C.C.-S., F.A.R.; Investigation: C.C.-S.; Resources: B.R., N.C.; Writing - original draft: C.C.-S., B.R., T.P., A.B., M.G., A.A.G.; Supervision: B.R., A.B., M.G., N.F., A.A.G.; Project administration: B.R., A.A.G.; Funding acquisition: A.A.G.

**Funding**

This work was partly funded by Fondazione Telethon (GGP19110 to A.A.G.).

**Data availability**

The data to support the findings of this study are available from the corresponding author upon reasonable request.

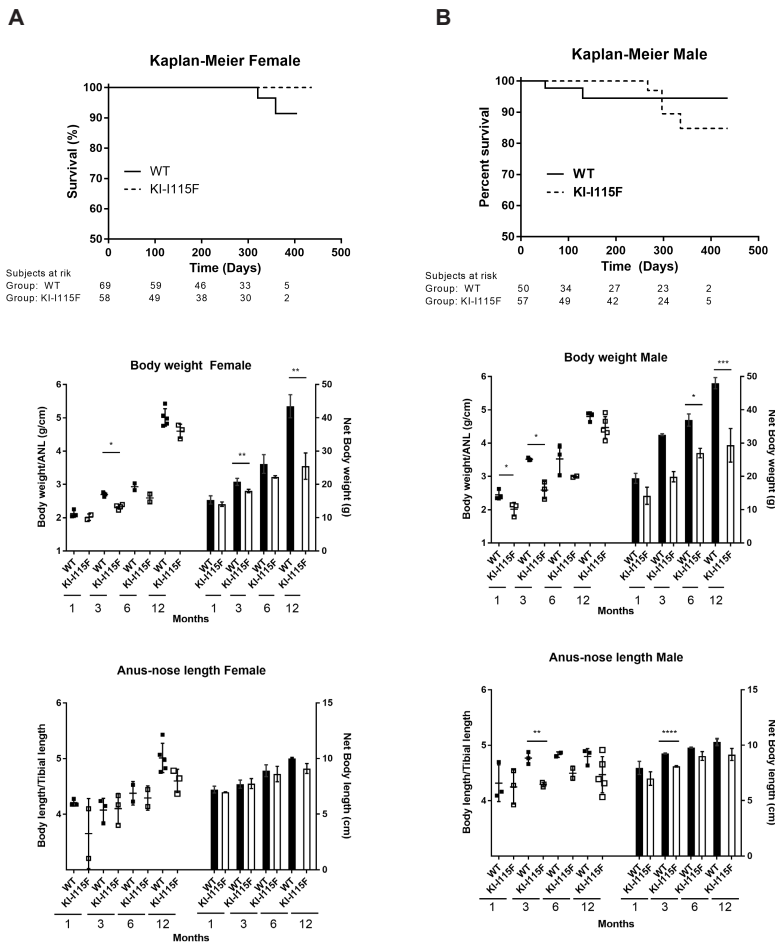
**Supplementary information**

Supplementary information available online at <http://dmm.biologists.org/lookup/doi/10.1242/dmm.041111.supplemental>

**References**

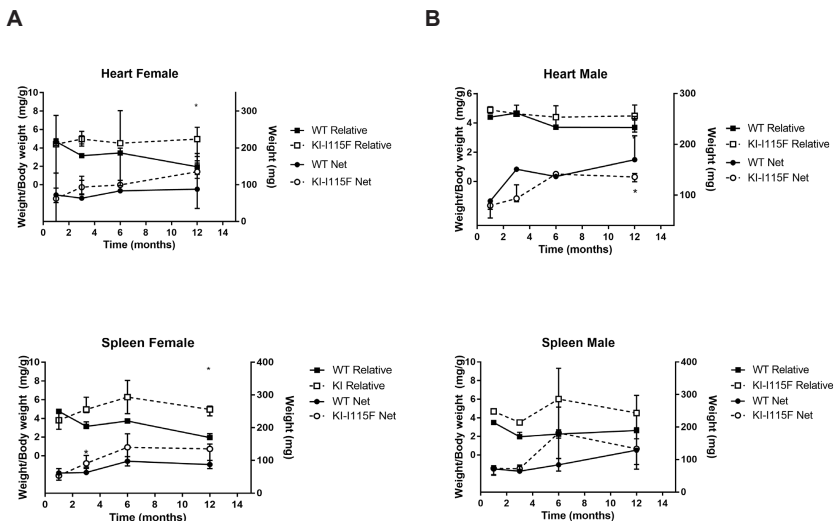
- Abel, A. M., Yang, C., Thakar, M. S. and Malarkannan, S. (2018). Natural killer cells: development, maturation, and clinical utilization. *Front Immunol.* **9**, 1-23. doi:10.3389/fimmu.2018.01869
- Berna-Erro, A., Redondo, P. C. and Rosado, J. A. (2012). Store-operated Ca(2+) entry. *Adv. Exp. Med. Biol.* **740**, 349-382. doi:10.1007/978-94-007-2888-2\_15
- Böhm, J. and Laporte, J. (2018). Gain-of-function mutations in STIM1 and ORAI1 causing tubular aggregate myopathy and Stormorken syndrome. *Cell Calcium* **76**, 1-9. doi:10.1016/j.ceca.2018.07.008
- Böhm, J., Chevessier, F., Koch, C., Peche, G. A., Mora, M., Morandi, L., Pasanisi, B., Moroni, I., Tasca, G., Fattori, F. et al. (2014). Clinical, histological and genetic characterisation of patients with tubular aggregate myopathy caused by mutations in STIM1. *J. Med. Genet.* **51**, 824-833. doi:10.1136/jmedgenet-2014-102623
- Dhanjal, T. S., Pendaries, C., Ross, E. A., Larson, M. K., Protsy, M. B., Buckley, C. D. and Watson, S. P. (2007). A novel role for PECAM-1 in megakaryocytokinesis and recovery of platelet counts in thrombocytopenic mice. *Blood* **109**, 4237-4244. doi:10.1182/blood-2006-10-050740
- Fahrner, M., Stadlbauer, M., Muik, M., Rathner, P., Stathopoulos, P., Ikura, M., Müller, N. and Romanin, C. (2018). A dual mechanism promotes switching of the Stormorken STIM1 R304W mutant into the activated state. *Nat. Commun.* **9**, 825. doi:10.1038/s41467-018-03062-w
- Feske, S. (2010). CRAC channelopathies. *Pflugers Arch.* **460**, 417-435. doi:10.1007/s00424-009-0777-5
- Feske, S., Picar, C. and Fischer, A. (2010). Immunodeficiency due to mutation in ORAI1 and STIM1. *Clin. Immunol.* **135**, 169-182. doi:10.1016/j.clim.2010.01.011
- Gamage, T. H., Gunnes, G., Lee, R. H., Louch, W. E., Holmgren, A., Bruton, J. D., Lengle, E., Kolstad, T. R. S., Revold, T., Amundsen, S. S. et al. (2018). STIM1 R304W causes muscle degeneration and impaired platelet activation in mice. *Cell Calcium* **76**, 87-100. doi:10.1016/j.ceca.2018.10.001
- Garibaldi, M., Fattori, F., Riva, B., Labasse, C., Brochier, G., Ottaviani, P., Sacconi, S., Vizzaccaro, E., Laschena, F., Romero, N. et al. (2016). A novel gain-of-function mutation in ORAI1 causes late-onset Tubular Aggregate Myopathy and congenital mirosis. *Clin. Genet.* **91**, 780-786. doi:10.1111/cge.12888
- Goonasekera, S. A., Davis, J., Kwong, J. Q., Accornero, F., Wei-LaPierre, L., Sargent, M. A., Dirksen, R. T. and Molkentin, J. D. (2014). Enhanced Ca<sup>2+</sup> influx from STIM1-Orai1 induces muscle pathology in mouse models of muscular dystrophy. *Hum. Mol. Genet.* **23**, 3706-3715. doi:10.1093/hmg/ddu079
- Grosse, J., Braun, A., Varga-Szabo, D., Beyersdorf, N., Schneider, B., Zeitmann, L., Hanke, P., Schropp, P., Mühlstedt, S., Zorn, C. et al. (2007). An EF hand mutation in Stim1 causes premature platelet activation and bleeding in mice. *J. Clin. Invest.* **117**, 3540-3550. doi:10.1172/JCI32312
- Harris, E., Hudson, J., Marsh, J., Marini Bettolo, C., Neri, M., Ferlini, A., Bushby, K., Lochmüller, H., Straub, B. and Barresi, R. (2015). A novel STIM1 mutation at p.340 causes tubular aggregate myopathy with mirosis without additional features of Stormorken syndrome. *Neuromuscul. Disord.* **25**, S289. doi:10.1016/j.nmd.2015.06.369
- Lacruz, R. S. and Feske, S. (2015). Diseases caused by mutations in ORAI1 and STIM1. *Ann. NY Acad. Sci.* **1356**, 45-79. doi:10.1111/nyas.12938
- Markello, T., Chen, D., Kwan, J. Y., Horkayne-Szakaly, I., Morrison, A., Simakova, O., Maric, I., Lozier, J., Cullinane, A. R., Kilo, T. et al. (2015). York platelet syndrome is a CRAC channelopathy due to gain-of-function mutations in STIM1. *Mol. Genet. Metab.* **114**, 474-482. doi:10.1016/j.ymgme.2014.12.307
- Misceo, D., Holmgren, A., Louch, W. E., Holme, P. A., Mizobuchi, M., Morales, R. J., De Paula, A. M., Stray-Pedersen, A., Lyle, R., Dalhus, B. et al. (2014). A dominant STIM1 mutation causes Stormorken syndrome. *Hum. Mutat.* **35**, 556-564. doi:10.1002/humu.22544
- Nesin, V., Wiley, G., Kousi, M., Ong, E.-C., Lehmann, T., Nicholl, D. J., Suri, M., Shahrazaila, N., Katsanis, N., Gaffney, P. M. et al. (2014). Activating mutations in STIM1 and ORAI1 cause overlapping syndromes of tubular myopathy and congenital mirosis. *Proc. Natl. Acad. Sci. USA* **111**, 4197-4202. doi:10.1073/pnas.1312520111
- Noury, J.-B., Böhm, J., Peche, G. A., Guyant-Marechal, L., Bedat-Millet, A.-L., Chiche, L., Carlier, R.-Y., Malfatti, E., Romero, N. B. and Stojkovic, T. (2017). Tubular aggregate myopathy with features of Stormorken disease due to a new STIM1 mutation. *Neuromuscul. Disord.* **27**, 78-82. doi:10.1016/j.nmd.2016.10.006
- Okuma, H., Saito, F., Mitsui, J., Hara, Y., Hatanaka, Y., Ikeda, M., Shimizu, T., Matsumura, K., Shimizu, J., Tsuji, S. et al. (2016). Tubular aggregate myopathy caused by a novel mutation in the cytoplasmic domain of STIM1. *Neurol Genet.* **2**, e50. doi:10.1212/NXG.0000000000000050
- Ong, H. L. and Ambudkar, I. S. (2015). Molecular determinants of TRPC1 regulation within ER-PM junctions. *Cell Calcium* **58**, 376-386. doi:10.1016/j.ceca.2015.03.008
- Putney, J. W. (2011). Origins of the concept of store-operated calcium entry. *Front. Biosci.* **3**, 980-984. doi:10.2741/s202
- Schiaffino, S. (2012). Tubular aggregates in skeletal muscle: just a special type of protein aggregates? *Neuromuscul. Disord.* **22**, 199-207. doi:10.1016/j.nmd.2011.10.005
- Shiotsuki, H., Yoshimi, K., Shimo, Y., Funayama, M., Takamatsu, Y., Ikeda, K., Takahashi, R., Kitazawa, S. and Hattori, N. (2010). A rotarod test for evaluation of motor skill learning. *J. Neurosci. Methods* **189**, 180-185. doi:10.1016/j.jneumeth.2010.03.026
- Silva-Rojas, R., Treves, S., Jacobs, H., Kessler, P., Messaddeq, N., Laporte, J. and Böhm, J. (2018). STIM1 overactivation generates a multi-systemic phenotype affecting skeletal muscle, spleen, eye, skin, bones, and the immune system in mice. *Hum. Mol. Genet.* **28**, 1579-1593. doi:10.1093/hmg/ddy446
- Stormorken, H., Holmsen, H., Sund, R., Sakariassen, K. S., Hovig, T., Jellum, E. and Solum, O. (1995). Studies on the haemostatic defect in a complicated syndrome. An inverse Scott syndrome platelet membrane abnormality. *Thromb. Haemost.* **74**, 1244-1251. doi:10.1055/s-0038-1649920
- Walter, M. C., Rossius, M., Zitzelsberger, M., Vorgerd, M., Müller-Felber, W., Ertl-Wagner, B., Zhang, Y., Brinkmeier, H., Senderek, J. and Schoser, B. (2015). 50 years to diagnosis: autosomal dominant tubular aggregate myopathy caused by a novel STIM1 mutation. *Neuromuscul. Disord.* **25**, 577-584. doi:10.1016/j.nmd.2015.04.005

### Figure S1



**Figure S1. Characterization of KI-STIM1115F mice in female and male animals. (A)** Sub-analysis of data for female animals. Top panel shows Kaplan-Meier for survival. Middle panel shows body weight at 1 (WT n=3, KI-1115F n=2), 3 (WT n=3, KI-1115F n=4), 6 (WT n=5, KI-1115F n=2) and 12 (WT n=3, KI-1115F n=3) months of age. Scatter plots and histograms show the means  $\pm$  S.E.M. of the indicated number of mice. Unpaired Student t-test with Welch's correction. \*  $P=0.0302$ , \*\*  $P\leq 0.0033$  versus WT. Bottom panel shows body length at 1 (WT n=3, KI-1115F n=2), 3 (WT n=3, KI-1115F n=3), 6 (WT n=2, KI-1115F n=2) and 12 (WT n=4, KI-1115F n=3). Scatter plots and histograms show the means  $\pm$  S.E.M. of the indicated number of mice. Unpaired Student t-test with Welch's correction versus WT. **(B)** Sub-analysis of data for male animals; Top panel shows Kaplan-Meier for survival. Middle panel shows body weight at 1 (WT n=3, KI-1115F n=3), 3 (WT n=3, KI-1115F n=3), 6 (WT n=2, KI-1115F n=5) months of age. Scatter plots and histograms show the means  $\pm$  S.E.M. of the indicated number of mice. Unpaired Student t-test with Welch's correction. \*  $P\leq 0.0455$ , \*\*\*  $P=0.0005$  versus WT. Bottom panel shows body length at 1 (WT n=3, KI-1115F n=3), 3 (WT n=3, KI-1115F n=3), 6 (WT n=2, KI-1115F n=2) and 12 (WT n=3, KI-1115F n=5) months of age. Scatter plots and histograms show the means  $\pm$  S.E.M. of the indicated number of mice. Unpaired Student t-test with Welch's correction. \*  $P=0.0093$ , \*\*\*\*  $P<10^{-4}$  versus WT.

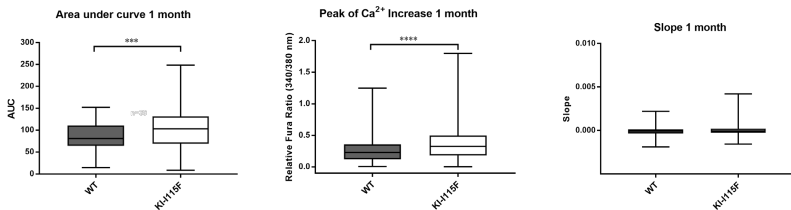
## Figure S2



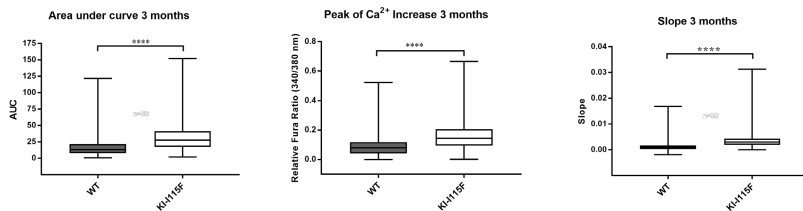
**Figure S2. Sub-analysis of heart and spleen size in female (A) and male (B) animals.** (A) Top panel represents heart weight and bottom panel represents spleen size weight at 1 (WT n=3, KI-115F n=2), 3 (WT n=3, KI-115F n=3), 6 (WT n=2, KI-115F n=2) and 12 (WT n=5, KI-115F n=3) months of age. Graph shows median and IQR of heart weight/body weight, or heart net weight. Mann-Whitney U test. \*  $P=0.0357$  versus WT. (B) Heart weight (top panel) and spleen weight (bottom panel) at 1 (WT n=3, KI-115F n=3), 3 (WT n=3, KI-115F n=3), 6 (WT n=2, KI-115F n=2) and 12 (WT n=3, KI-115F n=5) months of age. Graph shows median and IQR of heart weight/body weight, or heart net weight. Mann-Whitney U test. \*  $P=0.0357$  versus WT.

## Figure S3

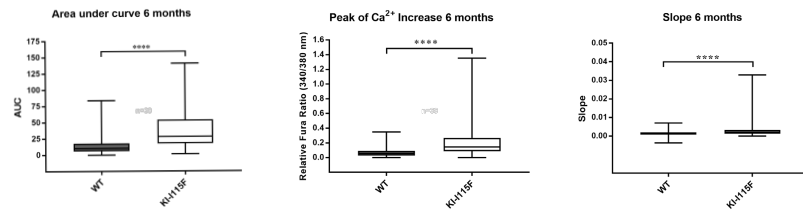
A



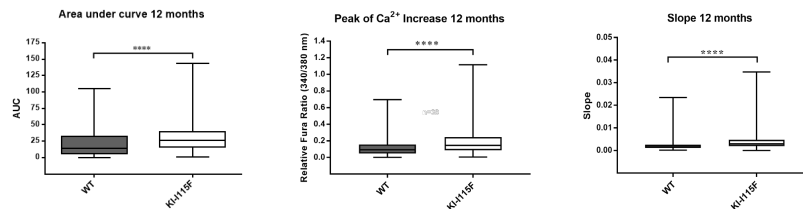
B



C

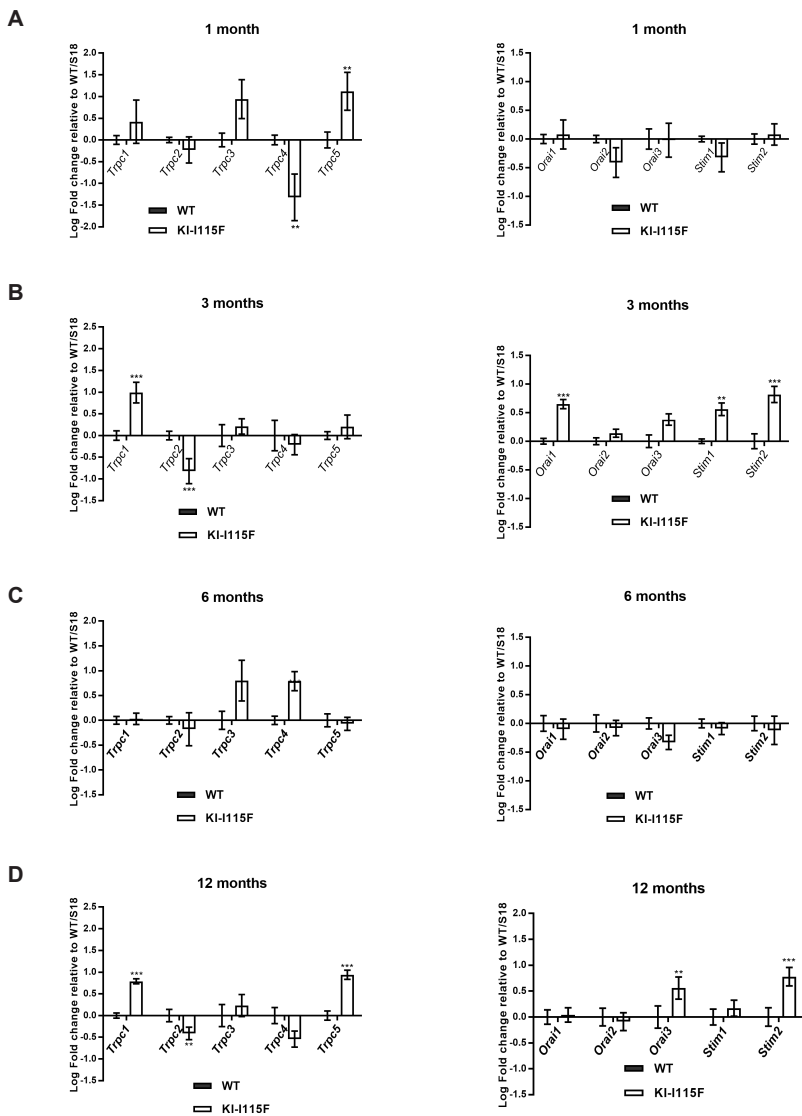


D



**Figure S3. SOCE alterations in myotubes.** Evaluation of the area under the curve (AUC), the peak amplitude, and the slope of the Ca<sup>2+</sup>-rise in WT and KI-115F at 1 (A), 3 (B), 6 (C) and 12 (D) months of age. Traces are the average of at least 180 myotubes from 6-well plates on two different experimental days. At all time-points, the experiments were performed on 4 different individual mice two males and two females per strain. Graph shows median and IQR of AUC, peak amplitude and slope of the Ca<sup>2+</sup>-rise. Mann-Whitney U test. AUC 1 months \*\*\* P=0.0005, peak amplitude 1 months \*\*\*\* P<0.0001 versus WT; AUC, peak amplitude and slope of Ca<sup>2+</sup>-rise 3 months \*\*\*\* P<0.0001 versus WT; AUC, peak amplitude and slope of Ca<sup>2+</sup>-rise 6 months \*\*\*\* P<0.0001 versus WT; AUC, peak amplitude and slope of Ca<sup>2+</sup>-rise 12 months \*\*\*\* P<0.0001 versus WT.

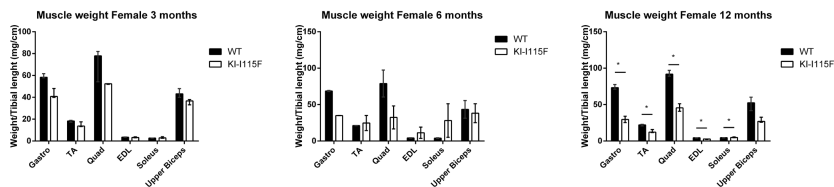
## Figure S4



**Figure S4. Gene expression alterations in muscle.** RT-PCR of SOCE genes in WT and KI-I115F at 1 (A), 3 (B), 6 (C) and 12 (D) months of age. Values represent mean  $\pm$  S.E.M and are expressed as  $\Delta\Delta C(t)$  of genes/S18 of four independent cultures. Unpaired two-tailed Student's t-test \*\*  $P \leq 0.00456$ , \*\*\*  $P \leq 0.000351$  versus WT.

## Figure S5

**A**

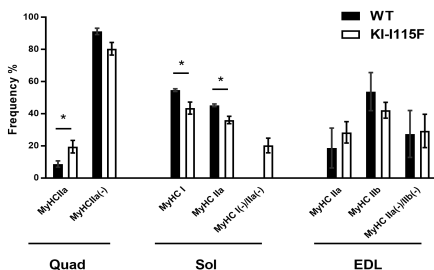


**B**



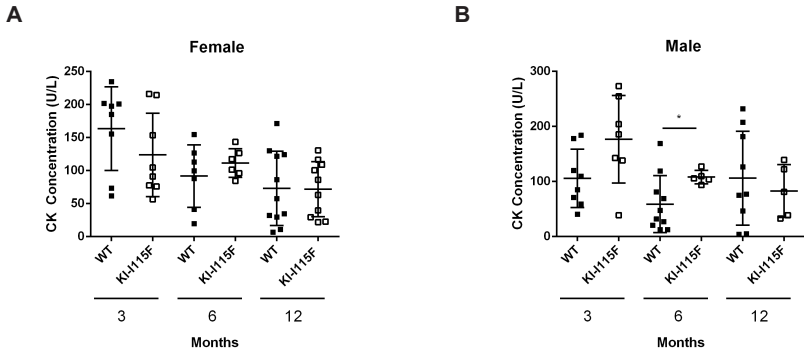
**Figure S5. Sub-analysis of muscle growth and damage in female (A) and male (B) animals. (A)** Muscle weight at 3 (WT n=3, KI-115F n=3), 6 (WT n=2, KI-115F n=2) and 12 months (WT n=5, KI-115F n=3) of age. (Gastro: gastrocnemius, TA: tibialis anterior, Quad: quadriceps, EDL: extensor digitorum longus). Histograms show median and IQR of muscle weights. Mann-Whitney U test. \*  $P=0.0357$  versus WT. **(B)** Muscle weight at 3 (WT n=3, KI-115F n=3), 6 (WT n=2, KI-115F n=2) and 12 months (WT n=3, KI-115F n=5) of age. (Gastro: gastrocnemius, TA: tibialis anterior, Quad: quadriceps, EDL: extensor digitorum longus). Histograms show median and IQR of muscle weights. Mann-Whitney U test. \*  $P=0.0357$  versus WT.

## Figure S6



**Figure S6. Muscle fiber frequency distribution in 12 months old WT and KI-115F mice.** Myosin heavy-chain (MyHC) immunofluorescence fiber staining (n=3) on quadriceps (Quad) for type Ila fibers (oxidative, fatigue resistant), on soleus (Sol) for type I and Ila fibers and on extensor digitorum longus (EDL) for type Ila and IIb (glycolytic) fibers. Negative myofibers for quadriceps represent type IIX and IIb fibers (MyHC IIa(-)) for soleus type IIX and IIb (MyHC I(-)/IIa(-)) and for EDL type IIX (MyHC IIa(-)/IIb(-)). The frequency is calculated above the total number of muscle fibers. Histograms show the means  $\pm$  S.E.M of the indicated number of mice. Unpaired Student t-test with Welch's correction. \*  $P<0.042$  versus WT.

## Figure S7

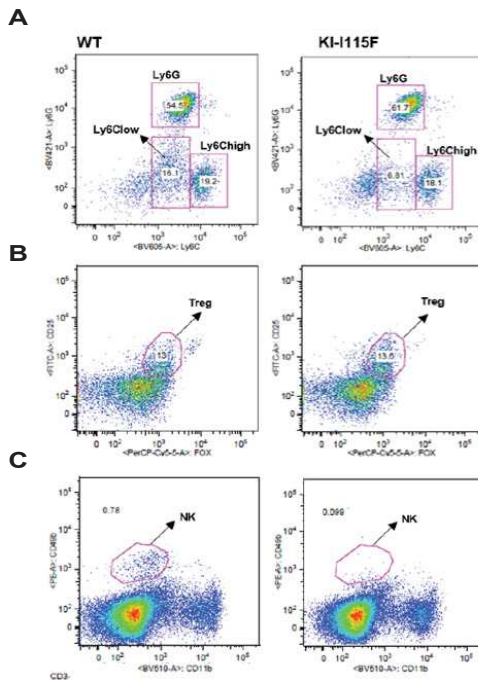


**Figure S7. Sub-analysis of Creatine Kinase plasma levels in female (A) and male (B) animals.**

(A) Scatter plots and histograms show the means  $\pm$  S.E.M at 3 months (WT n=8, KI-115F n=8), 6 months (WT n=7, KI-115F n=6), 12 months (WT n=11, KI-115F n=10) of age. Unpaired Student t-test with Welch's correction versus WT. (B) Scatter plots and histograms show the means  $\pm$  S.E.M at 3 months (WT n=8, KI-115F n=7), 6 months (WT n=10, KI-115F n=5), 12 months (WT n=9, KI-115F n=5) of age. Unpaired Student t-test with Welch's correction. \* P=0.016 versus WT.



## Figure S8

**Figure S8. Representative gating strategies in FACS analysis**

**(A)** Evaluation of monocytes and granulocytes in mouse blood using anti-Ly6C and anti-Ly6G antibodies.

**(B)** Evaluation of Treg cells in mouse spleen determined by anti-FOXP3 and anti-CD25 antibodies. **(C)** Evaluation of NK cells in mouse spleen using anti-CD11b and anti-CD49b antibodies. Please refer to the Material and method section for further details.

Table S1

Gene Symbol	Forward Primers	Reverse Primers
<i>Trpc1</i>	5'- GGACAGCCTCAGACATTCCA -3'	5'- CGGGCTAGCTCTTCATAATCA -3'
<i>Trpc2</i>	5'- AGAGGCAGAGCTGGAGTTCA -3'	5'- GGGGAATTTGAGCTTTTTGTT -3'
<i>Trpc3</i>	5'- GATCAATGTCTACAAGGGACT -3'	5'- TGCATTGCATGGAGAGTTTC -3'
<i>Trpc4</i>	5'- ACGCCATCAGAAAAGAGGTG -3'	5'- CCAAGATGATGGGTGTGATG -3'
<i>Trpc5</i>	5'- GAGGTGGTAGGAGCTGTGGA -3'	5'- TGCCAACATAATGGGAGTGA -3'
<i>Stim1</i>	5'- TCTGAAGAGTCTACCGAAGCAG -3'	5'- TGGAATTGAGGCTTCCCTTAG -3'
<i>Stim2</i>	5'- GACGAATGCGATCTGGTG -3'	5'- TTCAGTGAAGCAAGGTGGACT -3'
<i>Orai1</i>	5'- CCTGGCGCAAGCTTACTTA -3'	5'- TGCAGGCACTAAAGACGATC -3'
<i>Orai2</i>	5'- CACTGTCCTGGAGGAAGCTC -3'	5'- GGGCTGAGGTACTGGTACTT -3'
<i>Orai3</i>	5'-GAAACCGGAGGTGGACAG -3'	5'- GCTGGAGGCTTTGAGCATTAG -3'

Table S1. List of primers used

### **3.a.iii. Authors contribution:**

- ***Celia Cordero-Sanchez:***
  - Designed the experiments. Kaplan-meier. Mice, muscle and organs measurement. Calcium measurement. *In vivo* behavioural test. Platelets count. Supported bleeding test. Myeloid sample preparation. Script creation. Analysis of data and figure creation. Writing the draft. Managing of the mice colony.
- ***Beatrice Riva:***
  - Conceptualization. Supported calcium measurement: Supported Analysis. Writing the draft.
- ***Simone Reano:***
  - Mice, muscle and organs measurement. Grasping and hanging. Preparing CSA samples. H&E staining and CK measurements. Bleeding test.
- ***Nausicaa Clemente:***
  - Supported managing of the mice colony.
- ***Ivan Zaggia:***
  - Supported *ex vivo* experiments.
- ***Federico A. Ruffinatti:***
  - Analysis. Script creation.
- ***Alberto Potenzieri:***
  - Supported *ex vivo* experiments.
- ***Tracey Pirali:***
  - Writing the draft.
- ***Salvatore Raffa:***
  - Myeloid population experiments.
- ***Sabina Sangaletti:***
  - Myeloid population experiments.
- ***Mario P. Colombo:***
  - Myeloid population experiments.
- ***Alessandra Bertoni:***
  - Supervision.
- ***Matteo Garibaldi:***
  - Masson and Gomori Trichrome staining. Electron microscopy experiments. Writing the draft. Supervision.
- ***Nicoletta Filigheddu:***
  - Designed the experiments. Supervision.
- ***Armando A. Genazzani:***
  - Designed the experiments. Writing the draft. Supervision. Funding.



### ***3. PART I:***

## **Characterization of KI- STIM1<sup>I115F</sup> mouse model**

### ***b. Validation of KI-STIM1<sup>I115F</sup> mouse model for York Platelet Syndrome***

Under submission:

ID submitted manuscript: BLD-2021-014261



*i. Synopsis*

*Aim*

The aim of the present contribution is (i) to identify thrombocytopenia aetiology and (i) to evaluate SOC Entry inhibitor efficacy in the KI-STIM1<sup>I115F</sup> mouse model.

*The main findings of the manuscript are that:*

- (i) Thrombocytopenia presented in this mouse model is characterized by platelet pre-activation and hyper-aggregation.
- (ii) KI-STIM1<sup>I115F</sup> mouse model is valid not only for Tubular Aggregate Myopathy (TAM) but also for York Platelet Syndrome (YPS), validating the hypothesis that TAM, Stormorken Syndrome, and YPS are the spectra of the same disease (Bohm and Laporte, 2018a; Peche et al. 2020).
- (iii) CIC-39Na, a SOC Entry inhibitor, reverts thrombocytopenia and decreases blood loss in KI-STIM1<sup>I115F</sup> mice.

*Key take-home message:*

A SOC Entry inhibitor, CIC-39Na, reverts thrombocytopenia and bleeding diathesis in KI-STIM1<sup>I115F</sup> mice.

*Personal contribution:*

In the present contribution, I managed the colony and designed and performed all experiments except those contained in figure 5, under the supervision of Prof. Bertoni and Prof. Genazzani.





## ***CIC-39Na reverses the thrombocytopenia that characterizes Tubular Aggregate Myopathy***

Celia Cordero-Sanchez\*, Emanuela Pessolano\*, Beatrice Riva\*<sup>§</sup>, Nausicaa Clemente<sup>§</sup>, Silvio Aprile\*, Federico Alessandro Ruffinatti<sup>^</sup>, Paola Portararo<sup>‡</sup>, Nicoletta Filigheddu<sup>†</sup>, Ivan Zaggia<sup>†</sup>, Marta Serafini\*<sup>°</sup>, Tracey Pirali\*, Mario P. Colombo<sup>‡</sup>, Sabina Sangaletti<sup>‡</sup>, Alessandra Bertoni<sup>†,¶</sup>, Armando A. Genazzani\*<sup>¶</sup>

\*Department of Pharmaceutical Sciences, Università del Piemonte Orientale, Via Bovio 6, Novara (28100), Italy;

<sup>§</sup>Department of Health Sciences and Interdisciplinary Research Center of Autoimmune Diseases, Università del Piemonte Orientale, Via Solaroli 17, Novara (28100), Italy;

<sup>†</sup>Department of Translational Medicine, Università del Piemonte OrientaleUniversità del Piemonte Orientale, Via Solaroli 17, Novara (28100), Italy;

<sup>‡</sup>Department of Experimental Oncology and Molecular Medicine, Fondazione IRCCS Istituto Nazionale Tumori, Milano (20133), Italy;

<sup>¶</sup> The Authors wish it to be known that, in their opinion, the last 2 Authors should be regarded as joint Last Authors;

<sup>§</sup> present address: ChemiCare S.R.L. , Enne3, corso Trieste 15/a, Novara (28100), Italy;

<sup>°</sup> present address: Dept. of Chemistry, Chemistry Research Laboratory, University of Oxford, 12 Mansfield Road, OX1 3TA, UK;

<sup>^</sup> present address: Department of Life Sciences and Systems Biology, University of Turin, Via Accademia Albertina 13, Torino, Italy

Corresponding author: Armando A. Genazzani; Department of Pharmaceutical Sciences, University of Piemonte Orientale, Via Bovio 6, Novara (28100), Italy; armando.genazzani@uniupo.it; phone number: 0321 375 827- 0321 375 742 - 0321 375 830; fax: 0321 367 821.

**Text Word count: 3939**

**Abstract Word count: 166**

**Figure/table count: 5**

**Reference count: 31**

**Supplemental Tables: 2**

**Supplemental Figure: 1**

## Key Points

- Thrombocytopenia in a mouse model of tubular aggregate myopathy (KI-STIM1<sup>I115F</sup>) is characterized by platelet pre-activation and hyper-aggregation;
- CIC-39Na, a Store-Operated Calcium Entry inhibitor, reverts thrombocytopenia in KI-STIM1<sup>I115F</sup> mice and decreases blood loss.

## Abstract

Store-Operated Ca<sup>2+</sup>-Entry is a cellular mechanism that governs the replenishment of intracellular stores of Ca<sup>2+</sup> upon depletion caused by the opening of intracellular Ca<sup>2+</sup>-channels. Gain-of-function mutations of the two key proteins of Store-Operated Ca<sup>2+</sup>-Entry, STIM1 and Orai1, are associated with several ultra-rare diseases clustered as tubular aggregate myopathies. Our group has previously demonstrated that a mouse model bearing the STIM1 p.I115F mutation recapitulates the main features of the disease: muscle weakness and thrombocytopenia. Similar findings have been found in other mice bearing different mutations on STIM1. At present, no valid treatment is available for these patients. In the present contribution, we report that (i) platelets in tubular aggregate myopathy are characterized by pre-activation and hyper-aggregation; and (ii) CIC-39Na, a Store-Operated Ca<sup>2+</sup>-Entry inhibitor restores platelet number and counteracts the abnormal bleeding that characterizes these mice. This finding paves the way to a pharmacological treatment strategy for tubular aggregate myopathy patients as well as to a biomarker to be used in clinical trials in these slowly-progressing muscle disorders.

## Introduction

Store-Operated Ca<sup>2+</sup>-Entry (SOCE; also known as capacitative-calcium entry) is a cellular mechanism which governs the replenishment of intracellular stores of Ca<sup>2+</sup> upon depletion caused by the opening of intracellular Ca<sup>2+</sup>-channels<sup>1-3</sup> (e.g. as inositol-1,4,5-triphosphate receptors (IP<sub>3</sub>R)). This mechanism is orchestrated by two key proteins<sup>1-5</sup>: (i) ORAI (of which there are three isoforms), a calcium channel located in the plasma membrane; and (ii) STIM (of which there are two isoforms), a sensor of calcium located on the endo(sarco)plasmic reticulum membrane that triggers the mechanism when intraluminal Ca<sup>2+</sup>-concentrations drop<sup>2</sup>.

Gain-of-function mutations of STIM1 and ORAI1 lead to dominant ultra-rare genetic diseases that historically go under different names (e.g. Stormorken syndrome, York syndrome) but that may be clustered as tubular aggregate myopathies<sup>6</sup> (TAM). The characteristic histological findings of these disorders are tubular aggregates visible by electron microscopy in skeletal muscle<sup>7</sup>, while the primary clinical features are muscle weakness and painful cramps<sup>6</sup>. Over 15 dominant gain-of-function mutations have been reported on STIM1 and 6 dominant mutations have been reported on ORAI1<sup>8,9</sup>. These mutations lead to a wide range of symptom severity, from asymptomatic patients to early-onset muscle weakness and multisystemic diseases<sup>9</sup>. The full penetrance of the disorder is known as Stormorken syndrome and is characterized by the involvement of multiple districts alongside muscle<sup>9</sup>. Recently, Morin et al. have performed a systematic review of mutations and a genotype/phenotype correlation<sup>10</sup>. Importantly, thrombocytopenia is present in the totality of patients bearing the classical Stormorken STIM1 mutation at position 304 (e.g. R304W, R304Q) on the coiled-coiled domain thought to interact with ORAI1 and in about half of the patients that bear mutations in luminal EF-hand motifs of STIM1, responsible for sensing intraluminal calcium<sup>10</sup>. Historically, STIM1 mutations have been described as causing at times solely thrombocytopenia (York Syndrome)<sup>11,12</sup>, but further investigations have revealed that a muscle component is invariably evident also in these patients<sup>13</sup>. Bleeding episodes, likely correlated to thrombocytopenia, have also been described in patients that bear ORAI1 mutations<sup>10,14</sup>. It should be noticed that also mutations of one of the intra-luminal Ca<sup>2+</sup>-buffering proteins, calsequestrin, have been reported to lead to Tubular Aggregate Myopathy (TAM)<sup>15,16</sup>.

SOCE has a crucial role in platelet aggregation and thrombus formation<sup>17</sup>. Indeed, platelets from STIM-*knockout* animals display a reduced ability to switch to a pro-coagulant state<sup>18</sup>. The presence of thrombocytopenia in TAM patients is therefore not surprising.

Four separate animal models have been developed that recapitulate TAM. In our previous work<sup>19</sup>, we characterized a STIM1 mutated mouse model (KI-STIM1<sup>I115F</sup>) bearing a gain-of-function mutation (p.I115F) associated in humans with muscle and platelet involvement<sup>6</sup>. As expected, the p.I115F mutation in mice showed the muscular phenotype of TAM but also presented blood alterations. In particular, alongside an

increase in LyC6<sup>high</sup>, a decrease in LyC6<sup>low</sup> myeloid cells, and a reduction in splenic NK cells, the KI-STIM1<sup>1115F</sup> mouse model presented severe thrombocytopenia associated with a pathologically prolonged bleeding time. Two separate mouse lines bearing the p.R304W mutation have been generated and described in the literature<sup>20,21</sup>. In the mouse reported by Gamage et al.<sup>20</sup>, heterozygous R304W mice showed a normal number of platelets, which was associated with a significantly reduced expression of STIM1 and a consequent impairment of activation. Instead, in line with the KI-STIM1<sup>1115F</sup> mouse, the p.R304W mouse reported by Silva-Rojas et al.<sup>21</sup> manifested a marked reduction in platelet count. Importantly, Grosse et al.<sup>22</sup> reported a mouse model developed by random mutations in which an activating mutation on STIM1 (STIM1<sup>Sax/+</sup>), with no counter-part in human disorders, also resulted in thrombocytopenia and an associated bleeding disorder.

A number of SOCE modulators have been postulated as of therapeutic interest in disorders characterized by SOCE over-activation. L-651582 (CAI) was the first inhibitor to enter clinical trials for cancer. While its development was initially discontinued due to lack of promising efficacy in tumors, it is now gaining novel impulse in glioblastoma<sup>23</sup>. The most recent Phase Ib trial shows that the drug is tolerable with no dose-limiting toxicities. SOCE inhibitors are being tested also for other conditions, including acute pancreatitis, given the importance that Ca<sup>2+</sup> has in triggering exocytosis of zymogen granules<sup>24</sup>. In this respect, CM4620 (also known as Auxora) has completed Phase I trials and is now in Phase II (NCT03401190) for acute pancreatitis as well as in Phase I/II trials for asparaginase-associated acute pancreatitis, a rare condition triggered by asparaginase treatment (NCT04195347). The same molecule is also in Phase II for severe COVID-19 pneumonia (NCT04345614) for its potential to reduce pulmonary inflammation<sup>25</sup>. A small, Phase II study has been published on this compound showing that at a dose of 1.0 mg/Kg to 1.4 mg/Kg for four days it is well tolerated<sup>26</sup>. A third compound, RP3128, developed for autoimmune disorders, has published data on its first-in-human trial again showing that the drug was well tolerated with no limiting toxicities<sup>27</sup>. Importantly, it has been shown that two FDA- and EMA-approved drugs, teriflunomide and leflunomide bear at therapeutic doses inhibitory activity on SOCE<sup>28</sup>. The above emerging data therefore suggest that safety associated with SOCE inhibition is manageable.

Unfortunately TAM is an orphan disorder with no treatment and no known drug development programs ongoing. In light of this, in the present manuscript we decided to characterize the platelet dysfunction in the KI-STIM1<sup>1115F</sup> mouse model and to evaluate whether platelet number and function could be restored with chronic pharmacological SOCE inhibition. We now report that (i) KI-STIM1<sup>1115F</sup> mice are characterized by thrombocytopenia and by pre-activation and hyper-aggregation of platelets; and (ii) that CIC-39Na<sup>29</sup>, a SOCE inhibitor, is able to revert the thrombocytopenic phenotype in adult mice. The compound is able to increase platelet number and consequently reduce blood loss, providing for the first-time encouraging evidence of a pharmacological strategy with small molecules targeting SOCE for TAM.

## Methods

### 1. KI-STIM1<sup>fl15F</sup> mice maintenance

Procedures were approved by the local animal-health and ethical Committee (Università del Piemonte Orientale) and were authorized by the national authority (Istituto Superiore di Sanità; authorization N. 98/2021-PR). Care, husbandry, and initial characterization have been described elsewhere<sup>19</sup>.

### 2. Platelet isolation

Platelet-rich plasma (PRP) was obtained by collecting blood in Acid Citrate Dextrose solution (Citric acid 130 mM, Trisodic citrate 152 mM and Glucose 112 mM). Samples were then diluted in Tyrode solution (HEPES 10 mM, NaCl 137 mM, KCl 2.9 mM, NaHCO<sub>3</sub> 12 mM; pH 7.4) and centrifuged 200 g for 7 minutes with deceleration at 27 °C. To isolate platelets, 0.02 U/ml apyrase (A6237), 1 μM of prostaglandin E1 (P5515) and 10 μM of indomethacin (I7378-5G) provided by Sigma Aldrich, were added to PRP before re-centrifuged at 850 g for 6 minutes at 27 °C and suspended in Tyrode. Platelets were counted as previously described<sup>19</sup>.

### 3. Western blot

Washed platelets were lysed in RIPA buffer. Lysates were clarified by centrifugation at 14,000 g for 15 minutes at 4 °C and 15 μg of protein from each sample were loaded on SDS-PAGE gels.

All antibodies were prepared in TRIS-buffered saline solution containing 0.1% Tween-20 (T-TBS), and supplemented with 3-5% non-fat dried milk or 3-5% bovine serum albumin, according to manufacturer instructions.

### 4. Flow cytometry

#### a. Haematopoietic progenitors

Bone marrow cell suspensions were stained with a cocktail of PE-conjugated antibodies to Lin positive markers (CD3, CD11b, CD45R, Gr-1, F4/80, CD11c, Ter-119) and with antibodies to CD117 (c-Kit, PE-Cy7), SCA-1 (APC), CD34 (FITC), CD16/CD32 (PcP-Cy5.5), CD127 (IL-7Ra, BV421). Myeloid progenitors (CMP, GMP, MEP) were discriminated based on the expression of CD34 and CD16/CD32 within the gate of Lin-CD117+ cells. Common Lymphoid Progenitors were identified according to the expression of IL-7Ra+ within the Lin- gate. Reagents are shown in supplementary Table 1. Cells were detected using the BD FACSCanto II, BD LSRFortessa or BD Accuri C6 and analyzed with BD FACSDiva and FlowJo (9.3.2) software.

#### b. Platelets

Dilute whole-blood (25  $\mu$ L) or washed platelets ( $1 \times 10^6$  cells/sample) were incubated in dark for 30 minutes with Anti-Annexin V (640905, Biolegend), Anti-GPVI FITC (M011-1), Anti-Integrin  $\alpha 2$  FITC (M071-1), Anti-P-selectin FITC (CD62P), and Anti-active  $\alpha$ IIb $\beta$ 3 PE (JON/A, D200), Anti-GP $\alpha$ IIb PE (CD42b, M040-2) antibodies provided by Emfret Analytics, or Anti-GP $\alpha$ IIb CD41 FITC (553848; BD Biosciences). In some experiments washed platelets were stimulated with 0.1, 0.05 and 0.025 U/mL of thrombin (605195, Sigma Aldrich). All the analysis of the experiments with antibody incubation were performed referred to an unbinding control IgG FITC (sc-2340) or IgG PE (sc-2871), provided by Santa Cruz Biotechnology, Inc. For calcium measurement PRP was incubated with 2.5  $\mu$ M Fluo-4 AM (Life Technologies, Italy) for 30 minutes. Samples were measured by FACSCalibur flow cytometer and CellQuest software (Becton Dickinson).

### **5. Calcium Imaging experiments**

Washed platelets were loaded with 5  $\mu$ M Fura-2 AM (Life technologies, Italy) for at least 45 minutes and plated onto poly-L-lysine (P4832, Sigma-Aldrich)-coated glass coverslips for at least 30 minutes at RT. Calcium measurements were performed as previously described<sup>19</sup>.

### **6. Adhesion**

Washed platelets ( $2 \cdot 10^8$  cells/mL) were plated for 15 or 30 minutes on 13 mm glass coverslips coated with type I collagen or 0.5% BSA/PBS for 2 h at 37  $^{\circ}$ C,. Platelets were fixed with 3% paraformaldehyde-4% sucrose in PBS for 5 minutes at RT, permeabilized by 0.2% Triton-X100 for 5 minutes, and saturated with 2% BSA in PBS for 15 minutes. Platelets were stained with Alexa488-phalloidin (#8878; Cell Signalling Technology) for 30 minutes in the dark. Coverslips were washed twice with 0.2% BSA in PBS and mounted with 20% Mowiol<sup>®</sup> 4-88 (81381) and 2.5% Dabco (290734; Sigma Aldrich) in PBS. Platelets were viewed on a confocal microscope (Leica TCS SP2) and digital images (63X) were acquired. The number of adherent cells and the average cell area (index of platelet spreading) were determined using a purposely-developed script suitable for Image-J 2.1.0/1.53c.

### **7. Aggregation**

Washed platelets ( $1 \cdot 10^7$  cells/ml, 250  $\mu$ L) were stimulated at 37  $^{\circ}$ C with the indicate agonists in the presence of 1 mM MgCl<sub>2</sub> and aggregation was monitored for at least 5 min in CHRONO-LOG lumi-aggregometer. The analysis was performed using AggroLink CHRONO-LOG Software.

### **8. Study design of *in vivo* experiments**

Thirty-two 12-week-old mice (16 WT and 16 KI-STIM1<sup>1115F</sup>) were randomly distributed in four groups following sex, weight (27 - 28 g for WT and 23 - 24 g for KI-STIM1<sup>1115F</sup> mice) and platelet number (6.0 - 6.2·10<sup>8</sup> /mL for WT and 2.4 - 2.7·10<sup>8</sup> /mL for KI-STIM1<sup>1115F</sup> mice) evaluation.

Each strain, further divided in two subgroups, was anesthetized and Alzet osmotic minipumps (model 1002; volume: 100 µL; infusion rate: 0.25µL/h; duration: 2 weeks) were filled with saline vehicle or CIC-39Na (60 mg/kg, dissolved in saline) and implanted intraperitoneally. Before implantation, the minipumps were incubated in saline solution at 37 °C overnight.

Since KI-STIM1<sup>1115F</sup> mice did not show gender differences in penetrance of platelet disorders<sup>19</sup>, both sexes were considered for these *in vivo* treatments (Supplementary Table 2).

Each mouse was placed in a separate cage and its health impact was monitored twice a day for all the experimental period (30 days). All experimental procedures are summarized in **Figure 5A**. The hypothesis of the experiment was at least a 75% increase in platelet number at day 15 with an alpha error of 5% and a power of 80%. This led to groups of at least 5 animals. Not knowing the safety of the compound, it was decided to raise the group size to 8 animals.

#### **9. Platelet count in *in vivo*-treated mice**

Blood was drawn 48 h before and 5, 10, 12, 15, 22, 30 days after minipump implantation. Platelet count was determined as previously described<sup>19</sup> with the exception that the executor of the platelet count was blinded of group assignment.

#### **10. Tail bleeding assay and red blood detection**

15 and 30 days after minipump implantation, WT and KI-STIM1<sup>1115F</sup> mice were weighed, anesthetized, and placed in prone position. 2 mm of the tail tip was amputated and the tail, positioned vertically, was immersed in a falcon contained 14 mL of saline solution at 37 °C for 10 minutes. The precise bleeding time was calculated using a stop clock. If bleeding interruptions and resumes occurred, the sum of bleeding times over 10 minutes was calculated. At the end of the 10 minutes, the experiment was stopped, the tail was cauterized to stop bleeding. To determine blood loss, the falcon tube was centrifuged at 1000 RPM for 5 minutes at RT, supernatant was removed, and erythrocytes were resuspended in 300 µL of double-distilled water. The optical density of the resulting solution was then determined using a spectrophotometer (Victor<sup>3</sup> PerkinElmer) at 570 nm. At the end of experiment, animals were sacrificed by cervical dislocation.

#### **11. Evaluation of CIC-39Na plasma levels**

Blood was drawn 24 h before and 5, 10, 15, 22, 30 days after minipump implantation. 100 µL of blood extracted from the submandibular vein were mixed with 50 µL of EDTA solution (Sigma- Aldrich, Italy) and processed as follow. Aliquots of plasma samples (50 µL) were diluted by adding 50 µL of IS (BIP29Na final

concentration 100 µg/L) and 100 µL of acetonitrile. Samples were homogenized and centrifuged at 13,000 x g for 10 min, and supernatants (5 µL) were injected into LC-ESI-HRMS system. Plasma calibration standards were prepared using the same procedure by spiking the appropriate amount of CIC-39Na DMSO working solutions into blank plasma aliquots. The calibration curves ( $y = ax + b$ ), were constructed from the peak area versus plasma concentration using the weighted ( $1/x$ ) linear least-squares regression method (calibration range 1–10000 µg/L).

## **12. Statistical analysis**

The normality of data distributions was assessed using Shapiro–Wilk or KS normality tests. Data are presented as mean  $\pm$  SEM or median  $\pm$  IQR. Parametric (unpaired t-test and One-way analysis of variance (ANOVA) followed by Tukey’s post-hoc) or non-parametric (Mann-Whitney U test and One-way Kruskal-Wallis H test followed by Dunn’s post-hoc) statistical analysis were used for comparisons of data. All statistical assessments were two-sided and a value of  $P < 0.05$  was considered statistically significant. Statistical analyses were performed using GraphPad Prism software (GraphPad Software, Inc., USA).

For original data, please contact: [armando.genazzani@uniupo.it](mailto:armando.genazzani@uniupo.it)



## Results and discussion

### Thrombocytopenia drives an increased progenitor activity in the bone marrow

**Figure 1A** (left) confirms our previous findings<sup>19</sup> that KI-STIM1<sup>1115F</sup> mice display a significantly reduced number of platelets compared to WT animals. We therefore decided to investigate whether an alteration of haematopoietic progenitor differentiation was at the origin of the observed thrombocytopenia. To do so, we evaluated the frequency of the lymphoid progenitor population LSK, of the common myeloid progenitors (CMP), of the granulocyte-macrophage progenitors (GMP) and of the megakaryocyte-erythroid progenitors (MEP) within the bone marrow of WT and KI-STIM1<sup>1115F</sup> mice. As represented in **Figure 1B**, we observed a significant increase in the frequency of LSK stem cell compartment in KI-STIM1<sup>1115F</sup>. Within LK cells, the frequency of CMP was not different among WT and KI-STIM1<sup>1115F</sup> mice, however the latter group showed increased GMP paralleled by decreased MEP. Overall, the data would therefore suggest that there is either a defect in differentiation in the megakaryocyte lineage in KI-STIM1<sup>1115F</sup> mice or that the thrombocytopenia drives a positive feedback on stem cells and progenitors. As red cells are the other final progeny of CMP, we decided to investigate the haematocrit of KI-STIM1<sup>1115F</sup> mice, but no statistical difference could be observed and, on the contrary, a slight increase in red blood cells in KI-STIM1<sup>1115F</sup> is noticeable (**Figure 1A**, right). None of the previous studies on mice had evaluated haematopoietic precursors and therefore no comparison can be made. Nonetheless, our data would appear to show that thrombocytopenia is not mainly arising from a defect originating in the bone marrow but to higher use of the megakaryocyte lineage. This would be in accord with the higher platelet turnover that has been reported in STIM1<sup>Sax/+</sup> mice<sup>22</sup>.

### KI-STIM1<sup>1115F</sup> mice show an increased activation and aggregation

We next analyzed platelet activation. Hence, we measured the plasma membrane expression of two platelet identifying markers (CD1 and CD42b) and then the main platelet receptors in resting conditions (**Figure 2A**): integrin  $\alpha 2$ , GPVI, P-selectin and active  $\alpha \text{IIb}\beta 3$ . We found a decreased expression of integrin  $\alpha 2$  and an increased exposure of P-selectin and active  $\alpha \text{IIb}\beta 3$  in KI-STIM1<sup>1115F</sup> platelets. This is accord to the report that basal P-selectin and active  $\alpha \text{IIb}\beta 3$  in STIM1<sup>Sax/+</sup> animals are increased<sup>22</sup> and led us to speculate that circulating platelets in KI-STIM1<sup>1115F</sup> mice are pre-activated. Pre-activation in KI-STIM1<sup>1115F</sup> platelets can lead to (i) unresponsiveness or (ii) hyper-responsiveness. In order to distinguish between these two, we measured P-selectin and active  $\alpha \text{IIb}\beta 3$  exposure upon stimulation with thrombin (**Figure 2B, 2C**). Hyper-exposure of both P-selectin and active  $\alpha \text{IIb}\beta 3$  in KI-STIM1<sup>1115F</sup> platelets was evident under basal conditions as well as at the lower concentrations of thrombin tested (0.0025 U/mL and 0.025 U/mL) while smaller or no differences were evident at higher concentrations (0.1 U/mL). When analyzing in detail the co-exposure of the two markers, we noticed that a small sub-population of KI-STIM1<sup>1115F</sup> platelets expose only active  $\alpha \text{IIb}\beta 3$  under basal and stimulated conditions (**Figure 2B**). This is also evident in STIM1<sup>Sax/+</sup> <sup>22</sup>suggesting that the majority of KI-

STIM1<sup>115F</sup> platelets are hyper-responsive, but a small percentage (around 10%) of KI-STIM1<sup>115F</sup> platelets are unable to undergo full activation.

We next evaluated what could the functional consequences be of the above changes in terms of adhesion and aggregation. **Figure 3A** shows the number and the area of adhered platelets measured on collagen type I coated-glass coverslips after 15 and 30 minutes. No large differences could be observed, although the area of adhesion after 30 minutes was significantly larger in KI-STIM1<sup>115F</sup> platelets, suggesting an increase in spreading. These results differ from those reported in STIM1<sup>Sax/+</sup> platelets, where adhesion in a perfusion test demonstrated that platelets were unable to adhere<sup>22</sup>. We next proceeded to explore aggregation induced by thrombin (0.1 U/mL and 0.05 U/mL). At high thrombin concentrations, there was no difference in the maximal aggregation (aggregation; **Figure 3B**) but KI-STIM1<sup>115F</sup> platelets aggregated slower (slope; **Figure 3B**). At sub-maximal thrombin concentrations (0.05 U/mL), the slope was similar between the two groups but more aggregation occurred.

### **Ca<sup>2+</sup>-signaling is at the basis of the platelet dysfunction**

As mentioned in the introduction, in one of the TAM mouse models<sup>20</sup>, the number of platelets was found normal and this was associated with a significantly reduced STIM1 expression. We next evaluated the level of STIM1 in KI-STIM1<sup>115F</sup> platelets. As shown in **Figure 4A**, by Western blotting we observed that STIM1 was significantly reduced with no concurrent decrease in ORAI1. Given that the platelets collected from KI-STIM1<sup>115F</sup> mice are significantly reduced, these data might suggest that circulating platelets belong to those clones that express the least amount of STIM1, as the others most likely either aggregated or underwent cell death.

Although conscious of looking only at a sub-population, we nonetheless decided to explore Ca<sup>2+</sup>-signaling. We have previously shown that in myotubes from patients affected by TAM there is an increased basal cytosolic Ca<sup>2+</sup><sup>19,30</sup>. In order to evaluate whether this occurs also in platelets, we determined basal calcium by Fluo-4 and indeed found a significant increase in fluorescence, showing that basal Ca<sup>2+</sup> was elevated in these cells (**Figure 4B**). An increased Ca<sup>2+</sup> could lead to death, but this was not the case since we did not find an increase in membrane phosphatidylserine exposure (**Supplemental Figure 1**), a well-known biomarker of cell death<sup>31</sup> at least in the circulating population. Enhanced basal calcium and absence of difference in phosphatidylserine exposure were also seen in other TAM models<sup>20,22</sup>. It is possible, despite we have no evidence of this, that higher STIM1-expressing platelets indeed undergo cell death.

We then evaluated the Ca<sup>2+</sup>-responses to thrombin. As shown in **Figure 4C**, in KI-STIM1<sup>115F</sup> platelets the response to thrombin was potentiated, in analogy to the results obtained in receptor exposure experiments (**Figure 2C**). Despite this, when Ca<sup>2+</sup> was added to the extracellular medium to unmask thrombin-induced SOCE, KI-STIM1<sup>115F</sup> platelets showed a lower influx of Ca<sup>2+</sup> in comparison to WT. This is similar to the results

described on STIM1<sup>Sax/+</sup> platelets<sup>22</sup>, where thapsigargin-induced SOCE was lower compared to WT, and might be attributable to the increased release induced by thrombin, to an incomplete store filling attributable to a STIM-mediated Ca<sup>2+</sup>-leak or to the lower expression of STIM1.

### **SOCE inhibition leads to reversal of the platelet defects in KI-STIM1<sup>I115F</sup> mice**

TAM is a monogenic disorder and the above data strengthen the notion that the over-activation of SOCE is responsible for thrombocytopenia. It could therefore be postulated that counteracting the pathological activity of STIM1 with a negative SOCE modulator could restore the defect. To explore this, we made use of CIC-39Na, which we have previously shown to have an IC<sub>50</sub> of around 800 nM at inhibiting SOCE in HEK cells and a good aqueous solubility. We also evaluated whether CIC-39Na was able to inhibit SOCE triggered by the STIM1 p.I115F mutation by using myotubes from 6-month old KI-STIM1<sup>I115F</sup> mice. Indeed, this was the case with an IC<sub>50</sub> of around 1 μM (SOCE inhibition at 1 μM = 49.8 ± 3.6 and at 3 μM = 77.3 ± 4.8). For this proof-of-principle experiment, we decided to intraperitoneally implant minipumps that allowed to have a constant infusion of CIC-39Na for about 2 weeks, thereby reducing animal manipulation. Preliminary experiments showed that a dose of 60 mg/Kg/day *i.p.* was tolerated by mice for two weeks and we therefore aimed to deliver a similar amount per day *via* infusion. To monitor pump efficiency, blood samples were taken from treated WT and KI-STIM1<sup>I115F</sup> mice at day 5, 10, 15, 22 and 30 (**Figure 5A**). The average plasma drug concentration found when pooling data from day 5, 10 and 15 (in which the drug is supposed to be released) was 251 μg/L corresponding to 625 ± 89 nM, below the estimated IC<sub>50</sub>. Animals were kept for a further 15 days and, during this time, drug concentrations dropped time-dependently to 97 ± 48 nM at day 22 and 9.7 ± 2.1 nM at day 30. Treatments were well tolerated and animals did not show any visible sign of suffering. To strengthen this, usually KI-STIM1<sup>I115F</sup> mice are characterized by small weight, and treated animals instead gained weight compared to their controls (**Supplemental Figure 2**).

As shown in **Figure 5B**, treatment of WT mice with CIC-39Na led to a small but significant increase in platelet count at day 5 that recovered in the following determinations. Treatment of KI-STIM1<sup>I115F</sup> mice led to a striking increase in platelet number at 5 days which was maintained up to 15 days. This was paralleled by a significant decrease in blood loss compared to its control (**Figure 5C**) and to a significant decrease in bleeding time (**Figure 5D**). After 30 days, in which drug release from the pump was significantly reduced, platelet number showed a significant drop from the peak (**Figure 5B**), and, similarly, blood loss (**Figure 5C**) and bleeding time (**Figure 5D**) were increased.

In conclusion, TAM is a monogenic disorder and therefore we tested whether blunting the activity of SOCE, the altered signaling pathway, could counteract thrombocytopenia. Indeed, we found that chronic administration of a SOCE inhibitor is able to normalize platelet count and bleeding. Our results have important repercussions. First, we have paved the way for a treatment strategy for the platelet disorder

which affects more than half of the sufferers of this ultra-rare disorder. While we have tested a compound which is still in preclinical evaluation, there are compounds that are already in clinical trials for other indications that could be re-purposed to this aim with an appropriate clinical trial. Second, given the observation that a SOCE-mediated dysfunction is amenable of intervention with a SOCE inhibitor, this finding is the prelude to testing this or other compounds also for the muscular component of TAM. Importantly, given that TAM is a slowly-progressive disease, clinical trials with hard muscular end-points could be challenging. Were preclinical models to show a correlation between platelet number and muscle phenotype amelioration, improvement of thrombocytopenia could therefore be used as a valid, relevant biomarker of efficacy, thereby facilitating clinical trial design.

## **Acknowledgements**

The present study was supported by research funding from the Italian Telethon Foundation to Armando Genazzani. PoC instrument funding from LINKS Foundation and Compagnia di San Paolo, PoC UPO-Regione Piemonte art. 12 L.R. n. 4 05/04/2018 to Beatrice Riva.

The authors wish to thank ChemiCare S.R.L. for providing CIC-39Na.

## **Authorship Contributions**

A.A.G and A.B. contributed equally in supervision, A.A.G. provided funding. A.A.G, A.B, and C.C-S. conceived the design of experiments. C.C-S., E.P., N.C., B.R., F.A.R., P.P., N.F., I.Z., M.S., M.P.C., S.S., T.P. performed experiments and analysed the results. A.A.G and C.C-S. wrote the manuscript. All authors have given approval to final version of manuscripts.

## **Disclosure of Conflicts of Interest**

B.R. is an employer of Chemicare, of which she also owns stocks. T.P. owns stocks of Chemicare, a company that owns the rights to CIC-39Na. All other Authors have no competing interests.

## **References**

1. Berna-Erro A, Redondo PC, Rosado JA. Store-Operated Ca<sup>2+</sup> Entry. Vol 740.; 2012. doi:10.1007/978-94-007-2888-2\_15
2. Putney JW. Origins of the concept of store-operated calcium entry. *Front Biosci.* 2011;S3(1):980. doi:10.2741/202
3. Prakriya M, Lewis RS. Store-operated calcium channels. *Physiol Rev.* 2015;95(4):1383-1436. doi:10.1152/physrev.00020.2014
4. Liou J, Kim ML, Heo WD, et al. STIM is a Ca<sup>2+</sup> sensor essential for Ca<sup>2+</sup>-store-depletion-triggered Ca<sup>2+</sup> influx. *Curr Biol.* 2005;15(13):1235-1241. doi:10.1016/j.cub.2005.05.055
5. Soboloff J, Spassova MA, Tang XD, Hewavitharana T, Xu W, Gill DL. Orai1 and STIM reconstitute store-operated calcium channel function. *J Biol Chem.* 2006;281(30):20661-20665. doi:10.1074/jbc.C600126200
6. Lacruz RS, Feske S. Diseases caused by mutations in ORAI1 and STIM1. *Ann N Y Acad Sci.* 2015;1356(1):45-79. doi:10.1111/nyas.12938
7. Schiaffino S. Tubular aggregates in skeletal muscle: Just a special type of protein aggregates? *Neuromuscul Disord.* 2012;22(3):199-207. doi:10.1016/j.nmd.2011.10.005
8. Ticci C, Cassandrini D, Rubegni A, et al. Expanding the clinical and genetic spectrum of pathogenic variants in STIM1. *Muscle Nerve.* Published online August 26, 2021. doi:10.1002/mus.27391

9. Silva-Rojas R, Laporte J, Böhm J. STIM1/ORAI1 Loss-of-Function and Gain-of-Function Mutations Inversely Impact on SOCE and Calcium Homeostasis and Cause Multi-Systemic Mirror Diseases. *Front Physiol.* 2020;11. doi:10.3389/fphys.2020.604941
10. Morin G, Biancalana V, Echaniz-Laguna A, et al. Tubular aggregate myopathy and Stormorken syndrome: Mutation spectrum and genotype/phenotype correlation. *Hum Mutat.* 2020;41(1):17-37. doi:10.1002/humu.23899
11. White JG, Ahlstrand GG. Giant electron dense chains, clusters and granules in megakaryocytes and platelets with normal dense bodies: an inherited thrombocytopenic disorder III. Platelet analytical electron microscopy. *Platelets.* 2003;14(5):305-312. doi:10.1080/0953710031000137046
12. Markello T, Chen D, Kwan JY, et al. York platelet syndrome is a CRAC channelopathy due to gain-of-function mutations in STIM1. *Mol Genet Metab.* 2015;114(3):474-482. doi:10.1016/j.ymgme.2014.12.307
13. Roman J, Palmer MI, Palmer CA, Johnson NE, Butterfield RJ. Myopathy in the York Platelet Syndrome: An Underrecognized Complication. *Case Rep Pathol.* 2018;2018:5130143. Published 2018 Aug 12. doi:10.1155/2018/5130143
14. Nesin V, Wiley G, Kousi M, et al. Activating mutations in STIM1 and ORAI1 cause overlapping syndromes of tubular myopathy and congenital miosis. *Proc Natl Acad Sci U S A.* 2014;111(11):4197-4202. doi:10.1073/pnas.1312520111
15. Barone V, Del Re V, Gamberucci A, et al. Identification and characterization of three novel mutations in the CASQ1 gene in four patients with tubular aggregate myopathy. *Hum Mutat.* 2017;38(12):1761-1773. doi:10.1002/humu.23338
16. Böhm J, Lornage X, Chevessier F, et al. CASQ1 mutations impair calsequestrin polymerization and cause tubular aggregate myopathy. *Acta Neuropathol.* 2018;135(1):149-151. doi:10.1007/s00401-017-1775-x
17. Gresele P, Lopez JA, Kleiman NS, Page CP. Platelets in thrombotic and non-thrombotic disorders: Pathophysiology, pharmacology and therapeutics: An update. *Platelets Thromb Non-Thrombotic Disord Pathophysiol Pharmacol Ther an Updat.* Published online 2017:1-1445. doi:10.1007/978-3-319-47462-5
18. Gilio K, Van Kruchten R, Braun A, et al. Roles of platelet STIM1 and orai1 in glycoprotein VI- and thrombin-dependent procoagulant activity and thrombus formation. *J Biol Chem.* 2010;285(31):23629-23638. doi:10.1074/jbc.M110.108696
19. Cordero-Sanchez C, Riva B, Reano S, et al. A luminal EF-hand mutation in STIM1 in mice causes the clinical hallmarks of tubular aggregate myopathy. *DMM Dis Model Mech.* 2020;13(2). doi:10.1242/dmm.041111

20. Gamage TH, Gunnes G, Lee RH, et al. STIM1 R304W causes muscle degeneration and impaired platelet activation in mice. *Cell Calcium*. 2018;76(October):87-100. doi:10.1016/j.ceca.2018.10.001
21. Silva-Rojas R, Treves S, Jacobs H, et al. STIM1 over-activation generates a multi-systemic phenotype affecting the skeletal muscle, spleen, eye, skin, bones and immune system in mice. *Hum Mol Genet*. 2019;28(10):1579-1593. doi:10.1093/hmg/ddy446
22. Grosse J, Braun A, Varga-Szabo D, et al. An EF hand mutation in Stim1 causes premature platelet activation and bleeding in mice. *J Clin Invest*. 2007;117(11):3540-3550. doi:10.1172/JCI32312
23. Omuro A, Beal K, Mcneill K, et al. JOURNAL OF CLINICAL ONCOLOGY Multicenter Phase IB Trial of Carboxamidotriazole Orotate and Temozolomide for Recurrent and Newly Diagnosed Glioblastoma and Other Anaplastic Gliomas. *J Clin Oncol*. 2018;36:1702-1709. doi:10.1200/JCO
24. Gerasimenko JV, Gryshchenko O, Ferdek PE, et al. Ca<sup>2+</sup> release-activated Ca<sup>2+</sup> channel blockade as a potential tool in antipancreatitis therapy. *Proc Natl Acad Sci U S A*. 2013;110(32):13186-13191. doi:10.1073/pnas.1300910110
25. Miller J, Bruen C, Schnaus M, et al. (2020). Auxora versus standard of care for the treatment of severe or critical COVID-19 pneumonia: Results from a randomized controlled trial. *Critical Care*, 2020;24(1):1–9. doi:10.1186/s13054-020-03220-x
26. Bruen C, Miller J, Wilburn J, et al. Auxora for the Treatment of Patients with Acute Pancreatitis and Accompanying Systemic Inflammatory Response Syndrome: Clinical Development of a Calcium Release-Activated Calcium Channel Inhibitor. *Pancreas*. 2021;50(4):537-543. doi:10.1097/MPA.0000000000001793
27. Barde PJ, Viswanadha S, Veeraghavan S, Vakkalanka S V., Nair A. A first-in-human study to evaluate the safety, tolerability and pharmacokinetics of RP3128, an oral calcium release-activated calcium (CRAC) channel modulator in healthy volunteers. *J Clin Pharm Ther*. 2021;46(3):677-687. doi:10.1111/jcpt.13322
28. Rahman S, Rahman T. Unveiling some FDA-approved drugs as inhibitors of the store-operated Ca<sup>2+</sup> entry pathway. *Sci Rep*. 2017;7(1):12881. Published 2017 Oct 16. doi:10.1038/s41598-017-13343-x
29. Serafini M, Cordero-Sanchez C, Di Paola R, et al. Store-Operated Calcium Entry as a Therapeutic Target in Acute Pancreatitis: Discovery and Development of Drug-Like SOCE Inhibitors. *J Med Chem*. 2020;63(23):14761-14779. doi:10.1021/acs.jmedchem.0c01305
- Garibaldi M, Fattori F, Riva B, et al. A novel gain-of-function mutation in ORAI1 causes late-onset tubular aggregate myopathy and congenital miosis. *Clin Genet*. 2017;91(5):780-786. doi:10.1111/cge.12888
30. Garibaldi M, Fattori F, Riva B, et al. A novel gain-of-function mutation in ORAI1 causes late-onset tubular aggregate myopathy and congenital miosis. *Clin Genet*. 2017;91(5):780-786. doi:10.1111/cge.12888

31. Schoenwaelder SM, Yuan Y, Josefsson EC, et al. Two distinct pathways regulate platelet phosphatidyserine exposure and procoagulant function. *Blood*. 2009;114(3):663-666. doi:10.1182/blood-2009-01-200345

### **Abbreviations**

CMP: common myeloid progenitors

EMA: European Medicines Agency

FDA: Food and Drug Administration

GMP: granulocyte-macrophage progenitor

IP<sub>3</sub>R: inositol-1,4,5,-triphosphate receptor

MEP (Megakaryocyte-erythroid progenitor).

PRP: Platelet-rich plasma

TAM: Tubular aggregate myopathy.

SOCE: Store-Operated Ca<sup>2+</sup>-Entry

### **Figure Legends**

**Figure 1. Blood and progenitor characterization of WT and KI-STIM1<sup>I115F</sup> mice.** (A) Circulating number of platelets and erythrocytes; Unpaired t-test (WT n=7 and KI-STIM1<sup>I115F</sup> n=12; p-value; \*\*\*=0.0002); Mann-Whitney U test (WT n=7 and KI-STIM1<sup>I115F</sup> n=6), respectively. (B) Frequency of the indicated progenitor cells; Mann-Whitney U test (WT n=6 and KI-STIM1<sup>I115F</sup> n=7; p value: \*\*=0.0120; \*=0.0221).

**Figure 2. Membrane receptors in WT and KI-STIM1<sup>I115F</sup> platelets.** (A) Basal exposure of the indicated membrane receptors; Unpaired t-test (WT n=6 and KI-STIM1<sup>I115F</sup> n=7; p value: \*\*≤0.0074, \*=0.0319); (B) Representative flow cytometry results upon thrombin stimulation; (C) Thrombin dose-Response in WT and KI-STIM1<sup>I115F</sup> mice. Data represent percentage of fluorescence of the response obtained in WT with 0.1 u/ml of thrombin. Mann-Whitney U test (WT and KI-STIM1<sup>I115F</sup> n=3-5; p-value: \*\*\*=0.0005, \*\*=0.0017, \*≤0.0419)

**Figure 3. Adhesion and aggregation of WT and KI-STIM1<sup>I115F</sup> platelets.** (A) Number and area of adhered platelets. Unpaired Mann-Whitney test (15': WT n= 6 and KI-STIM1<sup>I115F</sup> n= 4; 30': WT n= 6 and KI-STIM1<sup>I115F</sup> n= 4); p value: p value: \*\*\*\*<0.0001); (B) Amount and speed of platelet aggregation. Unpaired t-test (THR 0.1 u/ml: WT and KI-STIM1<sup>I115F</sup> n= 5; THR 0.05 u/ml: WT and KI-STIM1<sup>I115F</sup> n= 4; p value: \*\*=0.0039); Unpaired t-test (Both THR (thrombin) 0.1 u/ml and THR 0.05 u/ml: WT and KI-STIM1<sup>I115F</sup> n= 4; p-value: \*\*=0.0044).

**Figure 4. Ca<sup>2+</sup>-signaling in WT and KI-STIM1<sup>I115F</sup> platelets.** (A) Densitometry analysis of Western blots for STIM1; Unpaired t-test (WT and KI-STIM1<sup>I115F</sup> n=6; p value: \*\*\*\*<0.0001); (B) Resting Ca<sup>2+</sup> in platelets; Unpaired t-test (WT and KI-STIM1<sup>I115F</sup> n=8; p value: \*=0.0257); (C) Ca<sup>2+</sup>-responses to thrombin in platelets;

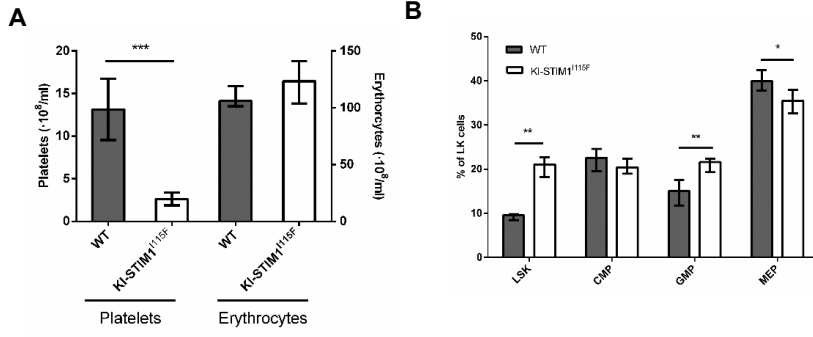


Cells were challenged with thrombin in  $\text{Ca}^{2+}$ -free conditions and then extracellular  $\text{Ca}^{2+}$  was re-added to trigger SOCE. At least 430 platelets from 3 separate mice per group were analyzed in at least 2 different experimental day.

**Figure 5. *In vivo* effect of CIC-39Na in WT and KI-STIM1<sup>115F</sup> mice.**

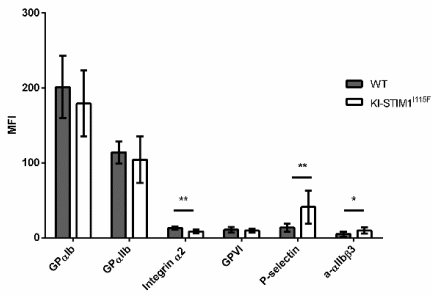
(A) Study design of *in vivo* treatments in WT and KI-STIM1<sup>115F</sup> mice. (B) Platelet count in the four treated groups (WT Vehicle (saline), WT CIC-39Na (60mg/kg), KI-STIM1<sup>115F</sup> Vehicle (saline) and KI-STIM1<sup>115F</sup> CIC-39Na (60mg/kg)). Non parametric Kruskal-Wallis H test followed by Dunn's post-hoc. P-value: \*= 0.0334 for each experimental point vs WT Vehicle. p value: #=0.0154, ##=0.016; ###=0.0001 for each experimental point vs KI-STIM1<sup>115F</sup>. (C) Absorbance values relative to blood lost in the four treated groups. Non parametric Kruskal-Wallis H test followed by Dunn's post-hoc. P-value: p value: #=0.0208 for each experimental point vs KI-STIM1<sup>115F</sup>. (D) Bleeding time in mice treated with Vehicle or CIC-39Na. p value: #=0.0304 for each experimental point vs KI-STIM1<sup>115F</sup>. Data reported in B, C, D represent the mean  $\pm$  SEM of 8 animals for each group from two independent experiments.

Figure 1

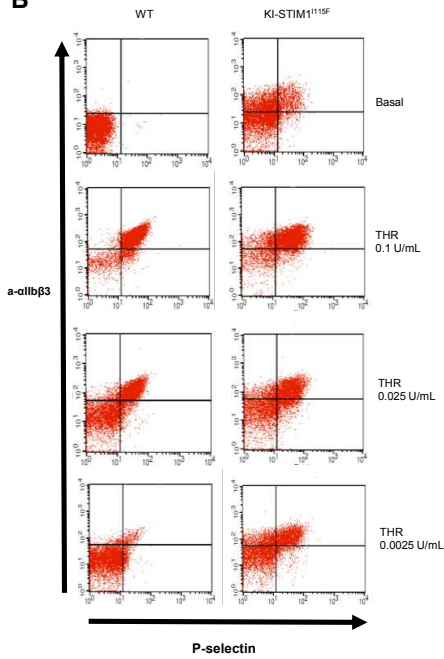


**Figure 2**

**A**



**B**



**C**

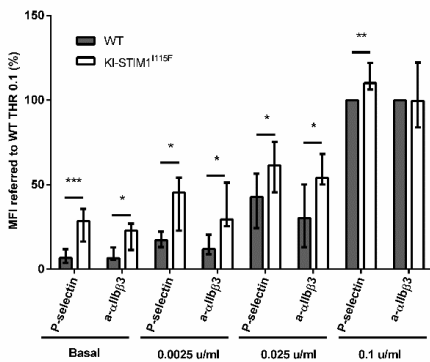
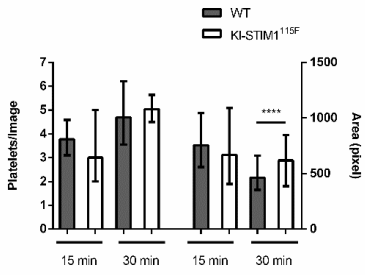
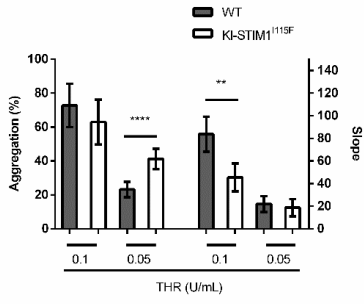


Figure 3

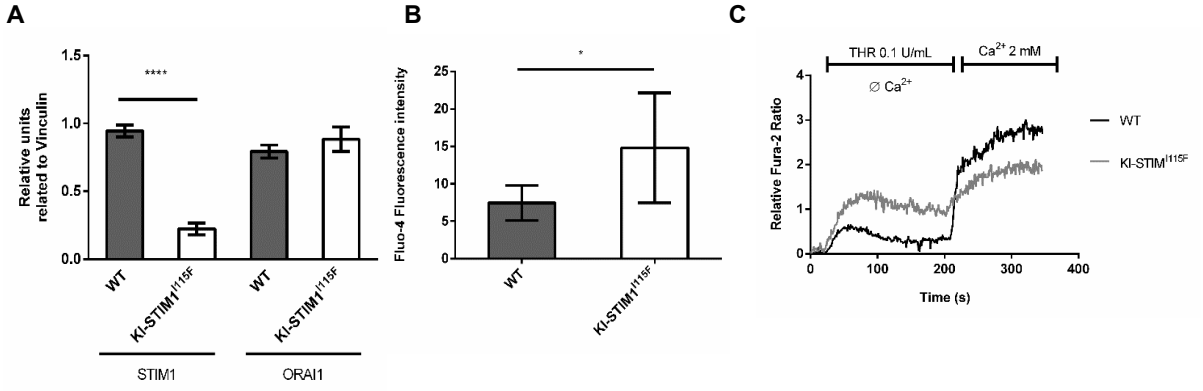
A



B

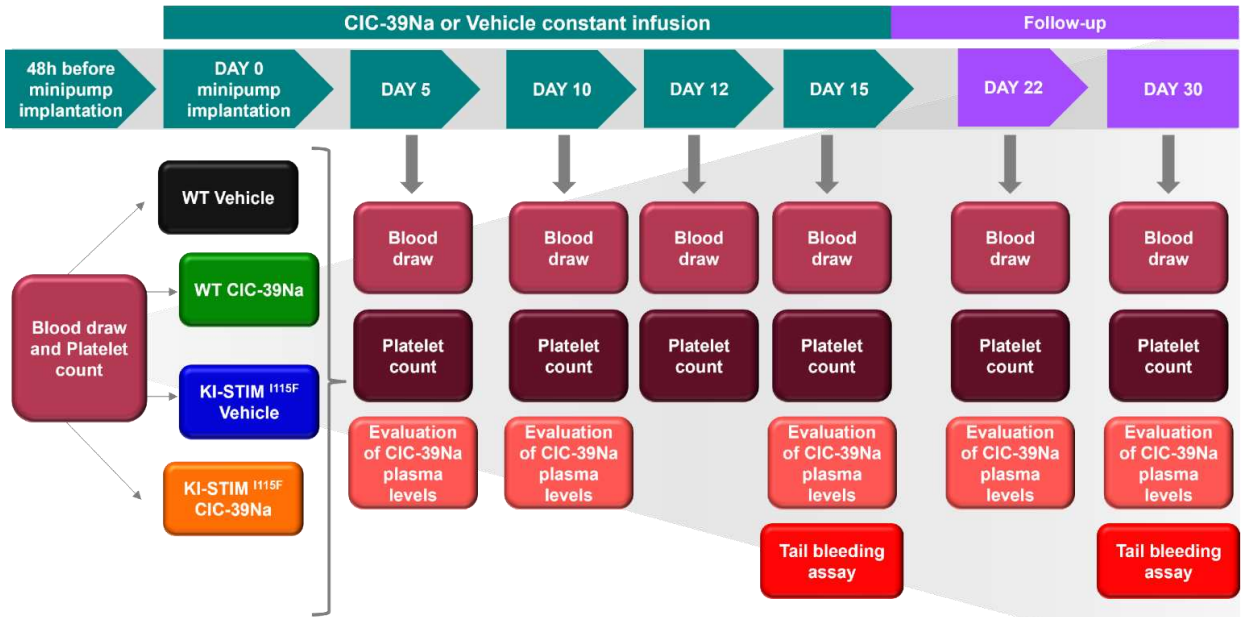


**Figure 4**

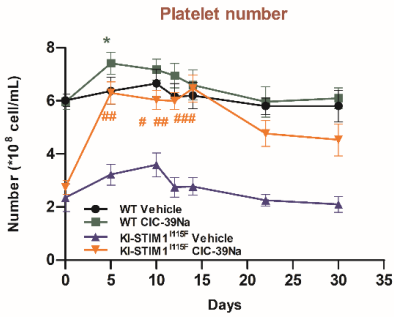


**Figure 5**

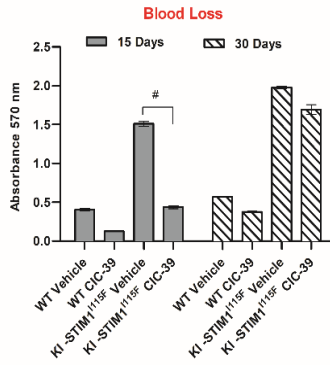
**A**



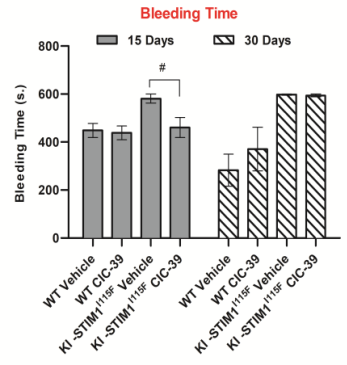
**B**



**C**



**D**



**Supplementary data**

Antibodies		
Name	Company	Clone/Cat. number
CD117 (cKit)	eBioscience	2B8/cat#25-1171-82
CD11b	eBioscience	M1/70/cat#12-0112-85
CD11c	TONBO Biosc.	N418/cat#50-011-U100
CD16/32	eBioscience	93/cat#45-0161-82
CD34	eBioscience	RAM34/cat#11-0341-82
CD3e	TONBO Biosc.	145-2C11/cat#50-0031-U500
CD45R	BD	RA3-6B2/cat#561078
F4/80	TONBO Biosc.	BM8.1/cat#50-4801-U100
Gr-1	eBioscience	RB6-8C5/cat#12-5931-85
IL-7R $\alpha$	eBioscience	SB/cat#199/562959
SCA-1	eBioscience	D7cat#17-5981-83
Ter-119	BD	TER-119/cat#553673

**SupTable1. Reagent table of haematopoietic precursors.**

Groups	Strain	Treatment	N.
1	WT	Saline vehicle	8 (5 male; 3 female)
2	WT	CIC-39Na	8 (5 male; 3 female)
3	KI-STIM1 <sup>I115F</sup>	Saline vehicle	8 (5 male; 3 female)
4	KI-STIM1 <sup>I115F</sup>	CIC-39Na	8 (5 male; 3 female)

**SupTable2. Treatment groups of the study**

## Supp Figure 1

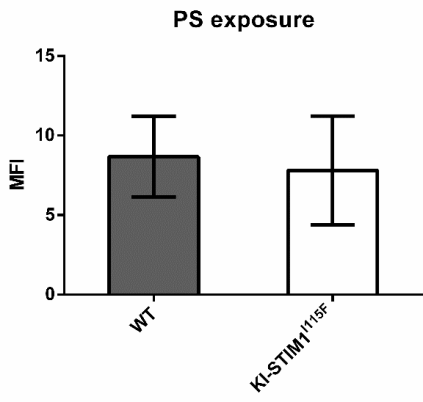


Figure 1.- Phosphatidylserin (PS) exposure by flow cytometry. Unpaired t-test (WT n=7 and KI-STIM1<sup>I115F</sup> n=9)



### **3.b.iii. Authors contribution:**

- ***Celia Cordero-Sanchez:***
  - Designed the experiments. *Ex vivo* experiments. Analysis. Script and figure creation. Writing the draft. Management of the mice colony.
- ***Emanuela Pessolano:***
  - *In vivo* experiment. Management of the mice colony.
- ***Beatrice Riva:***
  - Supported *in vivo* and *ex vivo* experiments.
- ***Nausicaa Clemente:***
  - Supported *in vivo* experiments and supported managing of the mice colony.
- ***Silvio Aprile:***
  - Chemical measurement of compound experiment.
- ***Federico Alessandro Ruffinati:***
  - Analysis. Script creation.
- ***Paola Portararo:***
  - Haematopoietical progenitors experiments.
- ***Nicoletta Filigheddu:***
  - Supported *ex vivo* experiments.
- ***Ivan Zaggia:***
  - Supported *ex vivo* experiments.
- ***Marta Serafini:***
  - Synthesis of the compounds.
- ***Tracey Pirali:***
  - Synthesis of the compounds.
- ***Mario P. Colombo:***
  - Haematopoietical progenitors experiments.
- ***Sabina Sangaletti:***
  - Haematopoietical progenitors experiments.
- ***Alessandra Bertoni:***
  - Designed the experiments. Supervision. Writing the draft.
- ***Armando A. Genazzani:***
  - Designed the experiments. Writing the draft. Supervision. Funding.



## ***4.PART II:***

### ***Development of small molecules***

#### ***a. Screening of putative Store-Operated Calcium Entry inhibitors***



## *i. Synopsis*

### *Aim*

The aim of the present contribution is to identify a lead compound as SOC Entry inhibitor manageable for human use in a chemical library based on Synta66 derivate.

*The main findings of the manuscripts are that:*

- (i) Identification of compound 34 as the lead compound;
- (ii) Compound 34 remarkably reduces SOC Entry at nanomolar concentrations, is selective and not cytotoxic;
- (iii) Compound 34 possess suitable drug pharmacokinetic properties;
- (iv) Compound 34 is effective in an acute pancreatitis mouse model.

### *Key take-home message*

The present contribution demonstrates that the lead compound 34, also known as CIC-39Na, is effective in an *in vivo* model of acute pancreatitis.

### *Personal contribution*

My contribution in this project has been (i) the biological screening performed in the identification of a hit compound and (ii) the *in vivo* sample collecting for pharmacokinetic experiments under the supervision of Prof. Pirali and Prof. Genazzani.



## Store-Operated Calcium Entry as a Therapeutic Target in Acute Pancreatitis: Discovery and Development of Drug-Like SOCE Inhibitors

Marta Serafini, Celia Cordero-Sanchez, Rosanna Di Paola, Irene P. Bhela, Silvio Aprile, Beatrice Purghè, Roberta Fusco, Salvatore Cuzzocrea, Armando A. Genazzani, Beatrice Riva, and Tracey Pirali\*

Cite This: *J. Med. Chem.* 2020, 63, 14761–14779

Read Online

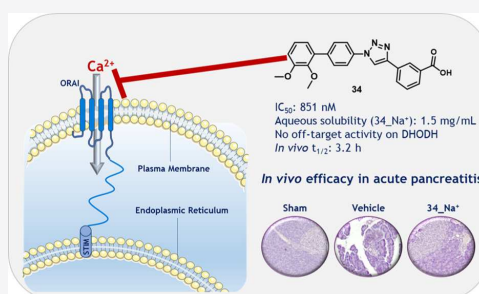
ACCESS |

Metrics &amp; More

Article Recommendations

Supporting Information

**ABSTRACT:** Store-operated calcium entry (SOCE) is important in the maintenance of calcium homeostasis and alterations in this mechanism are responsible for several pathological conditions, including acute pancreatitis. Since the discovery of SOCE, many inhibitors have been identified and extensively used as chemical probes to better elucidate the role played by this cellular mechanism. Nevertheless, only a few have demonstrated drug-like properties so far. Here, we report a class of biphenyl triazoles among which stands out a lead compound, **34**, that is endowed with an inhibitory activity at nanomolar concentrations, suitable pharmacokinetic properties, and *in vivo* efficacy in a mouse model of acute pancreatitis.



## INTRODUCTION

Acute pancreatitis (AP) is an inflammatory life-threatening disorder. It is characterized by autodigestion of the pancreas, which causes inflammation, edema, vacuolization, necrosis, and, in the worst scenario, induces injury of remote extrapancreatic organs. AP represents an urgent and unmet need as it affects about 35 individuals per 100,000 person-years worldwide,<sup>1</sup> with a mortality rate between 1.5 and 4.2%, and no effective pharmacological treatment is available.<sup>1,2</sup>

Among the triggers of AP is an intracellular Ca<sup>2+</sup> overload in pancreatic acinar cells (PACs) that induces the uncontrolled release of intracellular digestive proenzymes. While there are numerous mechanisms that control intracellular Ca<sup>2+</sup> concentrations, store-operated Ca<sup>2+</sup> entry (SOCE) appears to have a pivotal role in the induction of Ca<sup>2+</sup> overload in PACs.<sup>3</sup>

SOCE<sup>4</sup> is represented by the influx of Ca<sup>2+</sup> activated in response to the depletion of the stores from the endoplasmic reticulum (ER)<sup>5</sup> and is associated with the electrophysiological current named *I*<sub>CRAC</sub> (CRAC, calcium release-activated channel).<sup>6</sup> The exact molecular mechanism behind this cellular event was elucidated between 2005 and 2006, when the principal components of SOCE machinery, STIM and Orai, were discovered.<sup>7</sup> At present, three Orai isoforms (Orai1–3) and two STIM isoforms (STIM1–2) are known. STIM is a single-span protein located on the ER membrane and behaves as a sensor: the depletion of ER Ca<sup>2+</sup> stores induces a conformational change of STIM that, after oligomerization, interacts with Orai. The latter is a plasma membrane Ca<sup>2+</sup>

channel that allows for Ca<sup>2+</sup> influx from the extracellular environment, eventually refilling the intracellular Ca<sup>2+</sup> stores.

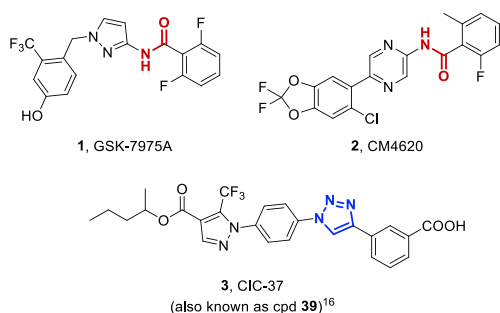
Other crucial proteins known to participate in SOCE are transient receptor potential canonical (TRPC) channels,<sup>8</sup> which were previously believed to be the primary contributors of Ca<sup>2+</sup> rise in PACs and therefore mainly responsible for AP.<sup>5b,9</sup> Yet, more recent studies have demonstrated that the metabolic alcohol products that are among the mediators of acinar cell damage induce the opening of IP<sub>3</sub>Rs, Ca<sup>2+</sup> channels located in the ER, resulting in the depletion of the ER stores and in the activation of STIM1.<sup>10</sup> This event leads to Ca<sup>2+</sup> entry through the Orai1 opening, sustaining toxic intracellular Ca<sup>2+</sup> elevation and pointing to Orai1 as a key culpable for AP damage.<sup>10</sup>

Gerasimenko *et al.* demonstrated that a selective CRAC channel blocker, GSK-7975A (**1**, Figure 1), with no inhibitory activity on TRP-channel currents, is able to decrease the overload of cytosolic Ca<sup>2+</sup> in a concentration-dependent manner and to prevent the activation of the necrotic cell death pathway in both mouse and human PACs,<sup>11</sup> confirming the involvement of Orai in AP and its druggability.

Received: July 27, 2020

Published: November 30, 2020





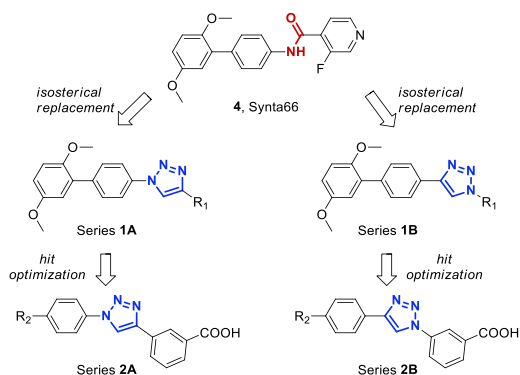
**Figure 1.** Negative modulators of SOCE reported in the literature.

Furthermore, GSK-7975A, together with another SOCE inhibitor, CM4620 (**2**, [Figure 1](#)), were demonstrated to be protective in three different murine models of chemically induced AP.<sup>12</sup> Based on these preclinical evidences, CM4620 has entered clinical trials,<sup>13</sup> with a Phase II trial for AP already completed and an ongoing Phase I/II trial for a rare condition in which AP is triggered by asparaginase treatment (asparaginase-associated AP). This rare condition (incidence between 7 and 18%) is a well-known complication of childhood acute lymphoblastic leukemia (ALL) treatment that is often responsible for the early discontinuation of drug treatments.<sup>3b</sup> As the increase in  $\text{Ca}^{2+}$  induced by asparaginase and the related necrosis of PACs depend on CRAC channels, recent findings have described the inhibition of CRAC channels as the most promising therapeutic approach in this pathology.<sup>3a,14</sup>

Among the several medicinal chemistry campaigns aimed at developing SOCE inhibitors,<sup>15</sup> in 2018 our research group described a class of SOCE modulators, named pyrtriazoles,<sup>16</sup> that were designed based on a known chemical probe for SOCE, Pyr6.<sup>17</sup> Among the reported compounds, a promising candidate (**3**, [Figure 1](#)) able to significantly ameliorate cerulein-induced AP in rodents without signs of toxicity was identified. Nevertheless, the pharmacokinetic (PK) profile of **3**, with its relatively short half-life (mouse, i.p., 1.3 h) and high volume of distribution (32 L/kg), prompted us to undertake a medicinal chemistry campaign aimed at developing more drug-like SOCE modulators.

Among the previously reported SOCE modulators, **Synta66** (**4**, [Figure 2](#)) is a CRAC channel blocker able to inhibit  $I_{\text{CRAC}}$  with an  $\text{IC}_{50}$  of 1.4–3.0  $\mu\text{M}$ .<sup>18</sup> Although its precise mechanism on SOCE remains unknown, assays performed in siRNA knock-down of Orai1 mast cells have suggested that **Synta66** might be selective for the channel.<sup>18a</sup> Furthermore, experiments in vascular smooth muscle cells have demonstrated that it does not interfere with STIM1 clustering.<sup>19</sup> Thanks to its inhibitory activity toward Orai1, an increasing number of *in vitro* and *in vivo* studies have used **Synta66** as a chemical probe to gain better insight into  $I_{\text{CRAC}}$  biology. Moreover, the compound is selective over a panel of other ion channels or receptors, including  $\text{Ca}^{2+}$  ATPase pump, voltage-gated  $\text{Ca}^{2+}$  and  $\text{Na}^{+}$  channels, and TRPC1/5 channels,<sup>18a,b,19</sup> indicating this molecule as a reliable starting point to develop new SOCE modulators.

In the present contribution, we describe a family of biphenyl triazoles that inhibit SOCE and are endowed with potency in the nanomolar range, good PK profile, and efficacy in



**Figure 2.** Modifications of **Synta66** moieties to synthesize biphenyl triazoles.

counteracting cerulein-induced AP. While the compounds had been initially designed as mere isosteres of **Synta66**,<sup>20</sup> replacement of the arylamide moiety with the triazole ring ([Figure 2](#)) gave unpredictable results in terms of structure–activity relationships (SARs) and unmasked the fact that this represents a completely new class of modulators.

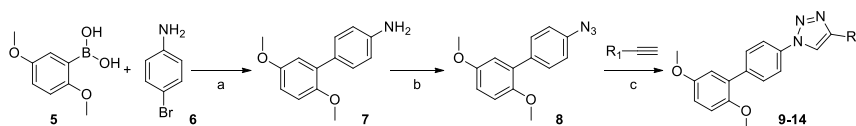
## RESULTS AND DISCUSSION

**SAR Study around 2-Fluoro-4-pyridine Gives Less-Active Compounds Compared to Synta66 on SOCE.** Starting from the structure of **Synta66**, the amide moiety was replaced with a 1,4-disubstituted 1,2,3-triazole ring by a click chemistry approach.<sup>21</sup> To this aim, azide **8** and alkyne **17** were prepared according to [Schemes 1](#) and [2](#). **8** was synthesized starting from (2,5-dimethoxyphenyl)boronic acid and 4-bromoaniline, which reacted in a Suzuki cross-coupling reaction to give intermediate **7**. Compound **7** underwent a diazotization-azidation reaction to afford the desired azide **8** with a yield of 60%. Alkyne **17** was prepared from (2,5-dimethoxyphenyl)boronic acid and 4-bromobenzaldehyde, which, after a Suzuki cross-coupling reaction, gave intermediate **16** that reacted in the presence of Bestmann–Ohira reagent to give **17**.

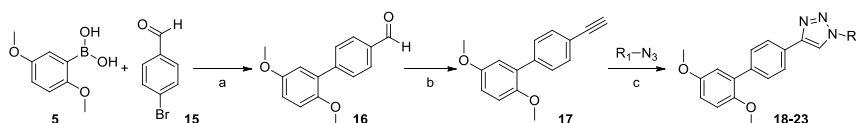
With these two compounds in hand, two click reactions were performed and compounds **9** and **18** ([Table 1](#)), displaying the same substructures as the reference compound **Synta66**, were obtained with a yield of 31 and 60%, respectively. **9** and **18** were tested for activity on SOCE in HEK cells, a human embryonic kidney (HEK) cell line, by fluorescence microscopy, as described elsewhere.<sup>16</sup> After 600 s,  $\text{Ca}^{2+}$  was added and intracellular levels were measured. Compared to **Synta66**, which exhibits an inhibition of  $90.8 \pm 1.7\%$ , compound **18** inhibited SOCE to a smaller extent ( $26.2 \pm 6.5\%$ ), whereas **9** showed a percentage of  $-4.9 \pm 21.3$ , indicating that the molecule slightly increased  $\text{Ca}^{2+}$  entry compared to control ([Table 1](#)). Therefore, the isosterical replacement of the aryl amide moiety with a triazole ring led to active molecules, although the activity was significantly reduced compared to the parent compound **Synta66**.

Prompted by this observation, we decided to investigate the SAR around the 2-fluoro-4-pyridine ring. To this aim, 10 additional molecules were designed and synthesized starting from azide **8** and alkyne **17** that were clicked with five different



Scheme 1. Synthesis of Compounds 9–14 (Series 1A)<sup>42</sup>

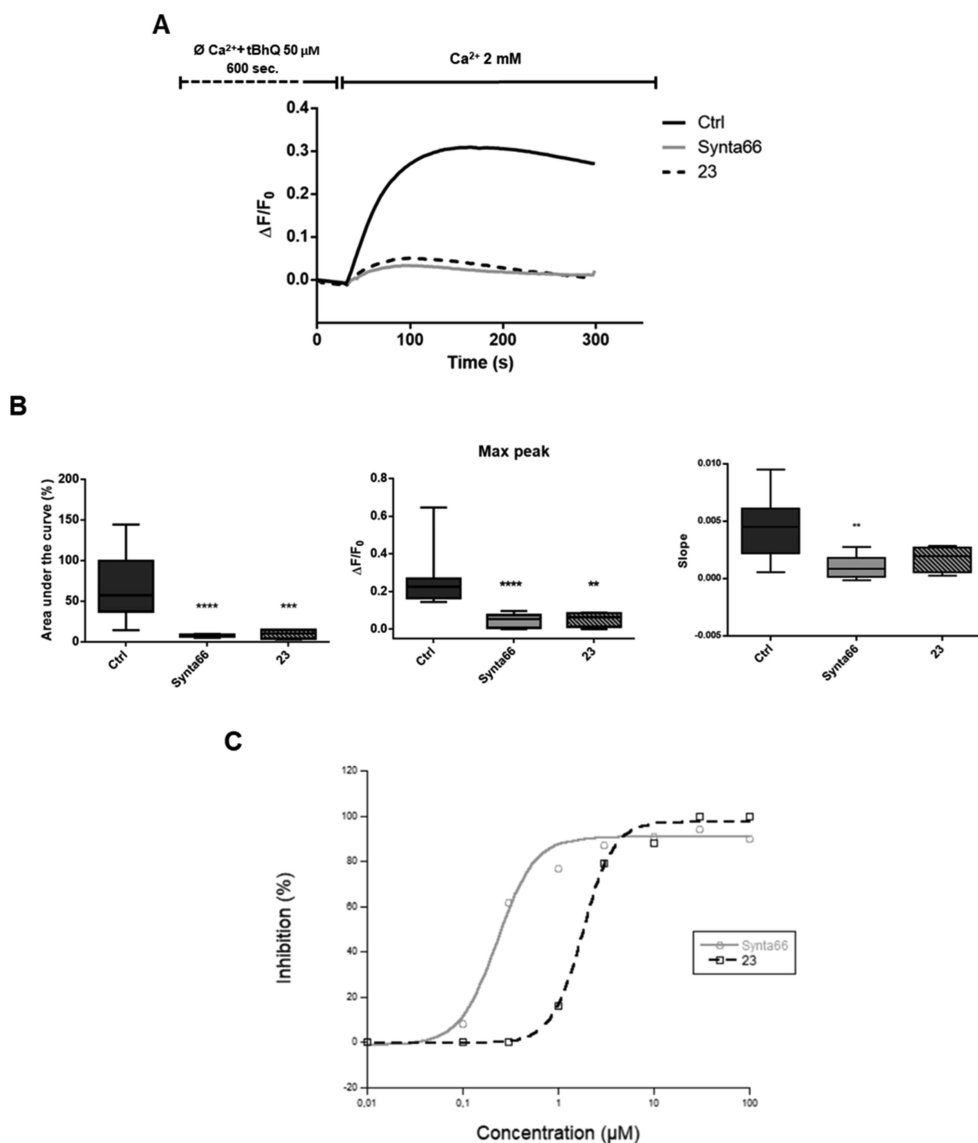
<sup>a</sup>Reagents and conditions: (a)  $K_2CO_3$ ,  $Pd(OAc)_2$ , EtOH, DMF, 80 °C, 3 h, 98%. (b)  $NaNO_2$ ,  $NaN_3$ , HCl,  $H_2O$ , rt, 5 h, 60%. (c) Sodium ascorbate,  $CuSO_4 \cdot 5H_2O$ , *t*-BuOH,  $H_2O$ , 50 °C, 16 h, 31–65%.

Scheme 2. Synthesis of Compounds 18–23 (Series 1B)<sup>42</sup>

<sup>a</sup>Reagents and conditions: (a)  $K_2CO_3$ ,  $Pd(OAc)_2$ , EtOH, DMF, 50 °C, 3 h, 99%. (b) Bestmann–Ohira reagent,  $K_2CO_3$ , MeOH, rt, 18 h, 82%. (c) Sodium ascorbate,  $CuSO_4 \cdot 5H_2O$ , *t*-BuOH,  $H_2O$ , 50 °C, 16 h, 60–99%.

Table 1. First Series of Compounds and Their Biological Activity in HEK Cells

series 1A					series 1B				
Cpd, Yield (%)	R <sub>1</sub>	% SOCE inhibition (10 μM)	% Viability (10 μM)	IC <sub>50</sub> (nM)	Cpd, Yield (%)	R <sub>1</sub>	% SOCE inhibition (10 μM)	% Viability (10 μM)	IC <sub>50</sub> (nM)
4, Synta66	-	90.8 ± 1.7	75.8 ± 8.0	228 ± 33					
9, 31%		-4.9 ± 21.3	-	-	18, 60%		26.2 ± 6.5	-	-
10, 37%		-12.8 ± 14.4	-	-	19, 79%		-1.7 ± 12.6	-	-
11, 65%		-14.0 ± 31.9	-	-	20, 78%		1.2 ± 33.4	-	-
12, 50%		0.0 ± 1.5	-	-			73.5 ± 1.4	-	-
13, 58%		79.9 ± 4.1	-	-	22, 75%		57.2 ± 8.3	-	-
14, 42%		76.2 ± 5.2	-	-	23, 99%		87.8 ± 2.9	71.8 ± 0.5	1790 ± 143

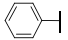
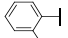
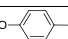
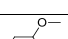
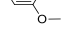
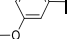
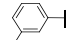
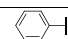
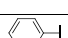
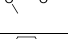
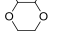
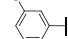
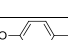
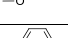


**Figure 3.** Effect of Synta66 (4) and 23 on SOCE in HEK cells. (A) Average Ca<sup>2+</sup>-traces of SOCE in the absence or presence of Synta66 or 23 (10 μM). Traces are the average of 200 cells. (B) Evaluation of the AUC, peak amplitude, and slope of the Ca<sup>2+</sup>-rise of the Ca<sup>2+</sup>-traces in the absence or presence of Synta66 or 23. The graph shows the median and IQR of the AUC, peak amplitude, and slope of the Ca<sup>2+</sup>-rise. Mann–Whitney *U* test of compounds vs control (\*\**p* < 0.0075 \*\*\*\**p* = 0.0002 \*\*\*\**p* < 0.0001). (C) Concentration–response curves of Synta66 and 23.

alkynes and azides, respectively, affording compounds 10–14 (series 1A, Figure 2) and 19–23 (series 1B, Figure 2). All the synthesized triazoles were tested as described above. Five compounds (9, 10, 11, 19, 20) evoked a variable Ca<sup>2+</sup> entry, leading to a remarkable standard error and suggesting that they were not able to reliably inhibit SOCE (Table 1). Moreover, only four molecules (13, 14, 21, 23) out of 12 inhibited SOCE by a considerable level (arbitrarily chosen to be >70%).

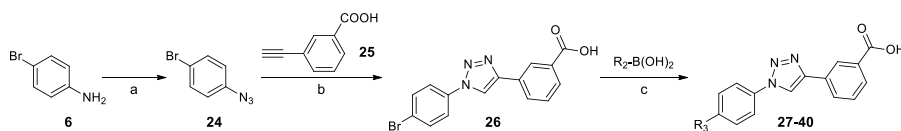
The most active compound, 23 (87.8 ± 2.9% of inhibition) showed an inhibitory activity comparable to Synta66 (90.8 ± 1.7%; Figure 3A). The effects of both compounds on SOCE were characterized analyzing the area under the curve (AUC), peak amplitude, and slope. As shown in Figure 3B, both Synta66 and 23 significantly reduced AUC and peak amplitude compared to control. Whereas only Synta66 showed a significant effect on the slope, it was apparent that also 23 had a similar effect. To determine the IC<sub>50</sub> value, we obtained

Table 2. Second Series of Compounds and Their Biological Activity in HEK Cells

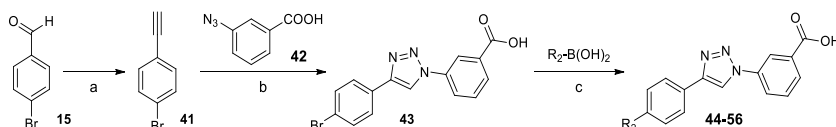
R <sub>2</sub>	series 2A				series 2B			
	Cpd, Yield (%)	% SOCE inhibition (3 μM)	% Viability (10 μM)	IC <sub>50</sub> (nM)	Cpd, Yield (%)	% SOCE inhibition (3 μM)	% Viability (10 μM)	IC <sub>50</sub> (nM)
-	4, Synta66	86.7 ± 3.7	75.8 ± 8.0	228 ± 33				
	27, 55%	51.0 ± 31.9	-	-	44, 55%	1.8 ± 3.1	-	-
	28, 67%	45.9 ± 14.5	-	-	45, 22%	12.0 ± 18.9	-	-
	29, 86%	56.4 ± 21.0	-	-	46, 98%	53.0 ± 3.8	-	-
	30, 52%	25.8 ± 22.3	-	-	47, 46%	-22.8 ± 0.9	-	-
	31, 68%	85.1 ± 9.0	85.1 ± 1.9	807 ± 216	48, 61%	29.5 ± 22.7	-	-
	32, 18%	0.0 ± 13.1	-	-	-	-	-	-
	33, 80%	23.6 ± 33.7	-	-	49, 99%	0.0 ± 0.7	-	-
	34, 76%	96.5 ± 2.4	85.6 ± 1.3	851 ± 54	50, 76%	93.3 ± 5.1	93.1 ± 2.4	781 ± 37
	35, 76%	70.9 ± 7.9	90.5 ± 1.6	1621 ± 463	51, 91%	44.1 ± 17.1	-	-
	36, 86%	73.8 ± 11.3	94.3 ± 3.6	802 ± 160	52, 98%	75.4 ± 28.8	-	-
	37, 43%	54.3 ± 6.3	-	-	53, 56%	39.6 ± 7.6	-	-
	38, 75%	77.5 ± 8.2	93.5 ± 4.4	1198 ± 154	54, 99%	81.1 ± 7.0	71.7 ± 0.3	-
	39, 33%	67.3 ± 44.6	-	-	55, 58%	0.0 ± 4.29	-	-
	40, 46%	74.7 ± 6.3	91.1 ± 2.9	361 ± 42	56, 41%	88.9 ± 7.5	92.3 ± 3.1	866 ± 301

the concentration–response curves for both compounds (Figure 3C). **23** showed an IC<sub>50</sub> of 1.79 ± 0.14 μM, revealing approximately a 1 order of magnitude lower potency compared

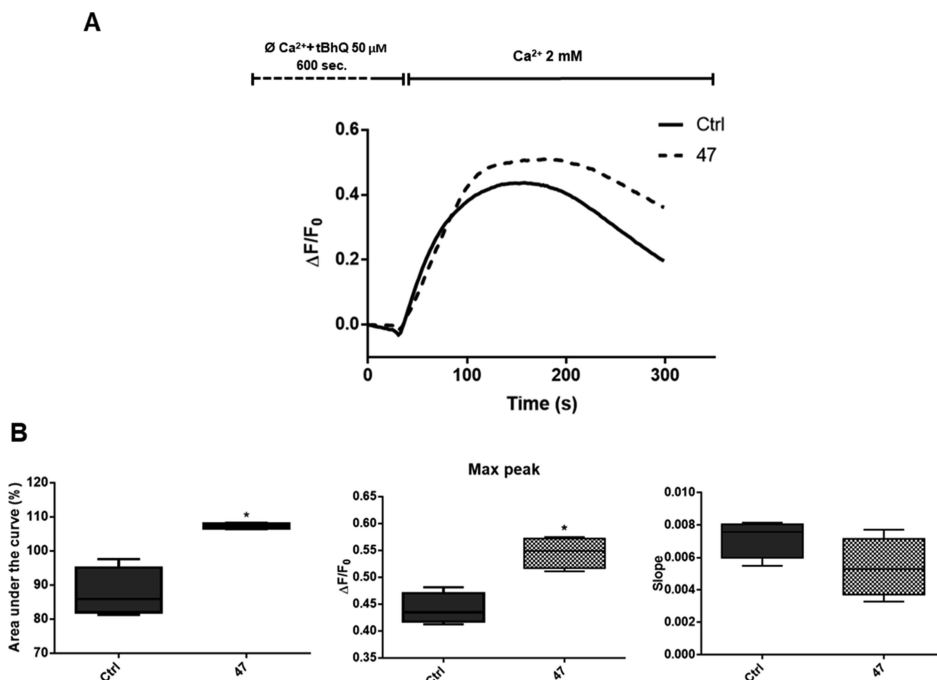
to **Synta66** (IC<sub>50</sub> = 228 ± 33 nM). Moreover, **23** was slightly cytotoxic, with a residual cell viability of 71.8% at 10 μM, a characteristic shared by **Synta66** (75.8 ± 8.0%). To assess the

Scheme 3. Synthesis of Compounds 27–40 (Series 2A)<sup>4t</sup>

<sup>4t</sup>Reagents and conditions: (a)  $\text{NaNO}_2$ ,  $\text{NaN}_3$ ,  $\text{HCl}$ ,  $\text{H}_2\text{O}$ , rt, 5 h, 81%. (b) Sodium ascorbate,  $\text{CuSO}_4 \cdot 5\text{H}_2\text{O}$ ,  $t\text{-BuOH}$ ,  $\text{H}_2\text{O}$ , 50 °C, 48 h, 87%. (c)  $\text{K}_2\text{CO}_3$ ,  $\text{Pd}(\text{OAc})_2$ ,  $\text{EtOH}$ ,  $\text{DMF}$ , 80 °C, 6 h, 18–86%.

Scheme 4. Synthesis of Compounds 44–56 (Series 2B)<sup>4t</sup>

<sup>4t</sup>Reagents and conditions: (a) Bestmann–Ohira reagent,  $\text{K}_2\text{CO}_3$ ,  $\text{MeOH}$ , rt, 18 h, 54%. (b) Sodium ascorbate,  $\text{CuSO}_4 \cdot 5\text{H}_2\text{O}$ ,  $t\text{-BuOH}$ ,  $\text{H}_2\text{O}$ , 50 °C, 16 h, 65%. (c)  $\text{K}_2\text{CO}_3$ ,  $\text{Pd}(\text{OAc})_2$ ,  $\text{EtOH}$ ,  $\text{DMF}$ , 80 °C, 6 h, 22–99%.



**Figure 4.** Effect of 47 on SOCE. (A) Average  $\text{Ca}^{2+}$ -traces of SOCE in the absence or presence of 47 ( $3 \mu\text{M}$  in HEK cells). Traces are the average of 200 cells. (B) Evaluation of the AUC, peak amplitude, and slope of the  $\text{Ca}^{2+}$ -rise in the absence or presence of 47. The graph shows the median and IQR of the AUC, peak amplitude, and slope of the  $\text{Ca}^{2+}$ -rise. Mann–Whitney  $U$  test of compound vs control ( $*p = 0.0286$ ).

cytotoxicity profile of the biphenyl triazoles, viability assays were performed on other molecules of the first series ( $10 \mu\text{M}$ ) and all the compounds showed a cell viability comparable to 23 (data not shown).

**SAR Study around 2,5-Dimethoxyphenyl Gives Compounds as Active as Synta66 on SOCE.** The above data demonstrate that all the synthesized biphenyl triazoles showed a reduced activity on SOCE compared to Synta66. We therefore synthesized a second series of compounds (series 2A

and 2B, Figure 2) where the 2,5-dimethoxyphenyl ring, the only structural motif that had been kept fixed in our preliminary SAR, was extensively modified (Table 2). Given that the most potent compound in the first series featured a 3-carboxyphenyl ring, we decided to select this moiety as the one to keep fixed. The choice was also guided by the fact that this substructure was the preferred substitution in our previous paper reporting pyrtiazoles (CIC-37, Figure 1) and by the

perception that the 3-carboxyphenyl substrate is a privileged scaffold in SOCE modulation.<sup>16</sup>

To obtain the second series of biphenyl triazoles, a Suzuki cross-coupling reaction was exploited, starting from two aryl bromides, **26** and **43**, that were coupled with different boronic acids. **26** and **43** were synthesized as depicted in Schemes 3 and 4. Click chemistry reaction between azide **24**, prepared from 4-bromoaniline by diazotization-azidation protocol, and alkyne **25** afforded the aryl bromide **26**. Similarly, **43** was obtained by clicking alkyne **41**, synthesized by reacting 4-bromobenzaldehyde in the presence of the Bestmann–Ohira reagent, with azide **42**.

Starting from these two intermediates, 28 Suzuki reactions were performed and compounds **27–40** (series 2A, Figure 2) and **44–56** (series 2B, Figure 2) were synthesized. One reaction was instead not successful.

As described above, all the compounds were initially tested at 10  $\mu\text{M}$  in HEK cells. This second series was significantly more potent compared to the first, and several molecules showed a noteworthy inhibitory activity, with percentage above 80% (data not shown). Therefore, in order to better discriminate between the different candidates, we decided to evaluate the effect of the compounds at 3  $\mu\text{M}$  on SOCE. For those compounds that displayed SOCE inhibitory activity  $\geq 70\%$ , cell viability assays, this time at 10  $\mu\text{M}$ , were then performed. For those molecules showing an inhibitory activity  $\geq 70\%$  and a cell viability  $\geq 85\%$ , the  $\text{IC}_{50}$  values were calculated (Table 2).

The biological results highlighted that removal of both the methoxy substituents from positions 2' and 5' (**27**,  $51.0 \pm 31.9\%$ ; **44**,  $1.8 \pm 3.1\%$ ), or the presence of the solely 2'-methoxy substituent (**28**,  $45.9 \pm 14.5\%$ ; **45**,  $12.0 \pm 18.9\%$ ), caused a significant reduction of activity compared to Synta66 with a remarkable variability. On the other hand, the additional methoxy group at position 4' made the inhibition rise to 50% (**29**,  $56.4 \pm 21.0\%$ ; **46**,  $53.0 \pm 3.8\%$ ). When the same insertion was performed at position 6', for one compound a drop in inhibitory activity occurred (**30**,  $25.8 \pm 22.3\%$ ), whereas for the other one (**47**) an increase in SOCE was surprisingly observed ( $-22.8 \pm 0.9\%$ , Figure 4A). The compound, tested at a concentration of 3  $\mu\text{M}$ , significantly increased the AUC of calcium entry and the peak amplitude (Figure 4B), that is, represents a positive modulator of SOCE.

Given the absence of effect on slope, it is highly likely that it affects channel closure or desensitization. Given that the focus of this study was to identify novel SOCE negative modulators for the treatment of AP, the profile of compound **47** was not investigated further, but its discovery supports the idea that minor structural modifications of SOCE inhibitors can interfere with channel gating and produce activators, as already observed for pyrtriazoles (AL-2T (**57**), NM-3G (**58**); Figure 5)<sup>16</sup> and for another recently described SOCE enhancer (IA65 (**59**), Figure 5).<sup>22</sup> **47** therefore represents an enhancer of SOCE from a third distinct class of modulators and provides grounds to develop models to understand the mechanism by which this occurs.

Compound **31** in which the methoxy group is removed from position 2' while bearing a 3'-methoxy substituent was more active ( $85.1 \pm 9.0\%$ ; Figure 6A) compared to Synta66, whereas the counterpart **48** was less active ( $29.5 \pm 22.7\%$ ). The substitution of the methoxy group with a hydroxyl (**32**,  $0.0 \pm 13.1\%$ ) or with a thioether (**33**,  $23.6 \pm 33.7\%$ ; **49**,  $0.0 \pm 0.7\%$ ) was instead not tolerated. Compounds **34** and **50** with a

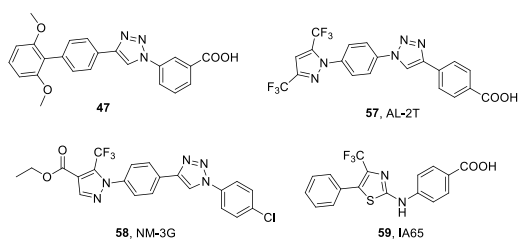


Figure 5. Structures of compound **47** and other positive modulators of SOCE reported in the literature.

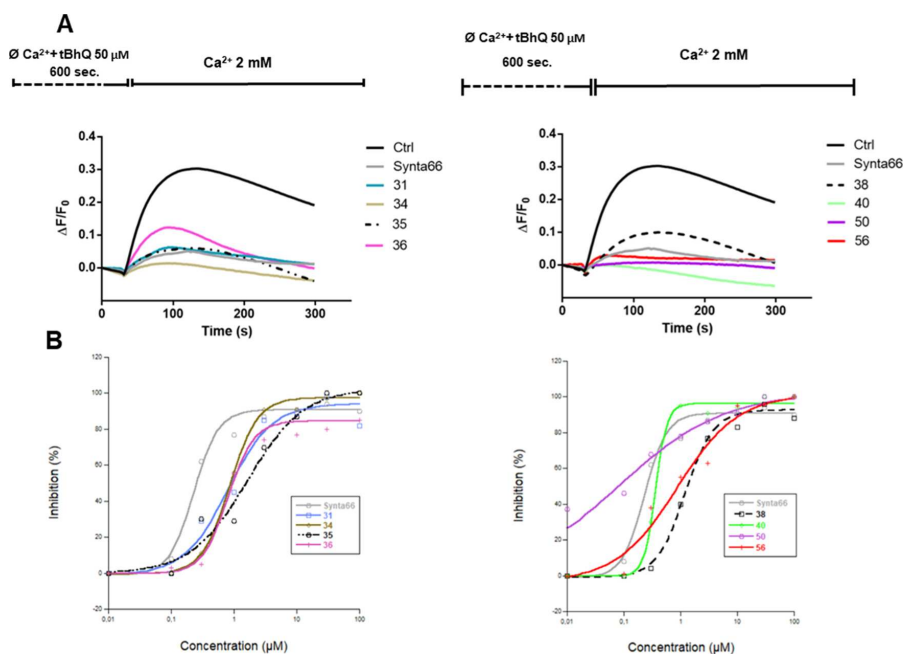
2',3'-dimethoxy phenyl substituent also showed a good activity ( $96.5 \pm 2.4$  and  $93.3 \pm 5.1\%$ , respectively; Figure 6A), whereas if the two methoxy groups were fused together to form a 1,4-dioxanyl ring, the activity was lower (**35**,  $70.9 \pm 7.9\%$  Figure 6A; **51**,  $44.1 \pm 17.1\%$ ). The 3',5'-dimethoxy phenyl substituent provided a good inhibitory activity, as in the case of **36**, which induced an inhibition of  $73.8 \pm 11.3\%$  (Figure 6A). On the other hand, **52** had a good inhibitory activity but due to its remarkable variability ( $75.4 \pm 28.8\%$ ), the compound was not selected for further studies. The reduction of SOCE inhibition was also observed with the 3',4'-dimethoxy phenyl substituent but to a less extent (**37**,  $54.3 \pm 6.3\%$ ; **53**,  $39.6 \pm 7.6\%$ ). When the substituents in 3' and 4' were fused together in a six-member 1,4-dioxanyl ring, the activity rose (**38**,  $77.5 \pm 8.2\%$ , Figure 6A; **54**,  $81.1 \pm 7.0\%$ ), whereas the 1,3-dioxolanyl was not tolerated in the case of **55** ( $0.0 \pm 4.3\%$ ) and led to a less active compound with a high standard error in the case of **39** ( $67.3 \pm 44.6\%$ ). Finally, a 2'-fluoro-5'-methoxy phenyl ring provided two compounds with remarkable activity on SOCE, **40** ( $74.7 \pm 6.3\%$ ) and **56** ( $88.9 \pm 7.5\%$ ), both reported in Figure 6A.

For all selected compounds (**31**, **34**, **35**, **36**, **38**, **40**, **50**, and **56**), the detailed analyses of the AUC, peak amplitude, and slope demonstrated that, similarly to Synta66, all compounds induced a drop in the three parameters, with **34** significantly reducing the AUC when compared to the reference compound. All these data are reported in the Supporting Information.

In summary, in the second series we were able to discover eight molecules with  $\text{IC}_{50}$  values in the nanomolar range (Figure 6B, Table 2).

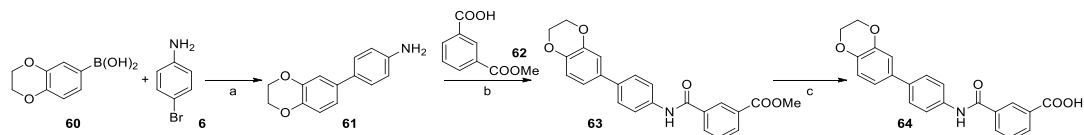
**Triazole is an Indispensable Feature of the New Class of Modulators and Reduces Off-Target Effects on DHODH.** To better elucidate the role of the triazole ring in the interaction with SOCE machinery, we synthesized analogues of **38** displaying the direct (**64**) and the inverse (**69**) amides, according to Schemes 5 and 6. Suzuki cross-coupling reaction between (2,3-dihydrobenzo[*b*][1,4]dioxin-6-yl)boronic acid and 4-bromoaniline afforded amine **61** that, after coupling with 3-(methoxycarbonyl)benzoic acid and hydrolysis of the methyl ester, yielded compound **64**. (2,3-Dihydrobenzo[*b*][1,4]dioxin-6-yl)boronic acid and methyl 4-iodobenzoate underwent a Suzuki cross-coupling reaction and, after deprotection of the carboxyl group, afforded intermediate **66**. Then, **66** was coupled with methyl 3-amino-benzoate and the methyl ester hydrolyzed to give compound **69**.

The triazole ring is reputed to be a nonclassical bioisostere of amides,<sup>20,21</sup> although we have shown in a number of



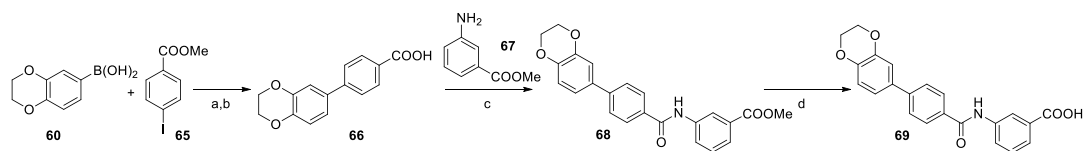
**Figure 6.** Effect of Synta66 and selected biphenyl triazoles on SOCE in HEK cells. (A) Average Ca<sup>2+</sup>-traces of SOCE in the absence or presence of Synta66 or biphenyl triazoles (3  $\mu$ M). Traces are the average of 200 cells. (B) Concentration–response curves.

#### Scheme 5. Synthesis of Compound 64<sup>a</sup>



<sup>a</sup>Reagents and conditions: (a) K<sub>2</sub>CO<sub>3</sub>, Pd(OAc)<sub>2</sub>, EtOH, DMF, 80 °C, 6 h, 86%. (b) EDCl, DMAP, DIPEA, dry CH<sub>2</sub>Cl<sub>2</sub>, rt, 18 h, 77%. (c) NaOH, H<sub>2</sub>O, THF, 3 h, 60 °C, 81%.

#### Scheme 6. Synthesis of Compound 69<sup>a</sup>



<sup>a</sup>Reagents and conditions: (a) K<sub>2</sub>CO<sub>3</sub>, Pd(OAc)<sub>2</sub>, EtOH, DMF, 80 °C, 6 h. (b) NaOH, H<sub>2</sub>O, THF, 4 h, 60 °C, 85%. (c) EDCl, DMAP, DIPEA, dry CH<sub>2</sub>Cl<sub>2</sub>, rt, 18 h, 63%. (d) NaOH, H<sub>2</sub>O, THF, 4 h, 60 °C, 61%.

occasions that this is not necessarily always the case.<sup>23</sup> To investigate the function of the triazole in this setting, we evaluated the amides of 38 (64 and 69). Both molecules displayed a significantly reduced activity compared to the parent compound (Table 3). It should be noticed that such a difference was also observed when comparing Synta66 with its triazole-substituted close analogues (9 and 18; Table 1).

Surprisingly, 64, despite its low activity on SOCE, showed a significant cytotoxicity, with a residual viability after 24 h of 50% at 10  $\mu$ M in HEK cells, in contrast to its inverse amide 69

and 38, that did not affect cell viability. When attempting to rationalize this cytotoxicity, we noticed that 64 was structurally closely related to dihydroorotate dehydrogenase (DHODH) inhibitors.<sup>24</sup> Indeed, a *h*DHODH inhibitor usually includes a lipophilic moiety that guarantees the interaction with subsite 1 of the enzyme, together with a carboxylate moiety that interacts with the Arg136 residue located in subsite 2, two structural features that can be found in compound 64.

More surprisingly, a recent screening performed on an FDA database has highlighted that teriflunomide (70, Figure 7), a

Table 3. Amide Analogues of 38

Cpd,	X	% SOCE inhibition (3 $\mu$ M)	% Viability (10 $\mu$ M)	IC <sub>50</sub>
Yield (%)				
64, 81%		51.8 $\pm$ 9.5	50.3 $\pm$ 0.8	-
69, 61%		22.6 $\pm$ 5.6	95.3 $\pm$ 3.3	-

DHODH inhibitor approved for multiple sclerosis,<sup>25</sup> is endowed with a considerable inhibitory activity on SOCE (IC<sub>50</sub> = 4.3  $\pm$  1.0  $\mu$ M in HEK cells).<sup>26</sup> This led to asking whether 64 was a DHODH inhibitor and whether triazole-bearing analogues shared this feature. To investigate the involvement of DHODH, the cytotoxic activities of the two compounds bearing an amide substructure, 64 and 69, and of the five selected biphenyl triazoles, 31, 34, 36, 38, 40, were evaluated after 72 h at a high concentration (50  $\mu$ M) in HEK cells. Alongside, two well-characterized DHODH inhibitors, teriflunomide itself (70, Figure 7) and brequinar (71, Figure 7)<sup>27</sup> were used as reference compounds. Gratifyingly, the viability profile revealed that the biphenyl triazoles did not impair cell viability even at these high concentrations. For the arylamide-bearing molecules displaying a significant cytotoxicity (64 and Synta66), the involvement of the *de novo* pyrimidine synthesis pathway was evaluated by supplementing the medium with an excess of uridine that should counterbalance the effect of DHODH inhibition by triggering the *de novo* pathway.<sup>28</sup> As expected, brequinar and teriflunomide were cytotoxic and their effect was reverted by uridine addition. The cytotoxic effect of 64 was also fully reverted by uridine, supporting our hypothesis that this is a DHODH inhibitor and that the substitution with the triazole ring reduces the off-target effects (Figure 7). While this observation deserves additional investigations, it questions whether other previously reported inhibitors bearing an aryl amide moiety might have promiscuous effects on this enzyme. Indeed, most SOCE inhibitors bear an amide-linkage as part of the pharmacophor-

e.<sup>15e</sup> We preliminarily tested CM4620 and found that it was cytotoxic at 50  $\mu$ M in HEK cells but this cytotoxicity was not reverted by uridine, suggesting that it is not a DHODH inhibitor (not shown). A similar lack of effect was also observable for Pyr6, while no other arylamide SOCE inhibitor was tested.

Overall, these data corroborate previous evidence that the amide to triazole substitution is not merely bioisosteric (REF), as the presence of the triazole prevents off-target effects on DHODH.

**Biphenyl Triazoles as Sodium Salts Are More Soluble Than Synta66.** According to both potency and cell viability of the second series of modulators, the five most promising candidates were selected (31, 34, 36, 38, and 40), excluding those molecules that differed from these candidates only for the orientation of the triazole ring (50 and 56). To assess the druggability of the molecules, their thermodynamic aqueous solubility was evaluated. Unfortunately, the biphenyl triazoles showed poor aqueous solubility (about 0.20  $\mu$ g/mL, data not shown) comparable to that of Synta66 (0.28  $\mu$ g/mL, Table 4). To overcome this limitation, the candidates were salified as sodium salts and their aqueous solubility was reassessed (Table 4). Briefly, except for 36, all the tested biphenyl triazoles salts were soluble in water in the 0.67–1.53 mg/mL range. The presence of one or two methoxy substituents on the phenyl ring considerably increased the solubility compared to the 1,4-dioxanyl moiety of 38 as well as the addition of a fluorine atom that slightly improved the solubility of 40 compared to 31. Interestingly, the enhanced solubility given by the methoxy substituents is minimally driven by the decrease in hydrophobicity but rather by the disruption of the molecular symmetry, as shown by the 80-fold increase in aqueous solubility of 34 compared to 36. In addition, to assess the solubilization of the selected candidates in the aqueous vehicle used for *in vivo* administration, compounds 34 and 40 were dissolved at the nominal concentration of 6 mg/mL in saline solutions containing cosolvents (see methods section). Only 34 gave a limpid solution in saline containing 10% dimethyl sulfoxide (DMSO) + 20% PEG400, whose title was confirmed by LC–UV analysis, pointing to this compound as the best candidate for further *in vivo* evaluation.

**Biphenyl Triazoles Are More Metabolically Stable Than Synta66.** Next, the *in vitro* metabolic stability of the five candidates (31, 34, 36, 38, and 40) was evaluated in mouse

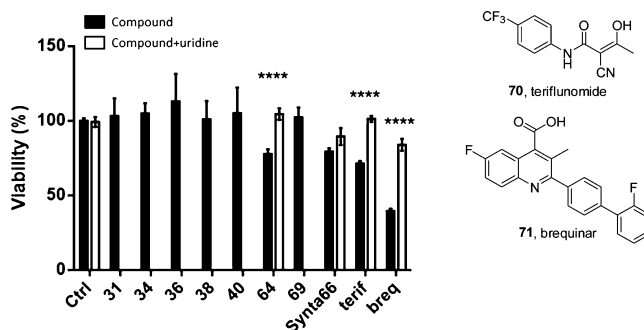
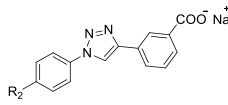
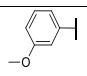
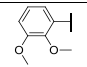
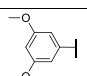
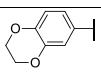
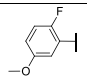


Figure 7. Effects of the selected compounds on DHODH. HEK cells were treated for 72 h at the concentration of 50  $\mu$ M with or without uridine (100  $\mu$ M). The graph shows average  $\pm$  SEM of cell viability, peak amplitude, and slope of the Ca<sup>2+</sup>-rise. A Student *t*-test was performed on compounds vs control (\*\*\*\**p* < 4.27  $\times$  10<sup>-6</sup>); (terif: teriflunomide, breq: brequinar).

**Table 4.** Aqueous Solubility and Metabolic Stability of the Selected Biphenyl Triazoles


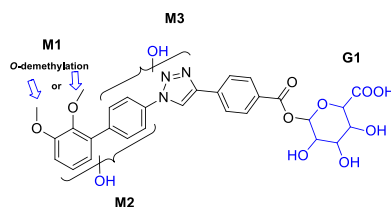
R <sub>2</sub>	Cpd	H <sub>2</sub> O solubility (μg/mL)	Metabolic stability <sup>a,b</sup>
-	4, Synta66	0.28	15%
	31_Na	855.57	91%
	34_Na	1528.18 <sup>a</sup>	75%
	36_Na	18.72	92%
	38_Na	668.34	94%
	40_Na	1168.36	93%

<sup>a</sup>Soluble at 6 mg/mL in saline containing 10% DMSO + 20% PEG400. <sup>b</sup>Residual substrate after 1 h incubation in MLMs.

liver microsomes (MLMs) activated by NADPH by measuring the substrate residual after 1 h. For comparative purposes, **Synta66** was incubated in the same conditions. All the salified biphenyl triazoles resulted in a quite stable microsomal oxidation, with a residual substrate in the range of 75–94% after incubation (Table 4). By contrast, **Synta66** resulted in a considerably less stable microsomal metabolism, with a substrate residual of only 15% after incubation, amide hydrolysis and *O*-demethylation metabolites showing the most extensive transformations (data not shown).

Next, the structural characterization of the metabolites of **34** was performed by high-resolution mass spectrometry (HRMS), processing the raw data with a workflow aimed at drug metabolite identification provided by Compound Discoverer 3.1 software (Thermo Scientific). Overall, data analysis highlighted the occurrence of three main transformations: *O*-demethylation (M1) followed by oxidation (M2) and hydroxylation (M3). Furthermore, incubation of **34** with MLMs in the presence of uridine diphosphate glucuronic acid (UDPGA) gave the corresponding acyl glucuronide metabolite G1 (Figure 8). Interestingly, data analysis did not highlight the formation of glutathione (GSH) adducts, suggesting that metabolism is not driven toward the formation of reactive species. Full data of metabolite structures and mass spectral data, as well as the metabolic pathways, are given in the Supporting Information.

**34 Is Effective In Vivo in AP.** To further characterize the compound, a PK analysis was performed in mice. Briefly, mice

**Figure 8.** Metabolic biotransformation of compound **34** in MLMs.

were injected with **34** (i.v., 7 mg/kg, once) and serial blood sampling was performed. **34** showed a half-life of 3.2 h, with a clearance of 0.5 L/h/kg, a volume of distribution of 2.3 L/kg, and a  $C_{max}$  of 16.8 mg/L (see the Supporting Information for the full set of PK parameters).

The PK profile of our candidate prompted us to investigate its efficacy in a cerulein-induced murine model of AP.<sup>29</sup> The compound was administered 30 and 150 min after the first cerulein injection at a dose of 10 mg/kg i.p. The hematoxylin/eosin (H&E) staining of the pancreatic tissues collected 5 h after the first cerulein injection demonstrated that the compound was able to significantly ameliorate the histological scores, with reduction of inflammation and edema typical of this disease (Figure 9), as expected from SOCE inhibitors with profiles compatible with systemic administration.<sup>16</sup>

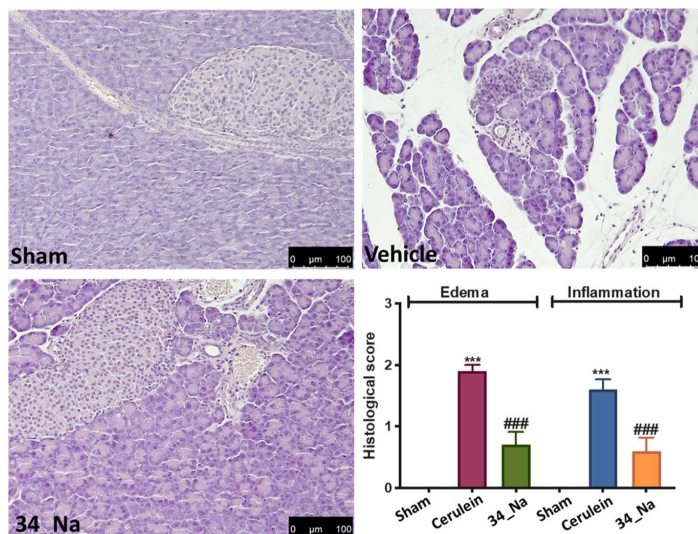
## CONCLUSIONS

This work stems from our previous discovery that the pytriazole derivative **3**, originally designed from known pyrazole inhibitors, is an inhibitor of SOCE ( $IC_{50} = 4.4 \mu M \pm 1.2$ ).<sup>16</sup> The compound demonstrated efficacy in the cerulein-induced model of AP despite its short half-life (i.p., 1.3 h). With the aim of discovering drug-like SOCE inhibitors endowed with a better PK profile, the replacement of the amide with the triazole ring in **Synta66**, another well-known SOCE inhibitor extensively employed as chemical probe, was attempted.

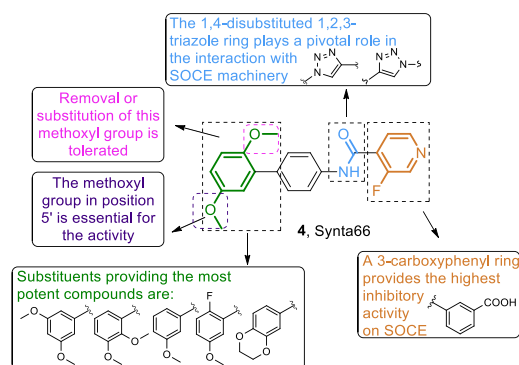
The synthetic strategy relied on a two-step process based on a click chemistry reaction, followed by a Suzuki coupling. The performed SAR study highlighted that the pharmacophore of this novel class of modulators includes the phenyl ring bearing a methyl or methylene ether group in the meta position, the phenyl ring featuring a carboxylic group in the meta position, and the triazole ring. The latter, when switched into the direct or inverse amide, not only leads to a decrease in SOCE inhibition (**64** and **69**) but also to a significant cytotoxicity (**64**), which may in part be reconducted to the fact that arylamide substructures may act on DHODH. The summary of the SAR investigations is schematized in Figure 10.

Our efforts resulted in compound **34** that compared to **Synta66** (i) displays a slightly decreased potency on SOCE ( $IC_{50} = 851 \pm 54 \text{ nM}$  vs  $228 \pm 33 \text{ nM}$ ) but, importantly, no detectable cytotoxicity in HEK cells up to 60  $\mu M$ ; (ii) shows a significantly higher *in vitro* metabolic stability in MLMs (75% vs 15% of residual substrate after 1 h); and (iii) is endowed with a carboxylic group that confers high aqueous solubility in the sodium salt form (1528  $\mu g/mL$  vs 0.28  $\mu g/mL$ ). This yields a favorable PK profile in mice (i.v.,  $t_{1/2}$  of 3.2 h) and efficacy in a mouse model of cerulein-induced AP.





**Figure 9.** Evaluation of compound 34 in AP. H&E sections of pancreatic tissues. Analysis was performed in a blinded manner and data represent the mean  $\pm$  SEM of 10 mice for each group. \*\*\* $p < 0.001$  versus Sham; ### $p < 0.001$  vs cerulein.



**Figure 10.** Graphical representation of SAR study around Synta66.

## EXPERIMENTAL SECTION

**Chemistry. General Experimental Methods.** Reagents and solvents were used without further purification, although, if required, they were distilled and stored on molecular sieves. Column chromatography was performed on silica gel. The following instrumentation was used: Stuart scientific SMP3 apparatus (melting point), FT-IR Thermo-Nicolet Avatar, FT-IR Bruker Alpha II, Jeol ECP 300 MHz ( $^1\text{H}$  NMR), Bruker AVANCE Neo 400 MHz or Jeol ECP 300 MHz ( $^{13}\text{C}$  NMR), Thermo Finnigan LCQ-deca XP-plus equipped with an ESI source and an ion trap detector or mass spectrometry (Thermo Scientific Q-Exactive Plus) equipped with a heated electrospray ionization source. Chemical shifts are reported in parts per million (ppm). All lead compounds displayed a purity of 95% or higher, determined by HPLC (see the Supporting Information). Boronic acids, azides, and alkynes are commercially available or were synthesized following procedures reported in the literature, except for compounds 73, 75, 77, and 78 (intermediates for the synthesis of 18, 21, 9, and 13, respectively) that were synthesized as reported in the Supporting Information.

**2',5'-Dimethoxy-[1,1'-biphenyl]-4-amine, (7).** 4-Bromoaniline 6 (2 g, 11.63 mmol) was solubilized in DMF (23 mL) and ethanol (23 mL) under nitrogen atmosphere. 2,5-(Dimethoxyphenyl)boronic acid 5 (3.17 g, 17.44 mmol), Pd(OAc)<sub>2</sub> (26.1 mg, 0.116 mmol), and K<sub>2</sub>CO<sub>3</sub> (3.2 g, 23.26 mmol) were added in order. The mixture was stirred at 80 °C for 3 h and at room temperature overnight. The reaction was then filtered under vacuo over a pad of celite, rinsed with ethanol, and evaporated. The crude product was purified by column chromatography using petroleum ether/ethyl acetate 7:3 v/v as eluent, affording compound 7 as a yellow solid (2.61 g, 11.40 mmol, 98%);  $^1\text{H}$  NMR (300 MHz, CDCl<sub>3</sub>):  $\delta$  7.39 (d,  $J = 6.9$  Hz, 2H), 6.97–6.88 (m, 2H), 6.84 (s, 1H), 6.70 (d,  $J = 6.9$  Hz, 2H), 3.82 (s, 3H), 3.76 (s, 3H). MS (ESI)  $m/z$ : 230 [M + H]<sup>+</sup>.

**4'-Azido-2,5-dimethoxy-1,1'-biphenyl, (8).** To a solution of 2',5'-dimethoxy-[1,1'-biphenyl]-4-amine (2 g, 8.73 mmol) in water (40 mL), HCl 37% (3.5 mL) was added dropwise and the resulting mixture was cooled down at 0 °C. Then, a solution of NaNO<sub>2</sub> (0.60 g, 8.73 mmol) in water (2 mL) was added and, after 10 min, a solution of NaN<sub>3</sub> (0.68 g, 10.48 mmol) in water (2 mL) was added dropwise. The reaction was stirred at room temperature for 5 h, diluted with ethyl acetate, and washed with water (2 $\times$ ). The organic layer was dried over sodium sulfate and the volatile was removed under vacuo. The crude material was purified by column chromatography using petroleum ether/ethyl acetate 98:2 v/v as eluent, yielding compound 8 as an orange solid (1.33 g, 5.24 mmol, 60%);  $^1\text{H}$  NMR (300 MHz, CDCl<sub>3</sub>):  $\delta$  8.31 (d,  $J = 7.1$  Hz, 2H), 7.75 (d,  $J = 7.1$  Hz, 2H), 6.92–6.83 (m, 3H), 3.85 (s, 3H), 3.79 (s, 3H).

**General Procedure A.** Compounds 9–14 were prepared from a suspension of 8 (74 mg, 0.29 mmol, 1 equiv) in water (320  $\mu\text{L}$ ) and *t*-BuOH (320  $\mu\text{L}$ ) and the relative alkyne (0.29 mmol, 1 equiv). Reactions were carried out overnight under vigorous stirring in the presence of sodium ascorbate 1 M (29  $\mu\text{L}$ ) and copper sulfate pentahydrate (0.0029 mmol, 0.01 equiv). Evaporation of the volatile and purification by silica gel column chromatography was performed.

**4-(1-(2',5'-Dimethoxy-[1,1'-biphenyl]-4-yl)-1H-1,2,3-triazol-4-yl)-3-fluoropyridine, (9).** Following general procedure A, the reaction of 8 and 4-ethynyl-3-fluoropyridine, after purification (petroleum ether/ethyl acetate 6:4 v/v as eluent), yielded 9 as a yellow solid (34 mg, 0.09 mmol, 31%); mp 165–166 °C.  $^1\text{H}$  NMR (300 MHz, CDCl<sub>3</sub>):  $\delta$  8.60–8.50 (m, 3H), 8.31 (d,  $J = 6.1$  Hz, 1H), 7.85 (d,  $J = 8.5$  Hz, 2H), 7.73 (d,  $J = 8.5$  Hz, 2H), 6.97–6.89 (m, 3H), 3.83 (s,











and then was left at rt overnight. HCl 3 N was added until pH 4 and the aqueous layer was extracted with ethyl acetate (x2). The collected organic phases were dried over sodium sulfate and evaporated. Purification by column chromatography (ethyl acetate as eluent) yielded compound **69** as a white solid (91.5 mg, 0.24 mmol, 61%); mp 234–235 °C dec. <sup>1</sup>H NMR (300 MHz, DMSO-*d*<sub>6</sub>): δ 10.39 (br s, 1H), 8.44 (s, 1H), 8.06–8.00 (m, 3H), 7.77 (d, *J* = 8.2 Hz, 2H), 7.69 (d, *J* = 7.4 Hz, 1H), 7.48 (t, *J* = 7.4 Hz, 1H), 7.25 (d, *J* = 8.2 Hz, 2H), 6.98 (d, *J* = 8.2 Hz, 1H), 4.30–4.29 (m, 4H). <sup>13</sup>C NMR (101 MHz, DMSO-*d*<sub>6</sub>): δ 167.8, 165.8, 144.3, 144.2, 143.1, 139.9, 133.3, 132.7, 131.9, 129.3, 128.8, 126.5, 124.9, 124.8, 121.6, 120.3, 118.1, 115.9, 64.7, 64.6. IR (neat)  $\bar{\nu}$ : 3310, 2924, 1693, 1650, 1485, 1302, 1069, 811, 752, 677 cm<sup>-1</sup>. MS (ESI) *m/z*: 376 [M + H]<sup>+</sup>. HRMS (ESI) *m/z*: (M + H)<sup>+</sup> calcd for C<sub>22</sub>H<sub>18</sub>NO<sub>5</sub>, 376.1179; found, 376.1172.

**In Vitro Metabolism Studies.** Phase I and II (glucuronidation) incubations were performed in MLMs (pooled male mouse CD-1, protein concentration: 20 mg/mL, purchased from Corning B.V. Life Sciences—Amsterdam, The Netherlands) using the procedure previously described<sup>16</sup> with the following modifications: 5 μM substrate concentration for the determination of the residual percentage and 50 μM for **34** metabolite characterization by HRMS; when metabolic activation was studied, 3 mM GSH trapping agent was added in the incubation mixture.

**Aqueous Solubility.** Thermodynamic aqueous solubility was determined as follows: about 3 mg of the tested compound was weighed and dissolved in 3 mL of deionized water. After vigorous mixing by vortex followed by sonication for 5 min, the resulting supersaturated solution was shaken horizontally overnight at 25 °C. After filtration over a syringe filter (pore 0.22 μm, regenerate cellulose membrane), 100 μL of DMSO was added to 1 mL of the filtered solution. The resulting solution was further diluted in water (typically 1:10) before LC–UV analysis. Aqueous solubility was calculated comparing the filtrate peak area to those of the tested compound DMSO solutions. Solubility in aqueous media was also checked in the following vehicles at the target concentration of 6 mg/mL: saline + 10% DMSO, saline + 10% DMSO + 20% PEG400, saline + 5% ethanol.

**Biology. Compounds.** A 50 mM stock solution of **Synta66**, CM4620, teriflunomide, brequinar, and all the biphenyl triazoles synthesized was dissolved in 100% DMSO and stored at +4/–20 °C. For each experiment, working concentrations of these compounds were freshly prepared by diluting DMSO to 0.1% in different physiologic solutions according to the experimental procedures (*i.e.*, Krebs–Ringer buffer, culture medium, Locke solution).

**Cell Culture and Calcium Imaging Experiments.** Screening, dose–response experiments, and calcium imaging experiments were performed in HEK cells (ATCC, Rock, ville, MD, USA), as already reported elsewhere.<sup>16</sup>

**3-(4,5-Dimethylthiazol-2-yl)-2,5-diphenyltetrazolium Bromide Assay.** Viability assays were performed in HEK cells that were plated in 24-well plates at the density of 20,000 cells per well. After 24 h, the cells were treated for other 24 h with the selected compounds. At the end of the treatments, the medium was removed and substituted with 300 μL of MTT reagent (Sigma-Aldrich Inc., Italy) at the final concentration of 0.25 mg/mL for 60 min at 37 °C. Reactions were then stopped and the crystals were solubilized by adding isopropyl alcohol/HCl (1 M) (Sigma-Aldrich Inc., Italy), before reading the absorbance at 570 nm, using the multiplate reader Victor3 V (PerkinElmer, Milan, Italy). To evaluate the effects on the DHODH enzyme, HEK cells were treated with the selected compounds in the absence or presence of 100 μM uridine for 72 h.

**PK Analysis and Analysis of Pancreatitis.** All animal experiments observe the regulations in Italy (D.M. 116192) as well as the EU regulations (O.J. of E.C. L 358/1 12/18/1986). Compound **34** was injected *i.v.* at a dose of 7 mg/kg in C57BL/6 mice. Blood was collected after 5, 15, 30, 60, 120, 240, 360 min and 24 h. Aliquots of plasma samples were analyzed as previously reported.<sup>16</sup> AP was induced in mice by *i.p.* injections of cerulein, as already reported elsewhere.<sup>16</sup>

**Statistical Analysis.** In *in vitro* experiments, data are presented as mean ± SEM or Median and interquartile range (IQR). The normality of data distributions was assessed using the Shapiro–Wilk test. Parametric (unpaired *t*-test and one-way analysis of variance (ANOVA) followed by Tukey's post-hoc) or nonparametric (Mann–Whitney *U* test and one-way Kruskal–Wallis *H* test followed by Dunn's post-hoc) statistical analysis was used for comparisons of data. All statistical assessments were two-sided and a value of *P* < 0.05 was considered statistically significant. Statistical analyses were performed using GraphPad Prism software (GraphPad Software, Inc., USA).

In *in vivo* experiments, results were analyzed by one-way ANOVA followed by a Bonferroni post hoc test for multiple comparisons.

## ■ ASSOCIATED CONTENT

### Supporting Information

The Supporting Information is available free of charge at <https://pubs.acs.org/doi/10.1021/acs.jmedchem.0c01305>.

Synthesis and characterization of compounds **73**, **75**, **77**, **78**; NMR spectra of **31**, **34**, **35**, **36**, **38**, **40**, **50**, **56**; biology (effect of **Synta66**, **31**, **34**, **36**, **38**, **40**, **50**, **56** on the AUC, peak amplitude, and slope of the Ca<sup>2+</sup>-rise in HEK cells); *in vitro* metabolism and *in vivo* PK analysis and thermodynamic aqueous solubility (PDF)

Molecular formula strings for compounds (CSV)

## ■ AUTHOR INFORMATION

### Corresponding Author

Tracey Piralì – Department of Pharmaceutical Sciences, Università del Piemonte Orientale, Novara 28100, Italy; ChemiCare S.r.l., Novara 28100, Italy; [orcid.org/0000-0003-3936-4787](https://orcid.org/0000-0003-3936-4787); Phone: +39 0321 375852; Email: [tracey.pirali@uniupo.it](mailto:tracey.pirali@uniupo.it)

### Authors

Marta Serafini – Department of Pharmaceutical Sciences, Università del Piemonte Orientale, Novara 28100, Italy  
Celia Cordero-Sanchez – Department of Pharmaceutical Sciences, Università del Piemonte Orientale, Novara 28100, Italy  
Rosanna Di Paola – Department of Chemical, Biological, Pharmaceutical and Environmental Sciences, Università di Messina, Messina 98166, Italy  
Irene P. Bhela – Department of Pharmaceutical Sciences, Università del Piemonte Orientale, Novara 28100, Italy  
Silvio Aprile – Department of Pharmaceutical Sciences, Università del Piemonte Orientale, Novara 28100, Italy; [orcid.org/0000-0003-4804-9543](https://orcid.org/0000-0003-4804-9543)  
Beatrice Purgè – Department of Pharmaceutical Sciences, Università del Piemonte Orientale, Novara 28100, Italy  
Roberta Fusco – Department of Chemical, Biological, Pharmaceutical and Environmental Sciences, Università di Messina, Messina 98166, Italy  
Salvatore Cuzzocrea – Department of Chemical, Biological, Pharmaceutical and Environmental Sciences, Università di Messina, Messina 98166, Italy  
Armando A. Genazzani – Department of Pharmaceutical Sciences, Università del Piemonte Orientale, Novara 28100, Italy; [orcid.org/0000-0003-1923-7430](https://orcid.org/0000-0003-1923-7430)  
Beatrice Riva – Department of Pharmaceutical Sciences, Università del Piemonte Orientale, Novara 28100, Italy; ChemiCare S.r.l., Novara 28100, Italy

Complete contact information is available at: <https://pubs.acs.org/doi/10.1021/acs.jmedchem.0c01305>

### Author Contributions

M.S. and C.C.-S. contributed equally. B.R. and T.P. contributed equally. The manuscript was written through contributions of all authors. All authors have given approval to the final version of the manuscript.

### Notes

The authors declare no competing financial interest.

### ACKNOWLEDGMENTS

M.S. is supported by Fondazione AIRC (Associazione Italiana per la Ricerca sul Cancro) fellowship for Italy (Rif. 22568). This work was partly funded by the Telethon Foundation (GGP19110) to A. A. G.

### ABBREVIATIONS

ALL, acute lymphoblastic leukemia; AP, acute pancreatitis; AUC, area under the curve; CDCl<sub>3</sub>, deuterated chloroform; CD<sub>3</sub>OD, deuterated methanol; CH<sub>2</sub>Cl<sub>2</sub>, dichloromethane; CRAC, calcium release-activated channels; DHODH, dihydroorotate dehydrogenase; DIPEA, diisopropylethylamine; DMAP, 4-dimethylaminopyridine; DMEM, Dubecco's modified Eagle's medium; DMF, dimethylformamide; DMSO, dimethyl sulfoxide; DMSO-*d*<sub>6</sub>, deuterated dimethyl sulfoxide; EDCl, 1-ethyl-3-(3-dimethylaminopropyl)carbodiimide; EGTA, ethylene glycol-bis(β-aminoethyl ether)-N,N,N',N'-tetraacetic acid; ER, endoplasmic reticulum; EtOH, ethanol; FBS, fetal bovine serum; Fura-2, fluorescent calcium indicator 2; GSH, glutathione; H&E, hematoxylin and eosin; HEK cells, human embryonic kidney cells; HPLC, high-performance liquid chromatography; HRMS, high-resolution mass spectrometry; IC<sub>50</sub>, half-maximum inhibitory concentration; IP<sub>3</sub>R, inositol trisphosphate receptor; IR, infrared; KRB, Krebs-Ringer buffer; LC-UV, liquid chromatography-ultraviolet; MLMs, mouse liver microsomes; MeOH, methanol; mp, melting point; MTT, 3-(4,5-dimethylthiazol-2-yl)-2,5-diphenyltetrazolium bromide; NADPH, nicotinamide adenine dinucleotide phosphate; NMR, nuclear magnetic resonance; Orai, calcium release-activated calcium channel protein; PACs, pancreatic acinar cells; PEG, polyethylene glycol; PK, pharmacokinetic; SAR, structure-activity relationship; SEM, standard error of the mean; SERCA, sarco-endoplasmic reticulum calcium ATPase; SOCE, store-operated calcium entry; STIM, stromal interaction molecule; *t*-BHQ, *tert*-butylhydroquinone; *t*-BuOH, *tert*-butanol; THF, tetrahydrofuran; TLC, thin-layer chromatography; TRP, transient receptor potential channels; TRPC, transient receptor potential-canonical channels; UDPGA, uridine diphosphate glucuronic acid

### REFERENCES

- Lee, P. J.; Papachristou, G. I. New insights into acute pancreatitis. *Nat. Rev. Gastroenterol. Hepatol.* **2019**, *16*, 479–496.
- Forsmark, C. E.; Vege, S. S.; Wilcox, C. M. Acute pancreatitis. *N. Engl. J. Med.* **2016**, *375*, 1972–1981.
- (a) Gerasimenko, J. V.; Gerasimenko, O. V.; Petersen, O. H. The role of Ca<sup>2+</sup> in the pathophysiology of pancreatitis. *J. Physiol.* **2014**, *592*, 269–280. (b) Gerasimenko, J. V.; Peng, S.; Tsugorka, T.; Gerasimenko, O. V. Ca<sup>2+</sup> signalling underlying pancreatitis. *Cell Calcium* **2018**, *70*, 95–101.
- For review articles on SOCE, see: (a) Lewis, R. S. The molecular choreography of a store-operated calcium channel. *Nature* **2007**, *446*, 284–287. (b) Putney, J. W. Store-operated calcium entry: an historical overview. *Adv. Exp. Med. Biol.* **2017**, *981*, 205–214.

(c) Stathopoulos, P. B.; Ikura, M. Store operated calcium entry: from concept to structural mechanisms. *Cell Calcium* **2017**, *63*, 3–7.

(5) (a) Putney, J. W. A model for receptor-regulated calcium entry. *Cell Calcium* **1986**, *7*, 1–12. (b) Parekh, A. B.; Putney, J. W. Store-operated calcium channels. *Physiol. Rev.* **2005**, *85*, 757–810. (c) Prakriya, M.; Lewis, R. S. Store-operated calcium channels. *Physiol. Rev.* **2015**, *95*, 1383–1436.

(6) Hoth, M.; Penner, R. Depletion of intracellular calcium stores activates a calcium current in mast cells. *Nature* **1992**, *355*, 353–356.

(7) (a) Putney, J. W. Origins of the concept of store-operated calcium entry. *Front. Biosci., Scholar Ed.* **2011**, *3*, 980–984. (b) Putney, J. W. The physiological function of store-operated calcium entry. *Neurochem. Res.* **2011**, *36*, 1157–1165. (c) Berna-Ero, A.; Woodard, G. E.; Rosado, J. A. Orais and STIMs: physiological mechanisms and disease. *J. Cell Mol. Med.* **2012**, *16*, 407–424.

(8) (a) Ong, H. L.; Ambudkar, I. S. Molecular determinants of TRPC1 regulation within ER-PM junctions. *Cell Calcium* **2015**, *58*, 376–386. (b) Ong, H. L.; de Souza, L. B.; Ambudkar, I. S. Role of TRPC channels in store-operated calcium entry. *Adv. Exp. Med. Biol.* **2016**, *898*, 87–109.

(9) Kim, M. S.; Lee, K. P.; Yang, D.; Shin, D. M.; Abramowitz, J.; Kiyonaka, S.; Birnbaumer, L.; Mori, Y.; Muallem, S. Genetic and pharmacologic inhibition of the Ca<sup>2+</sup> influx channel TRPC3 protects secretory epithelia from Ca<sup>2+</sup>-dependent toxicity. *Gastroenterology* **2011**, *140*, 2107–2115.

(10) (a) Lur, G.; Sherwood, M. W.; Ebisui, E.; Haynes, L.; Peske, S.; Sutton, R.; Burgoyne, R. D.; Mikoshiba, K.; Petersen, O. H.; Tepikin, A. V. InsP<sub>3</sub> receptors and Orai channels in pancreatic acinar cells: colocalization and its consequences. *Biochem. J.* **2011**, *436*, 231–239. (b) Gukovskaya, A. S.; Pandol, S. J.; Gukovsky, I. New insights into the pathways initiating and driving pancreatitis. *Curr. Opin. Gastroenterol.* **2016**, *32*, 429–435.

(11) Gerasimenko, J. V.; Gryshchenko, O.; Ferdek, P. E.; Stapleton, E.; Hebert, T. O. G.; Bychkova, S.; Peng, S.; Begg, M.; Gerasimenko, O. V.; Petersen, O. H. Ca<sup>2+</sup> release-activated Ca<sup>2+</sup> channel blockade as a potential tool in antipain therapy. *Proc. Natl. Acad. Sci. U.S.A.* **2013**, *110*, 13186–13191.

(12) (a) Wen, L.; Voronina, S.; Javed, M. A.; Awais, M.; Szatmary, P.; Latawiec, D.; Chvanov, M.; Collier, D.; Huang, W.; Barrett, J.; Begg, M.; Stauderman, K.; Roos, J.; Grigoryev, S.; Ramos, S.; Rogers, E.; Whitten, J.; Velicelebi, G.; Dunn, M.; Tepikin, A. V.; Criddle, D. N.; Sutton, R. Inhibitors of ORAI1 prevent cytosolic calcium-associated injury of human pancreatic acinar cells and acute pancreatitis in 3 mouse models. *Gastroenterology* **2015**, *149*, 481–492. (b) Waldron, R. T.; Chen, Y.; Pham, H.; Go, A.; Su, H. Y.; Hu, C.; Wen, L.; Husain, S. Z.; Sugar, C. A.; Roos, J.; Ramos, S.; Luega, A.; Dunn, M.; Stauderman, K.; Pandol, S. J. The Orai Ca<sup>2+</sup> channel inhibitor CM4620 targets both parenchymal and immune cells to reduce inflammation in experimental acute pancreatitis. *J. Physiol.* **2019**, *597*, 3085–3105.

(13) CM4620 Injectable Emulsion Versus Supportive Care in Patients With Acute Pancreatitis and SIRS. [ClinicalTrials.gov](https://clinicaltrials.gov/Identifier/NCT03401190). Identifier: NCT03401190. Last update: May 3, 2019 (accessed Sep 13, 2020); (b) Study of CM4620 to Reduce the Severity of Pancreatitis Due to Asparaginase. [ClinicalTrials.gov](https://clinicaltrials.gov/Identifier/NCT04195347). Identifier: NCT04195347. Last update: September 10, 2020 (accessed Sep 13, 2020).

(14) Peng, S.; Gerasimenko, J. V.; Tsugorka, T.; Gryshchenko, O.; Samarasinghe, S.; Petersen, O. H.; Gerasimenko, O. V. Calcium and adenosine triphosphate control of cellular pathology: asparaginase-induced pancreatitis elicited via protease-activated receptor 2. *Philos. Trans. R. Soc. London, Ser. B* **2016**, *371*, 20150423.

(15) For review articles on SOCE modulators, see: (a) Sweeney, Z. K.; Minatti, A.; Button, D. C.; Patrick, S. Small-molecule inhibitors of store-operated calcium entry. *ChemMedChem* **2009**, *4*, 706–718. (b) Sweeney, Z. K.; Minatti, A.; Button, D. C.; Patrick, S. Small-molecule inhibitors of store-operated calcium entry. *ChemMedChem* **2009**, *4*, 706–718. (c) Tia, C.; Du, L.; Zhou, Y.; Li, M. Store-operated CRAC channel inhibitors: opportunities and challenges.



- Future Med. Chem.* **2016**, *8*, 817–832. (d) Lopez, J. J.; Albarran, L.; Gómez, L. J.; Smani, T.; Salido, G. M.; Rosado, J. A. Molecular modulators of store-operated calcium entry. *Biochim. Biophys. Acta* **2016**, *1863*, 2037–2043. (e) Stauderman, K. A. CRAC channels as targets for drug discovery and development. *Cell Calcium* **2018**, *74*, 147–159.
- (16) (a) Riva, B.; Griglio, A.; Serafini, M.; Cordero-Sanchez, C.; Aprile, S.; Di Paola, R.; Gugliandolo, E.; Alansary, D.; Biocotino, I.; Lim, D.; Grosa, G.; Galli, U.; Niemyer, B.; Sorba, G.; Canonico, P. L.; Cuzzocrea, S.; Genazzani, A. A.; Pirali, T. Pyrtriazoles, a novel class of store-operated calcium entry modulators: discovery, biological profiling, and in vivo proof-of-concept efficacy in acute pancreatitis. *J. Med. Chem.* **2018**, *61*, 9756–9783. (b) Pirali, T.; Riva, B.; Genazzani, A. A. Modulators of SOCE, Compositions and use thereof. WO 2017212414 A1, Dec 14, 2017.
- (17) (a) Schleifer, H.; Doleschal, B.; Lichtenegger, M.; Oppenrieder, R.; Derler, I.; Frischauf, I.; Glasnov, T.; Kappe, C.; Romanin, C.; Groschner, K. Novel pyrazole compounds for pharmacological discrimination between receptor-operated and store-operated  $\text{Ca}^{2+}$  entry pathways. *Br. J. Pharmacol.* **2012**, *167*, 1712–1722. (b) Kiyonaka, S.; Kato, K.; Nishida, M.; Mio, K.; Numaga, T.; Sawaguchi, Y.; Yoshida, T.; Wakamori, M.; Mori, E.; Numata, T.; Ishii, M.; Takemoto, H.; Ojida, A.; Watanabe, K.; Uemura, A.; Kurose, H.; Morii, T.; Kobayashi, T.; Sato, Y.; Sato, C.; Hamachi, I.; Mori, Y. Selective and direct inhibition of TRPC3 channels underlies biological activities of a pyrazole compound. *Proc. Natl. Acad. Sci. U.S.A.* **2009**, *106*, 5400–5405.
- (18) (a) Ng, S. W.; di Capote, J.; Singaravelu, K.; Parekh, A. B. Sustained activation of the tyrosine kinase Syk by antigen in mast cells requires local  $\text{Ca}^{2+}$  influx through  $\text{Ca}^{2+}$  release-activated  $\text{Ca}^{2+}$  channels. *J. Biol. Chem.* **2008**, *283*, 31348–31355. (b) Di Sabatino, A.; Rovedatti, L.; Kaur, R.; Spencer, J. P.; Brown, J. T.; Morisset, V. D.; Biancheri, P.; Leakey, N. A. B.; Wilde, J. I.; Scott, L.; Corazza, G. R.; Lee, K.; Sengupta, N.; Knowles, C. H.; Gunthorpe, M. J.; McLean, P. G.; MacDonald, T. T.; Kruidenier, L. Targeting gut T cell  $\text{Ca}^{2+}$  release activated  $\text{Ca}^{2+}$  channels inhibits T cell cytokine production and T-Box transcription factor T-Bet in inflammatory bowel disease. *J. Immunol.* **2009**, *183*, 3454–3462. (c) Xie, Y.; Holmqvist, M.; Mahiou, J.; Ono, M.; Sun, L.; Chen, S.; Zhang, S.; Jiang, J.; Chimmanamada, D.; Fleig, A.; Yu, C.-Y. Method for Modulating Calcium Ion-Release-Activated Calcium Ion Channels. CN 1826121 A, Feb 03, 2005; (d) Xie, Y.; Holmqvist, M.; Mahiou, J.; Ono, M.; Sun, L.; Chen, S.; Zhang, S.; Jiang, J.; Chimmanamada, D.; Yu, C.-Y. Compounds for Inflammation and Immune-Related Uses. U.S. Patent 8,314,134 B2, Feb 3, 2005.
- (19) Li, J.; McKeown, L.; Ojelabi, O.; Stacey, M.; Foster, R.; O'Regan, D.; Porter, K. E.; Beech, D. J. Nanomolar potency and selectivity of a  $\text{Ca}^{2+}$  release-activated  $\text{Ca}^{2+}$  channel inhibitor against store-operated  $\text{Ca}^{2+}$  entry and migration of vascular smooth muscle cells. *Br. J. Pharmacol.* **2011**, *164*, 382–393.
- (20) (a) Bonandi, E.; Christodoulou, M. S.; Fumagalli, G.; Perdicchia, D.; Rastelli, G.; Passarella, D. The 1,2,3-triazole ring as a bioisostere in medicinal chemistry. *Drug Discovery Today* **2017**, *22*, 1572–1581. (b) Kumari, S.; Carmona, A. V.; Tiwari, A. K.; Trippier, P. C. Amide Bond Bioisosteres: Strategies, Synthesis, and Successes. *J. Med. Chem.* **2020**, *63*, 12290–12358.
- (21) (a) Tron, G. C.; Pirali, T.; Billington, R. A.; Canonico, P. L.; Sorba, G.; Genazzani, A. A. Click chemistry reactions in medicinal chemistry: applications of the 1,3-dipolar cycloaddition between azides and alkynes. *Med. Res. Rev.* **2008**, *28*, 278–308. (b) Jiang, X.; Hao, X.; Jing, L.; Wu, G.; Kang, D.; Liu, X.; Zhan, P. Recent applications of click chemistry in drug discovery. *Expert Opin. Drug Discovery* **2019**, *14*, 779–789.
- (22) Azimi, I.; Stevenson, R. J.; Zhang, X.; Meizoso-Huesca, A.; Xin, P.; Johnson, M.; Flanagan, J. U.; Chalmers, S. B.; Yoast, R. E.; Kapure, J. S.; Ross, B. P.; Vetter, L.; Ashton, M. R.; Launikonis, B. S.; Denny, W. A.; Trebak, M.; Monteith, G. R. A new selective pharmacological enhancer of the Orail  $\text{Ca}^{2+}$  channel reveals roles for Orail in smooth and skeletal muscle functions. *ACS Pharmacol. Transl. Sci.* **2020**, *3*, 135–147.
- (23) (a) Pagliai, F.; Pirali, T.; Del Grosso, E.; Di Brisco, R.; Tron, G. C.; Sorba, G.; Genazzani, A. A. Rapid synthesis of triazole-modified resveratrol analogues via click chemistry. *J. Med. Chem.* **2006**, *49*, 467–470. (b) Pirali, T.; Pagliai, F.; Mercurio, C.; Boggio, R.; Canonico, P. L.; Sorba, G.; Tron, G. C.; Genazzani, A. A. Triazole-modified histone deacetylase inhibitors as a rapid route to drug discovery. *J. Comb. Chem.* **2008**, *10*, 624–627.
- (24) (a) Lolli, M. L.; Sainas, S.; Pippione, A. C.; Giorgis, M.; Boschi, D.; Dosio, F. Use of human dihydroorotate dehydrogenase (hDHODH) inhibitors in autoimmune diseases and new perspectives in cancer therapy. *Recent Pat. Anticancer Drug Discov.* **2018**, *13*, 86–105. (b) Leban, J.; Saeb, W.; Garcia, G.; Baumgartner, R.; Kramer, B. Discovery of a novel series of DHODH inhibitors by a docking procedure and QSAR refinement. *Bioorg. Med. Chem. Lett.* **2004**, *14*, 55–58. (c) Munier-Lehmann, H.; Vidalain, P.-O.; Tangy, F.; Janin, Y. L. On dihydroorotate dehydrogenases and their inhibitors and uses. *J. Med. Chem.* **2013**, *56*, 3148–3167.
- (25) (a) Davis, J. P.; Cain, G. A.; Pitts, W. J.; Magolda, R. L.; Copeland, R. A. The immunosuppressive metabolite of leflunomide is a potent inhibitor of human dihydroorotate dehydrogenase. *Biochemistry* **1996**, *35*, 1270–1273. (b) Palmer, A. M. Teriflunomide, an inhibitor of dihydroorotate dehydrogenase for the potential oral treatment of multiple sclerosis. *Curr. Opin. Invest. Drugs* **2010**, *11*, 1313–1323.
- (26) Rahman, S.; Rahman, R. Unveiling some FDA-approved drugs as inhibitors of the store-operated  $\text{Ca}^{2+}$  entry pathway. *Sci. Rep.* **2017**, *7*, 12881–12893.
- (27) Peters, G. J.; Sharma, S. L.; Laurensse, E.; Pinedo, H. M. Inhibition of pyrimidine de novo synthesis by DUP-785 (NSC368390). *Invest. New Drugs* **1987**, *5*, 235–244.
- (28) Sainas, S.; Pippione, A. C.; Lupino, E.; Giorgis, M.; Circosta, P.; Gaidano, V.; Goyal, P.; Bonanni, D.; Rolando, B.; Cignetti, A.; D'Amico, A.; Andersson, M.; Järva, M.; Friemann, R.; Piccinini, M.; Ramondetti, C.; Buccinnà, B.; Al-Karadaghi, S.; Boschi, D.; Saglio, G.; Lolli, M. L. Targeting Myeloid Differentiation Using Potent 2-Hydroxypyrazolo[1,5-a]pyridine Scaffold-Based Human Dihydroorotate Dehydrogenase Inhibitors. *J. Med. Chem.* **2018**, *61*, 6034–6055.
- (29) Paterniti, I.; Mazzon, E.; Riccardi, L.; Galuppo, M.; Impellizzeri, D.; Esposito, E.; Bramanti, P.; Cappellani, A.; Cuzzocrea, S. Peroxisome proliferator-activated receptor  $\beta/\delta$  agonist GW0742 ameliorates cerulein- and taurocholate-induced acute pancreatitis in mice. *Surgery* **2012**, *152*, 90–106.



## SUPPORTING INFORMATION

### Store-Operated Calcium Entry (SOCE) as a therapeutic target in acute pancreatitis: discovery and development of drug-like SOCE inhibitors

*Marta Serafini<sup>1#</sup>, Celia Cordero-Sanchez<sup>1#</sup>, Rosanna Di Paola<sup>2</sup>, Irene P. Bhela<sup>1</sup>, Silvio Aprile<sup>1</sup>, Beatrice Purghè<sup>1</sup>, Roberta Fusco<sup>2</sup>, Salvatore Cuzzocrea<sup>2</sup>, Armando A. Genazzani<sup>1</sup>, Beatrice Riva<sup>1,3\*</sup>, Tracey Pirali<sup>1,3\*#@</sup>*

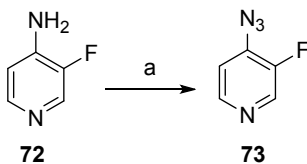
<sup>1</sup> Department of Pharmaceutical Sciences; Università del Piemonte Orientale; Novara, 28100; Italy; <sup>2</sup> Department of Chemical, Biological, Pharmaceutical and Environmental Sciences; Università di Messina; Messina, 98166; Italy; <sup>3</sup> ChemiCare S.r.l.; Enne3; Novara, 28100; Italy.

#### Table of contents

p. S2	Chemistry
p. S5	NMR Spectra of compounds <b>31, 34, 35, 36, 38, 40, 50, 56</b>
p. S13	Biology
p. S14	<i>In vitro</i> metabolism and pharmacokinetic
p. S17	Purity of lead compounds and thermodynamic aqueous solubility
p. S18	<i>In vivo</i> PK evaluation of compound <b>34</b>
p. S19	Metabolic stability data

## Chemistry

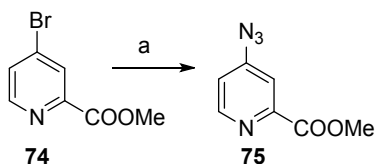
### Synthesis and characterization of azide **73**



Reagents and conditions: (a) NaNO<sub>2</sub>, NaN<sub>3</sub>, TFA, 0 °C, 2 h, 76%.

**4-Azido-3-fluoropyridine, (73).** To a solution of 3-fluoropyridin-4-amine **72** (150 mg, 1.33 mmol) in TFA (3.3 mL) NaNO<sub>2</sub> (111 mg, 1.61 mmol) was added at 0 °C. After 1 h, NaN<sub>3</sub> (1.88 g, 35.2 mmol) was added and the mixture was maintained under vigorous stirring. After 1 h, saturated aqueous NaHCO<sub>3</sub> solution was added until pH 8-9 and the aqueous phase was extracted with ethyl acetate (x2). The collected organic layers were dried over sodium sulfate and evaporated to give 4-azido-3-fluoropyridine **73** (139 mg, 1.01 mmol, 76%) as a pale brown oil. <sup>1</sup>H NMR (300 MHz, CDCl<sub>3</sub>): δ = 8.40 (d, *J* = 3.0 Hz, 1H), 8.30 (d, *J* = 5.2 Hz, 1H), 7.27 (dd, *J*<sub>S</sub> = 5.2 Hz, 3.1 Hz, 1H).

### Synthesis and characterization of azide **75**

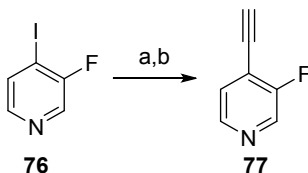


Reagents and conditions: (a) NaN<sub>3</sub>, DMF, H<sub>2</sub>O, 80 °C, 16 h, 59%.

**Methyl 4-azidopicolinate, (75).** Methyl 4-bromopicolinate **74** (300 mg, 1.91 mmol) was solubilized in DMF (2.2 mL) and water (0.11 mL) and NaN<sub>3</sub> (149 mg, 2.29 mmol) was added portionwise. The reaction was heated at 80 °C overnight. Then, the mixture was diluted with ethyl acetate and washed with water (x5). The organic phase was dried over sodium sulfate and evaporated to afford compound

**75** as a pale yellow solid (200 mg, 1.13 mmol, 59%). <sup>1</sup>H NMR (300 MHz, CDCl<sub>3</sub>): δ = 8.53 (d, *J* = 5.5 Hz, 1H), 7.74 (s, 1H), 7.31 (d, *J* = 5.5 Hz, 1H), 3.89 (s, 3H).

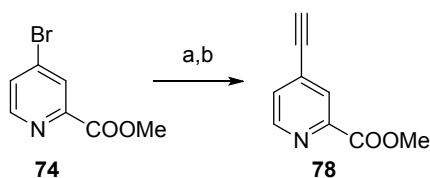
#### Synthesis and characterization of alkyne **77**



Reagents and conditions: (a) Ethynyltrimethylsilane, DIPEA, CuI, Pd(PPh<sub>3</sub>)<sub>2</sub>Cl<sub>2</sub>, DMF, rt, 2 h. (b) TBAF, THF, 0 °C, 30 min, 45%.

**4-Ethynyl-3-fluoropyridine (77). Step 1:** 3-Fluoro-4-iodopyridine **76** (118 mg; 0.53 mmol), DMF (1.2 mL), Pd(PPh<sub>3</sub>)<sub>2</sub>Cl<sub>2</sub> (35 mg; 0.05 mmol), CuI (9.52 mg; 0.05 mmol), DIPEA (0.36 mL; 2.11 mmol) and ethynyltrimethylsilane (0.22 mL; 1.59 mmol) were added in a Schlenk apparatus under nitrogen atmosphere. After 2 h the mixture was filtered over a pad of celite, the volatile was removed under reduced pressure and the reaction was worked up by dilution with ethyl acetate and washed with water (x1). The organic layer was washed with brine, dried over sodium sulfate and evaporated. The crude product was used in the next step without further purification. **Step 2:** 3-fluoro-4-((trimethylsilyl)ethynyl) pyridine was dissolved in THF (3.3 mL) at 0 °C. After 5 min TBAF (0.62 mL; 0.62 mmol) was added. After 30 min the volatile was removed under reduced pressure and the reaction was worked up by dilution with ethyl acetate and washing with water (x1). The crude material was purified by column chromatography using petroleum ether/ethyl acetate 98:2 and then petroleum ether/ethyl acetate 95:5 as eluents yielding 4-ethynyl-3-fluoropyridine **77** (28.9 mg, 0.23 mmol, 45%) as a brown oil. <sup>1</sup>H NMR (300 MHz, CDCl<sub>3</sub>): δ = 8.50 (s, 1H), 8.39 (d, *J* = 4.7 Hz, 1H), 7.38 (d, *J* = 5.5 Hz, 1H), 3.51 (s, 1H). MS (ESI): *m/z*: 122 [M + H]<sup>+</sup>.

## Synthesis and characterization of alkyne **78**

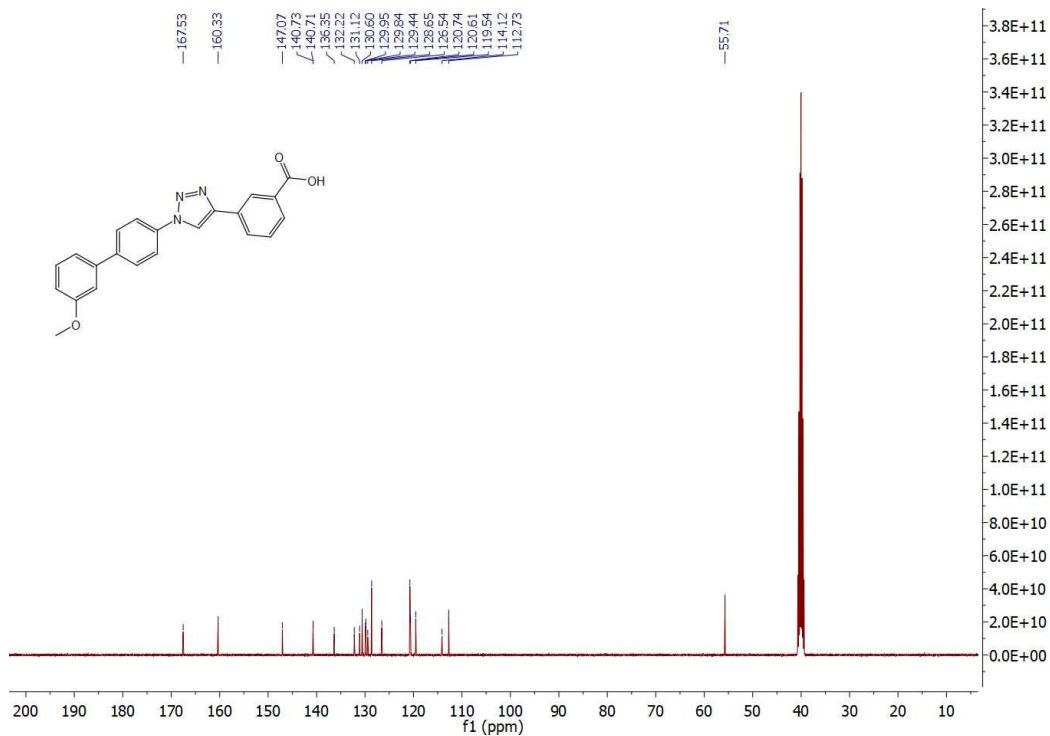
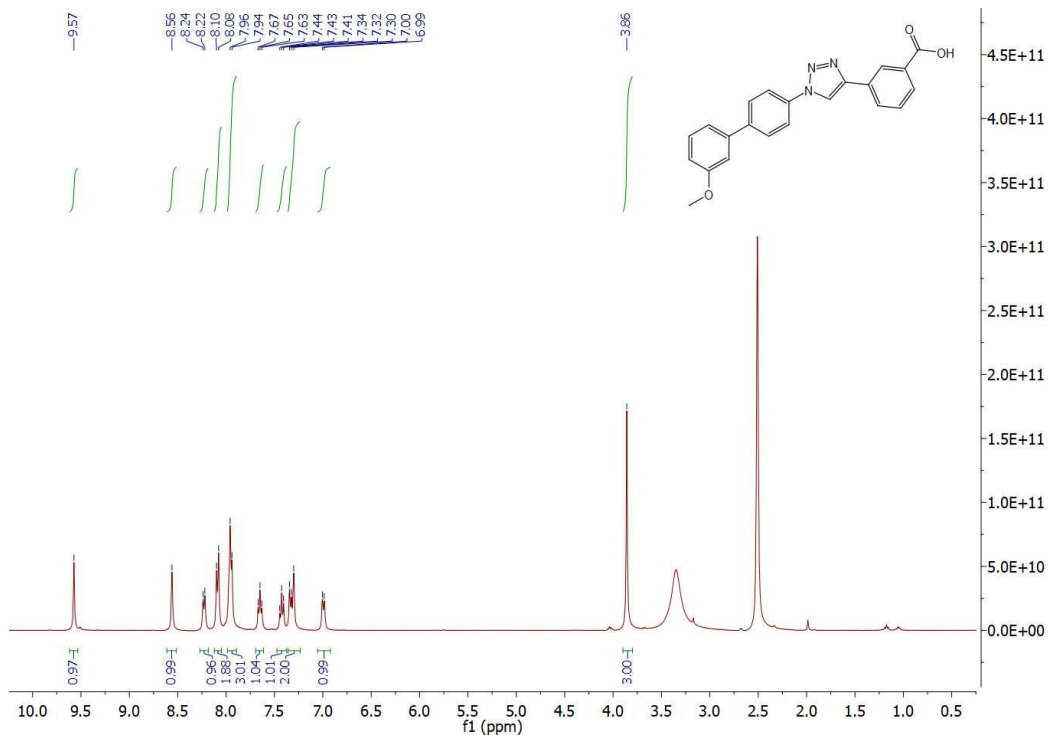


Reagents and conditions: (a) Ethynyltrimethylsilane, DIPEA, CuI, Pd(PPh<sub>3</sub>)<sub>2</sub>Cl<sub>2</sub>, toluene dry, 100 °C, 2 h, 99%. (b) CH<sub>3</sub>COOH, TBAF, THF, 0 °C, 30 min, 93%.

**Methyl 4-ethynylpicolinate, (78). Step 1:** To a solution of methyl 4-bromopicolinate **74** (300 mg, 1.39 mmol) in dry toluene (3 mL), DIPEA (0.48 mL, 2.79 mmol), CuI (24 mg, 0.12 mmol), Pd(PPh<sub>3</sub>)<sub>2</sub>Cl<sub>2</sub> (29.33 mg, 0.04 mmol) and ethynyltrimethylsilane (0.59 mL, 4.19 mmol) were added in a Schlenk apparatus. The reaction was stirred at reflux for 2 h under nitrogen atmosphere. Then, the mixture was filtered over a pad of celite and rinsed with ethyl acetate. The organic phase was washed with water (x1), dried over sodium sulfate and evaporated. The crude material was purified by column chromatography using petroleum ether/ethyl acetate 8:2 and petroleum ether/ethyl acetate 7:3 as eluents to give methyl 4-((trimethylsilyl)ethynyl)picolinate as a brown oil (322 mg, 1.38 mmol, 99%). <sup>1</sup>H NMR (300 MHz; CDCl<sub>3</sub>): δ = 8.69 (d, *J* = 4.8 Hz, 1H), 8.14 (s, 1H), 7.54 (d, *J* = 4.8 Hz, 1H), 4.06 (s, 3H), 1.19 (s, 9H). **Step 2:** methyl 4-((trimethylsilyl)ethynyl)picolinate (173 mg, 0.74 mmol) was dissolved in THF (1.5 mL). The mixture was cooled at 0 °C and CH<sub>3</sub>COOH (50.9 μL, 0.89 mmol) and TBAF (0.89 mL, 0.89 mmol) were added. The reaction was stirred at 0 °C for 30 min. The volatile was removed under vacuum, ethyl acetate was added and the organic layer was washed with water (x1). After drying over sodium sulfate and evaporation of the solvent, the crude material was purified by column chromatography using petroleum ether/ethyl acetate 6:4 and petroleum ether/ethyl acetate 5:5 as eluents to give compound **78** (111 mg, 0.69 mmol, 93%) as a brown solid. <sup>1</sup>H NMR (300 MHz, CDCl<sub>3</sub>): δ = 8.17 (s, 1 H), 7.96 (d, *J* = 6.5 Hz, 1H), 7.67 (d, *J* = 6.5 Hz, 1H), 7.40 (t, *J* = 6.5 Hz, 1H), 3.92 (s, 3H), 3.12 (s, 1H). MS (ESI): *m/z*: 161 [M + H]<sup>+</sup>.

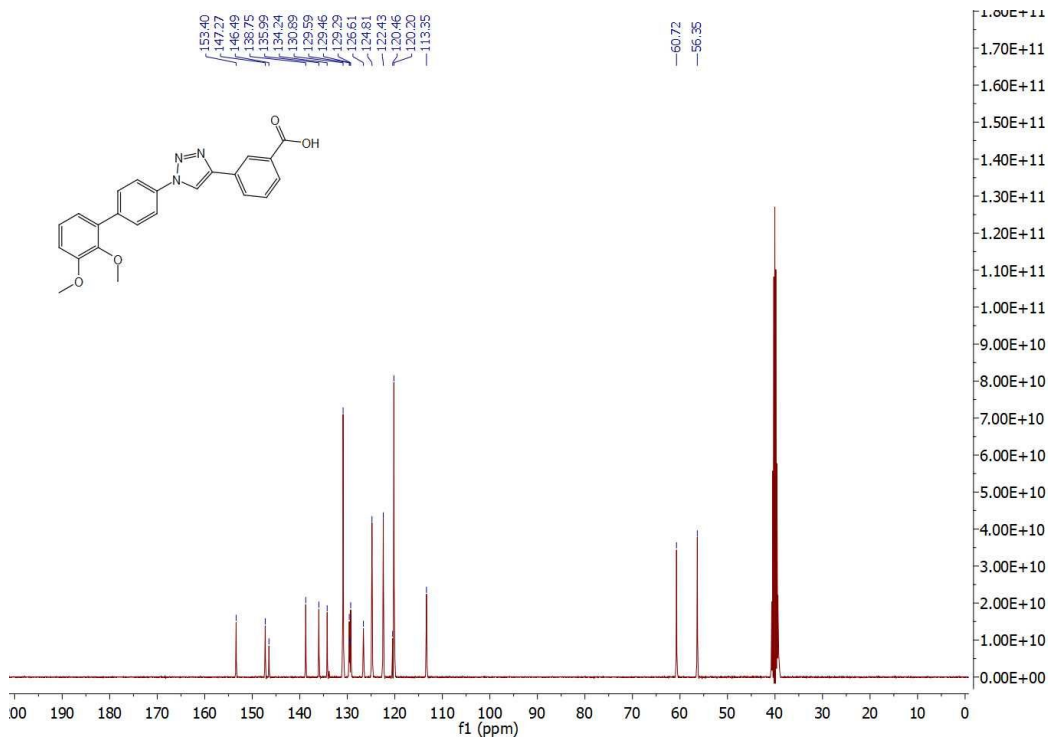
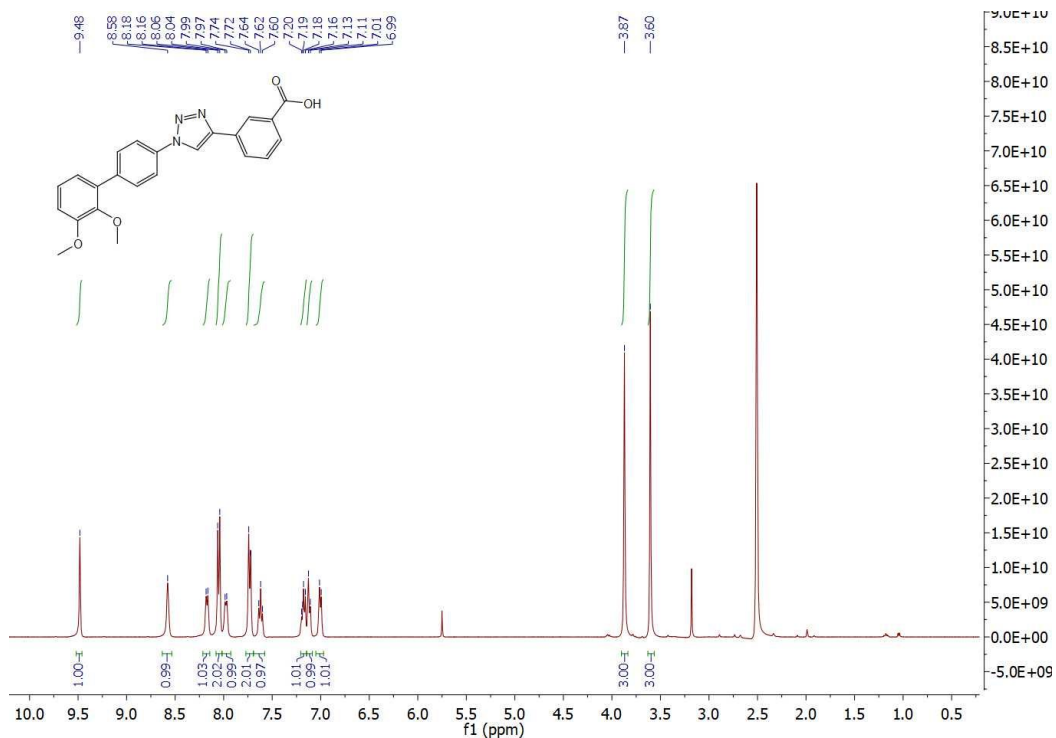
**NMR Spectra of compounds 31, 34, 35, 36, 38, 40, 50, 56.**

**31:  $^1\text{H}$  (DMSO- $d_6$ ),  $^{13}\text{C}$  (DMSO- $d_6$ )**

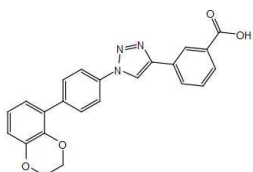
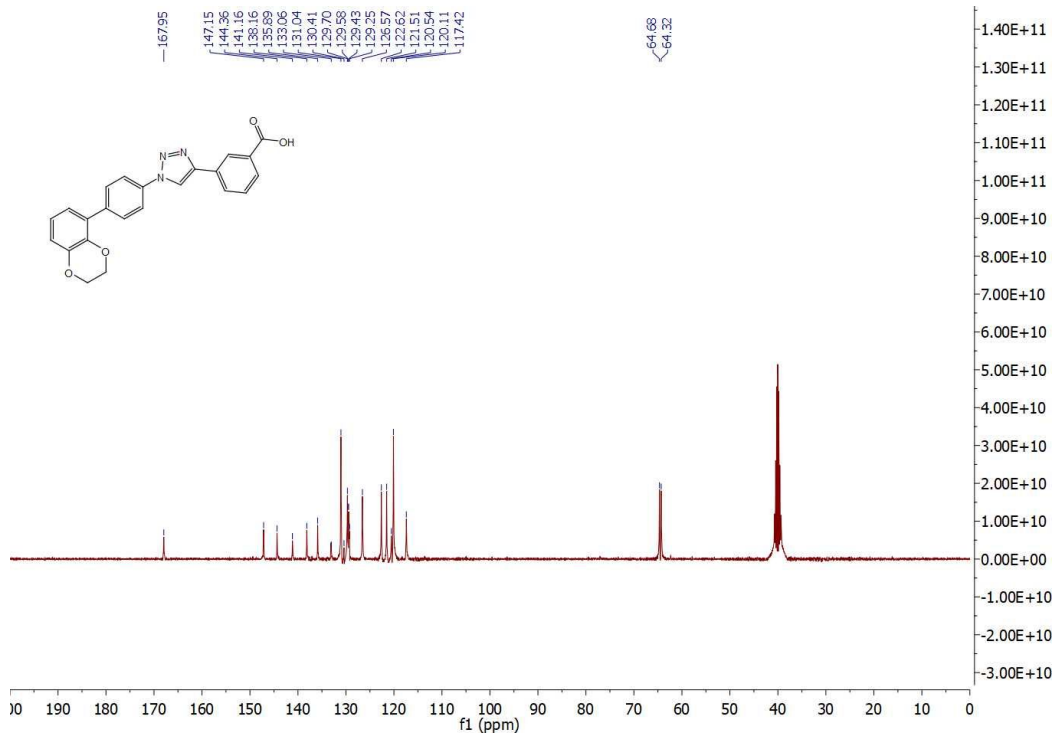
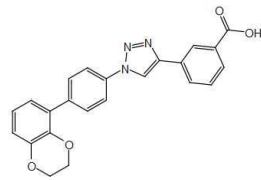
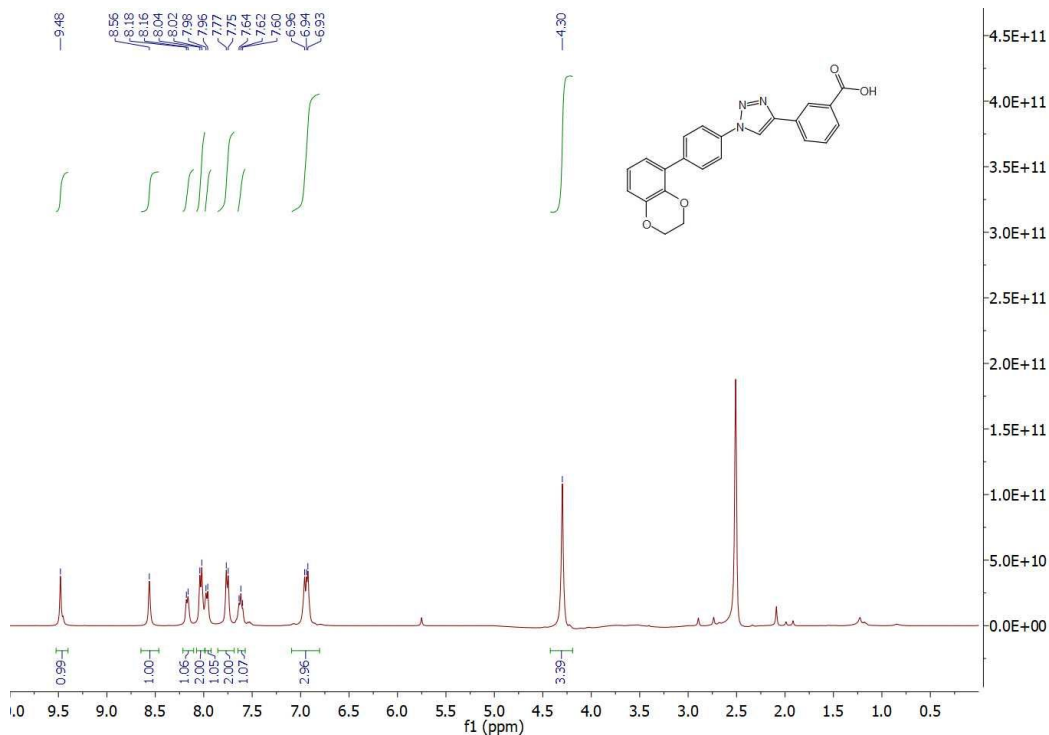




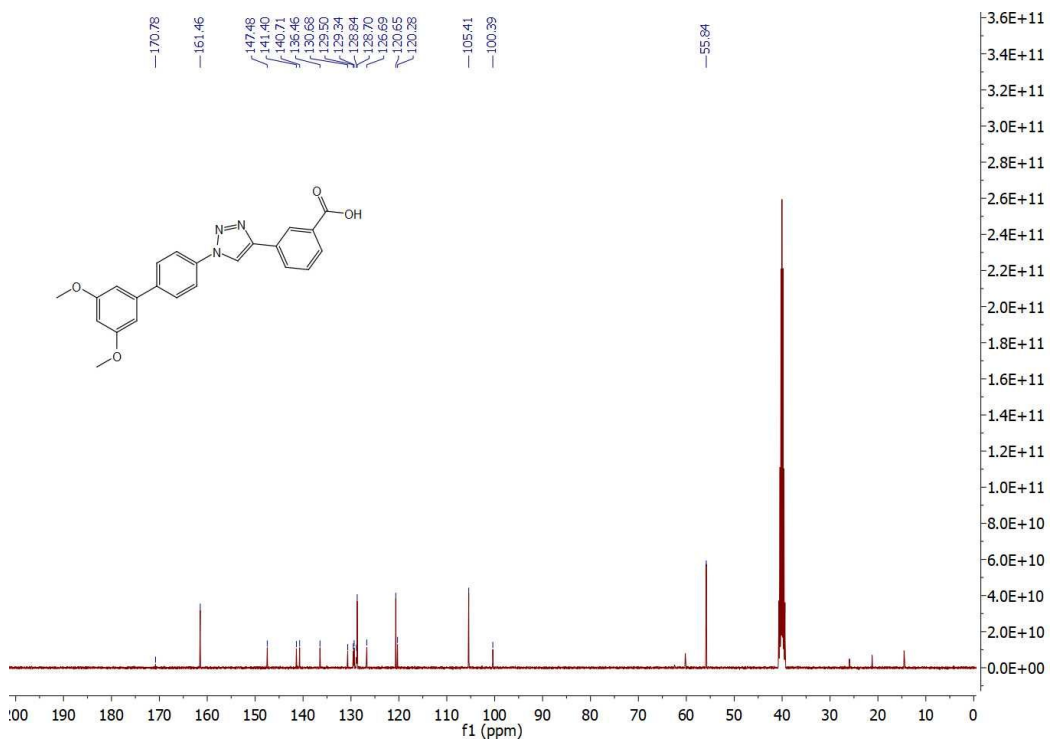
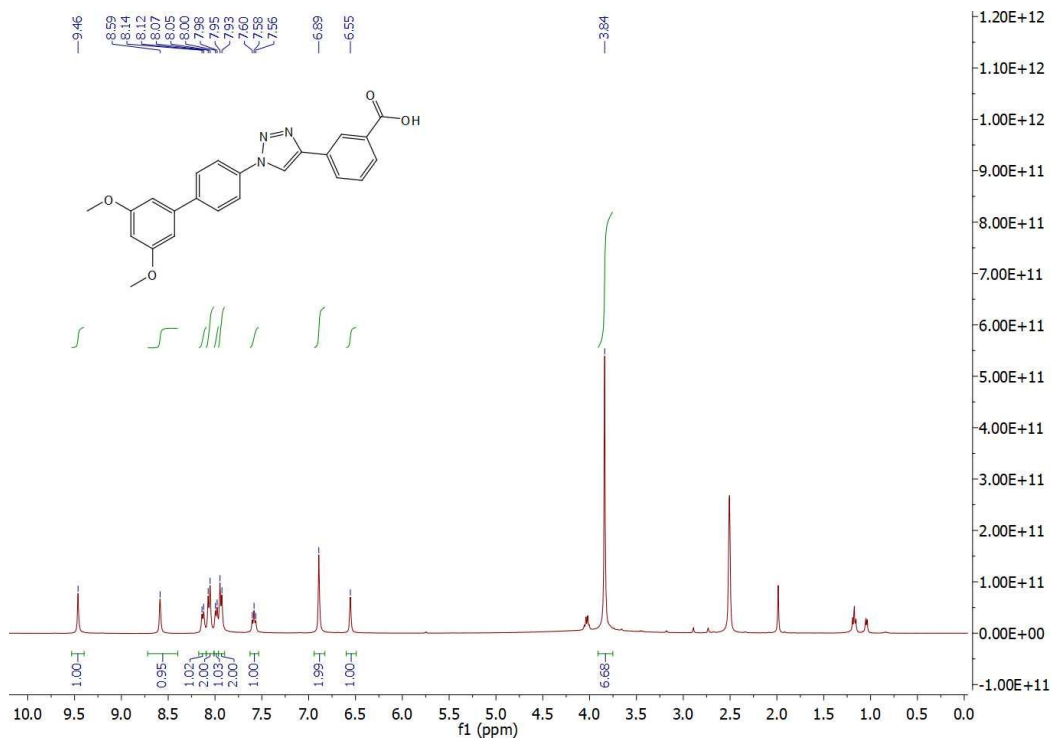
34:  $^1\text{H}$  (DMSO- $d_6$ ),  $^{13}\text{C}$  (DMSO- $d_6$ )



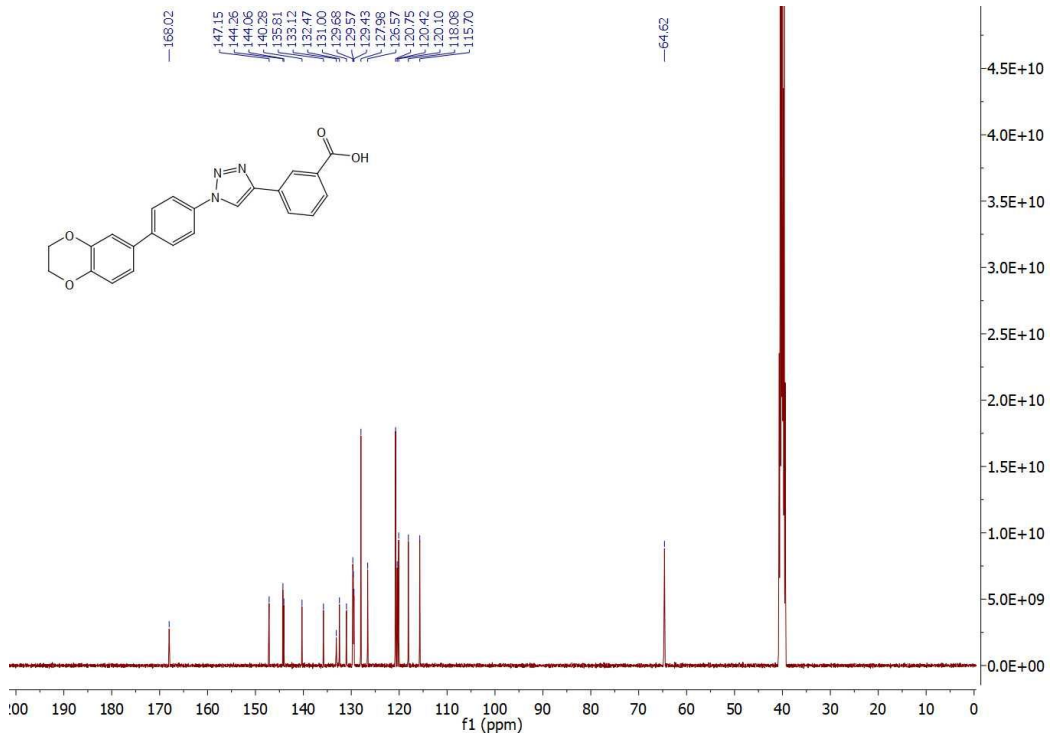
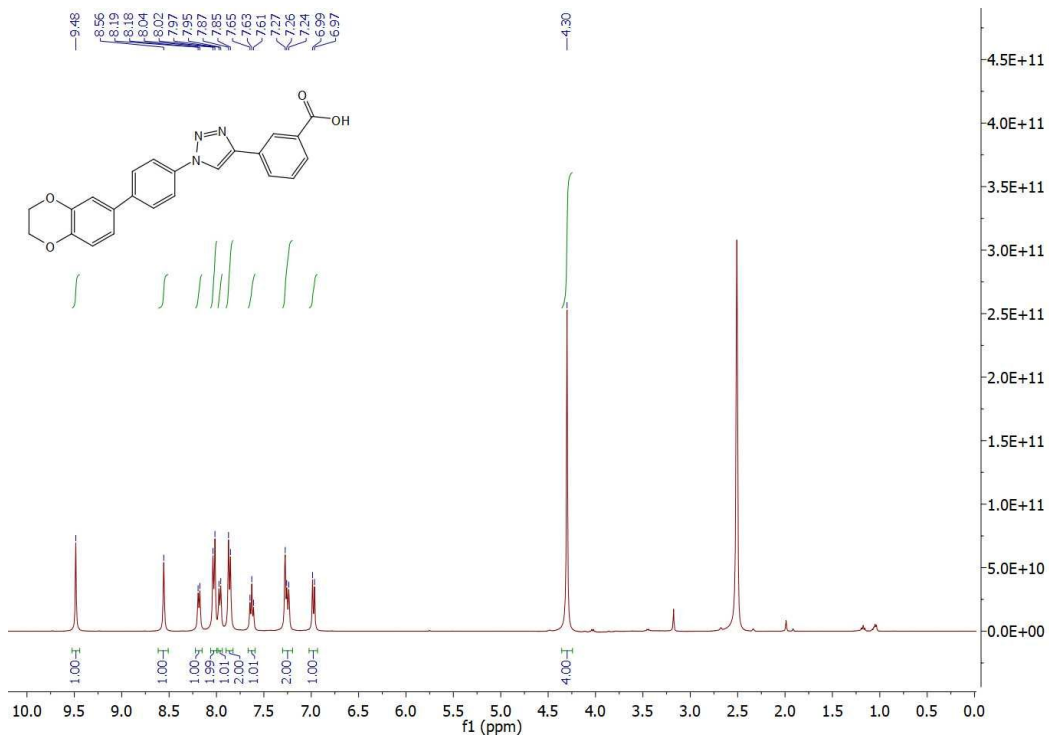
35: <sup>1</sup>H (DMSO-d<sub>6</sub>), <sup>13</sup>C (DMSO-d<sub>6</sub>)



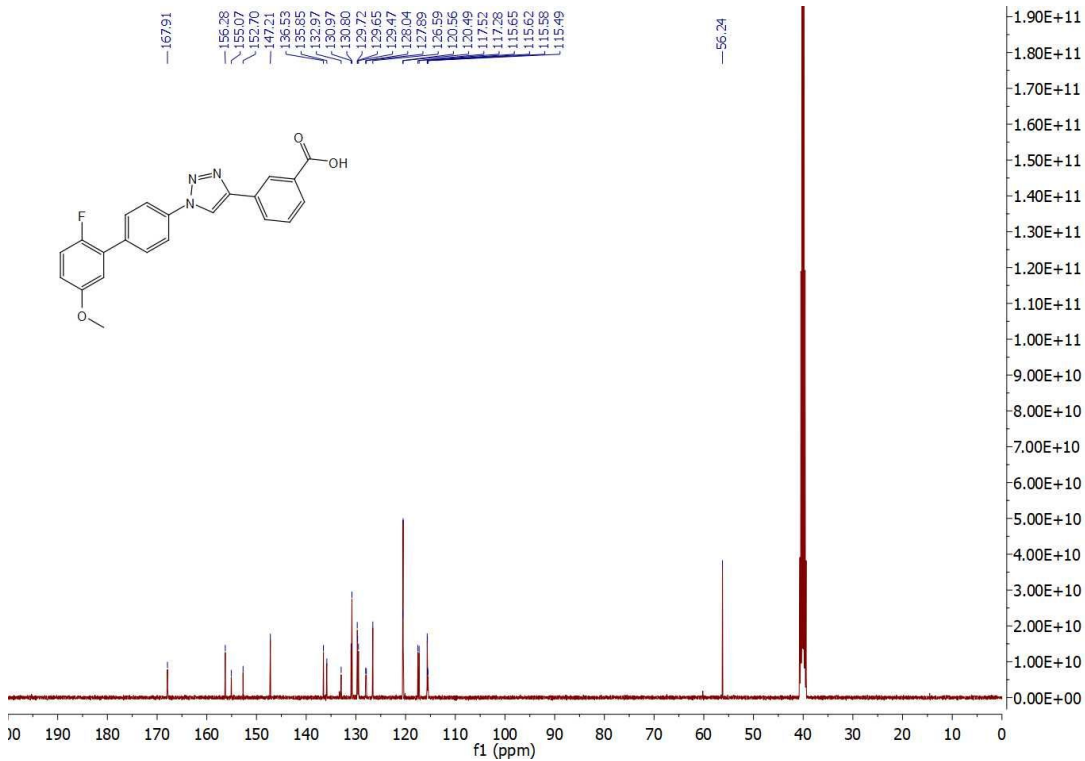
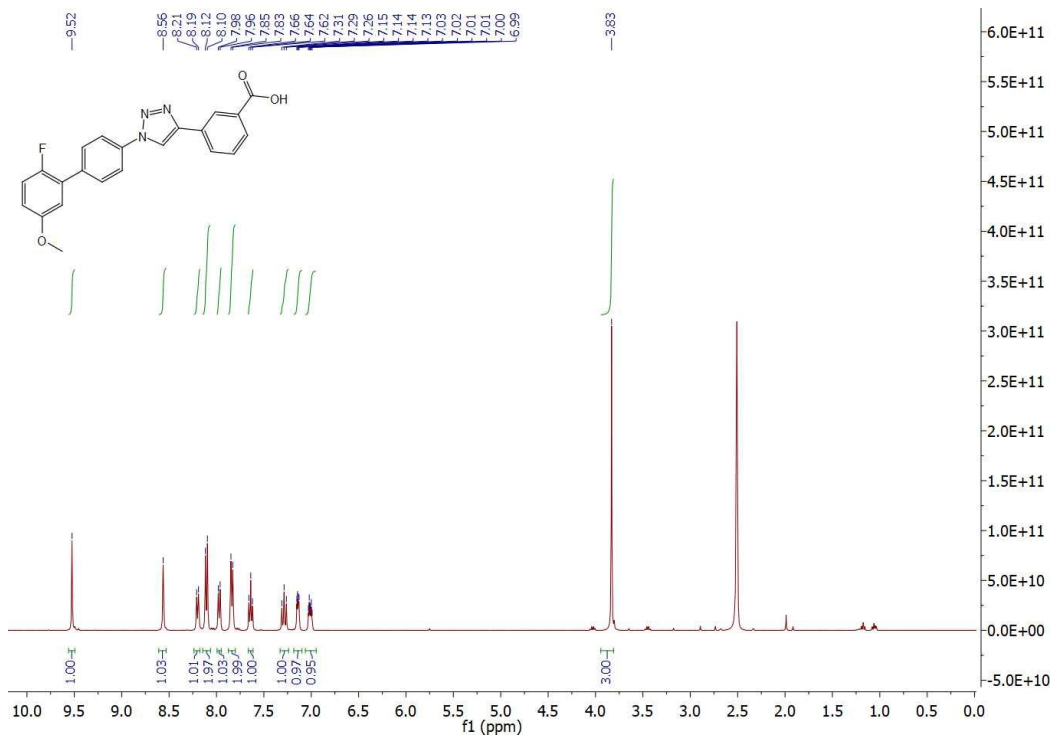
36:  $^1\text{H}$  (DMSO- $d_6$ ),  $^{13}\text{C}$  (DMSO- $d_6$ )



38: <sup>1</sup>H (DMSO-d<sub>6</sub>), <sup>13</sup>C (DMSO-d<sub>6</sub>)

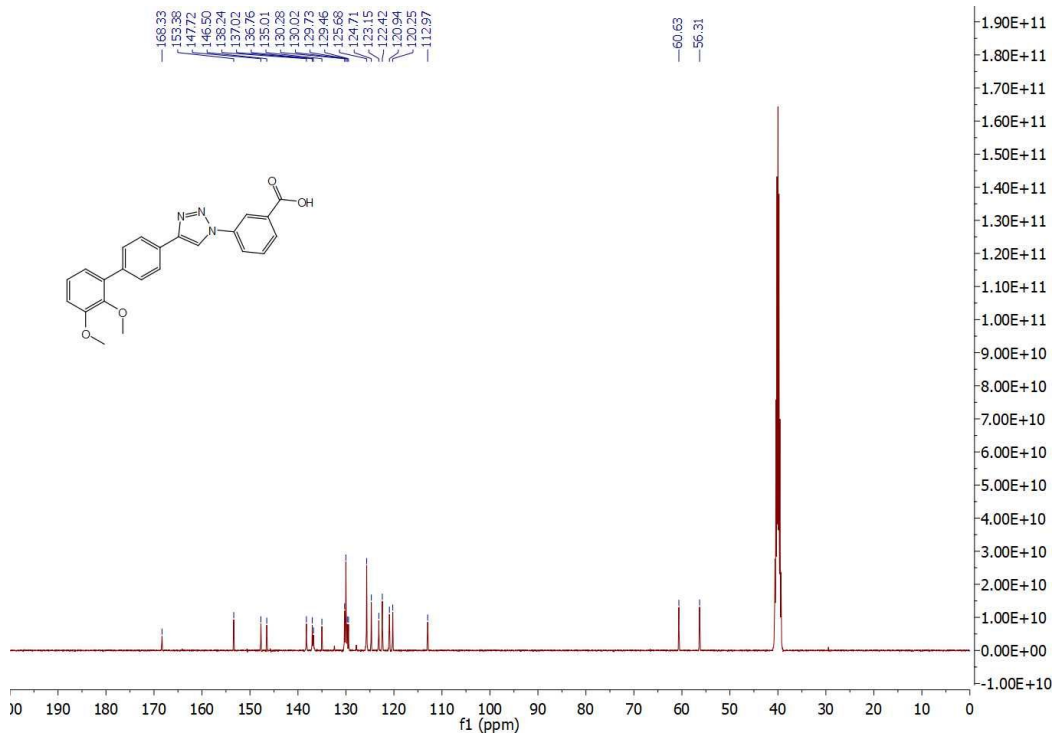
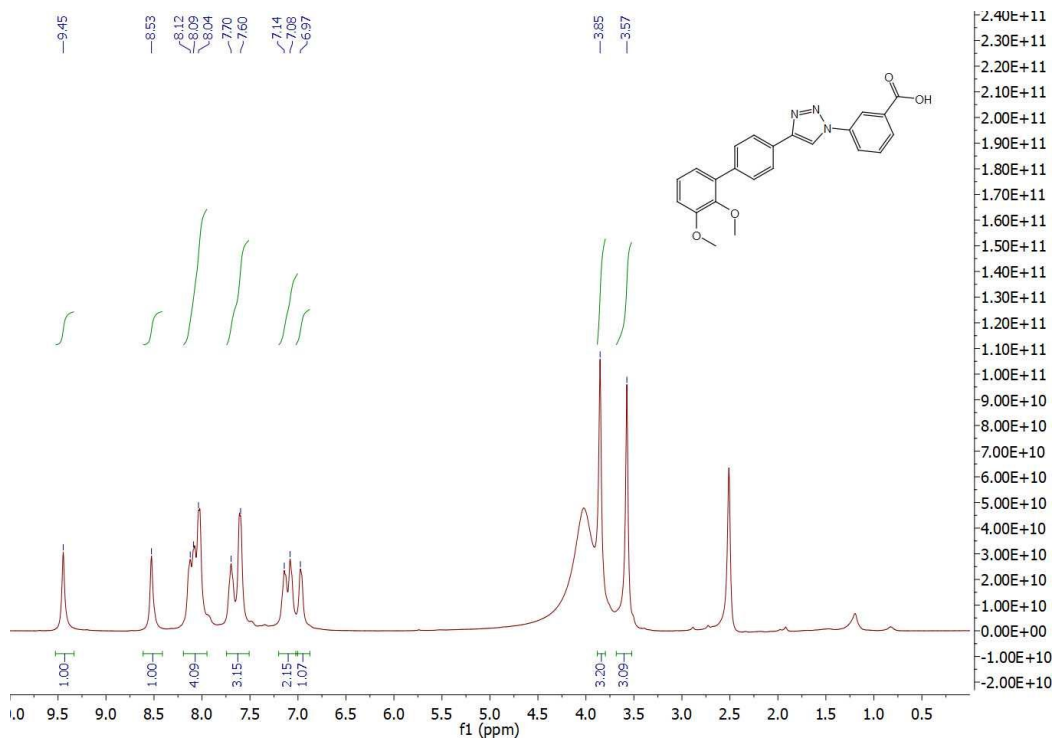


40:  $^1\text{H}$  (DMSO- $d_6$ ),  $^{13}\text{C}$  (DMSO- $d_6$ )

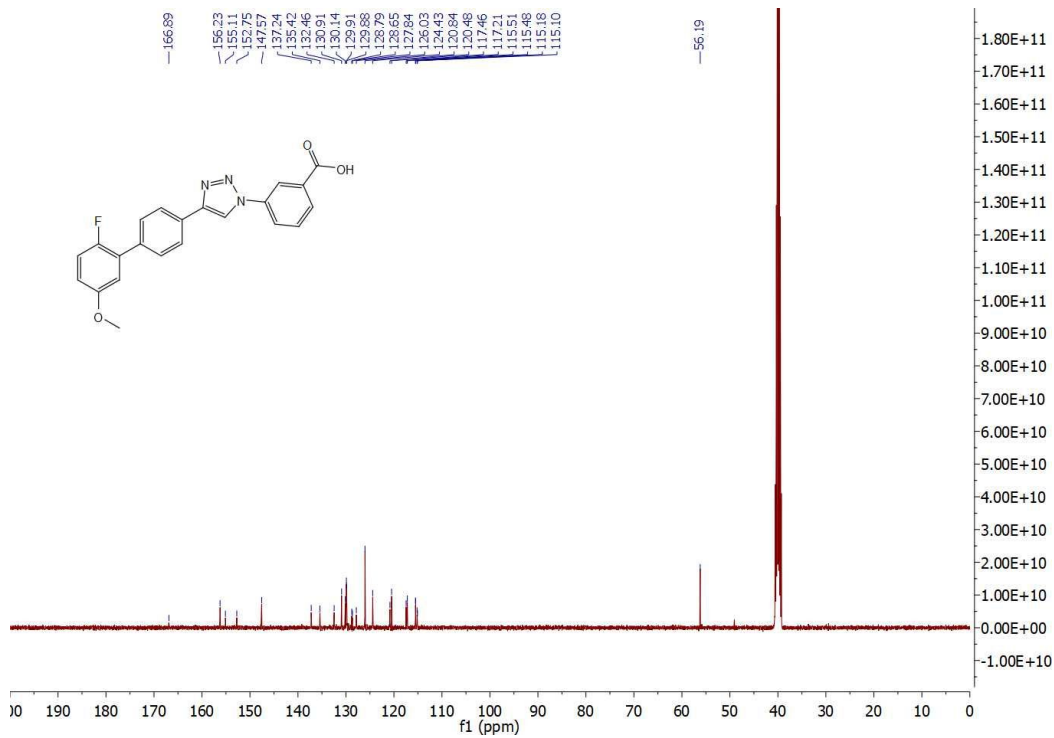
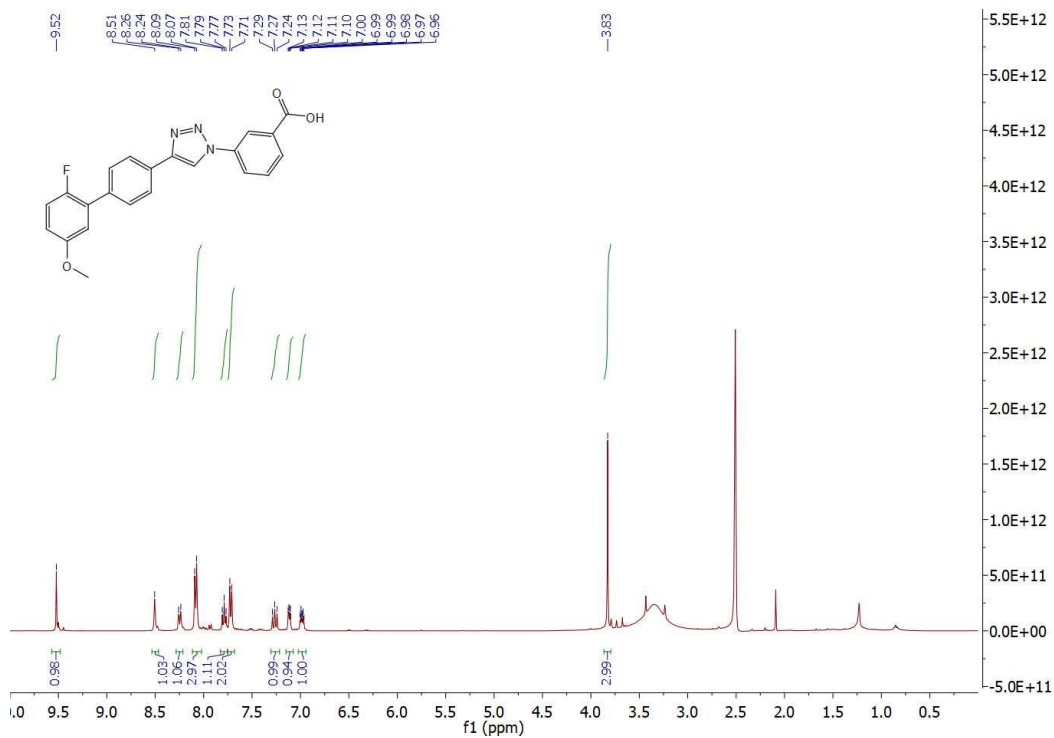


S11

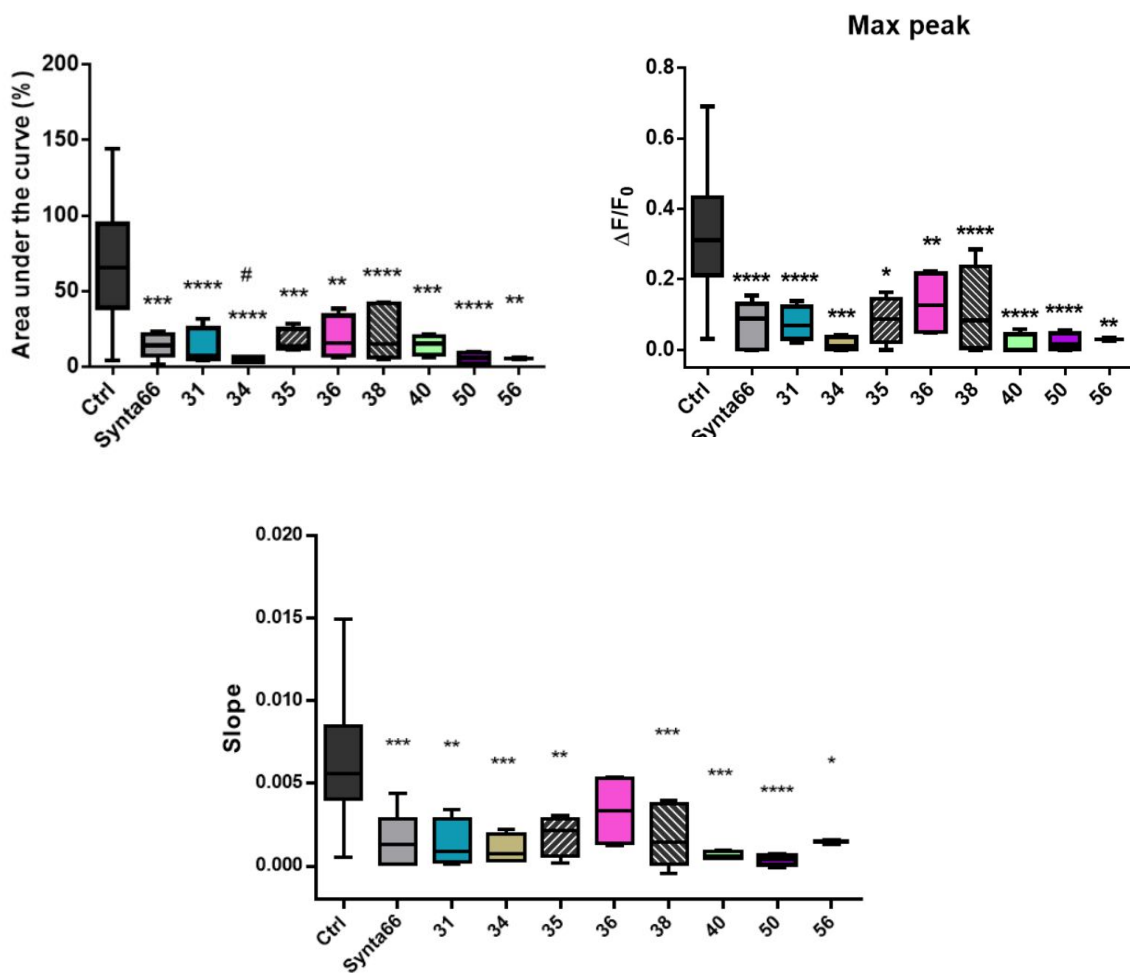
50: <sup>1</sup>H (DMS-d<sub>6</sub>), <sup>13</sup>C (DMSO-d<sub>6</sub>)



56: <sup>1</sup>H (DMSO-d<sub>6</sub>), <sup>13</sup>C (DMSO-d<sub>6</sub>)



## Biology



**Figure S1.** Evaluation of the area under the curve (AUC), peak amplitude, and slope of the  $\text{Ca}^{2+}$ -rise in the absence or presence of the indicated compounds. Graph shows median and IQR of the AUC, peak amplitude and slope of the  $\text{Ca}^{2+}$ -rise. Mann-Whitney U test of compound vs control (\*  $p < 0.0286$ , \*\*  $p < 0.0038$ , \*\*\*  $p < 0.0007$ , \*\*\*\*  $p < 0.0001$ ). Mann-Whitney U test. Mann-Whitney U test of compound vs Synta66 (# = 0.0485).



### **In vitro metabolism and pharmacokinetic.**

A Thermo Scientific Q-Exactive Plus system equipped with a Thermo Scientific Vanquish UHPLC system with a binary pump VF-P10, a split sampler VF-A10, and a column compartment VH-C10 were used. Data were acquired and processed using Xcalibur<sup>®</sup> software.

The operating conditions of the mass spectrometer were as follows: positive mode; sheath gas flow rate, 45 Auxiliary Units (A.U.), auxiliary gas flow rate, 10 A.U.; sweep gas flow rate, 2 A.U.; spray voltage, 3.50 kV; capillary temperature, 300 °C; auxiliary gas heater temperature, 300 °C.

#### ***1) LC-HRMS methods for metabolism studies.***

- Column: *Phenomex Kinetex C18 100 × 2.1 mm (2.6µm d.p.)* protected with a SecurityGuard<sup>®</sup> and kept at 40 °C (Torrance, CA, USA).
- Eluent:
  - A: 0.1% formic acid in water.
  - B: methanol.
- Flow rate: 0.250 mL/min.
- Injection volume: 5 µL.
- Gradient program: 0.00 min [B%=20%], 14.00 min [B%=90%], 16.50 min [B%=90%], 17.00 min [B%=20%], 22.00 min [B%=20%].

For metabolic stability assays, samples were acquired in positive full-MS and parallel reaction monitoring (PRM), using the parameters reported in Table S1 and monitoring the ions reported in the inclusion list S2.

PRM	
Microscans	1
Resolution	35.000
AGC target	1×10 <sup>5</sup>
Maximum IT	120 ms
Number of scan ranges	1
Loop count	1
MSX count	1
MSX isocronous ITs	on
Isolation window	1.5 <i>m/z</i>
Fixed first mass	180.0 <i>m/z</i>
Collision energy	CE:37
Mass scan range	150-850 <i>m/z</i>

**Table S1.** Parameters used for metabolic stability assays.

Compound	Mass [M+H] <sup>+</sup>	Formula [M]
Synta66	353.12960	C <sub>20</sub> H <sub>17</sub> FN <sub>2</sub> O <sub>3</sub>
<b>31</b>	372.13427	C <sub>22</sub> H <sub>17</sub> N <sub>3</sub> O <sub>3</sub>
<b>34</b>	402.14483	C <sub>23</sub> H <sub>19</sub> N <sub>3</sub> O <sub>4</sub>
<b>36</b>	402.14483	C <sub>23</sub> H <sub>19</sub> N <sub>3</sub> O <sub>4</sub>
<b>38</b>	400.12918	C <sub>23</sub> H <sub>17</sub> N <sub>3</sub> O <sub>4</sub>
<b>40</b>	390.12485	C <sub>22</sub> H <sub>16</sub> FN <sub>3</sub> O <sub>3</sub>

**Table S2.** Ions monitored for metabolic stability assays.

For metabolite characterization of compound **34**, samples were analysed in positive full-MS and dd-MS<sup>2</sup> (topN) modes using the parameters reported in Table S3.

Full MS		dd-MS <sup>2</sup> (topN)	
Microscans	1	Microscans	1
Resolution	70.000	Resolution	17.500
AGC target	1×10 <sup>6</sup>	AGC target	1×10 <sup>5</sup>
Maximum IT	200 ms	Maximum IT	60 ms
Number of scan ranges	1	Loop count	4
Scan range	150-850 <i>m/z</i>	MSX count	1
		TopN	4
		Isolation window	4.0 <i>m/z</i>
		Collision energy (CE)	37
		Minimum AGC target	6×10 <sup>3</sup>
		Intensity threshold	1×10 <sup>5</sup>
		Dynamic exclusion	3.0 s

**Table S3.** Parameters used for metabolite characterization of compound **34**.

## 2) LC-HRMS methods for pharmacokinetic analysis of compound 34.

- Column: Phenomenex Kinetex C18 150 × 2.1 mm (2.6 μm d.p.) protected with a SecurityGuard® and kept at 40 °C (Torrance, CA, USA).
- Eluent:
  - A: 0.1% formic acid in water.
  - B: acetonitrile.
- Injection volume: 5 μL.
- Analysis were performed in solvent and flow rate gradient elution (Table S4).

Time (min)	B%	Flow [mL/min]
0.00	30	0.300
5.00	98	0.300
7.00	98	0.400
7.50	30	0.400
10.00	30	0.300

**Table S4.** Solvent and flow rate gradient elution used for pharmacokinetic analysis of compound **34**.

Data were acquired in parallel reaction monitoring (PRM) mode monitoring the ions [M+H]<sup>+</sup> 402.14483 (C<sub>23</sub>H<sub>19</sub>N<sub>3</sub>O<sub>4</sub>) **34** and [M+H]<sup>+</sup> 390.12485 (C<sub>22</sub>H<sub>16</sub>FN<sub>3</sub>O<sub>3</sub>) **40** which was used as internal standard (IS). The operating conditions are reported in Table S5.

PRM	
Microscans	1
Resolution	35.000
AGC target	1×10 <sup>5</sup>
Maximum IT	120 ms
Number of scan ranges	1
Loop count	1
MSX count	1
MSX isocronous ITs	on
Isolation window	1.5 m/z
Fixed first mass	180.0 m/z
Collision energy	CE:32

**Table S5.** Operating conditions used for pharmacokinetic analysis of compound **34**.

### **Purity of lead compounds and thermodynamic aqueous solubility.**

A Shimadzu HPLC system (Shimadzu, Kyoto, Japan), consisting of two LC-10AD Vp module pumps, an SLC-10A Vp system controller, an SIL-10AD Vp autosampler, and a DGU-14-A on-line degasser were used for the analysis. The SPD-M10Avp photodiode array detector was used to detect the analytes. LC-Solution 1.24 software was used to process the chromatograms.

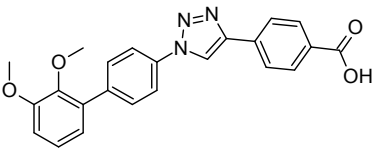
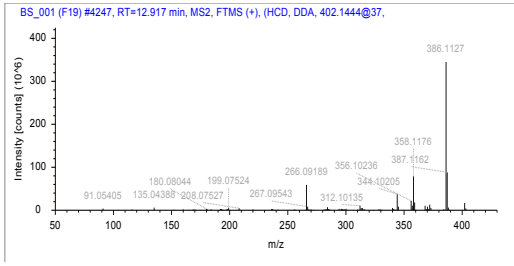
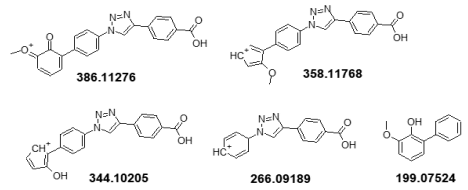
- Column: *Phenomenex Kinetex C18XB*, 150 × 4.6 mm (5 μm d.p.) protected with a SecurityGuard® (Torrance, CA, USA).
- Eluent:
  - A: 0.2% formic acid in water.
  - B: 0.2% formic acid in acetonitrile.
- Flow rate: 1 mL/min.
- Injection volume: 20 μL.
- Wavelength: 220 and 280 nm
- Gradient program: 0.00 min [B%=30%], 10.00 min [B%=90%], 12.50 min [B%=90%], 13.00 min [B%=30%], 18.00 min [B%=30%].

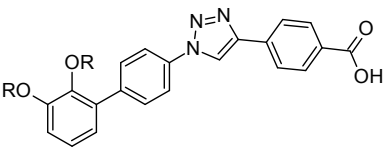
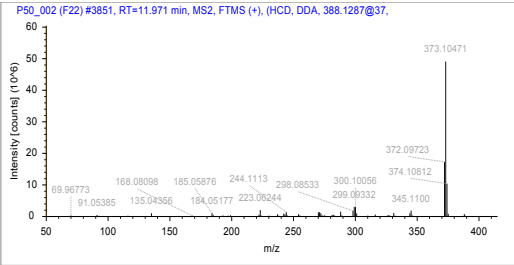
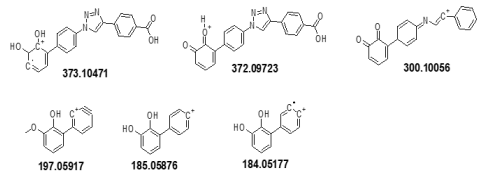
**In vivo PK evaluation of compound 34.**

**Table S6.** PK parameters of single administration of compound **34** (*e.v.*, 7 mg/kg, n=5)

<b>Parameter</b>	<b>Unit</b>	<b>Value</b>	<b>S.D.</b>
$t_{1/2}$	h	3.21	0.57
$T_{max}$	h	0.20	0.18
$C_{max}$	$\mu\text{g/L}$	16,834	4,829
$V_d$	L/Kg	2.30	0.76
Cl	L/h/Kg	0.50	0.15

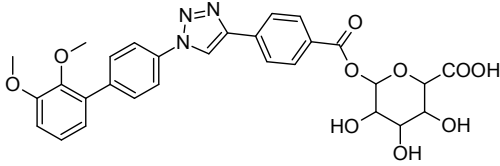
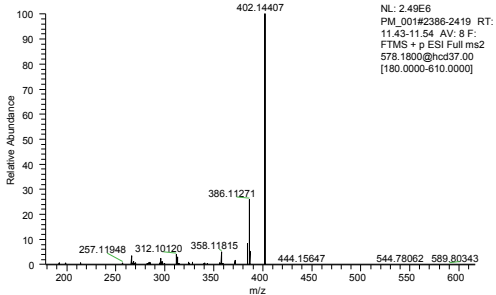
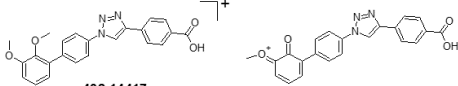
## Metabolic stability data.

34	Theoretical [M+H] <sup>+</sup>	Measured [M+H] <sup>+</sup>	Mass shift ppm	RT (min)
	402.1448	402.1444	1.08	12.917
MS <sup>2</sup> spectrum	Significant fragment ions			
				

M1	Theoretical [M+H] <sup>+</sup>	Measured [M+H] <sup>+</sup>	Mass shift ppm	RT (min)
 <p>R= H or Me</p>	388.1292	388.1287	1.24	11.971
MS <sup>2</sup> spectrum	Significant fragment ions			
				

M2	Theoretical [M+H] <sup>+</sup>	Measured [M+H] <sup>+</sup>	Mass shift ppm	RT (min)
<p>R= H or Me</p>	404.1241	404.1237	0.98	10.879
MS <sup>2</sup> spectrum	Significant fragment ions			
<p>P50_002 (F22) #3403, RT=10.879 min, MS2, FTMS (+), (HCD, DDA, 404.1237@37.</p>				

M3	Theoretical [M+H] <sup>+</sup>	Measured [M+H] <sup>+</sup>	Mass shift ppm	RT (min)
	418.1397	418.1390	1.79	11.815
MS <sup>2</sup> spectrum	Significant fragment ions			
<p>P50_002 (F22) #3787, RT=11.815 min, MS2, FTMS (+), (HCD, DDA, 418.1390@37.</p>				

G1	Theoretical [M+H] <sup>+</sup>	Measured [M+H] <sup>+</sup>	Mass shift ppm	RT (min)
	578.1769	578.1774	0.88	11.47
MS <sup>2</sup> spectrum		Significant fragment ions		
 <p data-bbox="530 538 650 614">           NL: 2.49E6            PM_001#2386-2419 RT:            11.43-11.54 AV: 8 F:            FTMS + p ESI Full ms2            578.1800@hcd37.00            [180.0000-610.0000]         </p>	 <p data-bbox="794 725 861 738"><b>402.14417</b></p> <p data-bbox="1042 725 1110 738"><b>386.11271</b></p>			



#### **4.a.iii. Authors contribution**

- ***Celia Cordero-Sanchez:***
  - *In vitro* experiments. Analysis. Writing the draft.
- ***Marta Serafini:***
  - Synthesis of the compounds. Writing the draft.
- ***Rosanna Di Paola:***
  - *In vivo* experiments.
- ***Irene P. Bhela:***
  - Synthesis of the compounds.
- ***Silvio Aprile:***
  - Metabolism experiments. Analysis.
- ***Beatrice Purghè:***
  - Metabolism experiments. Analysis.
- ***Roberta Fusco:***
  - Contributed data or analysis tools.
- ***Salvatore Cuzzocrea:***
  - Supervision.
- ***Armando A. Genazzani:***
  - Designed the experiments. Supervision. Funding.
- ***Beatrice Riva:***
  - Designed the experiments. Writing the draft.
- ***Tracey Pirali:***
  - Designed the experiments. Writing the draft



## 5.- Discussion and conclusions

In the present project, we characterized a *knock-in* mouse model (KI-STIM1<sup>I115F</sup>), proposing it as a model for tubular aggregate myopathy, in a C57Bl/6 background. The choice of this mutation was driven by the presence of these patients in the Italian setting and by the absence of other models that replicate mutations in the second EF-hand of STIM1, which are numerous as can be seen in Figure 7 of the introduction. Concretely, p.I115F mutation has been associated with both TAM and YPS, which we retained remarkable for increasing the understanding of the diseases.

The I115F mutation is located in the second EF-hand, responsible for stabilization of Ca<sup>2+</sup> binding. Undeniably, isoleucine (I) has a small non-reactive aliphatic side chain, which is typically involved in substrate recognition or binding, while phenylalanine (F) has an aromatic and very hydrophobic side chain, generally associated with Pi-Stacking interaction and specific binding to certain amino acids, as proline. (Betts and Russel. 2003). Substitution of isoleucine to phenylalanine directly leads to an increase in the topological polar surface area, from 63.3 to 83.1 Å<sup>2</sup> according to PubChem (AA – Isoleucine; AA-Phenylalanine). This substitution not only leads to the lack of the crucial isoleucine side-chain interaction affecting the stabilizing role of I115 in Ca<sup>2+</sup> binding but most probably has a steric effect that could head a conformational change of the second EF-hand. Consequently, the p.I115F mutation in STIM1 causes impairment in calcium-sensing and therefore, to an increased entry of calcium through ORAI1. Further crystallography studies should be performed to better understand in detail STIM1 structural consequences of STIM1 mutations.

Up to now, three mouse models have been described bearing STIM1 gain-of-function mutations. First, the group of Grosse (Grosse et al. 2007) has reported a mouse colony bearing the p.D84G STIM1 mutation, located in the first EF-hand. Stim1<sup>Sax/+</sup> mice presented severe thrombocytopenia, but no investigations have been done regarding muscle dystrophic-like phenotype. Recently, other two groups have generated mouse colonies bearing the p.R304 STIM1 mutation, located in the cytosolic domains (Gamage et al. 2018; Silva-Rojas et al. 2018) of the protein. Table 4 contains macroscopic features of all four models compared to TAM patients.

The KI-STIM1<sup>115F</sup> colony is fertile, homozygous pups are not viable, and, as expected, breeding follows the Mendelian ratio (1:1). As the rest of the TAM mouse models, KI-STIM1<sup>115F</sup> mice weigh less from 1 month of age, and this, experimentally, precludes blinding for behavioural experiments. At the same time, body weight differences provide a first early end-point to measure in the evaluation of treatments. The difference in KI-STIM1<sup>115F</sup> body weight is not caused by growth disturbances since the anus-nose length was normal, but it is due to the reduced muscle weight observed compared to WT. KI-STIM1<sup>115F</sup> present evident movement difficulties and a remarkable hunchback, a feature shared with homozygote Gamage mice (Gamage et al. 2018). Other symptoms of TAM patients as congenital miosis and ichthyosis have not been studied in the KI-STIM1<sup>115F</sup> mouse model. Instead, Stim1<sup>R304W/+</sup> mice presented a limitation of the movement of the eyes, namely gaze paresis, as observed in TAM patients (Silvio-Rojas et al. 2018). Besides, ichthyosis, a skin disorder barely present in TAM patients, has been occasionally observed in KI-STIM1<sup>115F</sup> mice. A photographic register should be performed to examine the severity of this symptom and determine its frequency in the KI-STIM1<sup>115F</sup> mice population.

**Table 4. Macroscopic features in TAM mouse models and TAM patients**

	Mouse model			TAM patients
	Stim1 <sup>R304W</sup>	Stim1 <sup>R304W/+</sup>	KI-STIM1 <sup>115F</sup>	
	Gamage et al. 2018	Silva-Rojas et al. 2018 and 2021	Cordero-Sanchez et al. 2019	Morin et al. 2020
<b>Body weight</b>	↓	↓	↓	Small stature
<b>Body length</b>	-	↓	N.D.	
<b>Congenital miosis</b>	-	Gaze paresis	-	Present
<b>Ichthyosis</b>	-	-	-	Present

Parameters not measured are indicated with dash (-). Red arrows indicate a decrease. Green arrows indicate an increase. N.D.: No differences.

### *Myopathy in KI-STIM1<sup>1115F</sup> mouse model*

In accord with the results obtained by the groups of Silvio-Rojas and Gamage (Silva-Rojas et al 2018; Gamage et al, 2018), KI-STIM1<sup>1115F</sup> mice show a strong myopathic picture. Table 5 contains a synopsis of the features observed in the different mouse models and patients. Myopathy in KI-STIM1<sup>1115F</sup> is characterized by a progressive muscle degeneration with a weight reduction of most of the muscle measured and the presence of (i) central nuclei fibers, (ii) necrotic and fibrotic tissue, (iii) endomysial inflammatory infiltrate, (iv) cytoplasmic fuscophilic areas, (v) smaller fibers frequency, and (vi) myofibrillar disorganization. Surprisingly, but in accord with Silvio-Rojas, the weight of the KI-STIM1<sup>1115F</sup> soleus is increased over WT. This is also present in a transgenic mouse model of muscular dystrophy overexpressing TRPC3 (Millay et al 2009). Millay et al. hypothesized the involvement of a “*sarcolemmal mechanism*”, so further studies have to be performed for explaining and understanding in deep this hypothesis. However, it has been recently shown that the degree of soleus hypertrophy depends on circadian rhythms after eccentric exercise (Chang et al. 2022). Chang et al. proposed mTOR/p70S6K signalling as the key mechanism of modulation in soleus muscle. The specific correlation of soleus hypertrophy and mTOR signalling could reasonably explain soleus hypertrophy since SOC entry activity has been related to mTOR signalling in different cell types (Ogawa et al. 2012; Abbonante et al. 2021).

Our model, similar to those reported in the literature, lacks the presence of tubular aggregates, the core histological hallmark of the disease, but displays “pseudo-aggregates”, which, unlike the human counterpart, are arranged chaotically. In addition, electron microscopy revealed mitochondria hypertrophy and crest loss, with occasional formation of circular structures in KI-STIM1<sup>1115F</sup> muscles. This alteration in mitochondrial morphology should be further studied, especially to identify oxidative stress due to calcium overload (Tsong-I et al. 2010) and dysfunction in the electron transport chain and/or bioenergetics imbalance (Cardenas et al. 2010). These experiments have been performed by Silvio-Rojas, revealing that mitochondrial respiration is not compromised in Stim1<sup>R304W/+</sup> mice, while the number of those in

muscle is drastically reduced, possibly contributing to muscle weakness (Silvio-Rojas et al. 2021).

Unfortunately, creatine kinase (CK) serum levels are physiological in KI-STIM1<sup>I115F</sup> mice, excluding this easy-read and general marker of muscle damage as a biomarker, contrary to the Silvio-Rojas group's results. Nevertheless, increased CK levels in TAM patients have incomplete penetrance, with no correlation with the mutation born.

In my thesis, I also investigated how the p.I115F mutation affects calcium signalling by measuring calcium in myotubes prepared from both WT and KI-STIM1<sup>I115F</sup> animals. Although neither alteration in basal calcium nor spontaneous oscillations were observed in KI-STIM1<sup>I115F</sup> myotubes, SOC Entry was over-activated. The absence of oscillations in KI-STIM1<sup>I115F</sup> myotubes is contrary to results observed in our lab in fibroblast patients bearing STIM1 mutations (unshown, Riva, et al. 2022, submitted). These differences could be associated with the maturation state of KI-STIM1<sup>I115F</sup> myotubes when the experiments were performed. In any case, fibroblasts of patients bearing ORAI1 mutations have been demonstrated to present these spontaneous oscillations, reasonable taking into account that ORAI1 is the calcium channel (Garibaldi et al. 2017).

Furthermore, no transcriptional alterations regarding Stim1 or other SOC or TRPC genes, were observed in our mice, fortifying the gain-of-function nature of the mutation. However, quantification of STIM1 and ORAI1 proteins in myotubes should be performed through western blotting to exclude transduction impairment or compensatory mechanisms. Besides, stored calcium studies based on aequorin probes targeting both ER and mitochondria should be performed to better understand calcium signalling defects.

By means of several behavioural test performances, the muscle functionality of KI-STIM1<sup>I115F</sup> mice was evaluated. On the one hand, both grip strength and hanging test demonstrated a normal performance of KI-STIM1<sup>I115F</sup> mice. On the other hand, rotarod and treadmill tests revealed an impairment in KI-STIM1<sup>I115F</sup> mice performance. These results illustrate the absence of alterations in forelimb strength or subacute muscle

function and coordination, but also suggest a defect in motor coordination, resistance, and fatigue. These data suggest that KI-STIM1<sup>I115F</sup> presents a prevalent running or sprinting impairment, as reported in TAM patients, with prevalent proximal muscle weakness (Walter et al. 2015). Balance impairment in KI-STIM1<sup>I115F</sup> mice has been discarded since hanging wire test performance was normal, and consequently, no signs of cerebellar deficit were revealed. All these results surprisingly differ from Silvio-Rojas and Gamage data, since mice showed impaired performance in grip strength and hanging test but normal performance in rotarod and treadmill test. This dissonance cannot be associated with the single mutation since some patients bearing one of the both I115F and R304W mutations present lower limb weakness with or without upper limb weakness even though most of the TAM patients have a predominantly lower limb weakness (Morin et al. 2020). However, for deeply studying muscle functionality, *ex vivo* experiments should be performed in KI-STIM1<sup>I115F</sup> muscles to measure specific muscle force and fatigue of the entire organ (Gamage et al. 2018; Silvio-Rojas et al. 2018).

All in all, the data obtained strongly demonstrates the face and construct validity of our mouse model, albeit some differences between the different animal models and the human phenotype are evident.

**Table 5. Myopathy disorder in TAM mouse models and TAM patients**

		Mouse model			TAM patients	
		Stim1 <sup>R304W</sup>	Stim1 <sup>R304W/+</sup>	KI-STIM1 <sup>I115F</sup>		
		Gamage et al, 2018	Silva-Rojas et al 2018 and 2021	Cordero-Sanchez et al. 2019	Morin et al. 2020; Riva et al. 2022.	
<b>CK serum levels</b>		-	↑	N.D.	N.D./ ↑	
<b>Myopathy</b>	Tubular aggregates	-	-	Chaotic	Organized	
	Muscle degeneration and/or regeneration	Present	Present	Present	Present	
	Muscle weight	G	↓	↓	↓	↓
		TA		-	↓	
		Q		-	↓	
		EDL		N.D.	N.D.	
		UB		-	↓	
Soleus	-	↑	↑			
<b>Mitochondria</b>	Morphology alteration	-	Present	Present	-	
	Functionality	-	N.D.	-		
<b>SOC Entry genes in myotubes</b>	Transcription	-	Downregulated	N.D.	N.D.	
	Transduction	↓	-	-	-	
<b>Calcium signalling in myotubes</b>	Basal calcium levels	↓	↑	N.D.	↑	
	Spontaneous Oscillations	-	-	Absent	Present	
	SOC Entry	N.D.	↑	↑	↑	
<b>Muscle Functionality</b>	Ex vivo muscle force measurement	N.D.	↓	-	Lower limb weakness	
	Open field	-	↓	-		
	Grip strength	-	↓	N.D.		
	Hanging test	-	↓	N.D.		
	Rotarod	-	N.D.	↓		
	Treadmill	↓	-	↓		

Parameters not measured have been indicated with dash (-). Red arrows indicate a decrease. Green arrows indicate an increase. N.D.: No differences; CK: Creatin kinase; G: gastrocnemius; TA: Tibialis anterior; Q: Quadriceps; EDL: extensor digitorum longus; UB: Upper biceps.



### ***KI-STIM1<sup>I115F</sup> mouse model is valid also for York Platelet Syndrome***

As (i) p.I115F mutation has been diagnosed as the driving mutation in both TAM and York Platelet Syndrome (YPS), and (ii) KI-STIM1<sup>I115F</sup> mice showed splenomegaly, a sign of bleeding dyscrasia, we studied also the bleeding phenotype. Table 6 contains all parameters regarding the blood disorder. Splenomegaly found in KI-STIM1<sup>I115F</sup> mice is not a common feature of TAM/ Stormorken patients, who occasionally present hyposplenism or asplenia. The principal feature of patients carrying STIM1 p.I115F or p.R304W mutations is the strong thrombocytopenia (Morin et al. 2020), observed in KI-STIM1<sup>I115F</sup> mice early in time and maintained during the life-span and also in the other three TAM mouse models. Hence, the platelet count is a realizable early and fast read-out identified KI-STIM1<sup>I115F</sup> mice.

Taking into account (i) the rareness of the disease, (ii) the different penetrance in patients, and (iii) the strong muscle phenotype, profoundly studying bleeding dyscrasia has not been a priority in the literature. For this reason, we wanted to further investigate the aetiology of thrombocytopenia in KI-STIM1<sup>I115F</sup> mice. We first hypothesized that a defect in the hematopoietic stem cell development could be the origin of the platelet lacking. This hypothesis was discarded as a significant increase in the frequency of lymphoid progenitor population (LSK) stem cell, common lymphoid progenitors (CLP), granulocyte-macrophage progenitors (GMP) were observed in KI-STIM1<sup>I115F</sup>. In agreement, megakaryocyte-erythroid progenitors (MEP) were decreased in KI-STIM1<sup>I115F</sup> mice compared to WT. Instead, no difference between WT and KI-STIM1<sup>I115F</sup> mice were found in red cells, the other final MEP progeny, neither in common myeloid progenitors (CMP) nor its progeny, granulocytes. This picture lets us conclude that thrombocytopenia leads to positive feedback on hematopoietic progenitors, most probably as an unsuccessful attempt of the organism to counteract thrombocytopenia. Simultaneously, these data could explain splenomegaly in KI-STIM1<sup>I115F</sup>, since abnormality of stem cells leads to spleen growth as reported in myeloproliferative neoplasms (MPN; Penna, 2021). Not only hematopoietic stem cells were studied, but also hematopoietic progeny. Contrary to the results of Silva-Rojas *et al.*, we did not observe an impairment of T cells nor neutrophils but reported an

alteration in monocyte subsets. Particularly, Ly6C<sup>high</sup> monocytes, associated with phagocytosis and pro-inflammatory processes, resulted in an increase in KI-STIM1<sup>1115F</sup> mice compared to WT, while Ly6C<sup>low</sup> monocytes, linked to tissue repair, were strongly decreased, in agreement with other TAM models. Moreover, as with other TAM mouse models, a strong decrease of KI-STIM1<sup>1115F</sup> NK has been observed, reasonable given the recent demonstration of the crucial role of STIM1 in NK maturation (Abel et al, 2018).

We then moved to investigate platelets. First, the principal resting and activation receptors were measured in both WT and KI-STIM1<sup>1115F</sup> mice at resting conditions. As reported in the Stim1<sup>Sax/+</sup> model, an increase in P-selectin and active  $\alpha$ IIB $\beta$ 3, and a decrease in integrin  $\alpha$ 2, receptors associated with platelet activation and rest state respectively, were observed, demonstrating the pre-activation status in KI-STIM1<sup>1115F</sup> platelets. This pre-activation does not lead to cell death since PS exposure was normal, contrary to TAM patients' platelets, which present an increased exposure of PS in the membrane. Instead, pre-activation of platelets can lead to (i) unresponsiveness or (ii) hyper-responsiveness. In order to distinguish between these two hypotheses, P-selectin and active  $\alpha$ IIB $\beta$ 3 exposure were measured under stimulation with thrombin at 0.1, 0.025, and 0.0025 u/ml. No differences in maximal thrombin response between WT and KI-STIM1<sup>1115F</sup> were observed, while hyper-exposure of both P-selectin and active  $\alpha$ IIB $\beta$ 3 occurred when stimulated with lower concentrations. All these results are in accord with platelets of patients bearing p.R304W mutation, where resting platelets showed increased exposure of the main activation receptors, indicating the pre-activation state. Furthermore, when PAR1 receptor was stimulated in platelets from patients, these platelets additionally exposed activation receptors, as KI-STIM1<sup>1115F</sup> platelets. However, patients' platelets were overall less responsive than healthy controls. This absence of response might be explained if patients' platelets were overcoming death, as it could be indicated by the increased PS exposure. (Misceo et al. 2014). During the analysis and in agreement with Grosse et al., we realized that a small sub-population of KI-STIM1<sup>1115F</sup> platelets constantly expose only active  $\alpha$ IIB $\beta$ 3 under all basal and stimulated conditions. These data suggest that despite the majority of KI-

STIM1<sup>1115F</sup> platelets are hyper-responsive, a small percentage (around 10%) are unable to fully activate.

Consequently, platelet functionality tests are crucial to demonstrate that this hyper-exposure of receptors directly leads to hyper-functionality. For this, static adhesion and aggregation assays were performed. Along the same line, the area of adhered KI-STIM1<sup>1115F</sup> platelets was higher in comparison to WT, demonstrating an increase in spreading after 30 minutes. Nonetheless, adhesion experiments should be performed also in a flow setting, in order to study functionality simulating physiological conditions. Instead, aggregation tests were performed by stimulation with 0.1 and 0.05 u/ml of thrombin. In high thrombin concentrations, KI-STIM1<sup>1115F</sup> platelets aggregated slower than WT but no differences in maximal aggregation were found. This event can be explained by the 10% of the platelet population that is unable to fully activate. In low thrombin concentrations, KI-STIM1<sup>1115F</sup> platelets hyper-aggregate but no differences in slope were found, in other words, the speed of aggregation was not altered. Therefore, these data confirm the hyper-responsiveness of KI-STIM1<sup>1115F</sup> platelets. Performance of clearance experiments would be useful for understanding *in vivo* life-span of platelets which could be even used as read-out during treatments. Besides, delta granule transport and secretion should be studied for identifying whether KI-STIM1<sup>1115F</sup> platelets have this deficiency, as in YPS platelets.

As in Grosse's mouse model and TAM patients bearing p.R304W mutation, also KI-STIM1<sup>1115F</sup> platelets present an increase in cytosolic basal calcium compared to WT, thus explaining the pre-activation state. In agreement, the calcium responses to thrombin were higher in KI-STIM1<sup>1115F</sup> platelets with respect to WT. This data sheds some light on the mechanism of hyper-exposure of receptors in a stimulated state since calcium has been demonstrated to be crucial for platelet activation. This hyper-signalling of calcium in absence of extracellular calcium demonstrates that, as reported in the literature, activation with thrombin evokes the emptiness of the calcium stores in platelets (Varga-Szabo et al. 2009). It would be extremely important to determinate calcium levels also in the dense tubular system since it seems that stores emptiness are higher in KI-STIM1<sup>1115F</sup> platelets. Even so, (i) delicateness of platelets and (ii) absence

of a nucleus makes extremely difficult or even impossible to use techniques of measuring calcium stores, for example with targeted aequorin.

In accord with Grosse's results, SOC Entry measured by the addition of calcium after the thrombin-store depletion was reduced in comparison with WT. Reduced SOC Entry in KI-STIM1<sup>I115F</sup> platelets could be explained by two hypotheses. On the one hand, SOC Entry reduction could be directly due to the reduction of the quantity of STIM1 protein in KI-STIM1<sup>I115F</sup> platelets with respect to WT observed by western blot. This reduction of STIM1 is absolutely reasonable if we take into account that we are probably studying the survived platelet population, and a lower expression of STIM1 might confer an evolutionary advantage. Independently, the hypothesis of SOC Entry reduction due to the lower quantity of STIM1 cannot fully explain neither higher basal calcium nor hyper-response to thrombin. On the other hand, constitutive activity of STIM1 would lead to higher basal cytosolic calcium levels and to hyper-response to thrombin, by the previous hyper-filling of the stores independently of luminal calcium levels. Since ORAI1 is a calcium channel that allows the passive calcium influx through the plasma membrane, higher cytosolic calcium levels after "fuller-stores" depletion could slow down the calcium entry through ORAI1, despite the STIM1 gain-of-function. In any case, in accord with Grosse's group and TAM patients, KI-STIM1<sup>I115F</sup> mice present bleeding dyscrasia with an increase in bleeding time and blood loss. Experiments of platelets clearance and proplatelet forming capacity of megakaryocytes should be performed to discriminate specifically the aetiology of thrombocytopenia.

Finally, the data obtained strongly demonstrates the main bleeding phenotype observed in YPS patients, validating the KI-STIM1<sup>I115F</sup> mouse model also for YPS and significantly contributing to base research of the disease. TAM, Stormorken syndrome, and YPS belong to a cluster of ultra-rare genetic orphan diseases. However, some authors consider the three of them as the spectra of the same disease with different penetrance (Bohm and Laporte, 2018; Markello et al. 2015; Morin et al. 2020; Silvio-Rojas et al, 2019). The present contribution strongly supports this hypothesis, since the KI-STIM1<sup>I115F</sup> model presents both pathological phenotypes diagnosed as both TAM and YPS in humans (Lacruz and Feske, 2015). Independently, due to the extremely low

frequency of each mutation, we strongly believe that both luminal and cytosolic STIM1 mutated mouse models are complementary. This variety directly increases the likelihood of success of the development of effective drugs as pharmaceutical therapy.

**Table 6. Blood disorder in TAM mouse models and TAM patients**

		Mouse model				TAM patients
		Stim1 <sup>Sax/+</sup>	Stim1 <sup>R304W</sup>	Stim1 <sup>R304W/+</sup>	KI-STIM1 <sup>II15F</sup>	
		Grosse et al. 2007	Gamage et al. 2018; and 2020	Silva-Rojas et al. 2018	Cordero-Sanchez et al. 2019	Morin et al. 2020; Lacruz and Feske, 2015; Misceo et al. 2014
<b>Splenomegaly</b>		Present	Present	Present	Present	Hyposplenism or asplenia
<b>Bone marrow structure alteration</b>		Present	Present	Present	-	-
<b>Hematopoietic stem cells alteration</b>		-	-	-	Present	-
<b>Blood cell population</b>	Granulocytes	-	-	Neutrophils	N.D.	-
				Eosinophils N.D.		
	Monocytes	-	-		Ly6C <sup>high</sup>	
					Ly6C <sup>low</sup>	
	Lymphocytes	-	-	N.D.	N.D.	
Treg	-	-		N.D.		
NK	-	-				
<b>Platelets</b>	Thrombocytopenia	Present	Present	Present	Present	Present
	Megakaryocyte's proplatelet forming		-	-	-	-
	Clearance		-	-	-	-
	Preactivation	Present	-	-	Present	Present
	PS exposure	-	N.D.	-	N.D.	
	Agonist's response		-	-		
	Adhesion and/or aggregation		-	-		-
	Basal calcium levels		-	-		
	Store emptiness		-	-		
	SOC Entry signalling		-	-		
<b>Bleeding time</b>			-	-		Bleeding diathesis

Parameters not measured have been indicated with dash (-). Red arrows indicate a decrease. Green arrows indicate an increase. N.D.: No differences; NK: Natural killer; PS: Phosphatidylserine.

***CIC-39Na, a SOC Entry inhibitor, reverts bleeding dyscrasia in the KI-STIM1<sup>II15F</sup> mouse model***

A full chemical library of putative SOC Entry inhibitors which derivate from Synta66 has been characterized. Synta66 is an inhibitor of SOC Entry used as a tool since (i) is selective also to other calcium channels, (i) has poor solubility, but (iii) is not metabolically stable. In this study CIC-39 (firstly named as 34) was identified as a SOC Entry inhibitor with suitable pharmacological properties. The first round of screening of the chemical library, composed of 23 compounds, revealed that both triazole and 3 – carboxy phenyl rings were essential to obtain a comparable inhibitory activity to Synta66. From the second round, compounds 31, CIC-39, 36, 38, and 40 were selected according to the screening criteria. The salt form of all of them resulted in more soluble in H<sub>2</sub>O and more metabolically stable than Synta66, demonstrating their more suitable properties for drugs. Only salted CIC-39 presented a good solubility in *in vivo* injection solution, making compound CIC-39Na the best SOC Entry inhibitor candidate. These results demonstrated that the methoxy group and fluorine atom increase solubility and positively influence metabolic stability. Two remarkable events were found in this first library. Surprisingly, one SOC Entry activator was found, compound 47, but no further studies have been done since it was out of the aim of this study, despite its possible interest in loss-of-function mutation. Considering the maintenance of the slope of calcium entry during calcium signalling assays, it is likely to affect closure or desensitization of ORAI1. The second event is the discovery of compound 64, a compound without the triazole group, which is drastically more toxic than the rest of the compound, which resulted chemically similar to a dihydroorotate dehydrogenase (DHODH) inhibitor. DHODH is an enzyme involved in pyrimidine synthesis, target of FDA-approved drugs as teriflunomide, also demonstrated to be a selective inhibitor of SOC Entry. This promising discovery leads us to demonstrate not only that compound 64 could be used as a putative inhibitor of DHODH and therefore, for treating rheumatoid arthritis but also that presence of triazole prevents off-target effects. The typical adverse event associated with DHODH inhibition (e.g. hyperlipidemia, altered hematological profile as leucopenia o lymphopenia, and liver function alteration) should be taken into consideration in the future development of compound 64 (Kaur et al 2021).

CIC-39Na showed an  $IC_{50}$  of 800 nM and 1  $\mu$ M at SOC Entry inhibition in HEK cells and in KI-STIM1<sup>1115F</sup> myotubes, respectively. Preliminary experiments of treatments with 60mg/Kg/day of CIC-39Na in KI-STIM1<sup>1115F</sup> mice were performed by intraperitoneally implanting minipumps for 14 days. Results showed that CIC-39Na is able to (i) increase body weight (not shown); (ii) increase the number of platelets; (iii) decrease of blood loss; and (iv) slightly decrease of bleeding time of KI-STIM1<sup>1115F</sup> mice compared to WT. Serum CIC-39Na concentration was 251  $\mu$ g/L corresponding to  $625 \pm 89$  nM, and effects were lost after 16 days.

The reversion of the thrombocytopenia and bleeding dyscrasias with CIC-39Na also demonstrate that counteracting SOC Entry is a viable and reliable therapeutic strategy. So, other SOC Entry inhibitors already in clinical trials can be re-purposed for this new therapeutic indication. Noticeably, CIC-39Na has been demonstrated to be also effective in acute pancreatitis, designating another therapeutic indication for CIC-39Na, which could be not unique, taking into consideration the demonstrated implication of SOC Entry in processes such as apoptosis or diseases as DMD or psoriasis. In any case, the recent emerging clinical data suggest that safety associated with SOC Entry inhibition is manageable. Noteworthy, small molecule drugs might present an economic advantage to other strategies such as protein supplements, RNA, or gene therapy, due to the simpler technology. Besides, pharmacological treatment has an easier and autonomous dosage guideline, increasing the quality of patients' life and facilitating their daily life.



### *Future expectations*

Currently, the identification of tubular aggregates by electron microscopy in muscle biopsies is the unique clinical procedure to diagnose TAM (Jain et al. 2008). This immensely invasive and specific procedure directly affects the natural history of the disease. It additionally difficults an arduous diagnosis in itself as ultra-rare disease. Evidently, this fact radically limits the capacity of registering TAM patients. New methods of diagnosis that may comprehend a cluster of rare diseases are of utmost importance.

Concomitantly, there is a serious lack of putative biomarkers to evaluate the prognosis of the disease. Given that (i) there is an imminent need of stabilizing biomarkers for the prognosis of the disease, and (ii) muscle biomarkers are generally more invasive than blood biomarkers, the objective of the next study is to individuate putative easy and non-invasive parameters realizable to monitor myopathy prognosis in both mice and human patients. For this reason, the next steps of the study will be to evaluate both RNA sequencing and proteomics of principal muscles in KI-STIM1<sup>1115F</sup> mice, in order to identify which gene transcription and/or proteins could act as a reliable muscle biomarker and correlate it with any easy serum readouts. For this, we will treat again KI-STIM1<sup>1115F</sup> mice with CIC-39Na in order to stipulate a correlation between blood and myopathy prognosis, as serum out-puts are generally less invasive than muscle read-out that does require mice sacrifice or is extremely invasive in patients. This bleeding read-out can be combined with body weight measure since amelioration of muscle degeneration progression would be expected. We hope that these blood parameters finding not only would be useful in mouse model platforms but feasible to be used also in patients, avoiding hard and invasive muscle outputs.

As far as I am concerned, the data obtained from our lab and that of others is close to be sufficient to bring any SOC entry inhibitor in clinical trials for TAM patients, independently of which one. Obviously, using a molecule that has already been studied in clinical trials, such as those indicated in Table 3 of the introduction, would speed up the process. Though the results obtained are promising, several crucial information is probably lacking yet. Up to now, no evidence of the effectiveness of molecules has been

demonstrated in motor function in mice, and indeed, we are currently conducting these experiments. Moreover, the effectiveness of SOC Entry inhibitors in every single mutation listed in Figure 7 of the introduction is unknown. To evaluate the effectiveness of our compound CIC-39Na in each mutation, SOC Entry measurements in patients' fibroblasts bearing different should be performed. Precision personalized medicine would guarantee the success of the treatment in each patient. For this reason, also the development of cellular models would be needed that permit the first screening to identify effective drugs in each mutation before testing in patients' fibroblasts. All these experiments were performed in our lab and results will be proximately published (not shown; Riva et al. 2022, submitted).

Since TAM is a chronic disease, data demonstrating long-term safety is also extremely necessary. Up to now, long-term safety in clinical trials of only PRCL-02 has been demonstrated up to 12 weeks. The overall treatment-emergent adverse events reported in literature comprehend nausea, dizziness, chromaturia, and psoriatic arthritis at the maximum tolerated dose (Bruen et al. 2021; Desai et al. 2004; NCT03614078). Adverse events observed have to be taken into account for future SOC Entry inhibitors development.

### *Conclusion*

Hence, the results of my thesis demonstrate that KI-STIM1<sup>I115F</sup> is a valid mouse model for both TAM/YPS that can be used as a solid platform for the development of putative SOC Entry inhibitors, as CIC-39Na. The existence of this mouse model specially guarantees the ability of test drug effectiveness in mutations in the second EF-hand of STIM1. Furthermore, this model is a confirmation of the hypothesis where TAM, Stormorken, and YPS are the spectra of the same disease and could be useful for the identification of putative biomarkers to be tested in patients. However, further aspects of the KI-STIM1<sup>I115F</sup> model should be more deeply investigated to better understand the disease, as mitochondria alteration, pseudo-aggregate identification, and inflammatory process involvement.

## 6- References

- Abbonante, V., Gruppi, C., Battiston, M., Zulian, A., Di Buduo, C. A., Chrisam, M., Sereni, L., Laurent, P.-A., Semplicini, C., Lombardi, E., Mazzucato, M., Moccia, F., Petronilli, V., Villa, A., Bello, L., Pegoraro, E., Bernardi, P., Braghetta, P., De Marco, L., ... Balduini, A. (2021). Ablation of collagen VI leads to the release of platelets with altered function. *Blood Advances*, 5(23), 5150-5163. <https://doi.org/10.1182/bloodadvances.2020002671>
- Abel, A. M., Yang, C., Thakar, M. S., & Malarkannan, S. (2018). Natural Killer Cells: Development, Maturation, and Clinical Utilization. *Frontiers in Immunology*, 9, 1869. <https://doi.org/10.3389/fimmu.2018.01869>
- Amcheslavsky, A., Wood, M. L., Yeromin, A. V., Parker, I., Freites, J. A., Tobias, D. J., & Cahalan, M. D. (2015). Molecular Biophysics of Orai Store-Operated Ca<sup>2+</sup> Channels. *Biophysical Journal*, 108(2), 237-246. <https://doi.org/10.1016/j.bpj.2014.11.3473>
- Amini, M., Chang, Y., Wissenbach, U., Flockerzi, V., Schlenstedt, G., & Beck, A. (2021). Activity of the yeast vacuolar TRP channel TRPY1 is inhibited by Ca<sup>2+</sup>-calmodulin binding. *Journal of Biological Chemistry*, 297(4), 101126. <https://doi.org/10.1016/j.jbc.2021.101126>
- Amor, N. B., Zbidi, H., Bouaziz, A., Isaac, J., Hernández-Cruz, J. M., Salido, G. M., Rosado, J. A., & Bartegi, A. (2009). Acidic-store depletion is required for human platelet aggregation. *Blood Coagulation & Fibrinolysis*, 20(7), 511-516. <https://doi.org/10.1097/MBC.0b013e32832f5104>

- Baba, Y., Hayashi, K., Fujii, Y., Mizushima, A., Watarai, H., Wakamori, M., Numaga, T., Mori, Y., Iino, M., Hikida, M., & Kurosaki, T. (2006). Coupling of STIM1 to store-operated Ca<sup>2+</sup> entry through its constitutive and inducible movement in the endoplasmic reticulum. *Proceedings of the National Academy of Sciences*, *103*(45), 16704-16709. <https://doi.org/10.1073/pnas.0608358103>
- Balghi, H., Robert, R., Rappaz, B., Zhang, X., Wohlhuter-Haddad, A., Evagelidis, A., Luo, Y., Goepp, J., Ferraro, P., Roméo, P., Trebak, M., Wiseman, P. W., Thomas, D. Y., & Hanrahan, J. W. (2011). Enhanced Ca<sup>2+</sup> entry due to Orail plasma membrane insertion increases IL-8 secretion by cystic fibrosis airways. *The FASEB Journal*, *25*(12), 4274-4291. <https://doi.org/10.1096/fj.11-187682>
- Barde, P. J., Viswanadha, S., Veeraraghavan, S., Vakkalanka, S. V., & Nair, A. (2021). A first-in-human study to evaluate the safety, tolerability and pharmacokinetics of RP3128, an oral calcium release-activated calcium (CRAC) channel modulator in healthy volunteers. *Journal of Clinical Pharmacy and Therapeutics*, *46*(3), 677-687. <https://doi.org/10.1111/jcpt.13322>
- Bergmeier, W., Oh-hora, M., McCarl, C.-A., Roden, R. C., Bray, P. F., & Feske, S. (2009). R93W mutation in *Orail* causes impaired calcium influx in platelets. *113*(3), 5.
- Berridge, M. J., Bootman, M. D., & Roderick, H. L. (2003). Calcium signalling: Dynamics, homeostasis and remodelling. *Nature Reviews Molecular Cell Biology*, *4*(7), 517-529. <https://doi.org/10.1038/nrm1155>

- Berridge, M. J., Lipp, P., & Bootman, M. D. (2000). The versatility and universality of calcium signalling. *Nature Reviews Molecular Cell Biology*, 1(1), 11-21. <https://doi.org/10.1038/35036035>
- Betts, M. J., & Russell, R. B. (s. f.). *Amino Acid Properties and Consequences of Substitutions*. 28.
- Bird, G. S., Hwang, S.-Y., Smyth, J. T., Fukushima, M., Boyles, R. R., & Putney, J. W. (2009). STIM1 Is a Calcium Sensor Specialized for Digital Signaling. *Current Biology*, 19(20), 1724-1729. <https://doi.org/10.1016/j.cub.2009.08.022>
- Böhm, J., Bulla, M., Urquhart, J. E., Malfatti, E., Williams, S. G., O'Sullivan, J., Szlauer, A., Koch, C., Baranello, G., Mora, M., Ripolone, M., Violano, R., Moggio, M., Kingston, H., Dawson, T., DeGoede, C. G., Nixon, J., Boland, A., Deleuze, J.-F., ... Laporte, J. (2017). ORAI1 Mutations with Distinct Channel Gating Defects in Tubular Aggregate Myopathy: HUMAN MUTATION. *Human Mutation*, 38(4), 426-438. <https://doi.org/10.1002/humu.23172>
- Böhm, J., Chevessier, F., Koch, C., Peche, G. A., Mora, M., Morandi, L., Pasanisi, B., Moroni, I., Tasca, G., Fattori, F., Ricci, E., Pénilsson-Besnier, I., Nadaj-Pakleza, A., Fardeau, M., Joshi, P. R., Deschauer, M., Romero, N. B., Eymard, B., & Laporte, J. (2014). Clinical, histological and genetic characterisation of patients with tubular aggregate myopathy caused by mutations in STIM1. *Journal of Medical Genetics*, 51(12), 824-833. <https://doi.org/10.1136/jmedgenet-2014-102623>

- Böhm, J., & Laporte, J. (2018). Gain-of-function mutations in STIM1 and ORAI1 causing tubular aggregate myopathy and Stormorken syndrome. *Cell Calcium*, 76, 1-9. <https://doi.org/10.1016/j.ceca.2018.07.008>
- Boncompagni, S., Michelucci, A., Pietrangelo, L., Dirksen, R. T., & Protasi, F. (2017). Exercise-dependent formation of new junctions that promote STIM1-Orai1 assembly in skeletal muscle. *Scientific Reports*, 7(1), 14286. <https://doi.org/10.1038/s41598-017-14134-0>
- Bootman, M. D., Berridge, M. J., & Roderick, H. L. (2002). Calcium Signalling: More Messengers, More Channels, More Complexity. *Current Biology*, 12(16), R563-R565. [https://doi.org/10.1016/S0960-9822\(02\)01055-2](https://doi.org/10.1016/S0960-9822(02)01055-2)
- Bootman, M. D., & Bultynck, G. (2020). Fundamentals of Cellular Calcium Signaling: A Primer. *Cold Spring Harbor Perspectives in Biology*, 12(1), a038802. <https://doi.org/10.1101/cshperspect.a038802>
- Brandman, O., Liou, J., Park, W. S., & Meyer, T. (2007). STIM2 Is a Feedback Regulator that Stabilizes Basal Cytosolic and Endoplasmic Reticulum Ca<sup>2+</sup> Levels. *Cell*, 131(7), 1327-1339. <https://doi.org/10.1016/j.cell.2007.11.039>
- Braun, A., Varga-Szabo, D., Kleinschnitz, C., Pleines, I., Bender, M., Austinat, M., Bösl, M., Stoll, G., & Nieswandt, B. (2009). Orai1 (CRACM1) is the platelet SOC channel and essential for pathological thrombus formation. *Blood*, 113(9), 2056-2063. <https://doi.org/10.1182/blood-2008-07-171611>
- Breedveld, F. C. (2000). Leflunomide: Mode of action in the treatment of rheumatoid arthritis. *Annals of the Rheumatic Diseases*, 59(11), 841-849. <https://doi.org/10.1136/ard.59.11.841>

- Bruen, C., Miller, J., Wilburn, J., Mackey, C., Bollen, T. L., Stauderman, K., & Hebbar, S. (2021). Auxora for the Treatment of Patients With Acute Pancreatitis and Accompanying Systemic Inflammatory Response Syndrome: Clinical Development of a Calcium Release-Activated Calcium Channel Inhibitor. *Pancreas*, 50(4), 537-543. <https://doi.org/10.1097/MPA.0000000000001793>
- Bulla, M., Gyimesi, G., Kim, J. H., Bhardwaj, R., Hediger, M. A., Frieden, M., & Demaurex, N. (2019). ORAI1 channel gating and selectivity is differentially altered by natural mutations in the first or third transmembrane domain. *The Journal of Physiology*, 597(2), 561-582. <https://doi.org/10.1113/JP277079>
- Cai, X. (2007). Molecular Evolution and Structural Analysis of the Ca<sup>2+</sup> Release-Activated Ca<sup>2+</sup> Channel Subunit, Orai. *Journal of Molecular Biology*, 368(5), 1284-1291. <https://doi.org/10.1016/j.jmb.2007.03.022>
- Cai, X., Zhou, Y., Nwokonko, R. M., Loktionova, N. A., Wang, X., Xin, P., Trebak, M., Wang, Y., & Gill, D. L. (2016). The Orai1 Store-operated Calcium Channel Functions as a Hexamer. *Journal of Biological Chemistry*, 291(50), 25764-25775. <https://doi.org/10.1074/jbc.M116.758813>
- Carafoli, E., Santella, L., Branca, D., & Brini, M. (2001). Generation, Control, and Processing of Cellular Calcium Signals. *Critical Reviews in Biochemistry and Molecular Biology*, 36(2), 107-260. <https://doi.org/10.1080/20014091074183>
- Cárdenas, C., Miller, R. A., Smith, I., Bui, T., Molgó, J., Müller, M., Vais, H., Cheung, K.-H., Yang, J., Parker, I., Thompson, C. B., Birnbaum, M. J., Hallows, K. R., & Foskett, J. K. (2010). Essential Regulation of Cell Bioenergetics by Constitutive

InsP3 Receptor Ca<sup>2+</sup> Transfer to Mitochondria. *Cell*, 142(2), 270-283.

<https://doi.org/10.1016/j.cell.2010.06.007>

Chang, S., Yoshihara, T., Tsuzuki, T., Natsume, T., Kakigi, R., Machida, S., & Naito, H. (2022). Circadian rhythms modulate the effect of eccentric exercise on rat soleus muscles. *PLOS ONE*, 17(2), e0264171.

<https://doi.org/10.1371/journal.pone.0264171>

Claeys, T., Goosens, V., Racé, V., Theys, T., Thal, D. R., Depuydt, C. E., & Claeys, K. G. (2020). Clinical and muscle MRI features in a family with tubular aggregate myopathy and novel STIM1 mutation. *Neuromuscular Disorders*, 30(9), 709-718. <https://doi.org/10.1016/j.nmd.2020.07.010>

Collins, S. R., & Meyer, T. (2011). Evolutionary origins of STIM1 and STIM2 within ancient Ca<sup>2+</sup> signaling systems. *Trends in Cell Biology*, 21(4), 202-211.

<https://doi.org/10.1016/j.tcb.2011.01.002>

Conte, E., Pannunzio, A., Imbrici, P., Camerino, G. M., Maggi, L., Mora, M., Gibertini, S., Cappellari, O., De Luca, A., Coluccia, M., & Liantonio, A. (2021). Gain-of-Function STIM1 L96V Mutation Causes Myogenesis Alteration in Muscle Cells From a Patient Affected by Tubular Aggregate Myopathy. *Frontiers in Cell and Developmental Biology*, 9, 635063.

<https://doi.org/10.3389/fcell.2021.635063>

Cordero-Sanchez, C., Riva, B., Reano, S., Clemente, N., Zaggia, I., Ruffinatti, F. A., Potenzieri, A., Pirali, T., Raffa, S., Sangaletti, S., Colombo, M. P., Bertoni, A., Garibaldi, M., Filigheddu, N., & Genazzani, A. A. (2019). A luminal EF-hand mutation in STIM1 in mice causes the clinical hallmarks of tubular aggregate



myopathy. *Disease Models & Mechanisms*, dmm.041111.

<https://doi.org/10.1242/dmm.041111>

Covington, E. D., Wu, M. M., & Lewis, R. S. (2010). Essential Role for the CRAC Activation Domain in Store-dependent Oligomerization of STIM1. *Molecular Biology of the Cell*, 21(11), 1897-1907. <https://doi.org/10.1091/mbc.e10-02-0145>

Davis, F. M., Goulding, E. H., D'Agostin, D. M., Janardhan, K. S., Cummings, C. A., Bird, G. S., Eddy, E. M., & Putney, J. W. (2016). Male infertility in mice lacking the store-operated Ca<sup>2+</sup> channel Orai1. *Cell Calcium*, 59(4), 189-197. <https://doi.org/10.1016/j.ceca.2016.02.007>

Davis, F. M., Janoshazi, A., Janardhan, K. S., Steinckwich, N., D'Agostin, D. M., Petranka, J. G., Desai, P. N., Roberts-Thomson, S. J., Bird, G. S., Tucker, D. K., Fenton, S. E., Feske, S., Monteith, G. R., & Putney, J. W. (2015). Essential role of Orai1 store-operated calcium channels in lactation. *Proceedings of the National Academy of Sciences*, 112(18), 5827-5832. <https://doi.org/10.1073/pnas.1502264112>

Davis, J. P., Cain, G. A., Pitts, W. J., Magolda, R. L., & Copeland, R. A. (1996). The Immunosuppressive Metabolite of Leflunomide Is a Potent Inhibitor of Human Dihydroorotate Dehydrogenase. *Biochemistry*, 35(4), 1270-1273. <https://doi.org/10.1021/bi952168g>

Derler, I., Plenk, P., Fahrner, M., Muik, M., Jardin, I., Schindl, R., Gruber, H. J., Groschner, K., & Romanin, C. (2013). The Extended Transmembrane Orai1 N-terminal (ETON) Region Combines Binding Interface and Gate for Orai1

Activation by STIM1. *Journal of Biological Chemistry*, 288(40), 29025-29034.

<https://doi.org/10.1074/jbc.M113.501510>

Desai, A. A., Innocenti, F., Janisch, L., DeMario, M., Shepard, D., Ramirez, J., Fleming, G. F., & Ratain, M. J. (2004). A phase I trial of pharmacokinetic modulation of carboxyamidotriazole (CAI) with ketoconazole in patients with advanced cancer. *Cancer Chemotherapy and Pharmacology*, 54(5), 377-384.

<https://doi.org/10.1007/s00280-004-0841-y>

Di Sabatino, A., Rovedatti, L., Kaur, R., Spencer, J. P., Brown, J. T., Morisset, V. D., Biancheri, P., Leakey, N. A. B., Wilde, J. I., Scott, L., Corazza, G. R., Lee, K., Sengupta, N., Knowles, C. H., Gunthorpe, M. J., McLean, P. G., MacDonald, T. T., & Kruidenier, L. (2009). Targeting Gut T Cell  $Ca^{2+}$  Release-Activated  $Ca^{2+}$  Channels Inhibits T Cell Cytokine Production and T-Box Transcription Factor T-Bet in Inflammatory Bowel Disease. *The Journal of Immunology*, 183(5), 3454-3462. <https://doi.org/10.4049/jimmunol.0802887>

Domínguez-Rodríguez, A., Díaz, I., Rodríguez-Moyano, M., Calderón-Sánchez, E., Rosado, J. A., Ordóñez, A., & Smani, T. (2012). Urotensin-II Signaling Mechanism in Rat Coronary Artery: Role of STIM1 and Orai1-Dependent Store Operated Calcium Influx in Vasoconstriction. *Arteriosclerosis, Thrombosis, and Vascular Biology*, 32(5), 1325-1332.

<https://doi.org/10.1161/ATVBAHA.111.243014>

Dubois, C., Vanden Abeele, F., Lehen'kyi, V., Gkika, D., Guarmit, B., Lepage, G., Slomianny, C., Borowiec, A. S., Bidaux, G., Benahmed, M., Shuba, Y., & Prevarskaya, N. (2014). Remodeling of Channel-Forming ORAI Proteins

Determines an Oncogenic Switch in Prostate Cancer. *Cancer Cell*, 26(1), 19-32.

<https://doi.org/10.1016/j.ccr.2014.04.025>

Eckstein, M., & Lacruz, R. S. (2018). CRAC channels in dental enamel cells. *Cell*

*Calcium*, 75, 14-20. <https://doi.org/10.1016/j.ceca.2018.07.012>

Endo, Y., Noguchi, S., Hara, Y., Hayashi, Y. K., Motomura, K., Miyatake, S.,

Murakami, N., Tanaka, S., Yamashita, S., Kizu, R., Bamba, M., Goto, Y.,

Matsumoto, N., Nonaka, I., & Nishino, I. (2015). Dominant mutations in ORAI1

cause tubular aggregate myopathy with hypocalcemia via constitutive activation

of store-operated Ca<sup>2+</sup> channels. *Human Molecular Genetics*, 24(3), 637-648.

<https://doi.org/10.1093/hmg/ddu477>

Fahrner, M., Grabmayr, H., & Romanin, C. (2020). Mechanism of STIM activation.

*Current Opinion in Physiology*, 17, 74-79.

<https://doi.org/10.1016/j.cophys.2020.07.006>

Feske, S. (2010). CRAC channelopathies. *Pflügers Archiv - European Journal of*

*Physiology*, 460(2), 417-435. <https://doi.org/10.1007/s00424-009-0777-5>

Feske, S. (2019). CRAC channels and disease – From human CRAC channelopathies

and animal models to novel drugs. *Cell Calcium*, 80, 112-116.

<https://doi.org/10.1016/j.ceca.2019.03.004>

Feske, S., Gwack, Y., Prakriya, M., Srikanth, S., Puppel, S.-H., Tanasa, B., Hogan, P.

G., Lewis, R. S., Daly, M., & Rao, A. (2006). A mutation in Orai1 causes immune

deficiency by abrogating CRAC channel function. *Nature*, 441(7090), 179-185.

<https://doi.org/10.1038/nature04702>

- Fngel, W. K., Bishop, D. W., & Cunningham, G. G. (s. f.). *Tubular Aggregates in Type II Muscle Fibers: Ultrastructural and Histochemical Correlation*. 19.
- Galán, C., Zbidi, H., Bartegi, A., Salido, G. M., & Rosado, J. A. (2009). STIM1, Orai1 and hTRPC1 are important for thrombin- and ADP-induced aggregation in human platelets. *Archives of Biochemistry and Biophysics*, 490(2), 137-144. <https://doi.org/10.1016/j.abb.2009.08.007>
- Gamage, T. H., Gunnes, G., Lee, R. H., Louch, W. E., Holmgren, A., Bruton, J. D., Lengle, E., Kolstad, T. R. S., Revold, T., Amundsen, S. S., Dalen, K. T., Holme, P. A., Tjønnfjord, G. E., Christensen, G., Westerblad, H., Klungland, A., Bergmeier, W., Misceo, D., & Frensen, E. (2018). STIM1 R304W causes muscle degeneration and impaired platelet activation in mice. *Cell Calcium*, 76, 87-100. <https://doi.org/10.1016/j.ceca.2018.10.001>
- Garibaldi, M., Fattori, F., Riva, B., Labasse, C., Brochier, G., Ottaviani, P., Sacconi, S., Vizzaccaro, E., Laschena, F., Romero, N. B., Genazzani, A., Bertini, E., & Antonini, G. (2017). A novel gain-of-function mutation in *ORAI1* causes late-onset tubular aggregate myopathy and congenital miosis: Novel *ORAI1* mutation causes mild TAM with miosis. *Clinical Genetics*, 91(5), 780-786. <https://doi.org/10.1111/cge.12888>
- Gavin, R. L., Koo, C. Z., & Tomlinson, M. G. (2020). Tspan18 is a novel regulator of thrombo-inflammation. *Medical Microbiology and Immunology*, 209(4), 553-564. <https://doi.org/10.1007/s00430-020-00678-y>
- Gehlert, S., Bloch, W., & Suhr, F. (2015). Ca<sup>2+</sup>-Dependent Regulations and Signaling in Skeletal Muscle: From Electro-Mechanical Coupling to Adaptation.

*International Journal of Molecular Sciences*, 16(1), 1066-1095.

<https://doi.org/10.3390/ijms16011066>

Gerasimenko, J. V., Gerasimenko, O. V., & Petersen, O. H. (2014). The role of Ca<sup>2+</sup> in the pathophysiology of pancreatitis. *The Journal of Physiology*, 592(2), 269-280. <https://doi.org/10.1113/jphysiol.2013.261784>

Gerasimenko, J. V., Gryshchenko, O., Ferdek, P. E., Stapleton, E., Hébert, T. O. G., Bychkova, S., Peng, S., Begg, M., Gerasimenko, O. V., & Petersen, O. H. (2013). Ca<sup>2+</sup> release-activated Ca<sup>2+</sup> channel blockade as a potential tool in antipancreatitis therapy. *Proceedings of the National Academy of Sciences*, 110(32), 13186-13191. <https://doi.org/10.1073/pnas.1300910110>

Gerasimenko, J. V., Peng, S., Tsugorka, T., & Gerasimenko, O. V. (2018). Ca<sup>2+</sup> signalling underlying pancreatitis. *Cell Calcium*, 70, 95-101. <https://doi.org/10.1016/j.ceca.2017.05.010>

Gilio, K., van Kruchten, R., Braun, A., Berna-Erro, A., Feijge, M. A. H., Stegner, D., van der Meijden, P. E. J., Kuijpers, M. J. E., Varga-Szabo, D., Heemskerk, J. W. M., & Nieswandt, B. (2010). Roles of Platelet STIM1 and Orai1 in Glycoprotein VI- and Thrombin-dependent Procoagulant Activity and Thrombus Formation. *Journal of Biological Chemistry*, 285(31), 23629-23638. <https://doi.org/10.1074/jbc.M110.108696>

Goonasekera, S. A., Davis, J., Kwong, J. Q., Accornero, F., Wei-LaPierre, L., Sargent, M. A., Dirksen, R. T., & Molkentin, J. D. (2014). Enhanced Ca<sup>2+</sup> influx from STIM1–Orai1 induces muscle pathology in mouse models of muscular

dystrophy. *Human Molecular Genetics*, 23(14), 3706-3715.

<https://doi.org/10.1093/hmg/ddu079>

Grabmayr, H., Romanin, C., & Fahrner, M. (2020). STIM Proteins: An Ever-Expanding Family. *International Journal of Molecular Sciences*, 22(1), 378.

<https://doi.org/10.3390/ijms22010378>

Gresele, P., Page C. P., Fuster V. & Vermynen, J. (2007). Platelets in Thrombotic and Non-Thrombotic Disorders: pathophysiology, pharmacology and therapeutics. *Journal of Thrombosis and Haemostasis*, 1, 613–614.

Grosse, J., Braun, A., Varga-Szabo, D., Beyersdorf, N., Schneider, B., Zeitlmann, L., Hanke, P., Schropp, P., Mühlstedt, S., Zorn, C., Huber, M., Schmittwolf, C., Jagla, W., Yu, P., Kerkau, T., Schulze, H., Nehls, M., & Nieswandt, B. (2007). An EF hand mutation in Stim1 causes premature platelet activation and bleeding in mice. *Journal of Clinical Investigation*, 117(11), 3540-3550.

<https://doi.org/10.1172/JCI32312>

Gukovskaya, A. S., Pandol, S. J., & Gukovsky, I. (2016). New insights into the pathways initiating and driving pancreatitis. *Current Opinion in Gastroenterology*, 32(5), 429-435.

<https://doi.org/10.1097/MOG.0000000000000301>

Hammad, A. S., & Machaca, K. (2021). Store Operated Calcium Entry in Cell Migration and Cancer Metastasis. *Cells*, 10(5), 1246.

<https://doi.org/10.3390/cells10051246>

Harisseh, R., Chatelier, A., Magaud, C., Déliot, N., & Constantin, B. (2013). Involvement of TRPV2 and SOCE in calcium influx disorder in DMD primary

human myotubes with a specific contribution of  $\alpha_1$ -syntrophin and PLC/PKC in SOCE regulation. *American Journal of Physiology-Cell Physiology*, 304(9), C881-C894. <https://doi.org/10.1152/ajpcell.00182.2012>

Harris, E., Burki, U., Marini-Bettolo, C., Neri, M., Scotton, C., Hudson, J., Bertoli, M., Evangelista, T., Vroiling, B., Polvikoski, T., Roberts, M., Töpf, A., Bushby, K., McArthur, D., Lochmüller, H., Ferlini, A., Straub, V., & Barresi, R. (2017). Complex phenotypes associated with STIM1 mutations in both coiled coil and EF-hand domains. *Neuromuscular Disorders*, 27(9), 861-872. <https://doi.org/10.1016/j.nmd.2017.05.002>

Hedberg C, Niceta M, Fattori F, et al. Childhood onset tubular aggregate myopathy associated with de novo STIM1 mutations. *J Neurol*. 2014;261(5):870-876. doi:10.1007/s00415-014-7287-x

Hoover, P. J., & Lewis, R. S. (2011). Stoichiometric requirements for trapping and gating of  $\text{Ca}^{2+}$  release-activated  $\text{Ca}^{2+}$  (CRAC) channels by stromal interaction molecule 1 (STIM1). *Proceedings of the National Academy of Sciences*, 108(32), 13299-13304. <https://doi.org/10.1073/pnas.1101664108>

Huang, G. N., Zeng, W., Kim, J. Y., Yuan, J. P., Han, L., Muallem, S., & Worley, P. F. (2006). STIM1 carboxyl-terminus activates native SOC, Icrac and TRPC1 channels. *Nature Cell Biology*, 8(9), 1003-1010. <https://doi.org/10.1038/ncb1454>

Hwang, S., & Putney, J. W. (2012). Orai1-mediated calcium entry plays a critical role in osteoclast differentiation and function by regulating activation of the transcription factor NFATc1. *The FASEB Journal*, 26(4), 1484-1492. <https://doi.org/10.1096/fj.11-194399>

- Hwang, S.-Y., Foley, J., Numaga-Tomita, T., Petranka, J. G., Bird, G. S., & Putney, J. W. (2012). Deletion of Orai1 alters expression of multiple genes during osteoclast and osteoblast maturation. *Cell Calcium*, 52(6), 488-500. <https://doi.org/10.1016/j.ceca.2012.10.001>
- Inoue, O., Suzuki-Inoue, K., Dean, W. L., Frampton, J., & Watson, S. P. (2003). Integrin  $\alpha 2\beta 1$  mediates outside-in regulation of platelet spreading on collagen through activation of Src kinases and PLC $\gamma 2$ . *Journal of Cell Biology*, 160(5), 769-780. <https://doi.org/10.1083/jcb.200208043>
- Jain, D., Sharma, M. C., Sarkar, C., Suri, V., Sharma, S. K., Singh, S., & Das, T. K. (2008). Tubular aggregate myopathy: A rare form of myopathy. *Journal of Clinical Neuroscience*, 15(11), 1222-1226. <https://doi.org/10.1016/j.jocn.2007.11.010>
- Jardin, I., Nieto-Felipe, J., Alvarado, S., Diez-Bello, R., Lopez, J. J., Salido, G. M., Smani, T., & Rosado, J. A. (2021). SARAF and EFHB Modulate Store-Operated Ca $^{2+}$  Entry and Are Required for Cell Proliferation, Migration and Viability in Breast Cancer Cells. *Cancers*, 13(16), 4160. <https://doi.org/10.3390/cancers13164160>
- Jardin, I., & Rosado, J. A. (2016). STIM and calcium channel complexes in cancer. *Biochimica et Biophysica Acta (BBA) - Molecular Cell Research*, 1863(6), 1418-1426. <https://doi.org/10.1016/j.bbamcr.2015.10.003>
- Jinhui Zhu, Qingping Feng, and Peter B. Stathopoulos. 2017. "The STIM-Orai Pathway: STIM-Orai Structures – Isolated and in Complex" Store-Operated Ca $^{2+}$  Entry (SOCE) Pathways Chapter 2.



- Johny, J. P., Plank, M. J., & David, T. (2017). Importance of Altered Levels of SERCA, IP 3 R, and RyR in Vascular Smooth Muscle Cell. *Biophysical Journal*, 112(2), 265-287. <https://doi.org/10.1016/j.bpj.2016.11.3206>
- Kaur, H., Sarma, P., Bhattacharyya, A., Sharma, S., Chhimpa, N., Prajapat, M., Prakash, A., Kumar, S., Singh, A., Singh, R., Avti, P., Thota, P., & Medhi, B. (2021). Efficacy and safety of dihydroorotate dehydrogenase (DHODH) inhibitors “leflunomide” and “teriflunomide” in Covid-19: A narrative review. *European Journal of Pharmacology*, 906, 174233. <https://doi.org/10.1016/j.ejphar.2021.174233>
- Koenig, X., Choi, R. H., & Launikonis, B. S. (2018). Store-operated Ca<sup>2+</sup> entry is activated by every action potential in skeletal muscle. *Communications Biology*, 1(1), 31. <https://doi.org/10.1038/s42003-018-0033-7>
- la Marca, G., Giocaliere, E., Malvagia, S., Funghini, S., Ombrone, D., Della Bona, M. L., Canessa, C., Lippi, F., Romano, F., Guerrini, R., Resti, M., & Azzari, C. (2014). The inclusion of ADA-SCID in expanded newborn screening by tandem mass spectrometry. *Journal of Pharmaceutical and Biomedical Analysis*, 88, 201-206. <https://doi.org/10.1016/j.jpba.2013.08.044>
- Lacruz, R. S., & Feske, S. (2015). Diseases caused by mutations in *ORAI1* and *STIM1*: Mutations in *ORAI1* and *STIM1*. *Annals of the New York Academy of Sciences*, 1356(1), 45-79. <https://doi.org/10.1111/nyas.12938>
- Launikonis, B. S., Barnes, M., & Stephenson, D. G. (2003). Identification of the coupling between skeletal muscle store-operated Ca<sup>2+</sup> entry and the inositol

triphosphate receptor. *Proceedings of the National Academy of Sciences*, 100(5), 2941-2944. <https://doi.org/10.1073/pnas.0536227100>

Launikonis, B. S., & Ríos, E. (2007). Store-operated Ca<sup>2+</sup> entry during intracellular Ca<sup>2+</sup> release in mammalian skeletal muscle: SOCE during Ca<sup>2+</sup> release in muscle. *The Journal of Physiology*, 583(1), 81-97. <https://doi.org/10.1113/jphysiol.2007.135046>

Lee, P. J., & Papachristou, G. I. (2019). New insights into acute pancreatitis. *Nature Reviews Gastroenterology & Hepatology*, 16(8), 479-496. <https://doi.org/10.1038/s41575-019-0158-2>

Lewis, R. S. (2020). Store-Operated Calcium Channels: From Function to Structure and Back Again. *Cold Spring Harbor Perspectives in Biology*, 12(5), a035055. <https://doi.org/10.1101/cshperspect.a035055>

Li, J., McKeown, L., Ojelabi, O., Stacey, M., Foster, R., O'Regan, D., Porter, K. E., & Beech, D. J. (2011). Nanomolar potency and selectivity of a Ca<sup>2+</sup> release-activated Ca<sup>2+</sup> channel inhibitor against store-operated Ca<sup>2+</sup> entry and migration of vascular smooth muscle cells: Vascular Orai1 and CRAC inhibition. *British Journal of Pharmacology*, 164(2), 382-393. <https://doi.org/10.1111/j.1476-5381.2011.01368.x>

Li, Y., Yang, X., & Shen, Y. (2021). Structural Insights into Ca<sup>2+</sup> Permeation through Orai Channels. *Cells*, 10(11), 3062. <https://doi.org/10.3390/cells10113062>

Li, Z., Lu, J., Xu, P., Xie, X., Chen, L., & Xu, T. (2007). Mapping the Interacting Domains of STIM1 and Orai1 in Ca<sup>2+</sup> Release-activated Ca<sup>2+</sup> Channel

Activation. *Journal of Biological Chemistry*, 282(40), 29448-29456.

<https://doi.org/10.1074/jbc.M703573200>

Lian, J., Cuk, M., Kahlfuss, S., Kozhaya, L., Vaeth, M., Rieux-Laucat, F., Picard, C., Benson, M. J., Jakovcevic, A., Bilic, K., Martinac, I., Stathopoulos, P., Kacs Kovics, I., Vraetz, T., Speckmann, C., Ehl, S., Issekutz, T., Unutmaz, D., & Feske, S. (2018). ORAI1 mutations abolishing store-operated Ca<sup>2+</sup> entry cause anhidrotic ectodermal dysplasia with immunodeficiency. *Journal of Allergy and Clinical Immunology*, 142(4), 1297-1310.e11.

<https://doi.org/10.1016/j.jaci.2017.10.031>

Lilliu, E., Koenig, S., Koenig, X., & Frieden, M. (2021). Store-Operated Calcium Entry in Skeletal Muscle: What Makes It Different? *Cells*, 10(9), 2356.

<https://doi.org/10.3390/cells10092356>

Liou, J., Fivaz, M., Inoue, T., & Meyer, T. (2007). Live-cell imaging reveals sequential oligomerization and local plasma membrane targeting of stromal interaction molecule 1 after Ca<sup>2+</sup> store depletion. *Proceedings of the National Academy of Sciences*, 104(22), 9301-9306. <https://doi.org/10.1073/pnas.0702866104>

Liou, J., Kim, M. L., Do Heo, W., Jones, J. T., Myers, J. W., Ferrell, J. E., & Meyer, T. (2005). STIM Is a Ca<sup>2+</sup> Sensor Essential for Ca<sup>2+</sup>-Store-Depletion-Triggered Ca<sup>2+</sup> Influx. *Current Biology*, 15(13), 1235-1241.

<https://doi.org/10.1016/j.cub.2005.05.055>

López, J. J., Camello-Almaraz, C., Pariente, J. A., Salido, G. M., & Rosado, J. A. (2005). Ca<sup>2+</sup> accumulation into acidic organelles mediated by Ca<sup>2+</sup>- and

vacuolar H<sup>+</sup>-ATPases in human platelets. *Biochemical Journal*, 390(1), 243-252.

<https://doi.org/10.1042/BJ20050168>

Lur, G., Sherwood, M. W., Ebisui, E., Haynes, L., Feske, S., Sutton, R., Burgoyne, R. D., Mikoshiba, K., Petersen, O. H., & Tepikin, A. V. (2011). Ins P 3 receptors and Orai channels in pancreatic acinar cells: Co-localization and its consequences. *Biochemical Journal*, 436(2), 231-239.

<https://doi.org/10.1042/BJ20110083>

Mammadova-Bach, E., Nagy, M., Heemskerk, J. W. M., Nieswandt, B., & Braun, A. (2019). Store-operated calcium entry in thrombosis and thrombo-inflammation.

*Cell Calcium*, 77, 39-48. <https://doi.org/10.1016/j.ceca.2018.11.005>

Marcu, M., Zhang, L., Nau-Staudt, K., & Trifaro, J. (1996). Recombinant scinderin, an F-actin severing protein, increases calcium- induced release of serotonin from permeabilized platelets, an effect blocked by two scinderin-derived actin-binding peptides and phosphatidylinositol 4,5-bisphosphate. *Blood*, 87(1), 20-24.

<https://doi.org/10.1182/blood.V87.1.20.20>

Markello, T., Chen, D., Kwan, J. Y., Horkayne-Szakaly, I., Morrison, A., Simakova, O., Maric, I., Lozier, J., Cullinane, A. R., Kilo, T., Meister, L., Pakzad, K., Bone, W., Chainani, S., Lee, E., Links, A., Boerkoel, C., Fischer, R., Toro, C., ... Gunay-Aygun, M. (2015). York platelet syndrome is a CRAC channelopathy due to gain-of-function mutations in STIM1. *Molecular Genetics and Metabolism*,

114(3), 474-482. <https://doi.org/10.1016/j.ymgme.2014.12.307>

Maruyama, Y., Ogura, T., Mio, K., Kato, K., Kaneko, T., Kiyonaka, S., Mori, Y., & Sato, C. (2009). Tetrameric Orai1 Is a Teardrop-shaped Molecule with a Long,

Tapered Cytoplasmic Domain. *Journal of Biological Chemistry*, 284(20), 13676-13685. <https://doi.org/10.1074/jbc.M900812200>

Mazzucato, M., Pradella, P., Cozzi, M. R., De Marco, L., & Ruggeri, Z. M. (2002). Sequential cytoplasmic calcium signals in a 2-stage platelet activation process induced by the glycoprotein Iba mechanoreceptor. *Blood*, 100(8), 2793-2800. <https://doi.org/10.1182/blood-2002-02-0514>

McCarl, C.-A., Picard, C., Khalil, S., Kawasaki, T., Röther, J., Papolos, A., Kutok, J., Hivroz, C., LeDeist, F., Plogmann, K., Ehl, S., Notheis, G., Albert, M. H., Belohradsky, B. H., Kirschner, J., Rao, A., Fischer, A., & Feske, S. (2009). ORAI1 deficiency and lack of store-operated Ca<sup>2+</sup> entry cause immunodeficiency, myopathy, and ectodermal dysplasia. *Journal of Allergy and Clinical Immunology*, 124(6), 1311-1318.e7. <https://doi.org/10.1016/j.jaci.2009.10.007>

McNally, B. A., & Prakriya, M. (2012). Permeation, selectivity and gating in store-operated CRAC channels: Permeation, selectivity and gating in store-operated CRAC channels. *The Journal of Physiology*, 590(17), 4179-4191. <https://doi.org/10.1113/jphysiol.2012.233098>

McNally, B. A., Somasundaram, A., Jairaman, A., Yamashita, M., & Prakriya, M. (2013). The C- and N-terminal STIM1 binding sites on Orai1 are required for both trapping and gating CRAC channels: CRAC channel gating requires both STIM1 binding sites on Orai1. *The Journal of Physiology*, 591(11), 2833-2850. <https://doi.org/10.1113/jphysiol.2012.250456>

- McNally, B. A., Yamashita, M., Engh, A., & Prakriya, M. (s. f.). *Structural determinants of ion permeation in CRAC channels*. 6.
- Mercer, J. C., DeHaven, W. I., Smyth, J. T., Wedel, B., Boyles, R. R., Bird, G. S., & Putney, J. W. (2006). Large Store-operated Calcium Selective Currents Due to Co-expression of Orai1 or Orai2 with the Intracellular Calcium Sensor, Stim1. *Journal of Biological Chemistry*, 281(34), 24979-24990. <https://doi.org/10.1074/jbc.M604589200>
- Mignen, O., Thompson, J. L., & Shuttleworth, T. J. (2008). Orai1 subunit stoichiometry of the mammalian CRAC channel pore: CRAC channel subunit stoichiometry. *The Journal of Physiology*, 586(2), 419-425. <https://doi.org/10.1113/jphysiol.2007.147249>
- Millay, D. P., Goonasekera, S. A., Sargent, M. A., Maillet, M., Aronow, B. J., & Molkenin, J. D. (2009). Calcium influx is sufficient to induce muscular dystrophy through a TRPC-dependent mechanism. *Proceedings of the National Academy of Sciences*, 106(45), 19023-19028. <https://doi.org/10.1073/pnas.0906591106>
- Miller, J., Bruen, C., Schnaus, M., Zhang, J., Ali, S., Lind, A., Stoecker, Z., Stauderman, K., & Hebbar, S. (2020). Auxora versus standard of care for the treatment of severe or critical COVID-19 pneumonia: Results from a randomized controlled trial. *Critical Care*, 24(1), 502. <https://doi.org/10.1186/s13054-020-03220-x>
- Misceo, D., Holmgren, A., Louch, W. E., Holme, P. A., Mizobuchi, M., Morales, R. J., De Paula, A. M., Stray-Pedersen, A., Lyle, R., Dalhus, B., Christensen, G.,

Stormorken, H., Tjønnfjord, G. E., & Frengen, E. (2014). A Dominant STIM1 Mutation Causes Stormorken Syndrome. *Human Mutation*, *35*(5), 556-564. <https://doi.org/10.1002/humu.22544>

Morin, G., Biancalana, V., Echaniz-Laguna, A., Noury, J., Lornage, X., Moggio, M., Ripolone, M., Violano, R., Marcorelles, P., Maréchal, D., Renaud, F., Maurage, C., Tard, C., Cuisset, J., Laporte, J., & Böhm, J. (2020). Tubular aggregate myopathy and Stormorken syndrome: Mutation spectrum and genotype/phenotype correlation. *Human Mutation*, *41*(1), 17-37. <https://doi.org/10.1002/humu.23899>

Morin, G., Bruechle, N. O., Singh, A. R., Knopp, C., Jedraszak, G., Elbracht, M., Brémond-Gignac, D., Hartmann, K., Sevestre, H., Deutz, P., Hérent, D., Nürnberg, P., Roméo, B., Konrad, K., Mathieu-Dramard, M., Oldenburg, J., Bourges-Petit, E., Shen, Y., Zerres, K., ... Rochette, J. (2014). Gain-of-Function Mutation in STIM1 (P.R304W) Is Associated with Stormorken Syndrome. *Human Mutation*, *35*(10), 1221-1232. <https://doi.org/10.1002/humu.22621>

Münzer, P., & Borst, O. (2022). CRACKing the Molecular Regulatory Mechanism of SOCE during Platelet Activation in Thrombo-Occlusive Diseases. *Cells*, *11*(4), 619. <https://doi.org/10.3390/cells11040619>

Nesin, V., Wiley, G., Kousi, M., Ong, E.-C., Lehmann, T., Nicholl, D. J., Suri, M., Shahrizaila, N., Katsanis, N., Gaffney, P. M., Wierenga, K. J., & Tsiokas, L. (2014). Activating mutations in *STIM1* and *ORAI1* cause overlapping syndromes of tubular myopathy and congenital miosis. *Proceedings of the National*

*Academy of Sciences*, 111(11), 4197-4202.

<https://doi.org/10.1073/pnas.1312520111>

Ng, S. W., di Capite, J., Singaravelu, K., & Parekh, A. B. (2008). Sustained Activation of the Tyrosine Kinase Syk by Antigen in Mast Cells Requires Local Ca<sup>2+</sup> Influx through Ca<sup>2+</sup> Release-activated Ca<sup>2+</sup> Channels. *Journal of Biological Chemistry*, 283(46), 31348-31355. <https://doi.org/10.1074/jbc.M804942200>

Noble, M., Lin, Q.-T., Sirko, C., Houpt, J. A., Novello, M. J., & Stathopoulos, P. B. (2020). Structural Mechanisms of Store-Operated and Mitochondrial Calcium Regulation: Initiation Points for Drug Discovery. *International Journal of Molecular Sciences*, 21(10), 3642. <https://doi.org/10.3390/ijms21103642>

Noury, J.-B., Böhm, J., Peche, G. A., Guyant-Marechal, L., Bedat-Millet, A.-L., Chiche, L., Carlier, R.-Y., Malfatti, E., Romero, N. B., & Stojkovic, T. (2017). Tubular aggregate myopathy with features of Stormorken disease due to a new STIM1 mutation. *Neuromuscular Disorders*, 27(1), 78-82. <https://doi.org/10.1016/j.nmd.2016.10.006>

Numaga-Tomita, T., & Putney, J. W. (s. f.). *1 Role of STIM1 and Orai1-mediated calcium entry in Ca<sup>2+</sup>- 2 induced epidermal keratinocyte differentiation*. 28.

Ogawa, A., Firth, A. L., Smith, K. A., Maliakal, M. V., & Yuan, J. X.-J. (2012). PDGF enhances store-operated Ca<sup>2+</sup> entry by upregulating STIM1/Orai1 via activation of Akt/mTOR in human pulmonary arterial smooth muscle cells. *American Journal of Physiology-Cell Physiology*, 302(2), C405-C411. <https://doi.org/10.1152/ajpcell.00337.2011>



- Okuma, H., Saito, F., Mitsui, J., Hara, Y., Hatanaka, Y., Ikeda, M., & Shimizu, T. (s. f.). *Tubular aggregate myopathy caused by a novel mutation in the cytoplasmic domain of STIM*. 7.
- Omuro, A., Beal, K., McNeill, K., Young, R. J., Thomas, A., Lin, X., Terziev, R., Kaley, T. J., DeAngelis, L. M., Daras, M., Gavrilovic, I. T., Mellinghoff, I., Diamond, E. L., McKeown, A., Manne, M., Caterfino, A., Patel, K., Bavisotto, L., Gorman, G., ... Pentsova, E. (2018). Multicenter Phase IB Trial of Carboxyamidotriazole Orotate and Temozolomide for Recurrent and Newly Diagnosed Glioblastoma and Other Anaplastic Gliomas. *Journal of Clinical Oncology*, 36(17), 1702-1709. <https://doi.org/10.1200/JCO.2017.76.9992>
- Palty, R., & Isacoff, E. Y. (2016). Cooperative Binding of Stromal Interaction Molecule 1 (STIM1) to the N and C Termini of Calcium Release-activated Calcium Modulator 1 (Orai1). *Journal of Biological Chemistry*, 291(1), 334-341. <https://doi.org/10.1074/jbc.M115.685289>
- Palty, R., Stanley, C., & Isacoff, E. Y. (2015). Critical role for Orai1 C-terminal domain and TM4 in CRAC channel gating. *Cell Research*, 25(8), 963-980. <https://doi.org/10.1038/cr.2015.80>
- Parekh, A. B., & Putney, J. W. (2005). Store-Operated Calcium Channels. *Physiological Reviews*, 85(2), 757-810. <https://doi.org/10.1152/physrev.00057.2003>
- Peche, G. A., Spiegelhalter, C., Silva-Rojas, R., Laporte, J., & Böhm, J. (2020). Functional analyses of *STIM1* mutations reveal a common pathomechanism for

tubular aggregate myopathy and Stormorken syndrome. *Neuropathology*, 40(6), 559-569. <https://doi.org/10.1111/neup.12692>

Peng, T.-I., & Jou, M.-J. (2010). Oxidative stress caused by mitochondrial calcium overload: Peng & Jou. *Annals of the New York Academy of Sciences*, 1201(1), 183-188. <https://doi.org/10.1111/j.1749-6632.2010.05634.x>

Penna, A., Demuro, A., Yeromin, A. V., Zhang, S. L., Safrina, O., Parker, I., & Cahalan, M. D. (2008). The CRAC channel consists of a tetramer formed by Stim-induced dimerization of Orai dimers. *Nature*, 456(7218), 116-120. <https://doi.org/10.1038/nature07338>

Penna, D. (2021). New Horizons in Myeloproliferative Neoplasms Treatment: A Review of Current and Future Therapeutic Options. *Medicina*, 57(11), 1181. <https://doi.org/10.3390/medicina57111181>

Prakriya, M., & Lewis, R. S. (2006). Regulation of CRAC Channel Activity by Recruitment of Silent Channels to a High Open-probability Gating Mode. *Journal of General Physiology*, 128(3), 373-386. <https://doi.org/10.1085/jgp.200609588>

Prakriya, M., & Lewis, R. S. (2015). STORE-OPERATED CALCIUM CHANNELS. *Physiol Rev*, 95, 54.

Protasi, F., Pietrangelo, L., & Boncompagni, S. (2021). Calcium entry units (CEUs): Perspectives in skeletal muscle function and disease. *Journal of Muscle Research and Cell Motility*, 42(2), 233-249. <https://doi.org/10.1007/s10974-020-09586-3>

Putney, J. W. (1986). A model for receptor-regulated calcium entry. *Cell calcium*, 7, 1-12.

- Putney, J. W. (2014). Origins of the concept of store-operated calcium entry. *Front Biosci*, 8.
- Rahman, S., & Rahman, T. (2017). Unveiling some FDA-approved drugs as inhibitors of the store-operated Ca<sup>2+</sup> entry pathway. *Scientific Reports*, 7(1), 12881. <https://doi.org/10.1038/s41598-017-13343-x>
- Receptor regulation of calcium release and calcium permeability in parotid gland cells. (1981). *Philosophical Transactions of the Royal Society of London. B, Biological Sciences*, 296(1080), 37-45. <https://doi.org/10.1098/rstb.1981.0169>
- Ren, Q., Wimmer, C., Chicka, M. C., Ye, S., Ren, Y., Hughson, F. M., & Whiteheart, S. W. (2010). Munc13-4 is a limiting factor in the pathway required for platelet granule release and hemostasis. *Blood*, 116(6), 869-877. <https://doi.org/10.1182/blood-2010-02-270934>
- Rink, T. J. (1990). Calcium in Human platelets. *Annual Review of Physiology*, 52(4)
- Rink, T. J., and S. O. Sage. 1990. "Calcium Signaling in Human Platelets." *Annual Review of Physiology* 52(81): 431–49.
- Riva, B., Griglio, A., Serafini, M., Cordero-Sanchez, C., Aprile, S., Di Paola, R., Gugliandolo, E., Alansary, D., Biocotino, I., Lim, D., Grosa, G., Galli, U., Niemeyer, B., Sorba, G., Canonico, P. L., Cuzzocrea, S., Genazzani, A. A., & Pirali, T. (2018). Pyrtriazoles, a Novel Class of Store-Operated Calcium Entry Modulators: Discovery, Biological Profiling, and in Vivo Proof-of-Concept Efficacy in Acute Pancreatitis. *Journal of Medicinal Chemistry*, 61(21), 9756-9783. <https://doi.org/10.1021/acs.jmedchem.8b01512>

- Roos, J., DiGregorio, P. J., Yeromin, A. V., Ohlsen, K., Lioudyno, M., Zhang, S., Safrina, O., Kozak, J. A., Wagner, S. L., Cahalan, M. D., Velichelebi, G., & Stauderman, K. A. (2005). STIM1, an essential and conserved component of store-operated Ca<sup>2+</sup> channel function. *Journal of Cell Biology*, *169*(3), 435-445. <https://doi.org/10.1083/jcb.200502019>
- Rychkov, G. Y., Zhou, F. H., Adams, M. K., Brierley, S. M., Ma, L., & Barritt, G. J. (2022). Orai1- and Orai2-, but not Orai3-mediated *I*<sub>CRAC</sub> is regulated by intracellular pH. *The Journal of Physiology*, *600*(3), 623-643. <https://doi.org/10.1113/JP282502>
- Sabourin, J., Le Gal, L., Saurwein, L., Haefliger, J.-A., Raddatz, E., & Allagnat, F. (2015). Store-operated Ca<sup>2+</sup> Entry Mediated by Orai1 and TRPC1 Participates to Insulin Secretion in Rat β-Cells. *Journal of Biological Chemistry*, *290*(51), 30530-30539. <https://doi.org/10.1074/jbc.M115.682583>
- Sauer, A. V., Hernandez, R. J., Fumagalli, F., Bianchi, V., Poliani, P. L., Dallatomasina, C., Riboni, E., Politi, L. S., Tabucchi, A., Carlucci, F., Casiraghi, M., Carriglio, N., Cominelli, M., Forcellini, C. A., Barzaghi, F., Ferrua, F., Minicucci, F., Medaglini, S., Leocani, L., ... Aiuti, A. (2017). Alterations in the brain adenosine metabolism cause behavioral and neurological impairment in ADA-deficient mice and patients. *Scientific Reports*, *7*(1), 40136. <https://doi.org/10.1038/srep40136>
- Schattenkirchner, M. (2000). The use of leflunomide in the treatment of rheumatoid arthritis: An experimental and clinical review. *Immunopharmacology*, *47*(2-3), 291-298. [https://doi.org/10.1016/S0162-3109\(00\)00194-6](https://doi.org/10.1016/S0162-3109(00)00194-6)

- Schiaffino, S. (2012). Tubular aggregates in skeletal muscle: Just a special type of protein aggregates? *Neuromuscular Disorders*, 22(3), 199-207. <https://doi.org/10.1016/j.nmd.2011.10.005>
- Schiaffino, S., & Reggiani, C. (2011). Fiber Types in Mammalian Skeletal Muscles. *Physiological Reviews*, 91(4), 1447-1531. <https://doi.org/10.1152/physrev.00031.2010>
- Schulte, A., Bieniussa, L., Gupta, R., Samtleben, S., Bischler, T., Doering, K., Sodmann, P., Rittner, H., & Blum, R. (2022). Homeostatic calcium fluxes, ER calcium release, SOCE, and calcium oscillations in cultured astrocytes are interlinked by a small calcium toolkit. *Cell Calcium*, 101, 102515. <https://doi.org/10.1016/j.ceca.2021.102515>
- Shapovalov, G., Gordienko, D., & Prevarskaya, N. (2021). Store operated calcium channels in cancer progression. En *International Review of Cell and Molecular Biology* (Vol. 363, pp. 123-168). Elsevier. <https://doi.org/10.1016/bs.ircmb.2021.02.016>
- Silva-Rojas, R., Charles, A.-L., Djeddi, S., Geny, B., Laporte, J., & Böhm, J. (2021). Pathophysiological Effects of Overactive STIM1 on Murine Muscle Function and Structure. *Cells*, 10(7), 1730. <https://doi.org/10.3390/cells10071730>
- Silva-Rojas, R., Laporte, J., & Böhm, J. (2020). STIM1/ORAI1 Loss-of-Function and Gain-of-Function Mutations Inversely Impact on SOCE and Calcium Homeostasis and Cause Multi-Systemic Mirror Diseases. *Frontiers in Physiology*, 11, 604941. <https://doi.org/10.3389/fphys.2020.604941>

- Silva-Rojas, R., Treves, S., Jacobs, H., Kessler, P., Laporte, J., & Böhm, J. (s. f.). *STIM1 over-activation generates a multi-systemic phenotype affecting skeletal muscle, spleen, eye, skin, bones, and the immune system in mice*. 42.
- Smani, T., Shapovalov, G., Skryma, R., Prevarskaya, N., & Rosado, J. A. (2015). Functional and physiopathological implications of TRP channels. *Biochimica et Biophysica Acta (BBA) - Molecular Cell Research*, 1853(8), 1772-1782. <https://doi.org/10.1016/j.bbamcr.2015.04.016>
- Soboloff, J., Spassova, M. A., Tang, X. D., Hewavitharana, T., Xu, W., & Gill, D. L. (2006). Orai1 and STIM Reconstitute Store-operated Calcium Channel Function. *Journal of Biological Chemistry*, 281(30), 20661-20665. <https://doi.org/10.1074/jbc.C600126200>
- Stathopoulos, P. B., Li, G.-Y., Plevin, M. J., Ames, J. B., & Ikura, M. (2006). Stored Ca<sup>2+</sup> Depletion-induced Oligomerization of Stromal Interaction Molecule 1 (STIM1) via the EF-SAM Region. *Journal of Biological Chemistry*, 281(47), 35855-35862. <https://doi.org/10.1074/jbc.M608247200>
- Steinckwich, N., Myers, P., Janardhan, K. S., Flagler, N. D., King, D., Petranka, J. G., & Putney, J. W. (2015). Role of the store-operated calcium entry protein, STIM1, in neutrophil chemotaxis and infiltration into a murine model of psoriasis-inflamed skin. *The FASEB Journal*, 29(7), 3003-3013. <https://doi.org/10.1096/fj.14-265215>
- Stormorken, H. et al. 1995. "Studies on the haemostatic defect in a complicated syndrome. An inverse Scott syndrome platelet membrane abnormality?." *Thrombosis and haemostasis* 74(5): 1244-51.

- Sukumaran, P., Nascimento Da Conceicao, V., Sun, Y., Ahamad, N., Saraiva, L. R., Selvaraj, S., & Singh, B. B. (2021). Calcium Signaling Regulates Autophagy and Apoptosis. *Cells*, *10*(8), 2125. <https://doi.org/10.3390/cells10082125>
- Thompson, J. L., & Shuttleworth, T. J. (2013). How Many Orai's Does It Take to Make a CRAC Channel? *Scientific Reports*, *3*(1), 1961. <https://doi.org/10.1038/srep01961>
- Thornton, A. M., Zhao, X., Weisleder, N., Brotto, L. S., Bougoin, S., Nosek, T. M., Reid, M., Hardin, B., Pan, Z., Ma, J., Parness, J., & Brotto, M. (2011). Store-Operated Ca<sup>2+</sup> Entry (SOCE) Contributes to Normal Skeletal Muscle Contractility in young but not in aged skeletal muscle. *Aging*, *3*(6), 621-634. <https://doi.org/10.18632/aging.100335>
- Vaeth, M., Kahlfuss, S., & Feske, S. (2020). CRAC Channels and Calcium Signaling in T Cell-Mediated Immunity. *Trends in Immunology*, *41*(10), 878-901. <https://doi.org/10.1016/j.it.2020.06.012>
- Varga-Szabo, D., Authi, K. S., Braun, A., Bender, M., Ambily, A., Hassock, S. R., Gudermann, T., Dietrich, A., & Nieswandt, B. (2008). Store-operated Ca<sup>2+</sup> entry in platelets occurs independently of transient receptor potential (TRP) C1. *Pflügers Archiv - European Journal of Physiology*, *457*(2), 377-387. <https://doi.org/10.1007/s00424-008-0531-4>
- Varga-Szabo, D., Braun, A., & Nieswandt, B. (2009). Calcium signaling in platelets. *Journal of Thrombosis and Haemostasis*, *7*(7), 1057-1066. <https://doi.org/10.1111/j.1538-7836.2009.03455.x>

- Vig, M., Peinelt, C., Beck, A., Koomoa, D. L., Rabah, D., Koblan-Huberson, M., Kraft, S., Turner, H., Fleig, A., Penner, R., & Kinet, J.-P. (2006). CRACM1 Is a Plasma Membrane Protein Essential for Store-Operated Ca<sup>2+</sup> Entry. *Science*, 312(5777), 1220-1223. <https://doi.org/10.1126/science.1127883>
- Waldherr, L., Tiffner, A., Mishra, D., Sallinger, M., Schober, R., Frischauf, I., Schmidt, T., Handl, V., Sagmeister, P., Köckinger, M., Derler, I., Üçal, M., Bonhenry, D., Patz, S., & Schindl, R. (2020). Blockage of Store-Operated Ca<sup>2+</sup> Influx by Synta66 is Mediated by Direct Inhibition of the Ca<sup>2+</sup> Selective Orai1 Pore. *Cancers*, 12(10), 2876. <https://doi.org/10.3390/cancers12102876>
- Waldron, R. T., Chen, Y., Pham, H., Go, A., Su, H., Hu, C., Wen, L., Husain, S. Z., Sugar, C. A., Roos, J., Ramos, S., Lugea, A., Dunn, M., Stauderman, K., & Pandol, S. J. (2019). The Orai Ca<sup>2+</sup> channel inhibitor CM4620 targets both parenchymal and immune cells to reduce inflammation in experimental acute pancreatitis. *The Journal of Physiology*, 597(12), 3085-3105. <https://doi.org/10.1113/JP277856>
- Walter, M. C., Rossius, M., Zitzelsberger, M., Vorgerd, M., Müller-Felber, W., Ertl-Wagner, B., Zhang, Y., Brinkmeier, H., Senderek, J., & Schoser, B. (2015). 50 years to diagnosis: Autosomal dominant tubular aggregate myopathy caused by a novel STIM1 mutation. *Neuromuscular Disorders*, 25(7), 577-584. <https://doi.org/10.1016/j.nmd.2015.04.005>
- Wei-LaPierre, L., Carrell, E. M., Boncompagni, S., Protasi, F., & Dirksen, R. T. (2013). Orai1-dependent calcium entry promotes skeletal muscle growth and



limits fatigue. *Nature Communications*, 4(1), 2805.

<https://doi.org/10.1038/ncomms3805>

Wen, L., Voronina, S., Javed, M. A., Awais, M., Szatmary, P., Latawiec, D., Chvanov, M., Collier, D., Huang, W., Barrett, J., Begg, M., Stauderman, K., Roos, J., Grigoryev, S., Ramos, S., Rogers, E., Whitten, J., Velicelebi, G., Dunn, M., ... Sutton, R. (2015). Inhibitors of ORAI1 Prevent Cytosolic Calcium-Associated Injury of Human Pancreatic Acinar Cells and Acute Pancreatitis in 3 Mouse Models. *Gastroenterology*, 149(2), 481-492.e7.

<https://doi.org/10.1053/j.gastro.2015.04.015>

Xia, W., Li, Y., Wang, B., Chen, J., Wang, X., Sun, Q., Sun, F., Li, Z., & Zhao, Z. (2015). Enhanced Store-Operated Calcium Entry in Platelets is Associated with Peripheral Artery Disease in Type 2 Diabetes. *Cellular Physiology and Biochemistry*, 37(5), 1945-1955. <https://doi.org/10.1159/000438555>

Xing, J., Petranka, J. G., Davis, F. M., Desai, P. N., Putney, J. W., & Bird, G. S. (2014). Role of *Orai1* and store-operated calcium entry in mouse lacrimal gland signalling and function: Mouse lacrimal gland signalling and function. *The Journal of Physiology*, 592(5), 927-939.

<https://doi.org/10.1113/jphysiol.2013.267740>

Yen, M., Lokteva, L. A., & Lewis, R. S. (2016). Functional Analysis of Orai1 Concatemers Supports a Hexameric Stoichiometry for the CRAC Channel. *Biophysical Journal*, 111(9), 1897-1907.

<https://doi.org/10.1016/j.bpj.2016.09.020>

- Yoshioka, A., Shirakawa, R., Nishioka, H., Tabuchi, A., Higashi, T., Ozaki, H., Yamamoto, A., Kita, T., & Horiuchi, H. (2001). Identification of Protein Kinase C $\alpha$  as an Essential, but Not Sufficient, Cytosolic Factor for Ca<sup>2+</sup>-induced  $\alpha$ - and Dense-core Granule Secretion in Platelets. *Journal of Biological Chemistry*, 276(42), 39379-39385. <https://doi.org/10.1074/jbc.M102933200>
- Zhang, S. L., Yeromin, A. V., Zhang, X. H.-F., Yu, Y., Safrina, O., Penna, A., Roos, J., Stauderman, K. A., & Cahalan, M. D. (2006). Genome-wide RNAi screen of Ca<sup>2+</sup> influx identifies genes that regulate Ca<sup>2+</sup> release-activated Ca<sup>2+</sup> channel activity. *Proceedings of the National Academy of Sciences*, 103(24), 9357-9362. <https://doi.org/10.1073/pnas.0603161103>
- Zhang, S. L., Yu, Y., Roos, J., Kozak, J. A., Deerinck, T. J., Ellisman, M. H., Stauderman, K. A., & Cahalan, M. D. (2005). STIM1 is a Ca<sup>2+</sup> sensor that activates CRAC channels and migrates from the Ca<sup>2+</sup> store to the plasma membrane. *Nature*, 437(7060), 902-905. <https://doi.org/10.1038/nature04147>
- Zheng, L., Stathopoulos, P. B., Li, G.-Y., & Ikura, M. (2008). Biophysical characterization of the EF-hand and SAM domain containing Ca<sup>2+</sup> sensory region of STIM1 and STIM2. *Biochemical and Biophysical Research Communications*, 369(1), 240-246. <https://doi.org/10.1016/j.bbrc.2007.12.129>
- Zhou, Y., Ramachandran, S., Oh-hora, M., Rao, A., & Hogan, P. G. (2010). Pore architecture of the ORAI1 store-operated calcium channel. *Proceedings of the National Academy of Sciences*, 107(11), 4896-4901. <https://doi.org/10.1073/pnas.1001169107>

Zhu, Z.-D., Yu, T., Liu, H.-J., Jin, J., & He, J. (2018). SOCE induced calcium overload regulates autophagy in acute pancreatitis via calcineurin activation. *Cell Death & Disease*, 9(2), 50. <https://doi.org/10.1038/s41419-017-0073-9>



## **Abbreviations**

AIHA: Autoimmunity with haemolytic anemia

Ca<sup>2+</sup>: Calcium ion

CICR: Calcium-Induce Calcium-Release

CK: Creatine Kinase

CMP: Common Myeloid Progenitors

CRAC: Calcium Release-Activated Calcium

DHODH: Dihydroorotate Dehydrogenase

DMD: Duchenne Muscular Dystrophy

DTS: Dense Tubular System

ER: Endoplasmic Reticulum

ER/SR: Endo-Sarcoplasmic Reticulum

GMP: Granulocyte-Macrophage Progenitors

IC<sub>50</sub>: Inhibition Concentration 50

IP<sub>3</sub>R: Inositol-1,4,5-triphosphate Receptor

LSK: Lymphoid Progenitor Population

MPN: Myeloproliferative Neoplasm

MEP: Megakaryocyte-Erythroid Progenitors

Na<sup>+</sup>: Sodium ion.

NK: Natural Killer

PAR: Protease-Activated Receptor

PM: Plasma Membrane

PKC: Protein Kinase C

PS: phosphatidylserine

RYR: Ryanodine Receptors

SCID: Severe Combined Immunodeficiency

SERCA: Sarco(Endo)plasmic Reticulum Ca<sup>2+</sup> ATPase

SOC Entry: Store-Operated Calcium Entry.

SR: Sarcoplasmic Reticulum

STIM: Stromal Interaction Molecule

TAM: Tubular Aggregate Myopathy

TM: Transmembrane

YPS: York Platelet Syndrome

## List of publications (*Cordero-Sanchez, C.*) *h-index: 4*

- First author
  - Cordero-Sanchez, C. et al. “*CIC-39Na reverses the thrombocytopenia that characterizes Tubular Aggregate Myopathy*” Submitted. Manuscript ID: BLD-2021-014261.
  - Cordero-Sanchez, C. et al 2019. “*Store-Operated Calcium Entry (SOCE) as a therapeutic target in acute pancreatitis: discovery and development of drug-like SOCE inhibitors*”: Med Chem. 2020;63(23):14761-14779. doi:10.1021/acs.jmedchem.0c01305
  - Cordero-Sanchez, C. et al. 2019. “*A luminal EF-hand mutation in STIM1 in mice causes the clinical hallmarks of tubular aggregate myopathy.*” Dis Model Mech. 2019;13(2):dmm041111. doi:10.1242/dmm.041111
  - Cordero-Sanchez, C. et al 2019. “*Fluorescence-Based Functional Assays for Ca<sup>2+</sup>-Permeable ThermoTRP Channels.*” Methods Mol Biol. 2019;1987:99-110. doi:10.1007/978-1-4939-9446-5\_7
- Co-author
  - Riva B. et al. “*STIM1 and ORAI1 mutations leading to tubular aggregate myopathies are sensitive to the Store-operated Ca<sup>2+</sup>-entry modulators CIC-37 and CIC-39*” Submitted. Manuscript ID: CECA-D-22-00007
  - Aprile, S. et al. 2021. “*1,2,4-Oxadiazole-Bearing Pyrazoles as Metabolically Stable Modulators of Store-Operated Calcium Entry*” ACS Med Chem Lett. 2021;12(4):640-646. doi:10.1021/acsmedchemlett.1c00034
  - Riva, B. et al. 2018 “*Pytriazoles, a Novel Class of Store-Operated Calcium Entry Modulators: Discovery, Biological Profiling, and in Vivo Proof-of-Concept Efficacy in Acute Pancreatitis.*” J Med Chem. 2018;61(21):9756-9783. doi:10.1021/acs.jmedchem.8b01512
  - Riva, B. et al 2018 “*Oxaliplatin induces pH acidification in dorsal root ganglia neurons.*” Sci Rep. 2018;8(1):15084. doi:10.1038/s41598-018-33508-6

## Patent:

- Patent number: n. 102020000003692. “*Composti bifenilici come modulatori di SOCE, loro composizioni e usi.*”





*Celia Cordero Sanchez*

*16/09/1994, Huelva (Spain)*

*Ph.D. student, Novara (Italy)*

*biocelia.cordero@gmail.com*

*3395975803*

### *Academic training*

- 2018/Nowadays.- PhD student in Chemistry and Biology at Università del Piemonte Orientale at Novara, (Italy).
- 2016/2017.- Master degree in Biotechnology and Bioengineering (UMH, Subdelegate)
- 2012/2016.- Bachelor's degree in Biotechnology (UMH).

### *Animal experimentation education*

According to the Directive 2010/63/EU (Spanish legislation, article 15.2 R.D. 53/2013.)

- 2018.- Experimental animal Course: “*Designing procedures and projects with laboratory animals (b)*” (Category (d))
- 2015.- Experimental animal Course: “*Carrying out procedures on animals (a)*” (Category (c))
- 2015.- Experimental animal Course: “*Sacrifice of animals (d)*” (Category (b))

### *Professional experience*

- 2018, November - Nowadays: Ph.D. candidate in Chemistry and Biology supervised by Prof. Armando Genazzani at Università del Piemonte Orientale (UPO), Department of Pharmacological Sciences (Novara, Italy). In collaboration with ChemiCare S.R.L.
  - o “*Characterization of a mouse model for Tubular Aggregate Myopathy and development of small molecules*”.
  - o 8 months at the Pablo Olavide University (UPO), Andalusian Center for Development Biology CABD (Seville, Spain). Project: “*Screening for personalized precision medicine in Ataxia di Friedreich and Huntington disease*”.
- 2017 October – 2018 October.- Researcher at ChemiCare S.R.L. (Novara, Italy)
- 2017 April – June.- Erasmus+Traineeship at UPO, Department of Pharmacological Sciences (Novara, Italy).
- 2014 September – 2017 March.- Traineeship supervised by Prof. Asia Fernandez Carbajal in Molecular and Cellular Biology Institute (IBMC, now IDIBE) of Miguel Hernandez University (UMH, Elche, Spain). In collaboration with Antalgénics S.L. MSc and Bachelor's project.
  - o “*Searching for modulators of TRPM8 channel by High-throughput screening (HTS) methods*”. (Honor)
  - o Researching activities' grant (3 months).
- 2014 July.- Traineeship supervised by Prof. Rosa Leon Banares in Cellular Biology and Biochemistry Department, University of Huelva (UHU) (Huelva, Spain)
  - o *Isolation and identification of new archaea strain in hypersaline waters*”

## Publications (Cordero-Sanchez, C.) h-index: 4

### - First author

- Cordero-Sanchez, C. et al. “CIC-39Na reverses the thrombocytopenia that characterizes Tubular Aggregate Myopathy” Submitted. BLD-2021-014261.
- Cordero-Sanchez, C. et al 2019. “Store-Operated Calcium Entry (SOCE) as a therapeutic target in acute pancreatitis: discovery and development of drug-like SOCE inhibitors”: *Med Chem.* 2020;63(23):14761-14779. doi:10.1021/acs.jmedchem.0c01305
- Cordero-Sanchez, C. et al. 2019. “A luminal EF-hand mutation in STIM1 in mice causes the clinical hallmarks of tubular aggregate myopathy.” *Dis Model Mech.* 2019;13(2):dmm041111. doi:10.1242/dmm.041111
- Cordero-Sanchez, C. et al 2019. “Fluorescence-Based Functional Assays for Ca<sup>2+</sup>-Permeable ThermoTRP Channels.” *Methods Mol Biol.* 2019;1987:99-110. doi:10.1007/978-1-4939-9446-5\_7

### - Co-author





- Riva B. et al. “STIM1 and ORA11 mutations leading to tubular aggregate myopathies are sensitive to the Store-operated Ca<sup>2+</sup>-entry modulators CIC-37 and CIC-39” Submitted. Manuscript ID: CECA-D-22-00007
- Aprile, S. et al. 2021. “1,2,4-Oxadiazole-Bearing Pyrazoles as Metabolically Stable Modulators of Store-Operated Calcium Entry” *ACS Med Chem Lett.* 2021;12(4):640-646. doi:10.1021/acsmedchemlett.1c00034
- Riva, B. et al. 2018 “Pyrtriazoles, a Novel Class of Store-Operated Calcium Entry Modulators: Discovery, Biological Profiling, and in Vivo Proof-of-Concept Efficacy in Acute Pancreatitis.” *J Med Chem.* 2018;61(21):9756-9783. doi:10.1021/acs.jmedchem.8b01512
- Riva, B. et al 2018 “Oxaliplatin induces pH acidification in dorsal root ganglia neurons.” *Sci Rep.* 2018;8(1):15084. doi:10.1038/s41598-018-33508-6

## Patent

- Patent number: n. 102020000003692: *Composti bifenilici come modulatori di SOCE, loro composizioni e usi.* Patent license to ChemiCare S.L.R.

## Languages

- Nowadays preparing for C1 of Italian.
- 2014.- English: *FIRST (B2) certificated by Cambridge.*
- 2011.- French: *B1 certificated for DELF.* Cultural Foreign Exchange with Chambery (France) (15 days).

Language	Oral	Written	Comprehension
	B2	B2	B2
	B1 (DELF)	B1 (DELF)	B1 (DELF)
	High	Medium	High
		Mother tongue	

### *In vitro and ex vivo skills*

- **Molecular Biology:** RNA extraction. Western-blotting. PCR and q-RT-PCR. Bacterial transformation. Cellular transfection techniques. Site-directed mutagenesis techniques. Fibroblasts reprogramming of induced neurons or myoblasts. High-throughput screening techniques (Polastar Omega and Victor). High-throughput automated Patch Clamp (IonFlux). Calcium imaging. Iron metabolism studies. Cell viability assays. Flow cytometry.
- **Cellular Biology:** Extraction, growth, and maintenance of human and mice primary culture. Culture of stable cell lines.

### *In vivo skills*

Handling experience with mice and rats.

- **Behavioural test:** in mice (open field test, grasping, hanging, rotarod, treadmill, novel object recognition test) and rat (static pain measurement by pressure).
- **Extraction:** Mice muscle and organs. Mice blood (cheek, retro-orbital, intracardiac). Mice and rat dorsal root ganglion. Bone marrow, neuronal, spleen, and blood cell isolation in mice.

### *Computer skills*

- Basic Knowledge of: Pymol. Swiss PDB Viewer. VMD. Yasara. MartinView. Chemidraw. Ubuntu. R Programm. GraphPad. Kaleidagraph. FlowJo. ImageJ. Prezi.
- Intermediate Knowledge on Office programs: Excel. Word. Powerpoint.

### *Teaching and dissemination*

- 2020.- Dissemination video: “Enfermedades raras”  
[https://www.youtube.com/watch?v=G4f76870abw&ab\\_channel=CeliaCorSan](https://www.youtube.com/watch?v=G4f76870abw&ab_channel=CeliaCorSan)
- 2016.- Professor assistant on Molecular Modelling, Subject on Biotechnology degree at UMH. (35 hours)
- 2016.- Dissemination sessions of Transgenics and OGM given at *Pablo Neruda high school* of Huelva. *Sixto Marco’s high school* of Elche (Alicante). and *Jesuita’s school* of Elche (Alicante). (8 hours)

### *Complementary education*

- Scientific courses:
  - 2020.- “How to write in English an article of scientific research?”.- Casa de Lletres Editor (8 weeks)
  - 2016.- “Inside Cancer” .- University of Bath (6 weeks)
  - 2016.- “Genomic Medicine: Transforming patient Care in Diabetes” University of Exeter. (4 weeks)

- General courses:
  - 2020.- “*Hyperthinking: improve your day to day learning& creativity.*” – Digital Masterclass (Udemy platform).
  - 2020.- “*Stress management y Mindfulness*”.- University of Anáhuac Mayab.

### *Secondary author poster*

- 2016.- Secondary author in a poster published on XXIV National Meeting in Medicinal Chemistry, Perugia (Italy). Collaboration with IBMC.
  - “*Design, synthesis and biological activity of tryptamine-based derivatives as new TRPM8 modulators.*”
- 2014.- Secondary author in a poster published on XXXVII Spanish Society of Biochemistry and Molecular Biology (SEBBM). Collaboration with UHU.
  - “*Isolation and identification of new archaea strain in hypersaline waters*”

### *Personal abilities*

- 2019-2020.- Social network management of Emotion Master (responsible for Twitter)
- 2016.- Volunteer at “Blood donation marathon” UMH.
- 2008.- Participation in XXIV Maths Olympics of Thales (Spain).

### *Conference and seminars attendance*

- 2021.- 40° Congress and XXII Seminar of Italian Pharmacological Society (SIF) - Digital Edition (9-13 March)
- 2019.- 39° Congress and XXII Seminar of Italian Pharmacological Society (SIF) in Florence (Italy) (19-23 November)
- 2018.- XXI Seminar of Italian Pharmacological Society (SIF) in Bresso (Italy) (19-22 September)
- 2016.- II Awareness sessions on Biomedical researching HGUE-IBMC. (5.5 hours)
- 2016.- VI Dissemination session: Prometeo-GV-Progression of Diabetes and Obesity. (3 hours)
- 2016.- “*Roles of T-type calcium channels in chronic pain: from sensory afferents to spinal networks.*” Emman el Bourinet (2 hours)
- 2016.- Seminars of the Master’s degree (22 hours).
- 2016.- 39 congress of Spanish Society of Immunology (4 hours)
- 2015.- “*From the idea to the action*” – Pau Garcia Milà. (3 hours)
- 2015.- IX Congress of Spanish Federation of Biotechnologists at Salamanca.
- 2014 and 2016.- II and III Dissemination session “*And you, what is your research about?*” UMH (21 hours)
- 2014.- “*Genetics for Legos*” – conferences about genetics and its use. (8 hours)
- 2012/16.- IV-VIII Awareness sessions of San Alberto Magno – Experimental sciences Faculty of UMH (22.5 hours).
- 2011.- “*Coffee with sciences*”, a week of science activities on Andalusia. (5 hours)